Technical Report

TR-02-13

Final report of the TRUE Block Scale project

1. Characterisation and model development

Peter Andersson, Johan Byegård, Geosigma AB

Bill Dershowitz, Thomas Doe, Golder Associates Inc

Jan Hermanson, Golder Associates AB

Peter Meier, ANDRA

Eva-Lena Tullborg, Terralogica AB

Anders Winberg (ed), Conterra AB

April 2002

Svensk Kärnbränslehantering AB
Swedish Nuclear Fuel
and Waste Management Co
Box 5864
SE-102 40 Stockholm Sweden
Tel 08-459 84 00
+46 8 459 84 00
Fax 08-661 57 19
+46 8 661 57 19

Final report of the TRUE Block Scale project

1. Characterisation and model development

Peter Andersson, Johan Byegård, Geosigma AB

Bill Dershowitz, Thomas Doe, Golder Associates Inc

Jan Hermanson, Golder Associates AB

Peter Meier, ANDRA

Eva-Lena Tullborg, Terralogica AB

Anders Winberg (ed), Conterra AB

April 2002

Keywords: Block Scale, characterisation, fracture, hydraulic, hydrochemistry, model evolution, network, structure, tracer tests, TRUE.

Foreword

This report constitutes the first in a series of four final reports of the TRUE Block Scale Project, the latter run within the framework of the Tracer Retention Understanding Experiments at the SKB Äspö Hard Rock Laboratory, Sweden.

Funding organisations of the project are;

ANDRA (France)

ENRESA (Spain)

JNC (Japan)

NIREX (United Kingdom)

POSIVA (Finland)

SKB (Sweden)

The work done could not have been accomplished without the active participation and effort of field characterisation crews and analysis teams from the organisations and countries involved. Their contributions and the contribution of the co-ordinators and staff of the Äspö Hard Rock Laboratory are hereby acknowledged.

Abstract

The general objectives of the TRUE Block Scale Project /Winberg, 1997/ were to 1) increase understanding of tracer transport in a fracture network and to improve predictive capabilities, 2) assess the importance of tracer retention mechanisms (diffusion and sorption) in a fracture network, and 3) assess the link between flow and transport data as a means for predicting transport phenomena. During the period mid 1996 through mid 1999 a 200x250x100 m rock volume was characterised with the purpose of furnishing the basis for successful tracer experiments in a network of conductive structures in the block scale (10–100 m). In total five cored boreholes were drilled as part of the project in an iterative mode with a period of analysis following completion of characterisation, and with a strong component of interactivity with numerical modelling and experimental design, particularly towards the end of the characterisation. The combined use of pressure responses due to drilling and drilling records provided important early information/confirmation of the existence and location of a given structure. Verification of conductors identified from pressure responses was achieved through the use of various flow logging techniques. The usage of the Posiva difference flow log towards the end of the characterisation work enabled identification of discrete conductive fractures with a high resolution. Pressure responses collected during drilling were used to obtain a first assessment of connectivity between boreholes. The transient behaviour of the responses collected during cross-hole interference tests in packed-off boreholes were used to identify families of responses, which correlated well with the identified principal families of structures/fracture networks. The conductive geometry of the investigated rock block is made up of steeply dipping deterministic NW structures and NNW structures. High inflows in the boreholes were for the most part associated with geologically/geometrically identified conductors. The remainder of conductive fractures/structures was assigned to the background fracture population. The principal experience from the characterisation and subsequent construction of hydro-structural models is that it is difficult to decouple structural-geological and hydraulic data in building the hydro-structural model. For the most part the hydraulic and geological/structural information was integrated simultaneously in the interpretation. The major conducting structures and their extents between boreholes were determined. The basic hydro-structural model was established using information from the first three boreholes. No major changes to the model were required on the basis of the additional information acquired from the last two boreholes, but more detail was added in terms of a few additional structures and more information about heterogeneity. Difficulties remain with regards to the actual extent of interpreted deterministic structures outside the borehole array. The developed hydro-structural model combined with the understanding of the hydraulic behaviour obtained from performed cross-hole and tracer dilution tests made it possible to identify a target area for well-controlled tracer experiments. The central parts of the TRUE Block Scale rock volume contained water of mixed origin including Deep brine water that is older and more saline than Baltic seawater. The hydraulic head information showed an expected movement of water across the studied block towards the underground openings of the Äspö Hard Rock Laboratory. The gradient over the central part of the TRUE Block Scale rock volume was about 0.05 m/m. Ambient flow measurements from tracer dilution tests provided a

useful complement to other information available on the flow field. The tracer test design had to consider these ambient flows carefully to avoid losing tracer in the flow paths.

Transport parameters were presented for the wall rock of structures involved in the TRUE Block Scale tracer tests. Given the kinship between the TRUE-1 site and the TRUE Block Scale site, sorption distribution coefficients and diffusivity of intact Äspö diorite and site-specific wall rock material from the TRUE–1 site were imported for use in TRUE Block Scale. The main reason for using this approach was the similarities in lithology, structure orientation and water chemistry between the TRUE-1 and TRUE Block Scale sites. Elaborate mineralogical and geochemical studies were performed on material collected from structure intercepts of interest. In addition, fault breccia material was analysed in the laboratory. Together with assessments of the cation exchange capacity, assessment of mineralogical distribution and site-specific hydrogeochemical data volumetric distributions coefficients K_d for the fault breccia size fractions <0.125 mm and 0.125–2 mm were estimated. A comprehensive petrophysical programme was performed with the aim to assess the porosity and porosity distribution/texture related to relevant structure intercepts. Both conventional water saturation/water absorption techniques and impregnation techniques using ^{14}C-labelled polymethylmethaacrylate (PMMA) were employed.

Sammanfattning

De övergripande målen med TRUE Block Scale projektet var att 1) öka förståelsen av transport av lösta spårämnen i ett nätverk av sprickor och att förbättra möjligheter att göra modellbaserade förutsägelser av transport, 2) undersöka betydelsen av retentionsmekanismer (diffusion och sorption) i nätverk av sprickor, och 3) att undersöka kopplingen mellan hydrauliska parametrar och transportparametrar för att därigenom ge en möjlighet att förutsäga transport av lösta ämnen. Under perioden 1996 till 1999 karakteriseraes en bergvolym med dimensionerna 200x250x100 m, med målet att tillhandahålla en plattform för genomförande av väl kontrollerade spårförsök i blockskala (10–100 m). Totalt borrades fem kärnborrhål inom ramen för projektet. Borrningsprogrammet genomfördes iterativt med en period för analys och utvärdering avsatt efter varje avslutad borrningsinsats. Karakteriseringsarbetet genomfördes med ett starkt inslag av interaktivitet med mumerisk modellering och experimentdesign, speciellt mot slutet av karakteriseringen. Kombinerad analys av borrprotokoll och tryckresponser i avmanschetterade delar av borrhålen gav tidig och viktig information vad avser existens och läge av vattenförande strukturer. Verifikation av vattenförande strukturer tolkade från tryckresponser erhölls från olika typer av flödesloggnings-metoder. Utnyttjande av Posivas DIFF flödesmätare medgav mot slutet av undersökningarna en möjlighet att identifiera diskreta vattenförande sprickor med hög upplösning. Tryckresponser insamlade under borrninng gav en första bild av hydraulisk koppling mellan borrhålen. Tryckresponser som erhölls i avmanschetterade borrhål vid genomförda hydrauliska mellanhålsmätningar användes för att identifiera olika typresponser som kunde korreleras med identifierade huvudgrupper av strukturer/ nätverk. Geometrin hos identifierade deterministiska konduktiva strukturer domineras av brant stupande strukturer orienterade i nordvästlig och nordnordvästlig riktning. Observerade höga inflöden i borrhålen kunde genomgående associeras med geologiskt/geometriskt identifierbara strukturer. Resterade konduktiva sprickor och strukturer tillskrevs en population representerande bergets normalsprickighet. Den viktigaste erfarenheten från det genomförda karakteriseringsarbetet, och den efter-följande geologiska modelleringen, var att det är svårt att genomföra oberoende analys av den strukturgeologiska och hydrologiska informationen vid byggandet av en strukturmodell av vattenförande zoner. För det mesta samtolkades och integrerades strukturgeologiska och hydrogeologiska data. De huvudsakliga vattenförande strukturerna och deras utsträckning mellan borrhålen bestämdes. En grundläggande strukturmodell togs fram med underlag från de första tre undersökningsborrhålen. Inga större förändringar av modellen var påkallde av den information som erhölls från de två sita borrhålen. En större grad av detaljförfining av modellen erhölls dock, inklusive ett fåtal tillkommande strukturer och ytterligare information om heterogenitet. Svårigheter kvarstår dock att fastställa utsträckningen av de tolkade strukturerna utanför det område som täcks av borrhålen. Den konstruerade strukturmodellen, i kombination med en förståelse av den hydrauliska situationen erhållen från utförda interferenstester och utspädningsmätningar, gjorde det möjligt att identifiera ett målområde för väl kontrollerade spårförsök. De centrala delarna av den studerade bergvolymen uppvisade vattentyper av olika ursprung, bl a “brine” från större djup, som är äldre och mer salint

är östersjövatten (Baltic seawater). Registering av grundvattentryck visade en förväntad vattenrörelse genom den studerade bergvolymen mot Äspölaboratoriets underjords-anläggningar. Den hydrauliska gradienten genom de centrala delarna av den undersökta bergvolymen var cirka 5%. Utspädningsmätningar av naturligt grundvattenflöde i avmanschetterade sektioner av borrhålen gav kompletterande information om flödes-regimen. I samband med design av efterföljande spårförsök togs hänsyn till dessa bakgrundsflöden för att undvika massförluster.

Transportparametrar representerande sidoberget presenterades för de strukturer som var involverade i senare utförda spårförsök. Givet likheterna mellan TRUE-1 siten och TRUE Block Scale volymen, importerades sorptionskoefficienter och diffusiviteter för platsspecifikt geologiskt material och intakt oomvandlad Äspödiorit från TRUE-1 siten. Argumenten för denna import var likheter i litologi, orientering hos aktuella strukturer samt vad avser vattenkemi. Omfattande mineralogiska och geokemiska analyser geomfördes på material från strukturintercept av betydelse. Vidare analyserades brecciamaterial i laboratorium. Genom utnyttjade av jonbyteskapaciter för aktuella mineral erhållna från literaturen, uppskattade mineralogisk fördelning och platsspecifika hydrogeokemiska data skattades väden på sorptionskoefficienter (K_d) för breccia-fraktionerna <125 mm samt 0.125–2 mm. Ett omfattande program genomfördes för att bestämma porositet och porositetsfördelning i anslutning till viktiga strukturintercept. I samband med dessa undersökningar utnyttjades konventionell vattenabsorbtionsteknik samt impregnering med ^{14}C-dopad polymetylmetaacrylat (PMMA).

Executive Summary

Background and objectives

In 1996 ANDRA, POSIVA, NIREX, SKB and subsequently ENRESA and JNC, decided to carry out the TRUE Block Scale Experiment. The experiment being directly linked to the preceding detailed scale (L<10 m) First TRUE Stage /Winberg et al, 2000/ which focused on transport and retention studies in an interpreted single fracture. The general objectives of TRUE Block Scale /Winberg, 1997/ were to 1) increase understanding of tracer transport in a fracture network and improve predictive capabilities, 2) assess the importance of tracer retention mechanisms (diffusion and sorption) in a fracture network, and 3) assess the link between flow and transport data as a means for predicting transport phenomena.

Specifics of TRUE Block Scale characterisation

During the period mid 1996 through mid 1999 a 200x250x100 m rock volume was characterised at the Äspö HRL with the purpose of furnishing the basis for successful tracer experiments in a network of conductive structures at the block scale (10–100 m). The prerequisites for carrying out such tests are 1) a hydro-structural model based on which the planned tracer tests can be designed and evaluated, and 2) a resulting borehole array, which provides the necessary sink and source sections for such tests. The present report provides a description of the methods and the characterisation results, which were used to build the hydro-structural models.

In total five cored boreholes were drilled as part of the project in an iterative mode with a period of analysis following completion of characterisation and with a strong component of interactivity with numerical modelling and experimental design, particularly towards the end of the characterisation. Defined needs and requirements decided the geometry of a new borehole.

Characterisation tools and methodology

Location and geometry of conductive features

The identification of hydraulic structures in the TRUE Block Scale rock volume has been made and corroborated with a number of different methods. The combined use of pressure responses due to drilling and drilling records provided important early information/confirmation of the existence and location of a given structure. Verification of conductors identified from pressure responses was achieved through the use of various flow logging techniques. The usage of the Posiva difference flow log

during the later parts of the characterisation work has enabled identification of discrete conductive fractures with a flow rate as low as 0.002 l/min and with a spatial resolution of 0.1 m. Association of a hydraulic flow anomaly with a geological feature was for the majority of identified conductors achieved using the BIPS borehole television log and the BIPS-based BOREMAP corelog. The correlation is straightforward for the major inflow points, which for the most part correlate with readily identifiable geological structures. These structures make up identified deterministic structures that appear in multiple boreholes.

Connectivity of identified conductive structures

The connectivity of identified structures was assessed through a series of different measurements performed at different times of the characterisation sequence. During the drilling of a borehole, pressure responses were used to obtain a first assessment of connectivity between boreholes. Indexed pressure responses in the form of so-called response matrices were identified as an efficient means to compile and visualise complex connectivity relationships. The transient behaviour of the responses collected during cross-hole interference tests in packed-off boreholes were used to identify families of responses which have been shown to correlate well with the identified principal families of structures/fracture networks. In the case of the responses in the TRUE Block Scale rock volume, two main groupings can be identified; the #13/#20/#21 (#22, #23) and the #5/#6/#7 (#24) systems, cf Figure EX-1.

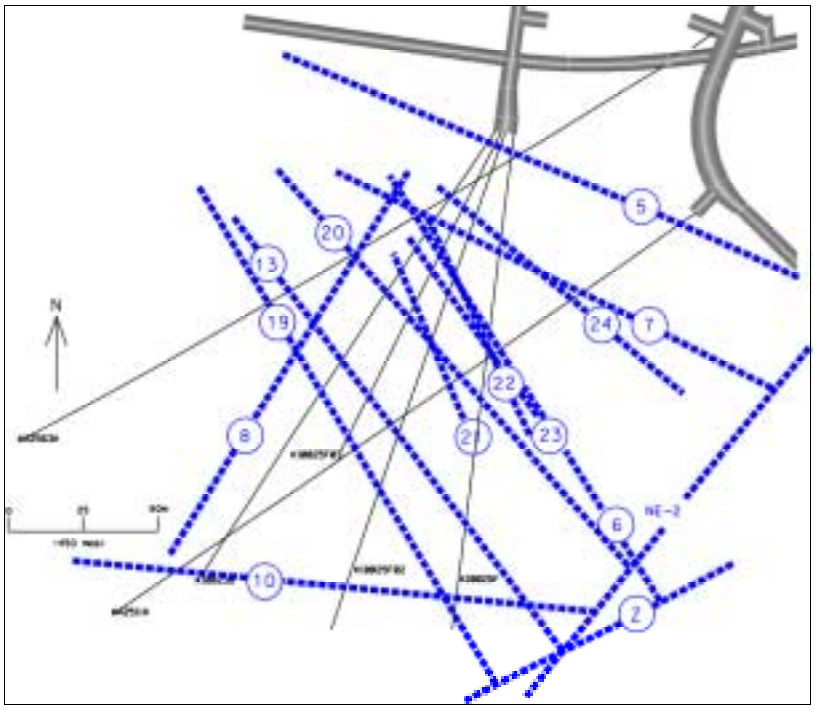

Figure EX-1. *Plan view of the Tracer Test Stage hydro-structural model with focus on the target volume of the block /Hermanson and Doe, 2000/.*

The majority of the identified structures are subvertical with steep dips (60–90 degrees). A subhorizontal fracture set can be identified, however, subhorizontal structures are regarded as subordinate conductors. The latter finding supported by observations in the neighbouring shafts.

Hydraulic tests

In the hydraulic characterisation of the TRUE Block Scale rock volume a selective approach was adopted. The selection of locations of more elaborate transient hydraulic tests was based on preceding flow logging in combination with the BIPS/BOREMAP logs. Towards the end of the characterisation programme, constant head flow and pressure build-up tests were integrated with short-term cross-hole interference tests in selected sections that enabled rapid establishment of packer positions in the new borehole. The established multi-packer borehole array was subsequently used for various types of cross-hole tests, including tracer dilution tests and tracer tests. By combining results from hydraulic interference tests with the corresponding tracer dilution tests it was possible to identify suitable sink and source sections for subsequent tracer tests.

Piezometer design

In the TRUE Block Scale Project two different piezometer (multi-packer system) designs were employed in 76-mm boreholes. The SKB/GEOSIGMA system, used in boreholes KA3510A, KI0025F and KI0025F02 is centred on a 20-mm central rod along which packers are positioned at selected intervals. An individual packer has 21 leadthroughs to facilitate circulation and pressure monitoring in up to seven sections and/or pressure monitoring in up to 21 sections. Circulation sections were equipped with dummy bodies to reduce the volume of the sections.

The ANDRA/Solexperts system installed in boreholes KI0023B and KI0025F02 consisted of up to 10 inflatable packers connected to a central tubing. All tubings and leadthroughs were led through the central tubing. All packers have individual inflation lines. All ten sections were equipped to facilitate circulation of fluids. No dummy materials in the test sections were required because the diameter of the central tubing is large in itself.

In the case of the early piezometers, KA2563A, KI0025F and KI0023B, the needs for re-instrumentation/optimisation was identified, and re-instrumentation was done repeatedly.

Building of hydro-structural models

Structural and geometrical aspects

The conductive geometry of the investigated rock block is made up of steeply dipping deterministic NW structures and NNW structures. High inflows and pressure responses in the boreholes were for the most part associated with geologically or geometrically identified conductors. Structures associated with more than one anomaly were in this context designated as deterministic structures in the hydro-structural model. The remainder of conductive fractures/structures, once the components of the deterministic structural model had been identified, were assigned to the background fracture population. It was identified that the first three boreholes (KA2563A, KI0025F and KI0023B) were required to develop the basic model of the network of major structures. The last two boreholes (KI0025F02 and KI0025F03) to a large extent confirmed and refined the model constructed on the basis of the first three boreholes. The fact that the hydro-structural model evolved substantially during the early phases of characterisation implied that that numerical scoping calculations and model assessments using complex 3D numerical models were not very useful and cost effective at that stage.

Hydraulic aspects

Low pressure responses in boreholes KI0025F02 and KI0025F03 suggested that Structure #13 is discontinuous, or possibly that some intercepts interpreted to be parts of Structure #13 are in fact associated with a different structure /Hermanson and Doe, 2000/. However, the interpreted discontinuity in Structure #13 based on pressure observation is disputed by tracer dilution responses in the test section in question /Andersson et al, 2000a/. An alternative cause for the noted lack of pressure response may be that some other water source acts as a reservoir and constant head boundary that reduces pressure responses to pumping in more distant observation sections. A possible candidate for such a reservoir is the fracture intersection zone (FIZ) formed by Structures #13 and #21 which is located close to intersections of Structure #13 in boreholes KI0025F02 and KI0025F03 where the low pressure responses occur. Additional support for the interpreted continuity of Structure #13 is provided by similar hydrogeochemistry associated with the interpreted intercepts.

Partial conclusions

- The principal experience from the characterisation and subsequent construction of a hydro-structural model is that it is difficult to decouple structural-geological and hydraulic data/elements in building the hydro-structural model,

- For the most part the hydraulic information and geological structural information are integrated simultaneously in the interpretation. However, at times a flow or head anomaly does not have a straightforward geological/geometrical interpretation, and a more thorough examination of the geological data is required,

- The main set of tools for determining the conductive geometry is combined borehole television (BIPS), flow logging (POSIVA difference flowmeter) and pressure responses from drilling/cross-hole interference tests,

- The major conducting structures and their extent between holes were determined. The basic hydro-structural model was established using information from the three first boreholes. No major changes to the model were required on the basis of the additional information acquired from the last two boreholes. However, additional detail i.a. in terms of improved understanding of the heterogeneity of some structures as well as new structures were interpreted towards the end of the characterisation. Difficulties remain with regards to the actual extent of interpreted deterministic structures outside the borehole array,

- In terms of hydraulic connectivity and hydraulic response characteristics the interpreted structures form two main groupings: the #20/#13-system and the #6/#7/#5-system, cf Figure EX-1, which are featured by distinct differences in response times and response characteristics,

- The developed hydro-structural model combined with the understanding of the hydraulic behaviour obtained from performed cross-hole and tracer dilution tests made it possible to identify a target area for well-controlled tracer experiments.

Conceptual flow model

The core of the TRUE Block Scale rock volume contains water types that range in salinity between 2000 and 6300 ppm Cl and are mainly mixed waters including Deep brine water and Baltic seawater. These water types may be coming from depth towards the underground openings along Structures #13 and #20.

The hydraulic head information showed an expected movement of water across the studied block towards the underground openings of the Äspö HRL. The gradient over the central part of the TRUE Block Scale rock volume was about 0.05 m/m which was in accord with what was deemed acceptable to achieve well-controlled tracer experiments. The gradient was observed to be steeper towards the underground openings. The head data were generally consistent within each structure.

The differences in hydraulic head as well as the chemical information indicated a hydraulic discontinuity between the core of the TRUE Block Scale rock volume and the overlying borehole KA2511A. Given the high level of connectivity between piezometer sections of KA2511A, this discontinuity may be a sub-horizontal conductor/lithological body that has not yet been penetrated by a borehole.

Ambient flow measurements from tracer dilution tests provided a useful complement to other available information on the flow field. The tracer test design had to consider these ambient flows carefully to avoid losing tracer in that the paths.

Transport parameters

A conceptual crossection of a typical conductive structure has been proposed, cf Figure EX-2. Transport parameters were presented for the wall rock of structures involved in the TRUE Block Scale tracer tests. Site-specific laboratory data were presented on the porosity and distribution of porosity of different geological members. Detailed mineralogical data were provided for all lithological members, including some results for fine-grained fault gouge. Given the kinship between the TRUE-1 site and the TRUE Block Scale site, sorption distribution coefficients and diffusivity of intact Äspö diorite and site-specific wall rock material from the TRUE–1 site experiments /Byegård et al, 1998/ have been imported for use in TRUE Block Scale. The main reason for using this approach was the similarities in lithology, structure orientation and water chemistry between the TRUE-1 and TRUE Block Scale sites.

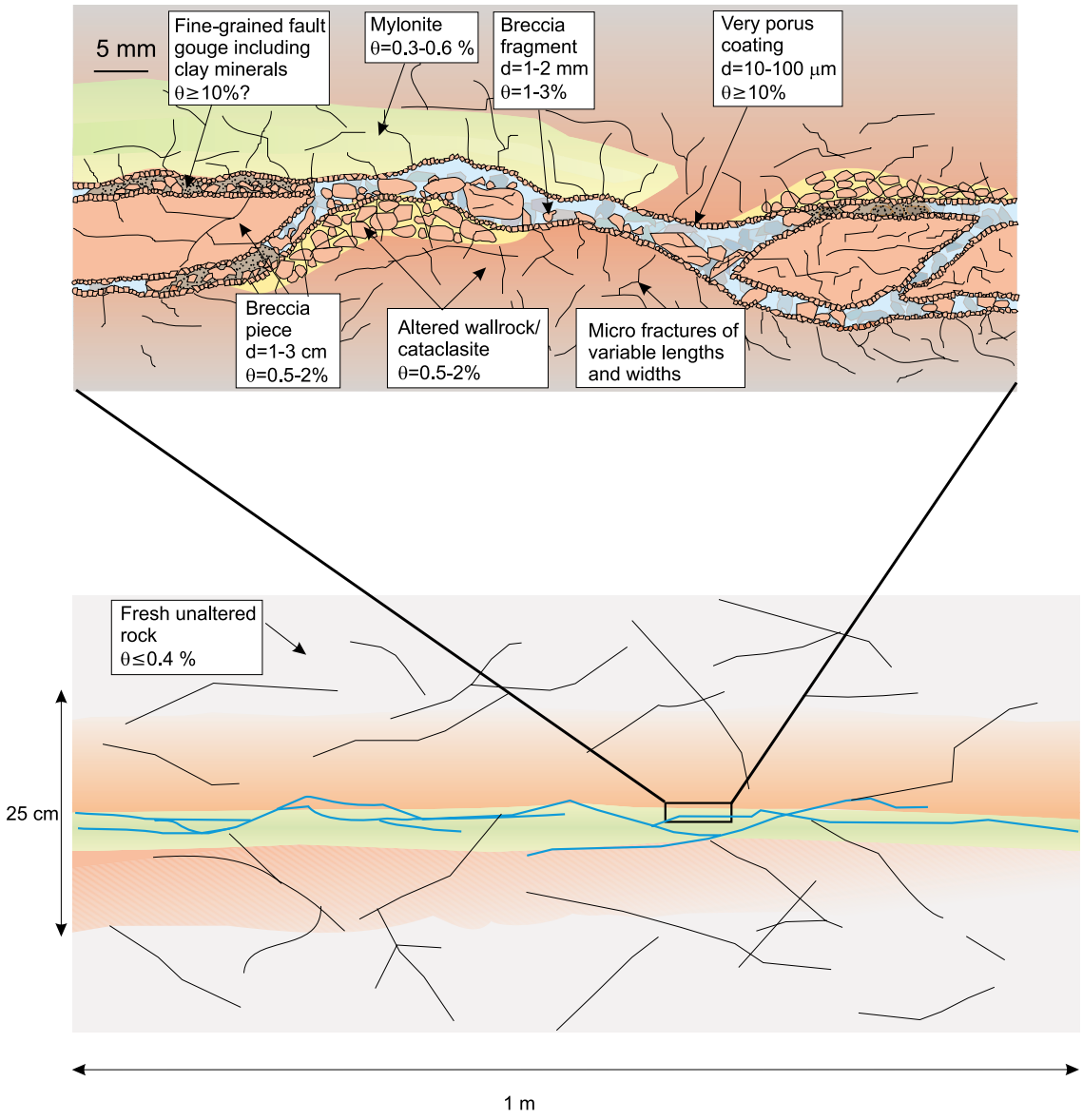

Figure EX-2. *Generalised conceptual model of a typical conductive structure involved in the tracer experiments.*

Elaborate mineralogical and geochemical studies were performed on material collected from structure intercepts of interest. In addition, fault breccia material has been analysed in the laboratory. Together with assessments of the cation exchange capacity, assessment of mineralogical distribution and site-specific hydrogeochemical data volumetric distributions coefficients K_d for the size fractions <0.125 mm and 0.125–2 mm were estimated. As an example the K_d values calculated for Cs for the <0.125 mm fraction was found to be significantly higher (K_d=0.093–0.28 m^3/kg) than that estimated for the 0.125–2 mm fraction (K_d=0.01 m^3/kg), which in turn was significantly higher than the measured value for intact Äspö diorite (K_d=0.0008 m^3/kg).

A comprehensive petrophysical programme was performed with the aim to assess the porosity and porosity distribution/texture related to relevant structure intercepts. Both conventional water saturation/water absorption techniques and impregnation techniques using ^{14}C-labelled PMMA /Hellmuth et al, 1999/ were employed. In this context, porosity determinations were performed also on 1–2 cm fault breccia pieces, and even on 1–2 mm fault breccia fragments from the investigated target structures. The results show average bulk porosities for the fault breccia pieces (about 0.4–0.8%) which are comparable to that of wall rock samples. The fault breccia fragments, however, show porosities varying between 1–3% (with highs >10%) /Kelokaski et al, 2001/, i.e. significantly higher than the corresponding altered wall rock.

What have we learned?

The characterisation of the TRUE Block Scale rock volume demonstrated the importance of monitoring all possible geological, hydraulic and hydrogeochemical entities and parameters during the development of the block scale experimental volume. The recording of pressure responses to drilling, combined with a record of the advancement of the drill bit proved to be an effective qualitative instrument in the construction/reconciliation of the hydro-structural model. In this context it is important in an underground research facility like Äspö HRL to keep a good record of any peripheral event which may affect the interpretation of the hydraulic and chemical situation in the investigated rock volume.

In order to obtain a useful basic model of the network of major structures, three boreholes were required (KA2563A, KI0025F, KI0023B) apart from the pre-existing KA2511A. The remaining two boreholes (KI0025F02 and KI0025F03) basically confirmed and refined the central part of the developed hydro-structural model. However, the latter two boreholes, and investigations involving them, refined the model and also added four additional structures and provided more information on i.a. heterogeneity within some of the interpreted deterministic structures.

Relatively simple and resource non-intensive characterisation tools were found to provide the basis for building a hydro-structural model satisfying the requirements for design, performance and evaluation of block scale tracer tests. A qualitative model was built from pressure responses to drilling and detailed flow logging. Careful correlation of flow logging results with borehole TV data allowed identification of the geological and structural characteristics of the conductive features. The detailed flow logging

results provided improved estimates of the statistics of transmissive fractures. Previous estimates, devoid of detailed flow logging, sufferred from an ambiguity in the determination of the frequency of conductive fractures. Quantification and further substantiation of the initial model was provided by transient single hole tests, crosshole interference tests and tracer dilution tests. Further support for the developed hydro-structural model and the experimental volume´s relation to other parts of the Äspö environment was provided by hydrogeochemical and isotope data.

Numerical modelling was originally regarded as a tool to help decision making in conjunction with all TRUE Block Scale hydro-structural model updates. It was found, however, that the effort of constructing elaborate discrete feature network models was not feasible during the early stages, because the hydro-structural models were not mature enough to justify usage complex and resource-intensive modelling approaches.

The TRUE Block Scale characterisation demonstrated the ability to build a hydro-structural model of a network of structures in the block scale (length scale of hundreds of meters). The model was subsequently verified using additional boreholes. The validity of the hydro-structural model, which should be regarded as a hypothesis in itself, will be subject to further testing as part of the evaluation of performed Phase C tracer tests. Of particular interest is the possible role of background fractures for transport in the investigated block scale rock volume.

Contents

1	**Introduction**	21
1.1	Background	21
1.2	Objectives	22
1.3	Introduction and overview	22
1.4	Previous experience of characterisation in the block scale	24
	1.4.1 Finnsjön	24
	1.4.2 El Berrocal	25
	1.4.3 Grimsel	25
	1.4.4 Kamaishi	26
	1.4.5 Stripa Mine (SCV)	28
	1.4.6 Whiteshell (URL)	29
	1.4.7 Äspö HRL	30
1.5	Rationale	31
	1.5.1 Performance assessment	31
	1.5.2 Site characterisation	31
	1.5.3 Modelling	31
	1.5.4 Transport and retention	32
1.6	Tested hypotheses	32
1.7	Outline of report series	33
1.8	Positioning and configuration of the experiment	34
	1.8.1 Positioning of experiment	34
	1.8.2 Definitions	35
1.9	Geological setting	36
	1.9.1 Lithology	36
	1.9.2 Deformation zones	39
	1.9.3 Small-scale features	40
	1.9.4 Hydraulic conductors and water-bearing fractures	40
2	**Overview of the site characterisation programme**	41
2.1	Experimental strategy and staging	41
	2.1.1 Scoping Stage	41
	2.1.2 Preliminary Characterisation Stage	42
	2.1.3 Detailed Characterisation Stage	42
	2.1.4 Tracer Test Stage	43
	2.1.5 Evaluation and Reporting Stage	43
2.2	Boreholes and installations	44
	2.2.1 Boreholes	44
	2.2.2 Installations	45
2.3	Methodology for developing hydro-structural model	50

3 Characterisation methods 53
3.1 Drilling 53
3.2 Borehole geophysics 53
3.2.1 Borehole radar with directional antenna 53
3.2.2 Borehole radar with high frequency antenna 55
3.2.3 Cross-hole seismic measurements 56
3.2.4 3D seismic measurements 56
3.2.5 Evaluation of geophysical methods used 59
3.3 Flow logging 59
3.3.1 Double packer flow logging 62
3.3.2 UCM (Ultrasonic Current Meter) flow logging 63
3.3.3 Posiva (DIFF) heat-pulse flow logging 64
3.3.4 Comparison and evaluation of flow logging methods 68
3.4 Core logging system – BIPS and BOREMAP 68
3.5 Drilling responses 71
3.6 Hydraulic tests 73
3.6.1 Purpose of hydraulic tests 73
3.6.2 Single-hole tests 73
3.6.3 Cross-hole hydraulic tests 77
3.7 Tracer dilution tests 81
3.8 Multiple-hole tracer tests 83
3.9 Porosity 84
3.10 Mineralogy 86
3.11 Geochemistry 87
3.12 Hydrogeochemistry 88
3.12.1 Sampling procedures 88
3.12.2 Analyses 88

4 Hydro-structural models 89
4.1 Location of the experiment to the –450 m level: The first structural model of the experimental volume 89
4.2 Scoping Stage: boreholes KA2563A and KA3510A 90
4.3 Preliminary Characterisation Stage: boreholes KI0025F and KI0023B 92
4.4 Detailed Characterisation Stage: borehole KI0025F02 95
4.5 Tracer Test Stage: borehole KI0025F03 96
4.6 Detailed geological description of the target structures 100
4.6.1 Structure #20 100
4.6.2 Structure #13 101
4.6.3 Structure #21 102
4.6.4 Hydraulic connectivity within Structures #13 and #21 103
4.6.5 Structure #22 105
4.6.6 Structure #23 105
4.6.7 Structure #24 106
4.7 Mineralogical and geochemical analyses 107
4.7.1 Lithology and mineralogy 107
4.7.2 Tectonisation and alteration 108
4.7.3 Characterisation of gouge materials 109
4.7.4 Stable isotopes 113
4.7.5 Uranium series analyses 115

4.8 Generalised detailed conceptual model of target structure 117
4.9 Hydraulic properties of the deterministic structures 119

5 Background fracturing 121
5.1 Fracture intensity 122
5.2 Fracture orientation 124
5.3 Transmissivity of fractures 125
5.4 Size distribution 127
5.5 Spatial pattern 127
5.5.1 Stationarity 127
5.5.2 Spacing and intensity distributions 128
5.5.3 Intensity distribution 130
5.6 Spatial model analysis 130
5.6.1 Fractal analysis 131
5.6.2 Geostatistical analysis 132
5.7 Summary of model of background fractures 133

6 Groundwater flow system 135
6.1 Introduction 135
6.2 Groundwater chemistry 136
6.2.1 General characteristics of Äspö groundwater chemistry 136
6.2.2 Variations in groundwater chemistry based on fluid resistivity logs 138
6.2.3 Results of groundwater geochemical sampling 138
6.3 Hydraulic head in the TRUE Block Scale volume 143
6.3.1 Analysis approach 144
6.3.2 Results 145
6.4 Background flow 147
6.5 Boundary conditions 151
6.5.1 Major bounding structures 151
6.5.2 Derivation of boundary conditions from site-scale models for the TRUE Block Scale rock volume 151

7 Retention characteristics 153
7.1 Overview 153
7.2 Porosity and density measurements 153
7.2.1 Introduction 153
7.2.2 Connected porosity from water saturation 155
7.2.3 Density distribution 157
7.2.4 Compact density measurements and total porosity 158
7.2.5 Porosity distribution – results from impregnations 160
7.2.6 Discussion and conclusion 163
7.3 Overview of data used to describe retention processes 165
7.4 Sorption coefficients for gouge material 166
7.4.1 Size fraction <0.125 mm 166
7.4.2 Size fraction 0.125–2 mm 170
7.5 Surface sorption coefficients 171
7.6 Diffusivities and sorption coefficients for the rock matrix 172

8 Recommended approach to block scale site characterisation 175
8.1 Overall premises and strategy 175
8.2 Identification of conductive structures 175
8.3 Assessment of fracture network connectivity 176
8.4 Use of borehole geophysics 176
8.5 Assessment of hydraulic material properties 177
8.6 Borehole piezometer design 178
8.7 Construction of hydro-structural models 179
8.8 Use of supporting hydrogeochemical data 180
8.9 Use of laboratory data 181

9 Discussion and conclusions 183
9.1 Characterisation tools and methodology 183
9.1.1 Location and geometry of conductive features 183
9.1.2 Connectivity of identified conductive structures 184
9.1.3 Hydraulic tests 185
9.1.4 Piezometer design 185
9.2 Building of hydro-structural models 186
9.2.1 Structural and geometrical aspects 186
9.2.2 Hydraulic aspects 187
9.2.3 Major conclusions 188
9.3 Conceptual flow model 188
9.4 Transport parameters 190
9.5 What have we learned? 190

10 Acknowledgement 192

11 References 193

Appendices 205

1 Introduction

1.1 Background

Concepts for deep geological disposal of spent nuclear fuel include multi-barrier systems for isolation of nuclear waste from the biosphere. Waste forms, and concepts for encapsulation of the waste and engineered barriers may vary between countries, but most concepts rely on a natural geological barrier which should provide a stable mechanical and chemical environment for the engineered barriers, and should also reduce and retard transport of radionuclides released from the engineered barriers. In case of an early canister damage, the retention capacity of the host rock for short-lived radionuclides such as Cs and Sr becomes important.

In planning the experiments to be performed during the Operating Phase of the Äspö Hard Rock Laboratory, the Swedish Nuclear Fuel and Waste management Company (SKB) identified the need for a better understanding of radionuclide transport and retention processes. The needs of performance assessment included improved confidence in models to be used for quantifying transport of sorbing radionuclides. It was also considered important from the performance assessment perspective to be able to show that adequate transport data and parameters (distribution coefficients, diffusivity, parameters similar to the "flow wetted surface area", etc) could be obtained from site characterisation, or field experiments, and that laboratory results could be related to retention parameters obtained in situ. To answer these needs, SKB in 1994 initiated a tracer test programme named the Tracer Retention Understanding Experiments (TRUE). The objectives of TRUE are given in Section 1.2.

The First Stage of TRUE /Winberg et al, 2000/ was performed in the detailed scale (0–10 m) and was focused on characterisation, experimentation and modelling of an interpreted single feature. Work performed included staged drilling of five boreholes, site characterisation, and installation of multi-packer systems to isolate interpreted hydraulic structures. Subsequent cross-hole hydraulic tests and a comprehensive series of tracer tests were used to plan a series of three tracer tests with radioactive sorbing tracers. The in situ tests were supported by a comprehensive laboratory programme performed on generic as well as on site-specific material from the studied interpreted feature. In addition techniques for characterisation of the pore space of the investigated flow paths using epoxy resin have been developed and successfully tested in situ.

The various phases of tracer tests performed as part of TRUE-1 were subject to blind model predictions and subsequent evaluation /Elert, 1999; Elert and Svensson, 2001/. The results of the TRUE-1 experiments showed clear evidence of diffusion, by some researchers attributed to diffusion into the rock matrix with associated sorption on inner surfaces. Other researchers claimed that the observed retention can be attributed to diffusion/sorption in gouge material. A distinction between the two alternative interpretations can only be achieved with a full implementation of the developed resin technology.

When the TRUE Programme was set up it was identified that the understanding of radionuclide transport and retention in the block scale (10–100 m) also required attention in terms of a separate experiment. This report is the first in a series of four reports and presents the results of the characterisation of the investigated TRUE Block Scale rock volume and the building of hydro-structural models.

1.2 Objectives

The overall objectives of the Tracer Retention Understanding Experiments (TRUE) are to:

- develop an understanding of radionuclide migration and retention in fractured rock,
- evaluate to what extent concepts used in models are based on realistic descriptions of a rock volume and if adequate data can be collected in site characterisation,
- evaluate the usefulness and feasibility of different approaches to model radionuclide migration and retention,
- provide in situ data on radionuclide migration and retention.

The specific objectives of the TRUE Block Scale Project given in the developed test plan /Winberg, 1997/ were to:

1. increase understanding of tracer transport in a fracture network and improve predictive capabilities,
2. assess the importance of tracer retention mechanisms (diffusion and sorption) in a fracture network,
3. assess the link between flow and transport data as a means for predicting transport phenomena.

1.3 Introduction and overview

The TRUE Block Scale project is an international partnership funded by ANDRA, ENRESA, Nirex, Posiva, PNC and SKB. The Block Scale project is one part of the Tracer Retention Understanding Experiments (TRUE) conducted at the Äspö Hard Rock Laboratory. The project which was initiated mid 1996 is divided into a series of consequtive stages /Winberg, 1997/;

- Scoping Stage.

- Preliminary Characterisation Stage /Winberg, 1999/.

- Detailed Characterisation Stage /Winberg, 2000/.
- Tracer Test Stage.
- Evaluation and Reporting Stage.

The staged approach also has an embedded iterative approach to characterisation and evaluation, cf Section 2.1, whereby the results of the characterisation of each drilled borehole have been used to plan the subsequent borehole. During the initial four stages of TRUE Block Scale, a total of 5 boreholes have been drilled and characterised as part of the project. Additional four boreholes have been completed as part of other adjacent projects and have been utilised as verification and monitoring boreholes. The principal characterisation tools used to establish the conductive geometry have been BIPS borehole imaging supported by logging with the Posiva difference flow meter and connectivity established from responses to drilling and performed crosshole interference tests. During the course of the project 6 versions of descriptive hydro-structural model have been developed.

At the conclusion of the Detailed Characterisation Stage in mid 1999, the feasibility of performing tracer tests in the identified network of structures in the block scale (10–100 m) had been firmly demonstrated /Winberg, 2000/. As a consequence a series of tests i.a. with radioactive sorbing tracers were performed as part of the Tracer Test Stage which has run from mid 1999 through 2000 /Andersson et al, 2001c/.

The respective updates of the hydro-structural model have been used to simulate, and in some cases perform blind predictions of, performed hydraulic and tracer tests /Winberg, 2000/. The analysis has been performed with various modelling approaches including Stochastic Continuum, Discrete Feature Network, Channel Network, the LaSAR approach /Cvetkovic et al, 2000/ and the so-called POSIVA approach /Hautojärvi and Taivassalo, 1994/.

In support of the in situ experimentation a series of laboratory investigations have been performed on geological material from the interpreted structures which make up the studied fracture network. The analyses performed include mineralogical and geochemical analyses, porosity determinations using water absorption and PMMA techniques, cf Chapters 3 and 7. In addition water samples collected during drilling and from packed off sections have been analysed for chemical composition and isotope content and used in support of the hydro-structural models, cf Chapter 6. Cation exchange capacity for fault breccia material from different intercepts, deduced from mineralogical composition, have been used in combination with ambient groundwater chemistry from the different test sections to estimate volumetric distribution coefficients (K_d), cf Chapter 7.

1.4 Previous experience of characterisation in the block scale

1.4.1 Finnsjön

Scale: Block Scale – Site Scale (500x1500x200 m)

At the Finnsjön test site, central eastern Sweden, a subhorizontal major fracture zone was investigated during 1984 through 1990. The objective of the study was to characterise the flow and transport properties of the zone and to localise potential pathways for groundwater flow and transport of solutes essential for the safety of a nuclear repository. At the site there are a number of gently dipping fracture zones (0–30 degrees) common to the foliated granodiorite at the site. Identification and characterisation of these fracture zones were accomplished through a broad range of geological, geophysical, geomechanical, geochemical and hydrological investigations.

Through these investigations, a gently dipping fracture zone, denoted Zone 2, was defined in an area of about 1500x500 m over a depth range of 100–300 m. The zone, which is about 100 m thick, was developed 1.7–1.6 Ga as a ductile shear zone at a depth of approximately 10–15 km, and repeated reactivation has occurred during Precambrian time and later /Ahlbom and Smellie, 1991/. The identified zone was selected for detailed studies aimed at understanding flow and transport in the zone, and its interactions with the surrounding bedrock. Hydraulic measurements on the zone included piezometry, single-hole hydraulic tests at different scales (section lengths), cross-hole interference tests, groundwater flow measurements, and tracer tests (converging and dipole flow fields). The tracer tests included both conservative and sorbing tracers.

It was found that the upper part of the zone is highly permeable with a transmissivity in excess of 10^{-3} m^2/s. The highly permeable sections have widths of about 0.5 m. This enhanced permeability as seen over a vast area was attributed to recent opening of the zone during the latest glaciation period. The performed cross-hole interference tests have shown that the identified highly conductive section is interconnected over distances of several hundred meters. Tracer experiments showed travel times differing by a factor 10 between 2 observation boreholes at approximately the same distance from an injection borehole. In situ measurements of natural groundwater flow showed that the flow was very high at the upper boundary of Zone 2, whereas near stagnant conditions prevailed at the lower boundary of the zone, and in the relict saline water body below the zone. The hydraulic head measurements as well as the groundwater chemistry suggested strongly that the low-angle Zone 2 acts as a hydraulic barrier, preventing groundwater from percolating downward through the zone. Subsequent modelling has shown that Zone 2 has a complicated structure, where transport occurs in a few well-defined pathways and that this observed heterogeneity must be an important component in transport models.

1.4.2 El Berrocal

Scale: Block Scale – Site scale (225x400x250 m)

The international El Berrocal project, located in an uranium deposit some 90 km SW of Madrid, Spain constituted an integrated exercise in geological, geochemical and hydrogeological characterisation with the ultimate aim to model and understand the past and present-day migration processes that control the behaviour and distribution of naturally occurring radionuclides in a granitic environment /Rivas et al, 1998/. The objectives were broadly focused on those particular processes which have relevance to safety assessments for geological repositories for radioactive waste /Guimerà et al, 1997/.

Performed studies included geological, structural, mineralogical, geochemical and hydrogeochemical studies at various scales. Tracer tests were performed at two sites involving a total of 5 boreholes /Guimerà et al, 1996/. Hydrogeological investigations were conducted as part of the planning of subsequent tracer tests and included hydraulic tests with double packer tests in 3 or 5 m section, piezometric investigations, and cross-hole interference tests performed to assess the hydraulic parameters of the rock between the two vertical wells. The interference tests were interpreted analytically under the assumption of a porous system and three different concepts; a conventional Theis approach (homogeneous), dual porosity and a recharge boundary. It was found that the dual porosity provided the best fit to the data, although due consideration of anisotropy had to be taken into account. The results were subsequently used to design tracer tests at the two sites. The field tracer programme included forced and non-forced injections in steady convergent flow fields. The programme also included tracer dilution tests, supporting laboratory tests and development of new downhole and injection/sampling equipment.

In subsequent modelling of the studied domain, it was found that a 3D model with embedded 2D structures, provided better model fits and a better predictive capability, and providing a good alternative for interpreting hydraulic tests in a geometrically complex environment. Cross-hole tests in this context provide the material properties of the 2D structures while single hole tests in the averagely fractured rock can be obtained from short time single hole tests.

It is concluded /Guimerà et al, 1997/ that reliable information has been obtained for a 10^6 m^3 volume of rock. Further, that the field and modelling methodologies developed are capable to face most of the requirements set by performance assessment of a geological repository.

1.4.3 Grimsel

At the Grimsel Test Site, central Switzerland, a fracture system flow test (BK) has been performed. The objective of this test /Liedke and Zuidema, 1988/ were to; 1) provide more information on transport of dissolved materials in fracture systems, 2) develop a technique for investigating fracture systems, and 3) develop and test equipment. The ultimate aim, 4) was to integrate the successive findings and developments into a

comprehensive strategy for site assessment. In total, some 10 boreholes were drilled in a fan-type array in which different types of hydraulic tests were conducted. The major conducting fractures and fracture zones were packed-off with multi-packer systems. In assessing solute transport, injections of brines were used. The background salinity of the Grimsel waters facilitates the use of brine and also enables use of borehole radar to map the evolving plume of migrating salt. The brine tracer tests performed in the BK site cover distances between 5 to 70m /Liedke et al, 1994/.

During Phase II and III of the Grimsel experiments, renewed attention has been given the BK site with comprehensive investigation programmes including fluid logging, hydraulic crosshole testing, combined salt/heat tracer tests and a project for integrating, visualising and modelling the site /Marschall and Vomvoris, 1995/. It has been identified that the most valuable information about the internal structure of the BK site stems from the fracture mapping of the drill cores and tunnel walls. The large number of boreholes drilled (N~20) provided a detailed description of boundaries, main fracture sets and their relevance for the flow system. However, the large number of boreholes was found to considerably disturb the flow conditions by short-circuiting hydraulic features. Not only did the overall connectivity increase, but also the hydraulic pressure distribution changed completely. As a result the NAGRA researchers strongly recommend to keep the number of boreholes down in future site characterisation, and to avoid preferential orientation of the boreholes, in order to avoid bias in inferred fracture orientations. Because of the strong element of short-circuiting, the long-term monitoring of pressure at the site did not fully meet expectations, and also affected performed hydraulic tests and tracers tests.

Despite the identified drawbacks and problem areas, the greatest benefit of the BK programme is found to be the development of equipment and methodologies for site characterisation. The most important data in building a conceptual hydrodynamic model of the BK site were the fluid logging and the hydraulic crosshole testing /Vomvoris and Frieg, 1992/, the challenge in their application to a fracture network and subsequent evaluation. Another interesting component in the Phase III research is the use of combined salt and heat tracer experiments. The use of combined flow fields and combined tracers were identified as means to obtain a better understanding of basic processes which govern flow and transport in fractured formations.

1.4.4 Kamaishi

Scale: Block Scale (approximately 80x80x20 m)

The Kamaishi mine, located on the north-eastern coast of the Honshu island, Japan, has been the setting for a comprehensive study on fluid flow and mass transport properties of fractured granite /Shimo et al, 1999/. The investigations have consisted of three major stages; 1) characterisation of the geometry and geology of the fracture system, 2) hydraulic characterisation of the fracture system and 3) tracer tests. The experimental area is located at a depth of about 350 m below surface. The geology is featured by metamorphic iron-bearing formations and intrusions of granodiorite. The test area is located in the latter rock type.

Initial characterisation, test design and definition of the testing program was largely driven by the discovery of a flow barrier in one of the boreholes drilled to investigate the boundary conditions. Minute measurements of pressure revealed a sudden increase in pressure from 200 kPa (20 m) to 2 MPa (200 m), indicating a barrier between the part of the fracture network being drained towards the mining works, and parts of the network with high pressure having poor connection to the underground openings. A strategy was developed which targeted the region featured by high groundwater pressure for tracer tests. This while the area could be reached by relatively short boreholes (<80 m) and since minor effects of the mine could be noted.

The experimental area was developed in an iterative fashion where the groundwater pressure in packed-off borehole sections were monitored during the drilling of each new borehole. A total of seven boreholes were drilled. After drilling, the new boreholes were flow-logged with a 1 m resolution and surveyed using borehole TV and core examination to identify the geological attributes associated with noted flow anomalies. More than 3000 fractures were mapped in the seven boreholes. The fractures identified as conductive showed an orange-coloured alteration halo, or mineral infillings of chlorite, calcite, stilbite and/or fine-grained dark green minerals. The highest degree of alteration was associated with the most fractured parts of the investigated volume /Sawada et al, 2000/.

The flow logging governed the positioning of the packers of the multi-packer system to be emplaced in each new borehole. Up to ten packers were used per borehole. The flow logging also provided estimates on transmissivity. A synthesis of performed pressure registrations indicated that the initial model with two regions with different pressure was too simplistic. At least six hydraulically isolated zones (compartments) were identified, characterised by similar static hydraulic head, and common response pattern to a given outer disturbance. The latter also included analysis of the transient response which showed distinct patterns between the compartments.

After completion a series of cross-hole pressure interference tests were run by withdrawing water from selected test sections. The test results confirmed the interpreted compartment geometry and provided additional information on hydraulic properties. Generalised flow dimension analysis provided information about the geometry of the conductive system and its properties. The diffusivity (T/S) was used to assess the connectivity of the studied fracture system.

Three of the fractures/zones identified in 2–5 boreholes were subsequently used for tracer tests in dipole configuration /Sawada et al, 2000/. A total of fifteen tests using NaCl as a tracer were performed in the three structures in dipole configuration with injection/withdrawal ratios varying between 1:1 to 1:8.

1.4.5 Stripa Mine (SCV)

Scale: >Block scale (150x150x150 m)

The Stripa mine has over a long period time, 1978 –1992, been a testing ground for development of techniques and methodologies for site characterisation for a geological repository. The Site Characterisation and Validation (SCV) Project was performed as a part of the OECD/NEA Stripa Project from 1986 to 1992. The objective of the project were to test the predictive capabilities of newly developed radar and seismic characterisation methods and numerical groundwater models /Olsson, 1992; NRC, 1996/. A basic experiment was designed to predict the distribution of water flow and tracer transport through a volume of granitic rock before and after excavation of a subhorizontal drift (the validation drift) and to compare these predictions with actual field measurements. A multidisciplinary characterisation programme was implemented from drifts and boreholes drilled from the drifts. The dimensions of the investigated volume is approximately 150x150x150 m.

Fractures in the drifts were mapped along scan lines and maps of the drift walls were produced at selected locations. Detailed maps were also made to study the variability in fracturing in fracture zones intersected by several drifts. All boreholes were mapped and oriented using TV logging. The fracture-mapping programme produced data on fracture orientations, trace lengths, mode of termination, and spacing. Cross-hole and single-hole radar measurements were conducted to determine the orientation and extent of fracture zones at the site. The directional antenna radar system developed for the project proved particularly useful while it provided data on the orientation of fracture zones based on measurements in a single borehole. Radar difference tomography was also used to show how saline tracer injected in a borehole became dispersed in the rock mass as it traversed three survey planes. Seismic techniques were used successfully to determine the orientation and extent of fracture zones. The physical properties of the rock in the vicinity of the boreholes were obtained using a comprehensive suite of geophysical borehole logs. It was identified that the sonic velocity, single point resistance and the normal resistivity were the most useful in identifying fractures and fracture zones.

A multi-packer probe was developed which allowed rapid testing of permeable features with a high spatial resolution. Single borehole tests were followed by cross-hole interference tests to define the properties of the fracture zones on the scale of the site (approximately 1000 m). The results of the hydraulic tests were used to check the hydraulic properties of the identified fracture zones obtained using geophysical techniques. The hydraulic programme also included monitoring of hydraulic head at 50 locations across the site. The latter measurements provided data on the hydraulic responses to various activities in the mine which could be used to characterise hydraulic connections across the site.

Characterisation of the SCV site was made in several stages. Initial data collection was followed by data interpretation and predictive modelling. Additional boreholes were then drilled to check the predictions based on the initial data set. These new data were then used to refine the conceptual model of the site and groundwater flow predictions. Finally, the predictions were checked by a series of dedicated experiments. In order to provide an adequate description of groundwater flow through the site, the identified

key issue for the characterisation work was to identify the important flow paths. An important element in this description is the possibility to distinguish fracture zones from the average fractured rock. In order to provide an objective measure for this distinction a binary representation based on a "fracture zone index" based on a principal component approach. The binary representation was subsequently used to construct a conceptual model of the site.

The final conceptual model of the SCV site was found to be consistent with field and test data. Major hydraulic responses were confined to the identified fracture zones, and there were few anomalies in the data that could not be explained. Between 80–90% of the flow was interpreted to occur through the identified fracture zones, as evidenced by single-hole and cross-hole hydraulic tests. Flow in fractured rock was dominated by a small fraction of the identified features. Flow in the fracture zones was concentrated in one or two fractures in the zones, and the transmissivity distribution in these fractures was found to be heterogeneous. The transmissivity of the fracture zones varied one to two orders of magnitude over a metre distance. Of the fractures in the averagely fractured rock, only a few were found to be transmissive. The staged approach employed, where data collection was followed by blind predictions and subsequent validation in several cycles, was found to be very useful.

1.4.6 Whiteshell (URL)

Scale: approximately 50x50x50 m

The Moderately Fractured Rock (MFR) Experiment /Frost et al, 1998; Jensen, 2001/ was initiated in 1993 at the Canadian Underground Research Laboratory (URL), Manitoba, with the intention to increase the knowledge of mass transport through fractured crystalline rock. The experiment is a multi-disciplinary undertaking involving the characterisation and numerical simulation of groundwater flow and mass transport in an approximately 100,000 m^3 volume of MFR located on the 240 metre Level of the URL. The primary objective of the experiment is to explore the validity of the Equivalent Porous Medium (EPM) approximation for simulation of mass transport through an interconnected fracture network. Experimental activities also intend to examine issues of relevance to geosphere Performance Assessment (PA) in the context of the characterisation and description of flow domain spatial variability, parameter scale dependence, and derivation of effective mass transport properties for abstracted PA model simulations.

The initial phase of the MFR experiment, which involved the characterisation and development of a conceptual flow model for the MFR domain, was completed in 1998. Characterisation activities included litho-structural mapping, fracture infilling mineralogy identification, hydrogeochemical sampling, cross-hole geophysical surveys, single and cross-bore hydraulic testing and hydraulic head monitoring within a array of ten sub-horizontal boreholes. An internally consistent conceptual flow model derived from these data provided a basis for a deterministic numerical realisation of ground-water flow using the 3-dimensional finite element code MOTIF. Calibration of this MFR mathematical model was achieved through comparison with inter-well hydraulic interference test results.

Phase II of the MFR experiment is underway including a sequence of tracer experiments at scales of 10 to 50 metres. As part of the experimental procedure, predictive pre-test estimates of tracer breakthrough are obtained using MOTIF for a given injection-withdrawal well geometry. Recently, modelling has incorporated the use of geostatistical techniques to explore the influence of permeability field variability on mass transport.

An additional series of tracer experiments will focus on understanding of the governing mass transport processes and mechanisms that, in part, will aid prioritisation of geoscience research activities and a re-examination of PA modelling strategies.

1.4.7 Äspö HRL

Scale: 50x50x50 m

Experiments where block scale sized rock volumes have been characterised at the Äspö HRL include the TRUE-1 rock block /Winberg, 1996; Winberg et al, 2000/.

Specific objectives of TRUE-1 were to investigate an experimental site with non-sorbing (conservative) and sorbing tracers in a simple test geometry. Further to show that available tracer test technology could be transferred to ambient Äspö HRL conditions, featured by high hydraulic pressure and high salinity of the groundwater at approximately 400 m depth. Secondary objectives included development and testing of methods for assessing the pore space of the investigated fracture system using injection of epoxy resin, followed by excavation and analysis. Although the TRUE-1 experiment was focused on a single fracture, effectively a rock block of 50x50x50 m was investigated as part of the selection of a suitable target feature. Many of the techniques and methodologies which have been employed in the TRUE Block Scale Project were inaugurated or tested in TRUE-1. The BIPS borehole TV technique was tested in an operating mode at Äspö HRL for the first time in TRUE-1. The POSIVA flow log was not tested, but a single packer flow log with a 0.5 m resolution was employed to correlate geological and hydraulic features in the boreholes. Unlike in TRUE Block Scale, the four experimental boreholes, KXTT1 to KXTT4, were drilled in close succession. Using a preliminary simplistic multi-packer assembly in each preceding borehole, it was possible to build a preliminary hydro-structural model. This model was subsequently refined using the BIPS and flow logging results in combination with crosshole interference responses obtained from the multi-packer installations in the boreholes.

The hydro-structural model developed by the project team /Winberg, 1996; Winberg et al, 2000/ is made up of four labelled features, Features A, B, C and D, of which Feature A was the focus for the subsequent dedicated experimentation. These features were bounded by four more prominent structures; Zones NNW-4, NW-2, NW-3 and NW-2'. The latter structures are interpreted to be in hydraulic contact with Feature A, as indicated by groundwater chemistry, hydraulic head and hydraulic responses. Features B and D are interpreted to be hydraulic features which are made up of a number of interconnected fractures. It should in this context be mentioned that alternative hydro-structural models, featuring a more intensely fractured bedrock have been developed by i.a. /Bossart et al, 2001/.

1.5 Rationale

1.5.1 Performance assessment

The block scale is important since it corresponds to the distance, "security distance" as defined by various national programs, between the periphery of a geological repository and the nearest major fracture zone. It is also assumed that the bulk of the retention provided by the natural bedrock barrier is provided in this region.

As a consequence, the block scale is also an important modelling issue, cf Section 1.5.3. Prioritised aspects are to understand the nature of transport paths in the block scale and the geological controls on retention, and to assess the flow wetted surface, or equitable entities, on the scale in question.

1.5.2 Site characterisation

The block scale is also important from a characterisation perspective. Firstly, to provide the necessary data from which the geometrical, conceptual and numerical models are built, which are used to assess a given site. In addition, the data collected in the block scale, whether obtained from the surface or from underground openings, are important for the detailed layout and design of a repository. This applies both to the positioning of storage tunnels and possible canister boreholes.

An experiment in the block scale hence provides a training ground for developing tools and methodologies to be employed in future site characterisation for a geological repository.

1.5.3 Modelling

The block scale (10–100 m) is an important scale in that it probably is the smallest scale at which the stochastic continuum approach can be used with good results for predicting flow and transport phenomena. At smaller scales, and possibly with a need to include higher degrees of complexity, discrete approaches are most likely the only alternative.

At the same time, the block scale constitutes a challenge for the more performance assessment related approaches. Despite the simplification of the natural system, are the model results adequate. Do they provide adequate descriptions of flow and transport, and are they not overly conservative?

One of the basic ideas embedded in the TRUE Programme is that experimentation at various scales, laboratory (<0.5 m), detailed scale (<10 m) and block scale (10–100 m) will provide a basis for improved understanding on how to model flow and transport and how to link transport models and transport parameters at different scales. It is expected that through this platform the uncertainties associated with extrapolation and prediction on a site scale (0.1–1 km) will be reduced. The TRUE Block Scale experiment here constitutes the higher end member of the studied experimental scales.

1.5.4 Transport and retention

The principal differences between the performed TRUE-1 experiments and TRUE Block Scale is obviously the difference in spatial scale. Of principal interest is whether the longer transport distances in themselves, through exposure to larger surface areas, will provide a higher degree of heterogeneity, and more retention.

In addition, the performance of tracer tests in a network of structures imply that flow paths/transport routes to a variable degree will be affected by the fracture intersection zones (FIZ) which connect intersecting structures. Although TRUE Block Scale does not provide an array with the specific aim to investigate FIZs, the results form the performed experiments may still provide indirect evidence of the possible effects of FIZs.

The results from the TRUE-1 experiments /Winberg et al, 2000/ showed a consistent relative order amongst the utilised radioactive sorbing tracers (in order from lowest sorptivity); $^{22}Na^{+} < {}^{47}Ca^{2+} \approx {}^{85}Sr^{2+} << {}^{86}Rb^{+} \approx {}^{133}Ba^{2+} < {}^{137}Cs^{+}$. This relative order was observed both in the laboratory and in situ. An interesting question for extrapolation to larger scales is whether this relative order is robust. Another result from TRUE-1 was that the retention obtained in the in situ tests was stronger than predicted based on laboratory data. The reasons for this are not fully clear but have been attributed to a) enhanced retention in an altered rim zone adjacent to the fractures, b) existence of porous gouge material, or c) three-dimensional flow field (larger flow wetted surface area).

Explicit evidence of existence of gouge material (fault breccia/fault gouge) was not found in the investigated Feature A at the TRUE-1 site /Winberg et al, 2000/, possibly due to poor core recovery. Performed modelling within the Äspö Task Force indicates that fine-grained fault gouge material could be responsible for the observed retention. In the network of structures investigated as part of TRUE Block Scale, however, there is a firm evidence for existence of fault breccia cf Section 4.7 and 7.2. Performed laboratory analyses, with all due respect to uncertainties about the distribution of gouge material, is expected to provide a means for assessing the contribution to retention from the rock matrix and gouge material, respectively.

1.6 Tested hypotheses

Three basic questions have been posed in relation to the performed tracer tests, their planning and evaluation tests /Winberg, 2000/. These are:

Q1) "What is the conductive geometry of the defined target volume for tracer tests within the TRUE Block Scale rock volume? Does the most recent structural model reflect this geometry with sufficient accuracy to allow design and interpretation of the planned tracer tests?"

Q2) "What are the properties of fractures and fracture zones that control transport in fracture networks?"

Q3) "Is there a discriminating difference between breakthrough of sorbing tracers in a detailed scale single fracture, as opposed to that observed in a fracture network in the block scale?"

On the basis of these questions corresponding hypotheses have been formulated /Winberg, 2000/, to be addressed by the tracer tests and the subsequent evaluation;

H1) "The major conducting structures of the target volume for tracer tests in the TRUE Block Scale rock volume trend north-west and are subvertical. Being subvertical, and subparallel, they do not form a conductive network in the designated target volume. For the purpose of testing fracture network flow and transport effects in the current borehole array, second-order NNW features are required to provide the necessary connectivity between the major conducting NW structures!"

H2a) "Fracture intersections have distinctive properties and have a measurable influence on transport in fracture/feature networks. These distinctive properties may make the intersection a preferential conductor, a barrier, or a combination of both!"

H2b) "In-plane heterogeneity and anisotropy have a measurable influence on transport of solutes in a block scale fracture network!"

H3) "It is not possible to discriminate between breakthrough curves of sorbing tracers in a single fracture from those obtained in a network of fractures!"

1.7 Outline of report series

The series of final report include the following four parts;

1. Characterisation and model development (this report).
2. Tracer tests /Andersson et al, 2002/.
3. Modelling of flow and transport /Poteri et al, 2002/.
4. Synthesis of flow, transport and retention in the block scale /Winberg et al, 2002/.

1.8 Positioning and configuration of the experiment

1.8.1 Positioning of experiment

A restriction in selecting a block for TRUE Block Scale was the overall usage of the experimental level of the Äspö HRL, cf Figure 1-1. The north-eastern part of the laboratory was allocated for the REX and TRUE-1 experiments. At the time of locating TRUE Block Scale, the eastern part of the tunnel spiral at the experimental level and south of the TBM assembly hall was used by the ZEDEX experiment, the Demonstration Repository facility and by the Long-Term Tests on Buffer materials. The area inside the tunnel spiral and north of the TBM was not used by any experiment. However, previous analysis had shown that the inner part of the laboratory show a high degree of hydraulic connectivity /Winberg et al, 1996/. In the western part of the laboratory the Chemlab experiment was in progress in borehole KA2512A. The latter experiment is sensitive to changes in the chemical composition of the groundwater, but does not create any hydraulic disturbances. The final part of the TBM tunnel was allocated for the development of the Prototype Repository project.

A set of desired experimental conditions were defined to be used in positioning the TRUE Block Scale experiment /Winberg, 1997/;

- Location outside tunnel spiral.
- Size of experimental block ~ 100x100x100 m.
- Location away from major fracture zones (i.e. EW-1 and NE-1).
- Access from multiple locations (vertically) in the laboratory.
- No adverse hydraulic interference from other activities in the laboratory.
- Transmissivity range of fractures making up the studied fracture network in the range; $T = 5 \cdot 10^{-8} – 5 \cdot 10^{-7}$ m^2/s.
- Small gradient ($I < 0.05$).
- Flow velocities such that diffusion can be made a measurable process.

The hydro-structural model of the experimental level available in mid 1996, cf Section 4.1, featured major northeasterly trending fracture zones delimiting the experimental level, where zones EW-1 and NE-1 and zones NNW-4 and NE-2 effectively bound the spiral tunnel. A number of possible minor fracture zones trending east-west to northwest, generally with steep to vertical dip, were also interpreted within the tunnel spiral.

Analysis of pressure responses in packed-off boreholes due to hydraulic events /Hermanson et al, 1996/ indicated that the western and southwestern parts of the experimental area is well connected to the central parts, but also that the highly conductive zone NNW-4 acts as a strong moderator to conveyance of pressure

perturbations between the eastern and western parts of the experimental level of Äspö HRL. On the basis of these inferences, the southwestern part of the experimental level was put forward as the most favourable location. The main reasons for this recommendation were;

1. Location of the TRUE Block Scale experiment in the southwestern part is not likely to create mutual disturbances between the TRUE Block Scale and the TRUE-1 and REX experiments.

2. A block positioned in the southwestern part can be readily accessed from two levels, from the experimental level (TBM part) and the access spiral tunnel some 150 m above.

3. A location in the southwestern part facilitates positioning outside the spiral tunnel thus avoiding complex hydraulic boundary conditions.

1.8.2 Definitions

The TRUE Block Scale site is located in the southwestern part of the experimental level at the Äspö HRL, cf Figure 1-1. The area covered by the developed borehole array is denoted "TRUE Block Scale rock volume" and has a lateral extent of 250x200 m, cf Figure 1-1, and extends between –500 masl to –350 masl in the vertical direction. The area containing the fracture network used in the tracer tests is about 100x100x50 m and is denoted the "TRUE Block Scale Tracer Test volume (TTV)", cf Figure 1-1.

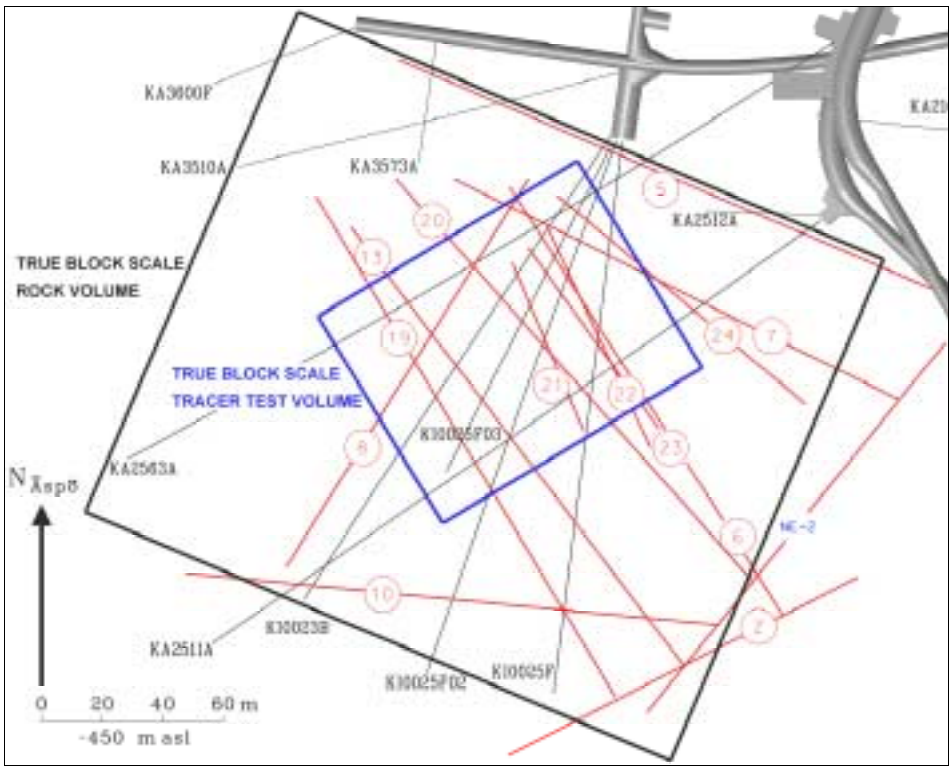

Figure 1-1. *Location of the TRUE Block Scale experiment and defined rock volumes.*

1.9 Geological setting

The regional setting of Äspö (Figure 1-2) has been established from an interpretation of geological field investigations and geophysical survey data, on a 25x25 kilometre scale. The Äspö region is characterised by granitoids belonging to the Transscandinavian Igneous Belt (TIB). The presence of some E-W elongated massifs of basic rocks have been inferred by positive magnetic and gravity anomalies /Gustafson et al, 1988/.

Information from all geophysical and geological investigations corroborates a tectonic picture dominated by one almost orthogonal system of 1st order lineaments trending N-S and E-W and extending in the order of 20–50 kilometres. The N-S zones most probably have vertical-subvertical dips and seem to be of a tensional character. The zones trending E-W are mostly vertical or moderately dipping to the north or south.

Besides the 1st order of E-W and N-S lineaments, there are also 2nd order zones trending NW and NE and forming another almost orthogonal system. The 2nd order zones are mostly in the order of 100 and 200 m wide and extend 1 to 20 km. The most prominent of the ENE trending zones, crossing the island of Äspö, is indicated by mylonites in some outcrops.

According to a general interpretation of the relative sequence of deformation most of the zones trending NE and NW are older than the N-S and E-W fracture zones, and most of the structures trending N-S are probably younger than the ones trending E-W /Munier, 1995/.

The 3rd order zones of lineaments, trending NNW and NNE, are interpreted as a conjugate shear set to a tensional fracture zone trending NS /Wikberg et al, 1991/.

1.9.1 Lithology

The dominant rocks on the Äspö island are TIB granitoids ranging in mineralogical composition from true granites (Ävrö granite) to granodioritic to quartz monzodioritic composition (Äspö diorites) /Kornfält and Wikman, 1988/. These granitoids were probably formed by continuous magma-mixing process as indicated by the presence of basic enclaves /Wikström, 1989/ and rather large irregular bodies of diorite/gabbroic rocks have been located in boreholes at great depth in the site area /Wikberg et al, 1991/. Some circular/semicircular structures in the area investigated are interpreted as granite diapirs. Fine-grained alkali granites are present as lenses and dikes intruding/ cutting the TIB-granitoids but most of the fine-grained granites have similar ages to these granitoids (c 1800 Ma) /Wikman and Kornfält, 1995/. Some others show, however, distinct contacts and may be associated with the c 1400 Ma anorogenic Götemar granite, which crops out 2 km north of Äspö /Åberg et al, 1984/. Across the island, there are a number of outcrops with greyish black, fine-grained basic rocks with a basaltic composition. They are very strongly altered and called greenstone and only constitute minor parts of the Äspö rock mass. Most of these metavolcanic rocks seem to be older than the Småland granite, based on the fact that they form sheets and xenoliths in the granitoid /Wikman and Kornfält, 1995/.

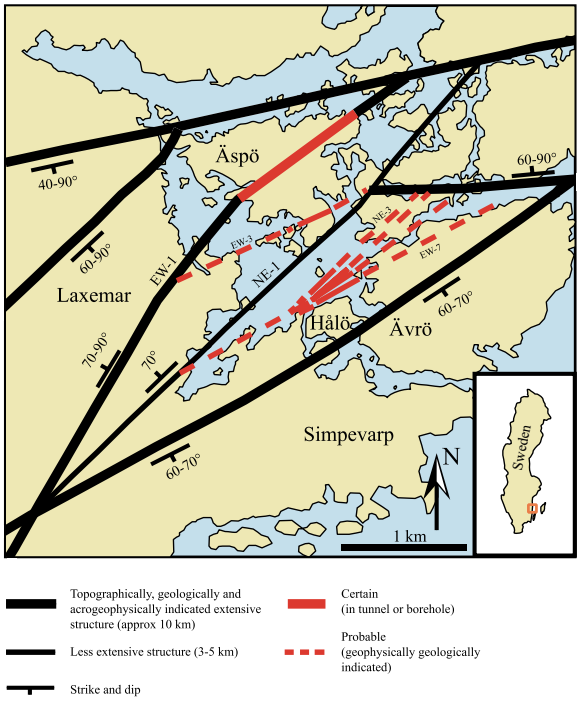

Figure 1-2. *The regional structural pattern over the Äspö Island in south eastern Sweden /from Rhén et al, 1997a/.*

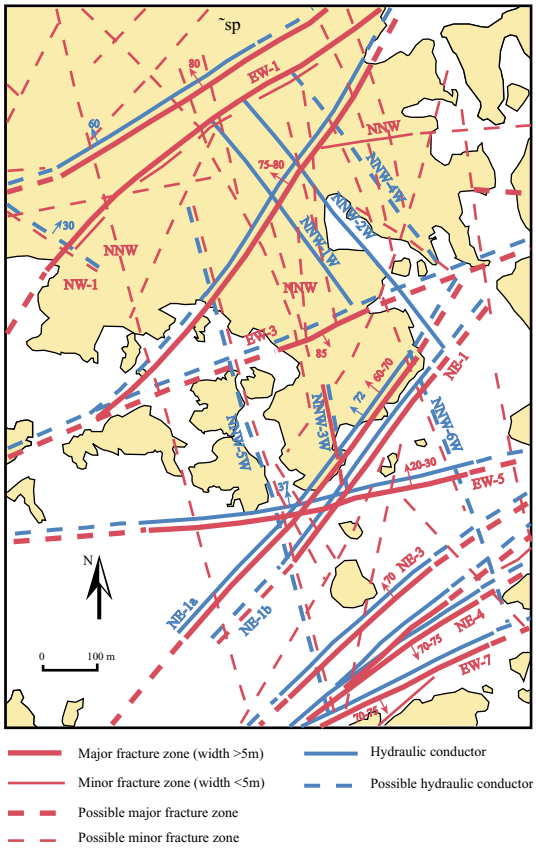

Figure 1-3. *Local structural pattern over the Äspö Island after /Rhén et al, 1997a/.*

The four main rock types that make up most of the rock mass in the Äspö area are described according to /Wikman and Kornfält, 1995/:

- The Äspö diorite is by far the most common group within the Äspö area. The typical facies is grey to reddish grey, medium-grained, with more or less scattered, large crystals of K-feldspars. Regarding the mineralogy (46% plagioclase, 15% quartz, 15% biotite, 12% K-feldspar), the rocks are typically granodiorites, quartz monzodiorites and quartz monzonites. Their age has been estimated to 1804 ± 3 M year old.

- The Småland (Ävrö) granite is brighter than the diorite, and presents a more reddish colour than Äspö diorites. This is partly due to more sparsely distributed phenocrysts of K-feldspars, and to a higher content of quartz and lower content of plagioclase. Macroscopically, the unaltered Småland (Ävrö) granite is medium to coarse-grained and somewhat porphyritic with a generally massive texture. The Ävrö granite is younger than the diorite, but the difference of age is assumed to be very small. Given linear relationships observed between titanium dioxides and zirconium content, these two rocks can be regarded as two varieties of the Småland granite of which the Ävrö granite is more evolved.

- The fine-grained granite occurs rather frequently, both on the surface of the Äspö island and its surroundings, as well as in the tunnel. It usually occurs as dikes and irregular veins, or even sheets, but the character is not so clear because of strong deformation, which has obscured contacts. The dykes usually vary in width between 0,1m and up to 5 metres, and are generally oriented NE-SW. The brittle deformation has caused a joint pattern in the fine-grained granites, often characterised by many short joints lying closely together. The most reliable dating test gave an age of 1794±16M years.

- The greenstones – fine-grained and medium to coarse-grained greenstone (diorites to grabbros) – are easily distinguished from the granitoid rocks by their very dark, greenish or greyish colour. As a rule they occur as minor inclusions or irregular, often elongated bodies within the granitoids and dioritoids following the common E-W foliation trend within the area. Except for smallest inclusions, the greenstones are often intensely penetrated by fine-grained, granitic material. These mafic rocks are assumed to be of volcanic origin and are always strongly altered.

The distribution of the four main rock types at different depths is quite similar, except for the first 100-meters where the Småland (Ävrö) granite occurs more frequently than the Äspö diorite.

1.9.2 Deformation zones

An almost vertical, penetrating foliation trending NE-ENE is the most dominant structural element in the 1800 Ma old Äspö granitoids and seems to be the oldest sign of the ductile deformation related to the subhorizontal NNW-SSE compression.

Intensified strain formed in the epidote-amphibolite facies is marked by gneissic zones trending NE-ENE, dipping to the NNW. Between 1700–1400 Ma, these old gneissic zones were reactivated as mylonitic shear-zones trending NE in a ductile/semiductile deformation phase. Strong foliation and mylonites trending E-W and dipping steeply to the north are common in the Äspö shear zone.

The first brittle faults probably developed in the region in response to the emplacement of younger granites. These faults and other ductile zones were reactivated several times. The rock mass became increasingly brittle as it was uplifted and exposed about 1000 Ma ago. Parts of the epidotic vein system were reactivated during this period and filled with calcite, chlorite, zeolites and fluorite /Munier, 1995/. Later, several km thick piles of Upper Palaeozoic molasse sediments related to the Caledonian orogeny covered the area and according to fission track data on titanites from the deep KLX02 borehole a thick sedimentary cover existed in the area 900–700 Ma ago /Tullborg et al, 1996/.

The Äspö HRL fracture zone pattern fits in a framework of major regional structures. Outcrop mapping on the island determined that most of the fracture zones on Äspö mainly strike E-W as well as coincide with the mylonite zones, also called Äspö shear zone EW-1, trending NE, which is the only extended regional fracture zone running across Äspö island, cf Figure 1-2. This prominent feature consists of at least two tabular segments that dip about 80°NNW to SSE and extends up to a width of 100 metres /Munier, 1995/. Local development of mylonites and epidote-rich shear zones along EW-1 controlled the orientation of later brittle deformation in the form of increasing fracturing and brecciation /Rhén et al, 1997b/. According to the fracture geometry and strike, the Äspö island is divided in two structural blocks, the north that appears to be more homogeneous, and the south block dominated by local fracture zones oriented N55°W (Figure 1-3).

The fracture distribution and density is related to the lithology, which has a bearing on the fault structure. The fault geometry is similar in the Äspö diorite and the Ävrö granite, and contacts are not preferentially reactivated by faults. In contrast, the fracture pattern is substantially different in the fine-grained granite in that the numbers of subparallel master faults as well as the density of fractures are an estimated factor 5–10 higher when compared with the other lithologies. Furthermore fractures in the fine-grained granite are usually poor in clay minerals, which implies that they have little ability for self-sealing, instead they are often water conducting. Greeenstones host a larger number of (small to intermediate) fracture zones than the other rock types according to /Munier, 1995/.

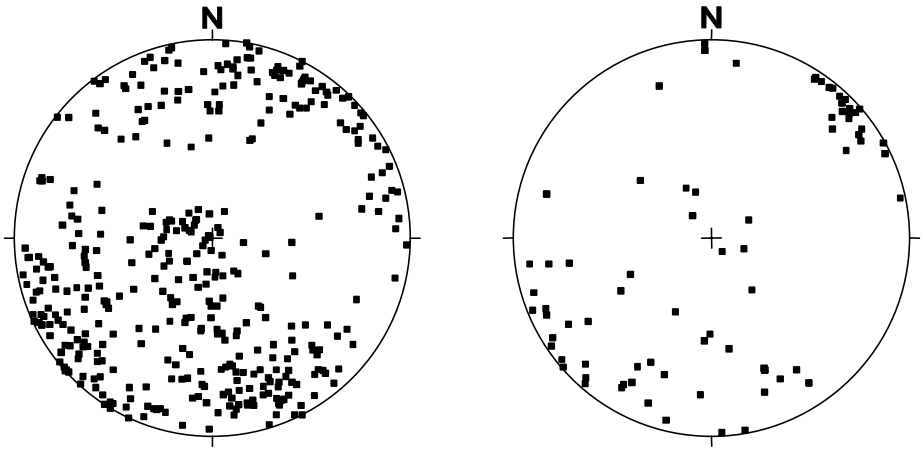

Figure 1-4. *Main fracture orientations shown as poles to fracture planes in a lower hemisphere equal area plot, examples from the TRUE Block Scale boreholes KI0025F02 (L=204.2 m) and KI0025F03 (L=147.2 m), respectively.*

1.9.3 Small-scale features

The main fracture sets coincide with the most conspicuous lineament directions (valleys) in the region. Combined data from fracture outcrops /Rhén et al, 1997a/ and tunnel mapping /Munier, 1995/ show the characteristic pattern of small-scale fractures at the scale of the Äspö Island. They mostly occur in a complex pattern of four predominant clusters (Figure 1-4) three are steeply dipping fracture sets and strike NS-NE, NNW and WNW. The fourth is a subhorizontal set trending E-W. The fracture sets are essentially similar within different rock types but differ in intensity with the highest intensity in the fine-grained Granites.

1.9.4 Hydraulic conductors and water-bearing fractures

Single hydraulic conductors are found both in Ävrö granite but also to a smaller extent in fine-grained granite /Munier, 1995; Rhén et al, 1997a; Mazurek et al, 1995/. However, given the irregular geometry it appears unlikely that the fine-grained granite alone can provide interconnected large-scale flow paths /Mazurek et al, 1995/.

Fractures containing water are assumed to relate to the latest rock fragmentation or fracture reactivation. The pattern of hydraulically active fractures (inferred in tunnel) consists of a single, steep set that strikes WNW. Less numerous but presumably equally important are steep fractures with NNW strikes. The dominant set of conductive fractures parallel the in situ axis of maximum compressive stress which is horizontal trends approximately 300°.

2 Overview of the site characterisation programme

2.1 Experimental strategy and staging

The TRUE Block Scale Project adopted a staged approach. The key element desired in the experimental strategy was expressed as; "Iterative characterisation with strong interaction between modelling and experimental work to ensure flexibility". This implies that site characterisation data from each new borehole should be used to update the hydro-structural model of the investigated block, whereby a successive refinement is obtained which is employed in the design, predictive modelling, performance and evaluation of block scale experiments. In the following, brief outlines are provided of the performed experimental stages and associated characterisation.

2.1.1 Scoping Stage

The "Scoping Stage" was intended to determine whether the identified experimental site fulfil the basic requirements stated in Section 1.8. The following specific objectives were defined;

- Assess whether the pre-allocated experimental volume meets the desired experimental conditions.
- Assess and suggest suitable spatial and temporal scales for tracer experiments.
- Assess under what conditions tracer tests using sorbing tracers can be performed.
- Recommend a preferred experimental approach.
- Propose necessary adaptation of down-hole equipment.
- Collect site-specific data from pilot boreholes.
- Update the descriptive model of the selected block scale rock volume.

One of the critical elements of the performed characterisation was that the drilling of the pilot borehole KA2563A (and KA3510A), cf Figure 2-1, was associated with difficulties involving high water inflows (KA2563A) and unsuccessful anchoring of the casing (KA3510A). This required use of cement grout at a number of locations to continue and finalise the drilling. In total, 2150 kg of grout was injected between L=89–156 m in KA2563A. Similarly in KA3510A a total of 1700 kg cement was injected between 2–47 m. The effects of the grouting campaign were discussed and assessed at a workshop in Stockholm, Oct 16–17 1996, where it was concluded that it

was possible to avoid the grouted portions and that there were no reasons to abandon the selected site.

Apart from the basic single hole characterisation, a cross-hole seismic investigation employing KA2511A and KA2563A was carried out.

The Scoping Stage was followed by a technical review meeting in October 1997 and a decision was subsequently taken to proceed in accordance with the test plan. The developed hydro-structural model is presented and discussed in Section 4.2.

2.1.2 Preliminary Characterisation Stage

The objectives of the Preliminary Characterisation Stage were to;

- Characterise the block in broad terms using a limited number of boreholes.
- Identify and quantify major conductive structures (fracture zones), fracture sets and boundary conditions.
- Assess connectivity of fracture networks using cross-hole interference tests in combination with tracer dilution tests.
- Perform preliminary assessment of transport parameters over longer distances using injection of tracers in conjunction with cross-hole interference tests.
- Assess representativness of selected block (in relation to overall Äspö conditions).

Field work included drilling, characterisation of boreholes KI0025F and KI0023B. A series of cross-hole hydraulic interference and tracer dilution tests were carried out /Andersson et al, 2001a/. One of the tracer dilution tests was prolonged and the breakthrough of the injected tracer was observed. In addition a 3D cross-hole seismic survey was carried out where the results were co-processed with old seismic data. The basic results of this stage is presented by /Winberg, 1999/. The developed hydro-structural model is presented in Section 4.3.

2.1.3 Detailed Characterisation Stage

The objectives of the Detailed Characterisation Stage were to;

- Reach a satisfactory basis for performing block scale tracer experiments through improved understanding of the structural geology and the hydraulic characteristics of the studied network of structures.
- Test different conservative tracers and to obtain site-specific transport parameters from analyses of geological material in the laboratory.
- Minimise the disturbance exerted by the borehole array on hydraulic and tracer tests.
- Assess the coupling between transport parameters and hydraulic parameters.

The field work included drilling and characterisation of borehole KI0025F02. In addition a comprehensive series of cross-hole hydraulic interference and tracer dilution and tracer tests were carried out /Andersson et al, 2001b/. The developed hydro-structural model is described in Section 4.4.

The majority of the defined objectives were accomplished and were subsequently discussed at technical review meetings held in November 1998 and in November 1999. However, site specific laboratory data were not available at the conclusion of the stage. This was due to a strategic decision to postpone such analyses until the geometry for the planned tests with sorbing tracers had been selected. Further, analysis of "flow accounting" /Black, 2001/ was not pursued as planned due to projected difficulties associated with the natural background flow. However, alternative steps to investigate the relation between hydraulic and transport parameters were taken /Billaux and Rachez, 2002/.

2.1.4 Tracer Test Stage

This stage included drilling and characterisation of the final borehole, KI0025F03, which was drilled to verify the March'99 hydro-structural model /Doe, 2001/ with an additional objective also to furnish additional injection points for tracer. The objectives of the Tracer Test Stage /Winberg, 2000/ were to;

- Assess and quantify the parameters which control radionuclide retention in a fracture network in the block scale.

- Assess the predictive capability of developed block scale transport models and characterisation tools for predicting transport of sorbing tracers, and to evaluate which model assumptions are most appropriate and important.

The work scope of this stage included, apart from drilling and characterisation of a new borehole, optimisation of existing multipacker installations. However, the main activity was the series of three tracer test phases; Phase A which was focused on identifying the best pumping (sink) section /Andersson et al, 2000a/, Phase B which was devoted to demonstrating sufficiently high mass recovery of non-sorbing species to allow usage of radioactive sorbing tracers /Andersson et al, 2000b/, and finally Phase C /Andersson et al, 2001c/, which included performance of four injections with radioactive sorbing tracers in three sections. The resulting hydro-structural model /Hermanson and Doe, 2000/ is discussed in Section 4.5.

2.1.5 Evaluation and Reporting Stage

The last of the five stages included evaluation of experimental data and modelling results an writing of the four final report defined in Section 1.7.

2.2 Boreholes and installations

2.2.1 Boreholes

The TRUE Block Scale borehole array is made up of 10 cored boreholes. Five of those have been drilled specifically within the TRUE Block Scale Project. The remainder have been drilled as part of the development of the spiral access tunnel, or as part of the characterisation for other projects, i.a. the Prototype Repository project. The boreholes are with two exceptions drilled using the triple-tube technique, cf Section 3.1. The boreholes penetrating the investigated rock volume are presented in Table 2-1 and Figure 2-1.

Table 2-1. Compilation of data on boreholes penetrating the TRUE Block Scale Rock volume. A detailed list of borehole coordinates, bearings and inclinations is provided in Appendix A. TT=Triple tube core barrel, Solexp.=ANDRA/Solexperts multipacker system.

Borehole Id	Diameter (mm)	Length (m)	Completed	Project
KA2511A	56	293.0	1993-09-05	Location of Turn 2
KA2563A	56	263.4	1996-08-24	TRUE Block Scale
KA3510A	76 TT	150.1	1996-09-09	Various
KI0025F	76 TT	193.8	1997-04-25	TRUE Block Scale
KI0023B	76 TT, Solexp.	200.7	1997-11-20	TRUE Block Scale
KI0025F02	76 TT, Solexp.	204.2	1998-08-25	TRUE Block Scale
KI0025F03	76 TT	141.7	1999-08-13	TRUE Block Scale
KA3548A	76 TT	30.0	1998-06-26	Prototype Repository
KA3573A	76 TT	40.1	1997-09-11	Prototype Repository
KA3600F	76 TT	50.1	1997-09-24	Prototype Repository

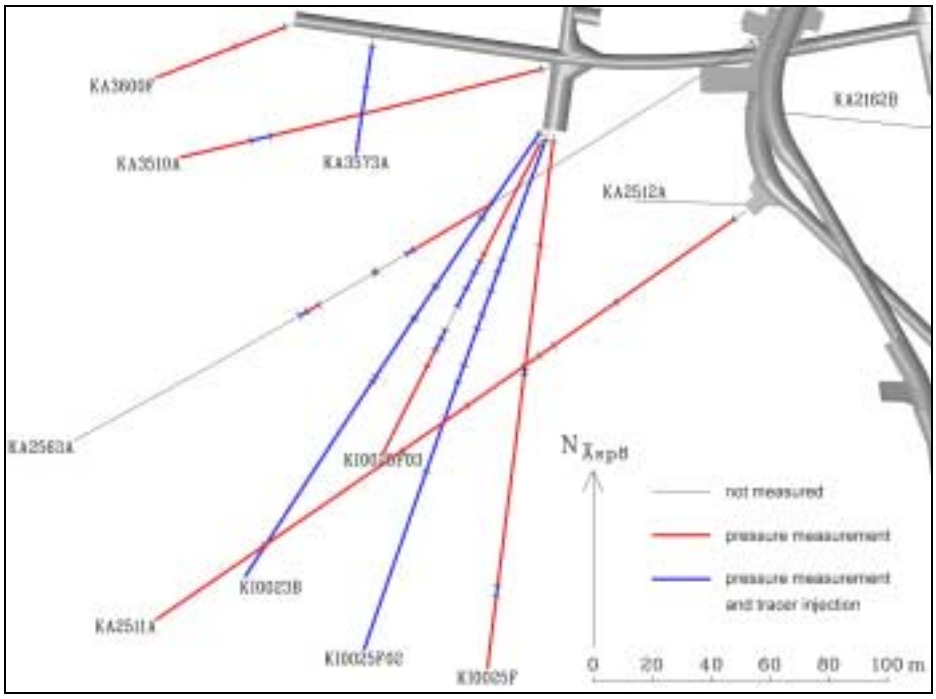

Figure 2-1. *TRUE Block Scale borehole array and definition of defined rock volumes in the investigated rock block. The figure also indicate the locations of packed off intervals in the boreholes (per June 2000).*

2.2.2 Installations

Of the boreholes listed in Table 2-1, seven have been instrumented as part of the project. The exceptions being the boreholes drilled as part of the Prototype Repository experiment. In the boreholes instrumented by the TRUE Block Scale Project, two types of packer equipment have been utilised; the so-called “SKB/GEOSIGMA system” and the “ANDRA/Solexperts system”. Brief descriptions of the two systems are provided below.

ANDRA/Solexperts system

The ANDRA system is installed in boreholes KI0023B and KI0025F02, cf Table 2-1 and Figure 2-1.

This multi-packer system consists of up to 10 inflatable packers connected by a central tubing providing up to ten test sections where pressure can be monitored and fluid can be circulated. Packer-inflation, interval-pressure and interval-injection/circulation lines are run through the central tubing, which provides protection from abrasive damage and allows a continuous line (i.e. no connectors) between the interval/packer and the control units.

The system comprises 4 main components, cf Figure 2-2:

- Inflatable packers.
- Central tubing.
- Control lines for packer inflation, pressure measurement, injection and tracer circulation.
- Surface control unit.

The packers consist of a stainless-steel body and a steel-reinforced fixed-end expansion element made of natural rubber (OD=72 mm). Each packer has 4 welded-in steel lines that extend approximately 20 cm beyond the packer end. The lines are for packer inflation, pressure-measurement, injection and circulation. The packers have a 6 MPa maximum working pressure in a 76 mm diameter borehole, allowing a maximum differential pressure of 50 MPa. All packers have separate inflation lines and are inflated using pressurised water. The packers are equipped with a swivel-nut coupling on the down-hole side, and a threaded coupling on the up-hole side of the packer. A stainless-steel sinter filter serves as a static mixer for tracer injection. The filter distributes the tracer evenly around the interval.

The packers are connected by a large-diameter stainless-steel central tubing through which all of the control lines are run. The tubing couplings are sealed with o-rings and can be hand-tightened. The certified working pressure for the tubing is 50 bar. Certain portions of the central tubing (important test sections) are coated with polyamide to increase the outside diameter to 68 mm in order to minimise the interval volume of the test sections.

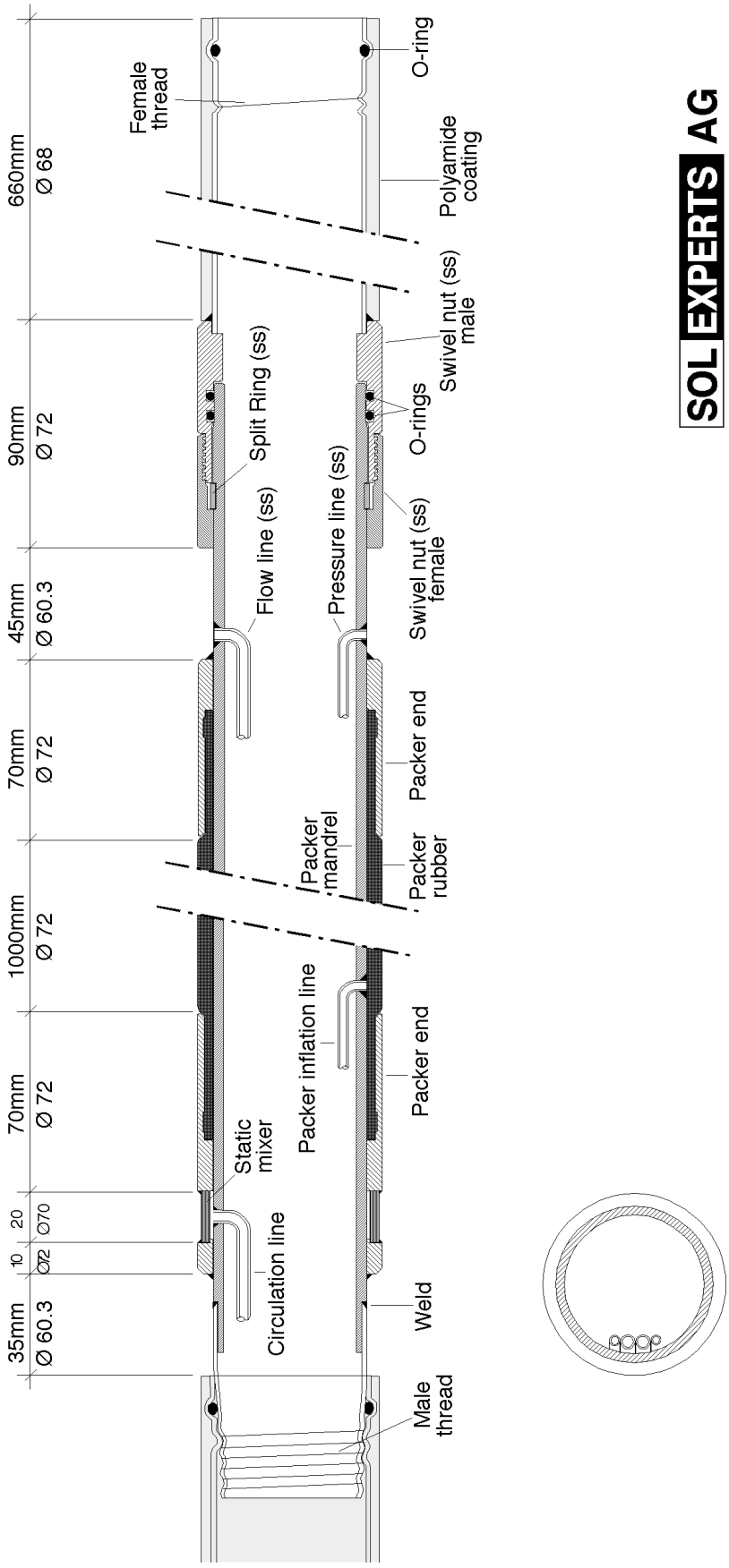

Figure 2-2. *Schematic illustration of the ANDRA/Solexperts packer system.*

The test intervals and packers are connected to the control units on the surface via polyamide control lines. Swagelok™ connectors are used for connecting the control lines to the packers and the control units. The surface control units consist of valves, connectors and manometers for packer inflation, pressure measurement and fluid injection/circulation.

The initial installation in borehole KI0023B suffered a failed tubing in the section L=87.2–2110.25 m due to a faulty central tubing which did not withstand the acting water pressure of about 42 bars. An attempt to extract the packer system for remediation failed, attributed to a rock piece protruding into the borehole and blocking movement. It was therefore decided to reinstate the packer system back to its original position. The remaining problem with the piezometer was a need to maintain ambient pressure in the faulty section to ensure functionality of the leadthroughs in the collapsed central tubing. This was achieved by placing a lid on the central tubing at the borehole collar. In addition, the inability to separate Structures #20 and #6 in section P7 (L=43.45–69.95 m) which is adjacent to the selected optimal pump section for tracer tests (KI0023B:P6). Repeated pre-tests have, however, shown that the effect of the faulty section and the short-circuit in section P7 are manageable, and do not affect the tracer test results to any significant degree.

SKB/GEOSIGMA System

The SKB/GEOSIGMA system is installed in all boreholes except KI0023B and KI0025F02, cf Table 2-1 and Figure 2-1.

The SKB/GEOSIGMA system for a 76 mm boreholes unlike the ANDRA/Solexperts system is based on a design with packers connected by 20 mm steel/aluminium rod. The equipment is made up of five main components;

- Packers of 90 Shore Polyurethane.
- 20 mm steel/aluminium rod.
- 6/4 or 4/2 polyethene lines used for circulation/inflation and pressure monitoring, respectively. All lines are bundled against the central rod.
- Dummy bodies of Delrine/High Density Polyethene are used to reduce the volume in the test sections equipped for circulation.
- Surface anchor.
- Surface control unit.

The packers have a maximum inflation pressure of 7 MPa and allow a differential pressure of maximum 6.4 MPa. The design allows a total of 21 leadthroughs in a 76 mm borehole, allowing up to 7 circulation sections and/or up to 21 sections where pressure can be monitored depending on how the leadthroughs are distributed. All packers are inflated with one common line. Figure 2-3 shows a schematic of the SKB/GEOSIGMA system.

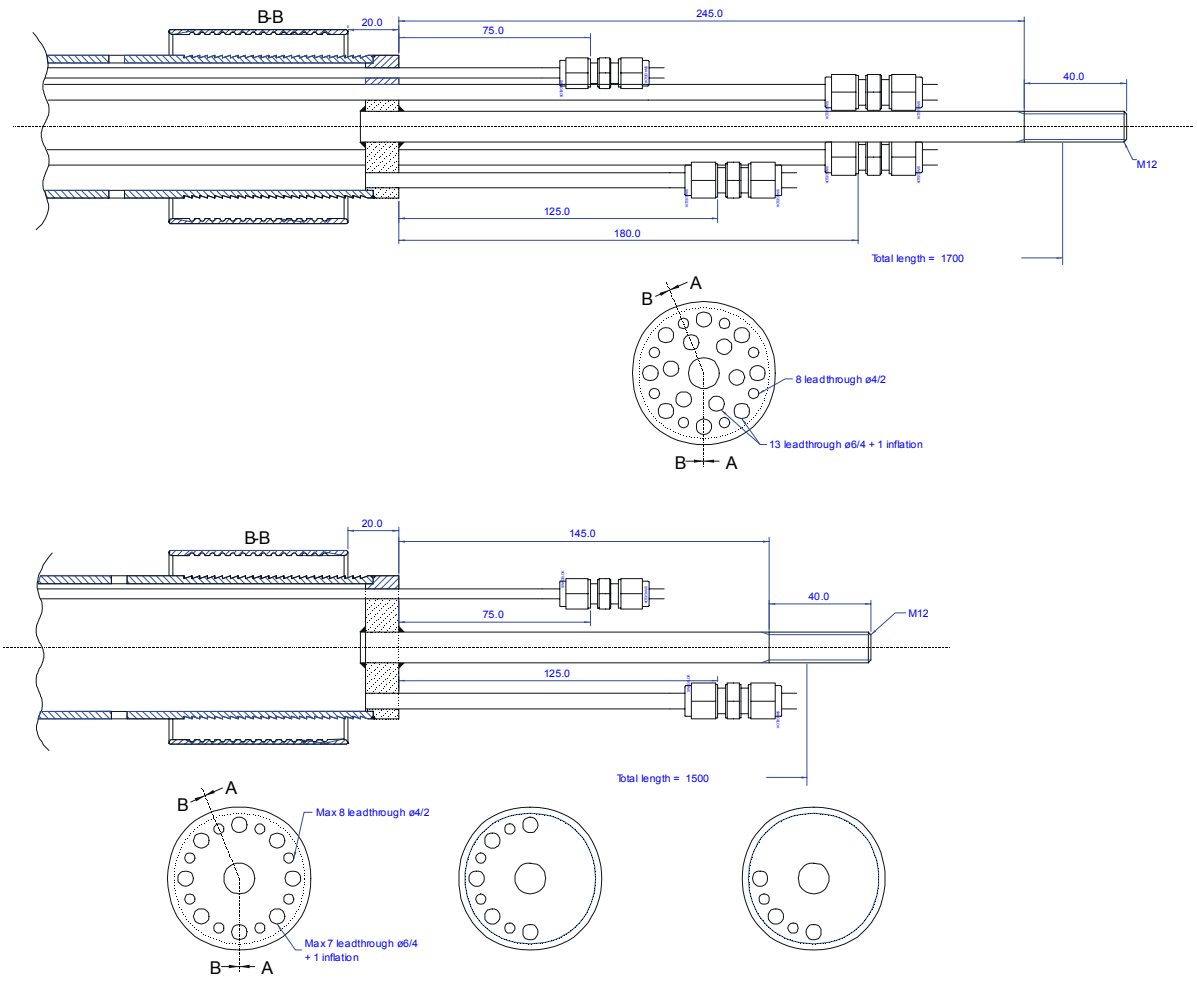

Figure 2-3. *Schematic description of the SKB/GEOSIGMA Packer system.*

Pressure transducers

Individual piezoelectric transducers of type Druck 520 have been used for monitoring pressure in the different test sections. The pressure transducers are mounted on racks in the close vicinity of each borehole. The transducers are connected to the Äspö Hard Rock Laboratory Hydro Monitoring System (HMS) which allows continuous control and access to pressure data.

Evolution of configuration of packers systems

The two 56 mm boreholes, KA2511A and KA2563A, have been reinstrumented repeatedly allowing for optimisation of the packer array in relation to the evolving hydro-structural model, and identification of testable parts of the studied network of structures.

The final configuration of the packer systems in the boreholes penetrating the TRUE Block Scale rock volume are listed in Appendix A.

2.3 Methodology for developing hydro-structural model

At an early stage in the project there was a strive towards making a distinction between parallel development of a structural-geologic and a hydraulic model. The idea being to test the ability to assess the hydraulic characteristics of geological features from geological observations, whether from direct observation (drill core) or from indirect observation (borehole TV imaging), or both. Geological structures at Äspö are however known to vary in character over distance /Mazurek et al, 1997/, and hence attempts to connect structure intercepts over distances ranging between 10–100 m are therefore difficult without prior knowledge of hydraulic data. Similarly, building a hydraulic model from single hole observations and cross-hole interference data, whether from drilling responses or cross-hole hydraulic tests, also leads to some type of geometric framework which subsequently needs to be clad in a geological context. The consequence being that building of a hydro-structural model requires an integrated effort employing both geological/structural data and hydraulic data.

The basic methodology for the interactive process has therefore been that the existing hydro-structural model has been used to predict the projected intercepts of interpreted deterministic structures along the length of a given new borehole, cf Chapter 4.

During the drilling careful records have been kept of the pressure responses in adjacent boreholes equipped with multi-packer systems. In addition, careful measurements have been made of the cumulative inflow to the borehole after each drill core uptake. Through the combined use of these data a rough verification of the existing model is obtained both in a geometrical (location) and quantitative hydraulic sense (inflow), cf Section 3.5. At the same time possible new conductive structures are tentatively identified.

Using the subsequent single hole characterisation data, POSIVA flow logging (Section 3.3) and BIPS/BOREMAP logs (Section 3.4) a refined and more detailed identification of conductive fractures along the new borehole is obtained. Using these data, updates are also obtained on various fracture statistics (orientation, frequency/intensity measures). The next step is to correlate the deterministic structures of the existing model to the new information on conductive structures, and if necessary define new structures. The final step constitutes an integrated hydraulic reconciliation where all hydraulic data; drilling responses, static hydraulic head, flow logs, single hole test results and results of cross-hole interference tests are used to substantiate the model and to assign material properties to the deterministic structures. More importantly, the hydraulic information is used to shed light on the sometimes complex connectivity pattern which in some cases may lead to subdivision of a given identified structure into two parts with two distinctly different hydraulic characteristics/response patterns. In addition the detailed integrated hydraulic analysis may also identify a conductor which is presently not associated with a geological structure.

Collected hydrogeochemical data can subsequently provide additional verification of the developed model.

The basic methodology for constructing the hydro-structural model is described in Figure 2-4.

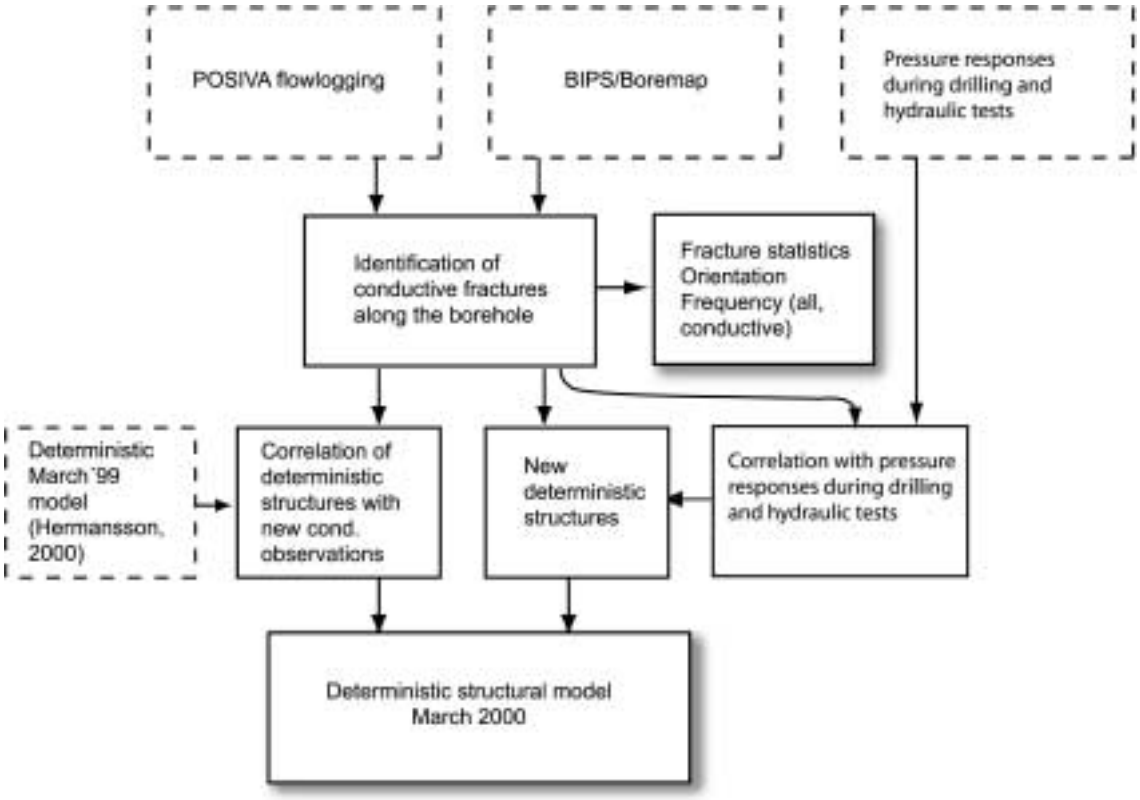

Figure 2-4. *Methodology for updating the hydro-structural model using available characterisation data.*

3 Characterisation methods

3.1 Drilling

All the boreholes which penetrate the investigated rock volume are cored boreholes. The 56 mm boreholes KA2511A and KA2563A have been drilled using conventional double tube core barrel. The 76 mm boreholes have been drilled with an ONRAM 1000 drill rig and a Triefus Triple Tube with NMLC with an OD of 75.6 mm, or a Hagby triple tube barrel with OD 76.3 mm. The resulting diameter of the core is 52 mm.

All boreholes are equipped with stainless steel casings of 2.5–3 m length glued to the rock using an epoxy resin.

Formation water, primarily from KA2598A, stored under a nitrogen atmosphere in plastic containers, was used as flushing water. A fluorescent tracer (Uranine) was used as an additive to trace remaining drilling water in water samples.

3.2 Borehole geophysics

The experience from previously performed site characterisation in Sweden is that traditional borehole geophysics does not contribute significantly to identification of conductive fractures and their connectivity and or extent. The exception being some of the electrical methods (single point resistance) and electromagnetic methods (borehole radar) and seismic methods (tubewave methods). However, in these cases it is for the most part major conductive fractures that are readily identified. However, in the case of the TRUE experiments also the very minute conductive fractures of the background fracture population are of importance. As a consequence the borehole geophysical programme utilised in TRUE Block Scale is of limited extent. Borehole radar with directional antenna has been used primarily in the initial phases of characterisation to primarily help delineate fracture geometry at distance from the boreholes. Cross-hole seismics and 3D seismics have been used to investigate the capability of the method given more effective seismic sources and processing algorithms. The primary focus have in the latter case been to identify the major conductive structures.

3.2.1 Borehole radar with directional antenna

Measurements with borehole radar with directional antenna have been performed in the cored boreholes KA2511A, KA2563A, KI0025F, KI0023B and KI0025F02. The objectives of the measurements were to determine the orientation and extent of fracture zones, and as far possible, conductive fractures intersecting the boreholes. In the case of

KI0025F02, high frequency antenna measurements were performed to improve the resolution near the borehole wall, cf Section 3.2.2.

The measurements with directional antenna have been performed using the RAMAC system. A general description of the RAMAC system and the interpretation of directional data is given by /Sandberg et al, 1990/. Due to the dimension of the boreholes (56/76 mm) compared to the dimension of the radar probe (48 mm), it has been necessary to use plastic centralisers in order to keep the probe in the centre of the borehole. The equipment consists of a transmitter and receiver with a 7 m spacing. The measurements have been carried in a single-hole reflection mode with a centre frequency of 45–50 MHz. Reflectors have been identified in DC-filtered and bandpass-filtered data. The DC-filtering corrects for voltage variations during measurement and sets all traces to an equal voltage level. The bandpass filter introduced towards the end of the project, effectively reduced high frequency ringing in the original radar data.

The angle of intersection relative to the borehole and the gravity azimuth (vertical down) have been determined for most reflectors. This gives the orientation of the reflectors relative to the borehole. Based on these data and the borehole geometry (deviation data), the orientation of the reflectors relative to north in the local Äspö coordinate system has been determined. An example of a three dimensional interpretation model from the measurement in KI0025F02 is given in Figure 3-1.

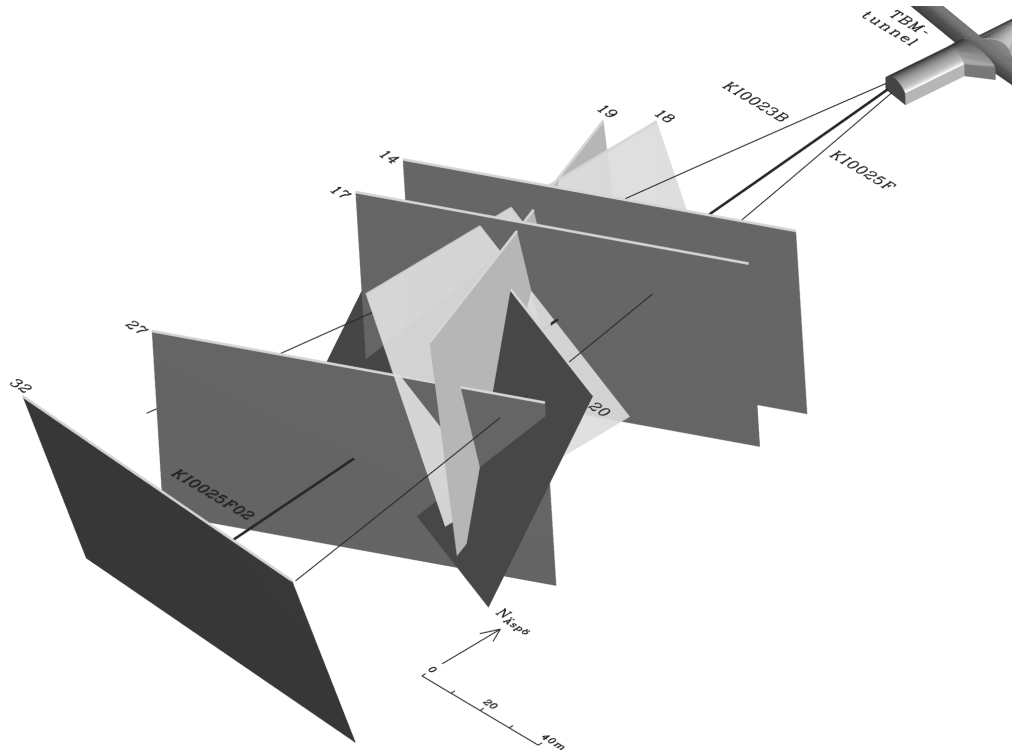

Figure 3-1. *Radar reflectors interpreted from measurements with RAMAC directional borehole radar in borehole KI0025F02. Perspective view from SE.*

In borehole KI0025F02, for example, a total of 36 reflectors were interpreted from the radar map, of which 32 were interpreted to intercept the borehole. It was also possible to correlate 25 of these reflectors with geological structures identified using BIPS. All 32 directional reflectors identified in the borehole were correlated the high frequency reflectors, cf Section 3.2.2.

A total of 47 discrete inflow anomalies have been identified from POSIVA flow logging in KI0025F02. The directional antenna measurements indicate that 17 of the interpreted reflectors (53%) can be correlated with flow anomalies, accounting for 36% of the flow anomalies.

A comparison of interpreted directional radar reflectors identified in KA2511A, KI0023B and KI0025F02 with those evaluated from the evaluation of the 3D seismics, cf Section 3.2.4, shows a good correspondence.

3.2.2 Borehole radar with high frequency antenna

Borehole radar measurement with the high frequency antenna was performed using the RAMAC/GPR system. The system consists of a transmitter/receiver system with a separation of 1.9 m. The centre frequency used is 250 MHz. Reflectors have been identified in DC-filtered and GRADIX-filtered data. The DC-filter corrects for voltage variations during measurement and sets all traces to an equal voltage level. The filter used in GRADIX reduces high frequency ringing in the original radar data. The angle of intersection relative to the borehole axis and the intersection length in the borehole has been determined for all visible reflectors. It is not possible to derive the absolute orientation of the identified reflectors.

As an example, the measurements with high frequency antenna in borehole KI0025F02 have indicated most of the sections in the borehole where conductive fractures have been identified from POSIVA flow logging, cf Section 3.3. A total of 151 reflectors were interpreted in the 250 MHz radar map, of which 146 were interpreted to intercept the borehole. Some 124 reflectors (85%) were correlated with geological structures mapped by BIPS. Possible reasons why 15% of the radar reflectors are not correlated with BIPS structures may be that (i) BIPS does not identify all fractures (resolution), (ii) some reflectors may be due to mineralogical content (e.g. sulphide minerals and biotite), (iii) some reflectors are detected outside the borehole, (iv) curvature in reflectors, the reflectors may intercept at another location than based on a linear extrapolation.

The high frequency antenna measurements showed that 38 reflectors could be associated with conductive fractures. This corresponds to 26% of the total number of high frequency reflectors. However, given that 46 inflow points have been identified by POSIVA flow logging, 83% of the total number of conductive fractures/inflow points (N=47) have been identified. This is a significant improvement compared to the directional antenna measurements, cf Section 3.2.1.

It was shown that the high frequency measurement provided an improved resolution compared to the directional antenna, implying that more details about geology, structure and fractures can be obtained. Also the positioning of fracture intercepts in the borehole is improved. The high-frequency measurement is thus a link between the more penetrative directional antenna and the core/BIPS/BOREMAP information. The major drawback is that the orientation of the reflectors cannot be deduced.

3.2.3 Cross-hole seismic measurements

This high frequency method was employed in 1997 and employed a piezoelectric source which was moved to 289 positions at 1 m intervals in KA2563A. The receiver chain was moved to 128 positions at 2.5 m spacing in borehole KA2511A. The source consists of a stack of piezoelectric crystals, a converter unit which transforms the energy in the piezo-stack to a seismic wave, and a power module which provides the high voltage required to drive the source. The receiver chain contains eight three (orthogonal) component accelerometers spaced at 5 m intervals. The Z component is oriented along the axis of the borehole. The receiver units were clamped against the borehole wall with a motor-driven side arm. A sampling frequency of 20 kHz was employed during the recording.

The basic processing of the results included assessment of velocity determinations. This analysis indicated an error in the calculated deviation of borehole KA2563A which amounted to several meters. The pre-processing included a series of steps including band-pass filtering between 1200–3600 Hz. Subsequent processing included CMP-stacking (Common Mean reflection Point) and pτ-transform and migration.

The basic results include migrated sections at various azimuth angles along where possible reflectors have been interpreted. Due to the fact that the two boreholes essentially are located in the same plane, the interpretation of absolute geometry of interpreted reflectors is ambiguous. The data were subsequently reprocessed jointly with new 3D seismic data, cf Section 3.2.4.

3.2.4 3D seismic measurements

Multi-offset VSP and HSP surveys were performed in the TRUE Block Scale rock volume in December 1997–January 1998. The VSP (Vertical Seismic Profiling) layout consisted of several source positions along the tunnels and a dense array of receivers (accelerometers) in borehole KI0023B. The HSP (Horizontal Seismic Profiling) layouts consisted of dense arrays of sources placed along tunnels several detectors placed ion borehole KI0023B.

The source employed was based on the Swept Impact Seismic Technique (SIST) which delivers 15–25 J of energy per impact at a mean impact rate of $25 s^{-1}$. The energy delivered in 20 seconds is thus 10kJ, which is equivalent to a mass of 1000 kg dropped

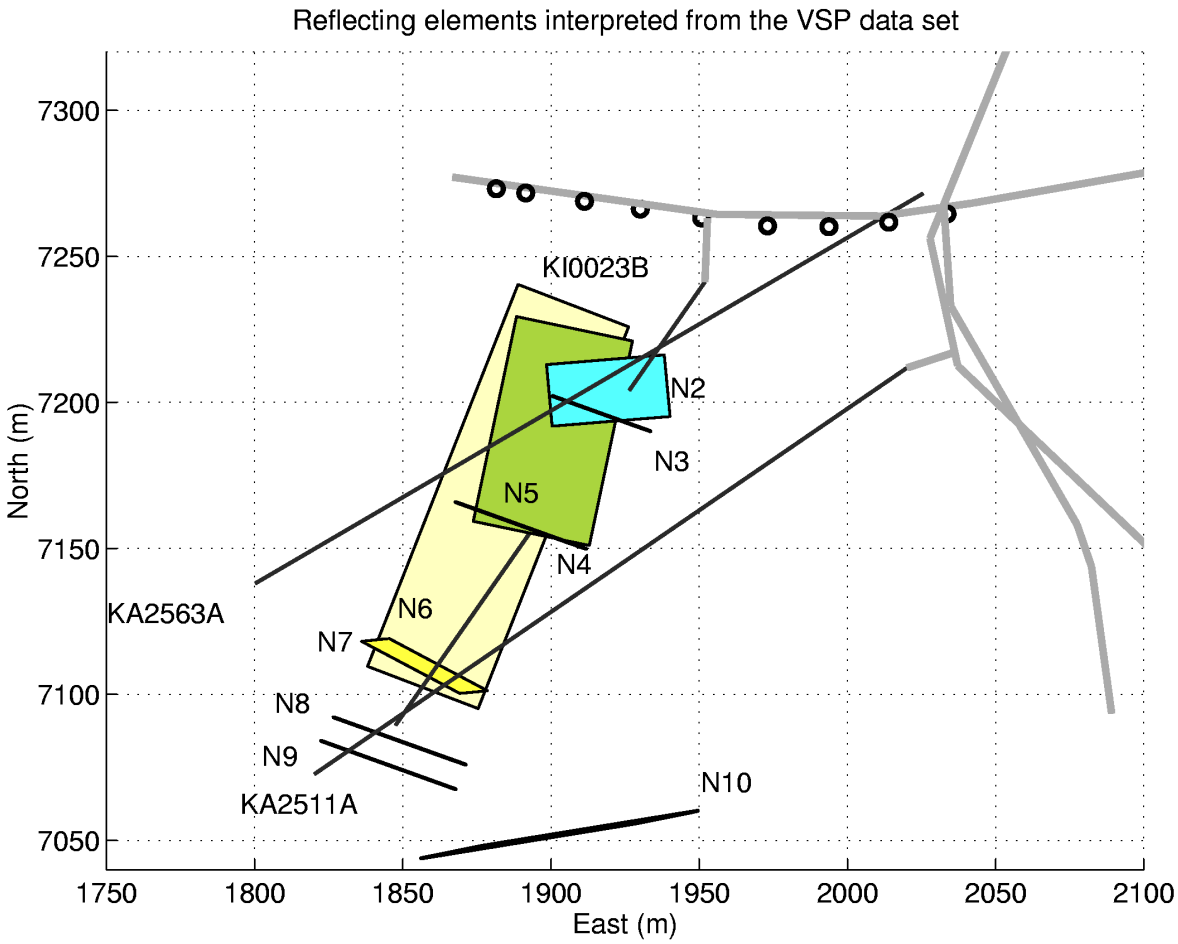

Figure 3-2. *Reflectors interpreted from the VSP data set seen in plane view. Colours only included to improve readability. Shot points for VSP along tunnel are also indicated.*

from 1 m. The mean frequency of the delivered pulse was 1000–1500 Hz. The estimated investigation depth range is 200–500 m. The receiver chain was made up of 24 accelerometers placed in eight 3-component modules with the Z component aligned with the borehole axis. The distance between the modules was 5 metres. The recording system consisted of 2 PCs each equipped with a 12-bit A/D conversion board. The system enabled sweeps of 10–20 seconds at a sampling rate of 150 µs per channel.

Processing included controlled conversion of the log sweeps and preconditioning of the signal followed by 3-D component image transformation. The analysis included reprocessing of the cross-hole data, cf Section 3.2.3, followed by a combined interpretation of the seismic data collected in the TRUE Block Scale rock volume 1997 and 1998.

The VSP data set, cf Figure 3.2, set reveals three subhorizontal structures of variable extent and separated about 40 metres apart between –470 to –520 masl. It should be noted that although these structures may gave a geological and geophysical signature, their hydraulic signature has been found to be insignificant, cf Section 4.3. The reflectors N8–N9 correspond to the deterministic Structure #10, N4 to Structure #19 and reflector N3 to Structure #7, cf Figure 4-6.

The cross-hole data reprocessing and evaluation, cf Figures 3-3 and 4-6, reveals three reflectors (C8–C10) which could be associated with the interpreted Structure #10, reflector C1 could be associated with Structure #7 and reflector C6 could be associated with Structure #8, the latter deemed to be of no or insignificant hydraulic significance.

In general, it appears that smaller structures, corresponding to the interpreted Structures #13, #20, #21, #22 and #23, are not seen by the seismics. This could be due to them being poor reflectors, possible subdued in the presence of other, more important reflectors. The measurement geometry also plays an important role in this context.

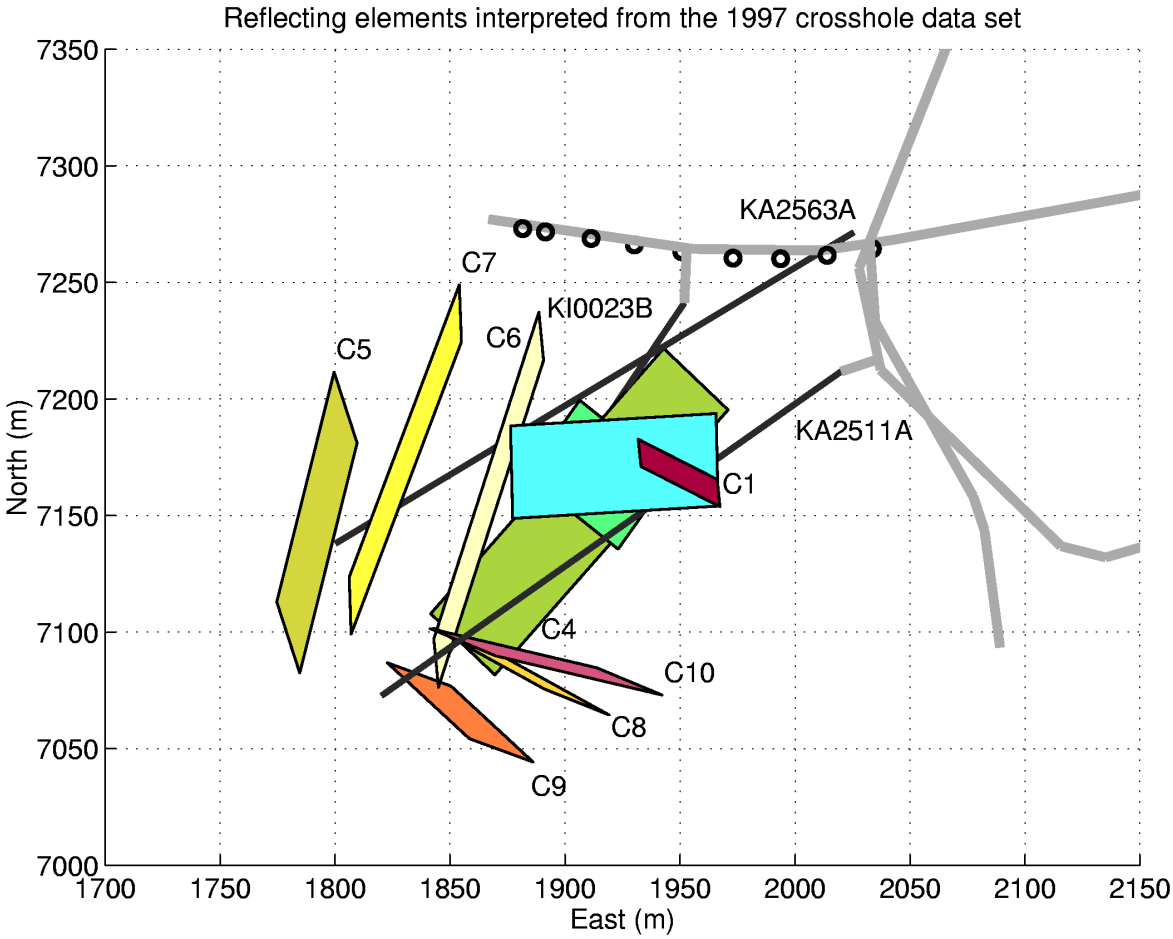

Figure 3-3. *Reflectors interpreted from the 1997 cross-hole data seen in plan view. Colours only included to improve readability. Shot points for VSP along tunnel are also indicated.*

3.2.5 Evaluation of geophysical methods used

The use of directional borehole radar has not in any significant way provided crucial and important data which could not be obtained more effectively and quantitatively from other sources, e.g. BIPS and flow logging. However, during an early phase of site characterisation (say one borehole completed), the directional borehole radar provides information which can be guiding in the planning of subsequent characterisation phases. It should however be pointed out that the difficulty to make use of the directional radar data at the Äspö HRL is mainly attributed to the relatively high salinity of the groundwater (approximately 1% TDS), which provides a higher attenuation of the radar signal, reducing its penetration depth. At Stripa /Gnirk, 1993/, with a less saline groundwater (approximately 0.1% TDS), the directional borehole radar was found to be a highly efficient tool to characterise the location and geometry of conductive structures.

The seismic work has identified larger structures than the ones involved in the subsequent tracer tests. Consequently, the current seismic methods can primarily be used to delineate the fracture zones which are bounding a block scale site. The identification of structures within a block of 100 m length scale has to be performed with other, and more direct geological and hydraulic techniques, of the type utilised in the TRUE Block Scale characterisation.

3.3 Flow logging

Flow logging is the main tool for locating the conductive portions of boreholes in the TRUE Block Scale project. Over the past several years, improvements in flow logging methods have increased the range of measurable flow rates and refined the spatial resolution of flow logs. These improvements can be seen in the evolution of the flow logging methods used in the TRUE Block Scale experiments. The initial flow logs in the project used packers and had a practical resolution of five meters. By the end of the experiment, flow-logging methods could provide nearly continuous flow measurements with resolution in the order of centimetres without the use of inflatable packers

As a hydrologic testing tool, flow logging has both advantages and disadvantages. The main advantage of flow logging is its speed and low cost. The main disadvantage of flow logging is that it only provides steady state estimates of transmissivity, unlike transient well tests, which can overcome effects of near-hole heterogeneities and give information on the geometry of the conducting feature away from the well.

The TRUE Block Scale project used flow logs and transient well tests in a complementary fashion. Because transient well tests are relatively expensive and time-consuming, it is not efficient to use them on short intervals over the entire lengths of the TRUE Block Scale boreholes. With the information from flow logging, one can limit the scope of transient well tests to short borehole intervals that contain the most significant conducting fractures.

Flow logging also provides information on fracture connectivity. Connectivity assessments look for changes in flow rates from specific fractures when pressures or flow rates are disturbed elsewhere in the fracture network. This approach was used to test various hypotheses regarding the existence and extent of Structure #9 within the TRUE Block, cf Section 4.4.

The True Block Scale project used three different flow-logging methods. The techniques used were (1) double packer logging, (2) ultrasonic current meter (UCM) logging, (3) and heat-pulse (Posiva) flow logging. Table 3-1 presents some of the characteristics of the logging tools, and in which boreholes each method was utilised. Packer logging and UCM flow logging were used first. Posiva flow logging was introduced later in the project. Portions of boreholes KA2563A and KA2511A were re-logged with the Posiva tool, in part for the purpose of re-configuring and optimising the piezometer arrays in these holes.

Table 3-1. Characteristics of flow logging methods and their application to TRUE Block Scale project boreholes. X=employed.

	Packer Flow Log	**UCM Ultrasonic Current Meter Flow Log**	**Posiva (DIFF) Heat Pulse Flow Log**
Spatial Resolution	1 to 5 m	1 m	0.1 m
Flow Range	0.0003–>45 l/m	0.044–132 l/m (76 mm hole)	0.002–5.0 l/m
Cumulative		Yes	
Discrete	Yes		Yes
KA2511A	/Gentzschein, 2001/		/Rouhiainen and Heikkinen, 2001b/
KA2563A	X	X	/Rouhiainen and Heikkinen, 2001b/
KI0025F	/Gentzschein, 2001/	X	
KI0023B	X	X	
KI0025F02		X	/Rouhiainen and Heikkinen, 2001a/
KI0025F03			/Rouhiainen and Heikkinen, 2001c/

Flow logging methods provide the basis for estimation of transmissivity using equations for steady-flow. Steady flow implies that the pressure and the flow rates around the borehole have reached a stable condition. Steady flow equations for transmissivity, *T*, have the form:

$$T = C\frac{Q}{\Delta h} \tag{3-1}$$

where *Q* is the flow rate from the test section and *Δh* is the difference in hydraulic head between the borehole and the head at some distance *R* in the rock where the flow to the borehole has a negligible effect on the pressure.

The constant *C* can take different forms, depending on what assumptions are used with respect to the flow geometry of the fracture network. The steady radial flow equation gives *C* as:

$$C = \frac{\ln R / r_w}{2\pi} \tag{3-2}$$

where r_w is the well radius. Another common expression for *C* is Moye's formula which makes assumptions to eliminate the uncertainty in *R*:

$$C = [1 + \ln(L / r_w)] / 2\pi \tag{3-3}$$

where *L* is the interval length. Practically speaking the different forms for calculating *C* do not yield significantly different results.

A larger concern in flow logging is the role that skin effects play in determining transmissivity. Skin effects involve the transmissivity of the fractures local to the borehole. If the borehole penetrates a fracture in a region where the transmissivity is less than the large-scale average value for the fracture, the steady-flow determination from flow logging will measure mainly the lower transmissivity skin. Thus, steady flow measurements tend to give underestimates as compared with values from transient tests, which provide information on both the skin as well as the larger scale transmissivity of the fractures.

Because flow logging generally provides input data for steady flow calculations, the main value and contribution of the flow log is to provide the location of conducting fractures and a partly qualitative estimate of their transmissivity. The intervals that flow logging identifies as containing significant fractures then become candidates for pressure build-up, or other transient tests. For the remaining low transmissivity portions of the boreholes, either the steady flow estimate or the lower measurement limit of the flow logging method may be a sufficient measure of transmissivity.

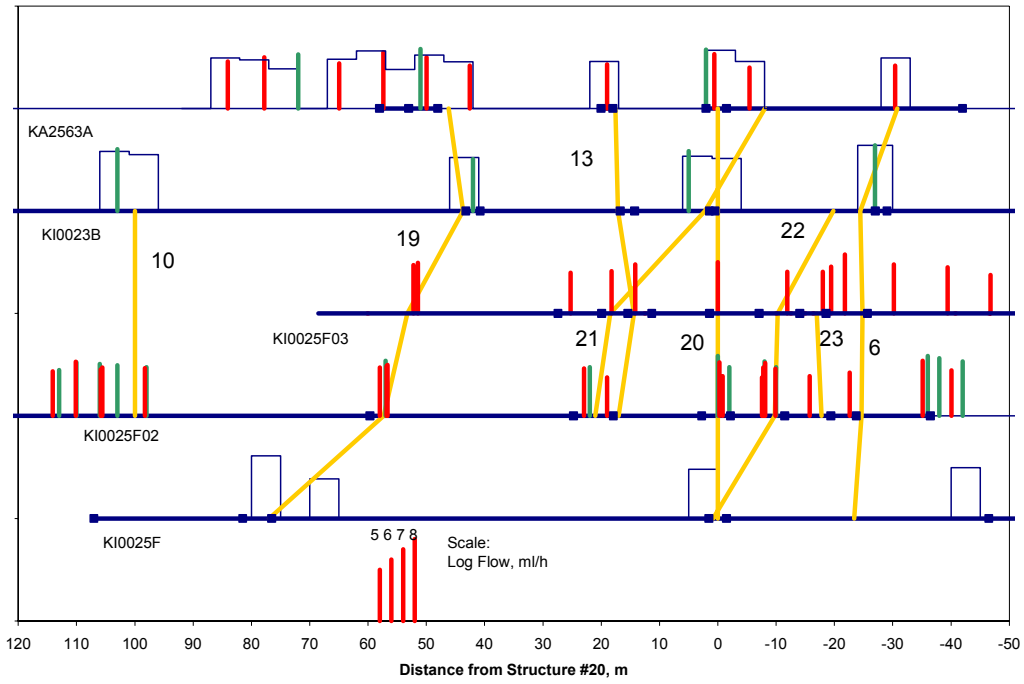

Figure 3-4. *Flow logging results for all boreholes except KA2511A. Packer logging: blue outlined bars, UCM: green bars, Posiva: red bars. Boreholes appear in relative positions. Depth is normalised to the location of Structure #20. Structures appear in orange.*

Figure 3-4 compares all the flow logging results, except for 1m packer logs in KA2563A and the logs from KA2511A. Note that this figure does not show a map view, but simply plots the length scales are shifted to position Structure #20 at the X-axis origin. Blue bars show the packer log results, green bars show the locations of UCM log anomalies, and red bars show Posiva log anomalies that exceed 5000 ml/hour. The bars are scaled logarithmically in units of ml/hour.

3.3.1 Double packer flow logging

The double packer system measures the flow rate out from an isolated section of borehole to determine that section's contribution to the total flow from the hole. The packer system contains piping that allows the flow from deeper sections to pass through the packer system. The entire borehole flows continuously, thus avoiding transient flow rates that would be associated with large pressure fluctuations in the borehole. Also, as the borehole flows continuously during the logging, one may safely assume the flow rates have reached a reasonably steady flow.

The double packer logging system uses two 1m long inflatable packers. The packers isolate a 5m section of borehole for most measurements, though forty 1m measurements were performed between 230–255 m and 260–275 m in KA2563A. The flow from the isolated interval follows a tube that feeds into a flow meter outside the borehole collar.

This flow meter and a transducer monitoring the pressure in the measurement section feed data to a data logger.

The packer flow logs used flow meters that could resolve flows between 0.0003 and 45 litres per minute. A single borehole interval required about 30 minutes to complete a measurement. One factor influencing the duration of the test was transient effects of packer inflation, which were greater for lower conductivity intervals.

The double packer flow logging method was applied to boreholes KA2511A, KA2563A, KI0025F, and KI0023B. The logging used 5m intervals except as noted above. Figure 3-4 shows the packer logging results.

3.3.2 UCM (Ultrasonic Current Meter) flow logging

Malå GeoScience of Malå, Sweden, developed the UCM probe from similar instruments that are used for marine applications. The probe measures the velocities of ultrasonic waves that it emits into the flow stream in opposite directions along the probe. The difference in transit time between the waves sent upstream and downstream is a function of the water velocity. The velocity also varies with temperature, pressure, and salinity. As the hole is open, the pressure is constant. However, temperature and salinity vary significantly along some TRUE Block Scale boreholes, hence the requirement for fluid resistivity and temperature logs to facilitate corrections to the flow meter data.

The probe measures the wave velocities along two pathways that are 90 degrees from one another along the circumference of the probe. In one hole (KI0023B) the flow rates from these two pathways gave different values for reasons that are not presently understood The probe is also optimised for 56 mm boreholes, such as KA2563A and KA2511A, rather than the other holes, which are 76 mm in diameter. Table 3-1 gives the flow resolutions of the UCM probe. As the probe measures flow velocity rather than flow, the sensitivity of the instrument varies with the hole diameter.

The UCM probe measures the flow rate from the open hole without any packers or sealing devices to isolate individual sections (unlike the packer logging or the Posiva logging). As a result, the flow rate at any location is the cumulative flow from the entire hole below the depth of the probe. It can be difficult to recognise small contributions to flow when there is a large flow from deeper parts in the hole. Hence, the UCM log indicates unambiguously only the few most significant flowing features in each hole.

UCM logs were run in boreholes KA2563A, KA2511A, KI0023B, KI0025F, and KI0025F02. An example of a UCM log from KI0025F02 is shown in Figure 3-5. This log shows the typical responses. Structures #19 and #20 show up clearly in most logs as well as either Structure #6 or #7. Structure #10 also appears clearly in KI0025F02 and KI0023B. Clearly identifiable flow anomalies are shown in Figure 3-4.

The most useful features of the UCM log may not be the flow log, but the complementary temperature and fluid resistivity logs. These logs provide considerable insights on the flow system. Different fracture networks in the TRUE Block Scale volume contain water with different origins, which is reflected in differences in geochemistry. Salinity is the primary factor, and fluid resistivity logs readily identify the major variations. A more detailed discussion of the implications of these measurements is contained in Chapter 6. Briefly, the temperature and resistivity logs show where waters with different sources enter the borehole based on shifts in either the temperature or resistivity. The typical pattern in the boreholes shows high resistivity in the deeper portions of the holes, which reflects lower salinity sources in Structure #10. Moving up the holes, the resistivity decreases as more saline water starts to enter the boreholes from Structures #19 and #20. Towards the borehole collars from Structure #20, progressively less saline water from shallower structures reverses the resistivity trend as less saline water enters from Structures as #6, #7, and #5. Again, these patterns appear in those holes that intersect Structure #10 (KI0025F02 and KI0023B) as well as in KA2563A. Borehole KI0025F, which does not intersect Structure #10 carries water with relatively low resistivity over its entire length until fresher waters from Structures #7 and #5 enter the hole near the collar.

The temperature logs also provide information on the flow system. In general, the temperatures decrease from the bottom of the holes to the collars. Water from Structure #20 appears to be cooler than the water flowing in from other structures, as the temperature logs show a sharp temperature drop where Structure #20 waters enter the hole.

3.3.3 Posiva (DIFF) heat-pulse flow logging

The Finnish radioactive waste program, under the management of Posiva Oy, developed a flow-logging tool for its site characterisation efforts /Rouhiainen, 2001/. The tool uses the principle of heat pulse flow logging. Heat-pulse flow logging tools determine lower- range flow velocities by measuring the travel time of water from a heater to a temperature sensor. At high flow rates this time delay becomes too short to measure, and the analysis method uses the velocity-dependent heating of the water, or the temperature dilution, to determine the flow rate.

Like the UCM flow meter, most heat pulse flow meters measure the cumulative velocity at various points along the borehole. The Posiva logging tool differs from most other heat-pulse logging tools in its isolation of short intervals of hole. The logging tool used for the TRUE Block Scale project uses rubber disks to isolate a smaller interval. Like the packer flow log, the tool allows the water from below the lower disk to flow along the borehole. The logging system was termed the differential or DIFF system.Within the project, the DIFF flow logs were commonly referred to as “Posiva flow logs”, and that terminology will be used here.

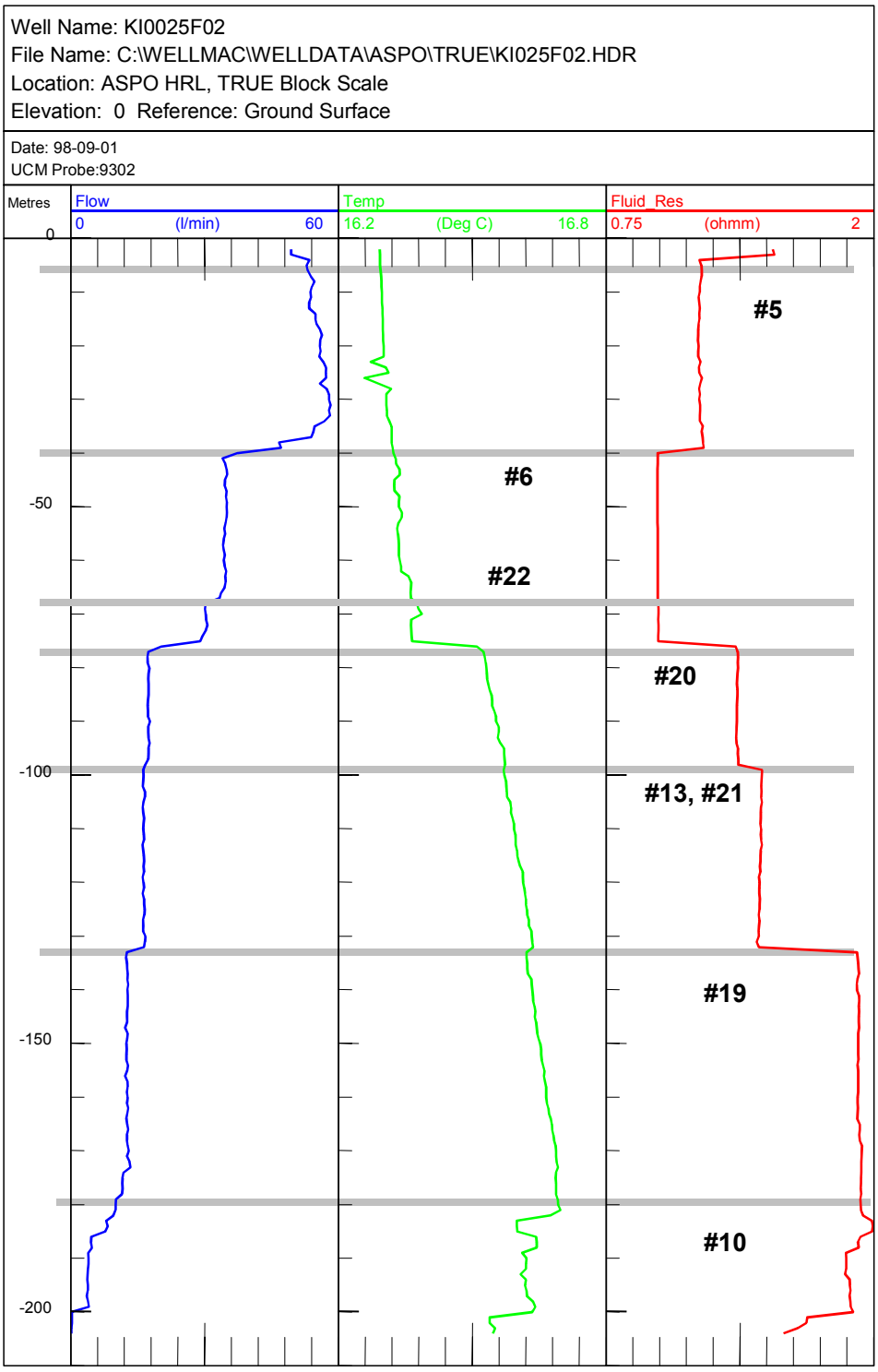

Figure 3-5. *Ultrasonic Current Meter (UCM) flow log for KI0025F02, approximate structure locations shown in grey horizontal lines.*

The Posiva DIFF flow logging tool resolves flow rates between 0.002 and 5 litres per minute. A number of major conductors in the TRUE Block Scale rock volume most likely exceeded the upper limit of flow, hence transmissivity values based on the upper limit of flow resolution are probably underestimated. This is not a serious problem, as these high-rate conductors were later targeted for detailed pressure build-up tests.

A particular characteristic of the Posiva flow logs is the logging of discrete intervals of the hole using the rubber disks. Unlike packers, the disks do not require inflation and deflation. The disks are effective in sealing intervals if pressure differences across the disks are small, which normally is the case. The rubber disks can be set to a range of spacing for coarse or detailed flow logging. Logging work for the TRUE Block Scale Project used both 5 m and 1 m disk spacing. Logging the hole in 0.1 m increments with the 1 m spacing of the disks allowed very fine, 0.1 m, resolution for the inflow to the boreholes. At this resolution the inflow points can be narrowed down to a few conductors or even to a single fracture. The flow measurements require about 12 minutes for each measurement point, and a 200-m underground hole takes about 13 hours to log.

Figure 3-6 shows an example of a Posiva flow log for KI0025F03 /Rouhiainen and Heikkinen, 2001c/. Because the sealing disks have a 1 m spacing, and the detailed measurements are carried out in 0.1 m increments, a flow anomaly will typically appear in ten consecutive measurements giving the appearance of a 1m square-shaped anomaly in the log. If more than one flow anomaly occurs within a 1m interval, the anomalies for the conductive features will overlap. One can determine the depth of the anomaly by noting the depth of the logging tool when the anomaly enters or leaves the 1m interval. The Posiva logging tool also measures the resistivity of the rock. These single-point values provide further resolution of the location of the conducting intervals/fractures.

The Posiva flow log was first introduced for logging KI025F02 /Rouhiainen and Heikkinen, 2001a/. The logging tool quickly showed its value for determining the location of inflow points into the boreholes in detail, and the log was used instead of UCM or Packer logging for the final hole, KI0025F03. Additional Posiva logs provided information on the location of conductors in KA2511A and KA2563A /Rouhiainen and Heikkinen, 2001b/. These logs were run in part to assist in identifying piezometer intervals when the instruments in those holes were last reconfigured.

The Posiva logs also played a role in resolving the importance of Structure #9 as a conductor. Structure #9 was thought to be a significant flow path between boreholes KI0023B and KA2563A. The role of flow logging in testing connectivity was to check for changes in flow rate in selected conductors in KA2563A, when piezometer intervals in KI0023B were opened or closed. Opening a conductor to flow in KI0023B was expected to change the flow from the conductor in KA2563A if the two intervals were connected. This test showed that Structure #9 did not provide a hydraulic connection between the two holes and was not a candidate for future tracer tests.

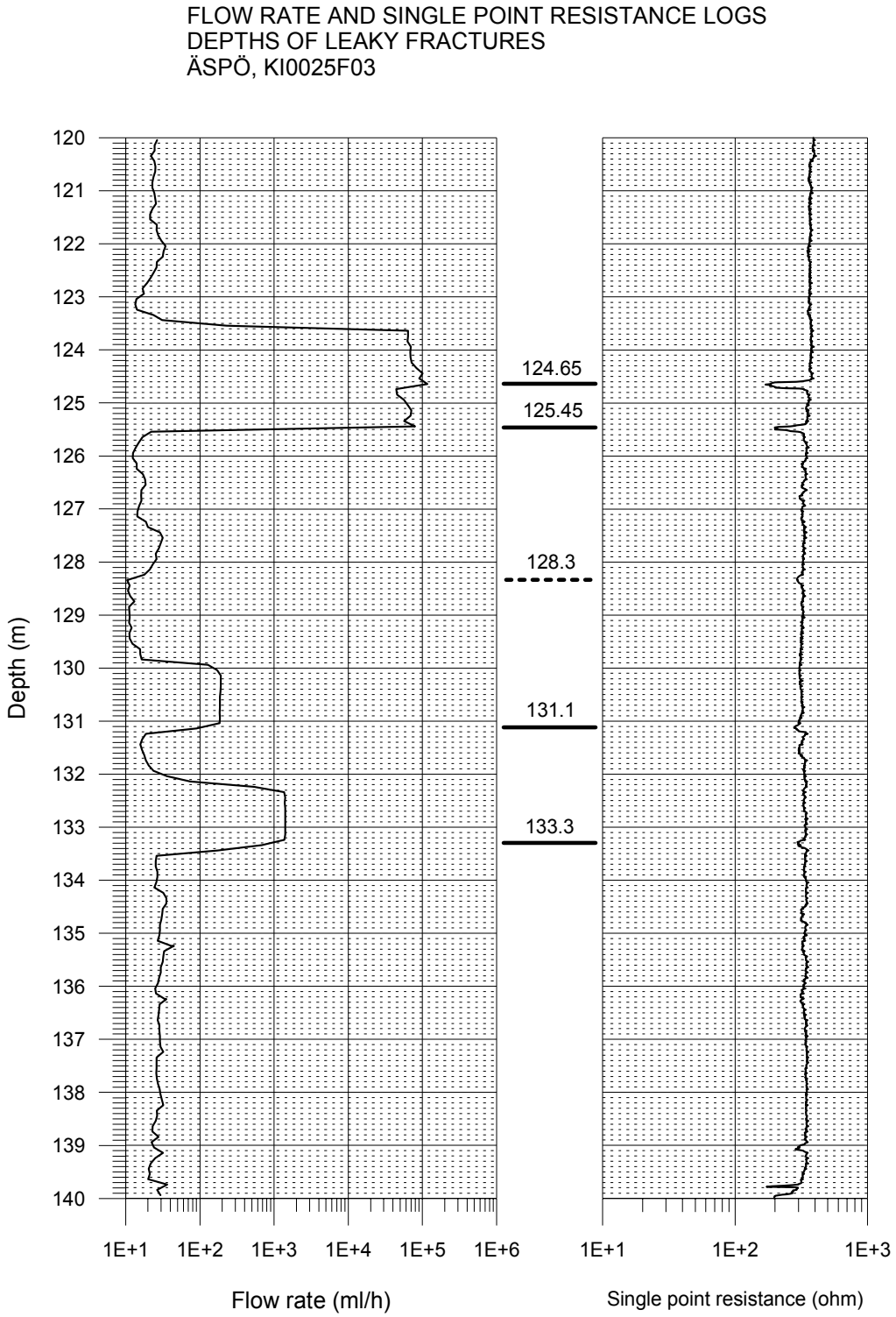

Figure 3-6. *Example of the POSIVA flow log of KI0025F03, section 120 to 140 m from /Rouhiainen and Heikkinen, 2001a/.*

3.3.4 Comparison and evaluation of flow logging methods

The flow logging methods used by the TRUE Block Scale project evolved over the duration of the project. Packer flow logging was initially used. The main advantage of packer logging is its simplicity and the relatively high assurance that borehole intervals are truly sealed and accurately measured flow from the intended section of the borehole. The major disadvantage to packer flow logging is the time required to perform the measurements. The coarse resolution is also a concern, which could be overcome by using shorter packer spacing. However, shorter packer spacing result in longer time requirements for testing.

The UCM ultrasonic flow log improved the process through its enhanced resolution over the period of the project. Early applications only found the few major conductors in the borehole (or none at all as in KI0025F). In KI0025F02, the last hole that was logged, most of the major structures produced measurable signals. The primary use of the UCM tool is to measure cumulative flow rather than flow from discrete intervals, which limits its resolution. The fluid resistivity and temperature logs, which provide data to correct the flow signal for temperature and salinity effects, proved very useful for identifying groundwater sources with strikingly different thermal and chemical signatures in different parts of the holes.

The Posiva flow log was introduced part way through the TRUE Block Scale Project, and it became the sole flow-logging tool for the last borehole, KI0025F03. The Posiva flow log provided logging results of very high resolution. Along with the single point resistivity logs, the flow logs can locate conducting fractures within a few centimetres. This level of resolution greatly aided the selection of intervals for the packers making up the piezometer arrays. The detailed flow logging also provided the main data source for evaluating the transmissivity and frequency of background fractures, i.e. the conducting fractures that were not associated with the numbered deterministic structures.

3.4 Core logging system – BIPS and BOREMAP

The boreholes have been logged using conventional core logging in combination with BIPS images of the borehole wall.

The BIPS method is characterised by a typical flat continuous 360° digital colour image of the borehole wall as shown in Figure 3-7. The image of the cylindrical borehole wall can be described as a “rolled out carpet”, where the vertical up side of an inclined borehole is in the centre of the image and the vertical down side is divided in the middle and displayed at the extreme left and right sides of the image, respectively. A cylindrical probe with a downhole looking TV camera facing a conical mirror, which reflects the borehole wall into the camera, is lowered or pulled along the borehole with a constant velocity. A trigged coded pulse collects images as the camera is moved along

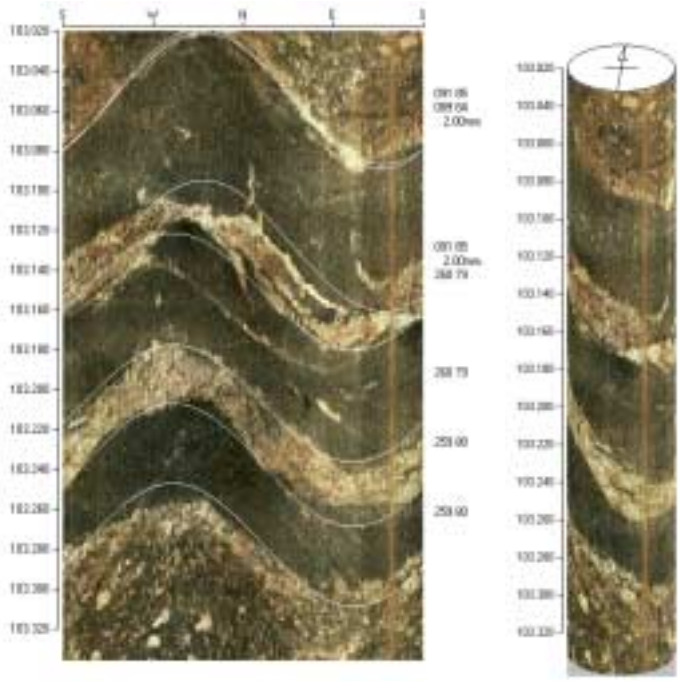

Figure 3-7. *Example of a planar unfolded BIPS image (left) and a cylindrical image (right). The sinusoidal lines show the interpreted orientation for (in this case) the rock contact between greenstone and Äspö Diorite.*

the borehole. An image processor converts the "cylindrical" image to an ordinary planar image. This image is then stored on magnetic-optical discs (MO-disks). As the relative orientation of the camera to the vertical up- or down sides is known at all times during the logging, the orientation of the planes of all structures within the borehole can be calculated, provided that the borehole geometry is known in terms of azimuth and inclination.

In a downward mode, the borehole is logged with a maximum velocity of 1.5 m/min. With normal resolution the images occupy about 1 MB of data storage space per metre logged borehole. About 200 m can be logged in one session. During the logging it is possible to observe fractures and veins on a monitor, as the probe moves along the borehole.

After the logging, the files stored on MO-disks are transferred to a PC equipped with mapping software (BOREMAP or BIPS mapping software) for orientation and mapping of structures in the borehole. Any planar structure crossing the borehole can be oriented and characterised in the mapping process.

Fractures in the crystalline rock found at Äspö HRL normally have a size (length) that is much larger than the borehole diameter. Further, the fractures are usually planar at the scale of the borehole diameter (0.076 m or less). Fractures therefore tend to have a sinusoidal appearance on the out rolled borehole wall image. By putting small digitised

markers on the sinusoidal-shaped structure, the system can calculate an orientation of the structure relative to the borehole direction. The borehole orientation (based on the drilling direction or deviation measurements) is used as reference for the orientation calculation of the mapped fractures, veins and rock contacts. The apparent width is measured as the calculated distance between two markers placed on the edges of the structure.

The mapping of the BIPS image is performed in combination with mapping of the core using the mapping system BOREMAP developed by SKB. The system allows for using the BIPS image as a complement to the more detailed information from the core. All geometrical information such as orientation and location along the borehole are taken from the BIPS image. The core makes it possible for the geologist to closely identify each fracture filling and other detailed characteristics. Information from both sources are entered into the BOREMAP database.

The structures are mapped using a standard characterisation chart, cf Table 3-2. The table consists of four main columns for describing the core/BIPS image. The header "Type" describes the type of structure (e.g. fracture, vein or contact). "Form" describes the form of the structure (e.g. planar, undulating or irregular). "Condition" describes the state of the structure (e.g. weathered, oxidised or open). "Remark" allows additional description of the mineralogy or infilling material observed in the structure (e.g. chlorite, quartz or aplite (fine-grained granite)). The rock types along the borehole are documented according to a similar characterisation sheet as shown above for fractures.

The mapping data in Table 3-2 are stored in the SKB site characterisation database (SICADA) together with mapping date and name of responsible geologist.

Table 3-2. Standard characterisation chart of the BIPS image analysis in BOREMAP.

No	Type	Form	Condition	Remark
0	Primary structure	Planar	Weathered	Quartz
1	Fracture	Undulating	Dull	Chlorite
2	Vein	Stepped	Cavities	Calcite
3	Fracture zone	Irregular	Open	Epidote
4	Contact	Network	Oxidized	Hematite
5	Structure	Breccia	Chloritisized	Pyrite
6	Alteration	Shear	Epitotized	Hybrid rock
7		Crushed	Tectonized	Clay
8		Flow structure		Granite
9		Foliation		Pegmatite
10				Aplite
11				Mylonite

3.5 Drilling responses

An important lesson learned from underground hydraulic experimentation is that every event or activity that disturbs the flow system is a source of information to characterise the studied rock volume. Drilling activities are very good examples of this principle, as the measurements of flow from boreholes during drilling and the associated pressure responses of the monitoring system are some of the simplest, but most useful data for developing the hydro-structural model of the TRUE Block Scale rock volume.

An analysis of drilling response data begins with the activity logs of the drilling of the borehole. The driller's logs include information on the time of starting and stopping each coring run, and the associated depth of the hole, and a measurement of the cumulative flow from the hole. Each core run requires entries in the driller's records, hence the information appears no less frequently than the length of a core barrel (in the case of TRUE Block Scale every three metres). A measurable change in outflow from the hole indicates the intersection of a new conductor, as the flow to the borehole increases to reflect that feature's contribution.

When the flow to the drilled hole increases, the groundwater pressure in some intervals of the piezometers in other boreholes typically respond with a pressure drop. The intervals that show such behaviour are those that either contain the conductor intersecting the new hole, or are part of the same network as that conductor. In other words, the new borehole becomes a short circuit for a conductor at initially ambient pressure to atmospheric pressure where the conductor intersect in the open hole being drilled.

For each borehole, the time line of the drilling progress and the pressure responses throughout the monitoring network were prepared. Vertical lines mark the times when the drillers observed significant changes in the water inflow to the hole. Figure 3-8 shows an example of one of these plots. Tabulations of inflow points in the new hole against the magnitudes of pressure responses in the neighbouring piezometers effectively mapped the network of conductive structures through the piezometer array.

Early in the site characterisation, the pressure responses from drilling are used to develop hypotheses about the conducting network. Candidate structures are those which have a flow point in one hole and a strong pressure response in another. Pressure interference responses to build-up or flow tests after the drilled hole has been instrumented with a piezometer can confirm these connections. Later in the site characterisation the network of conducting structures is largely established. Pressure responses to drilling then confirm the structural model and complement later flow logging to determine the exact intercept points of the structure in the new hole. The absence of a response from a known conducting feature may indicate that it does not intersect the new borehole. Such information provides a basis for locating where conductive structures may terminate in the rock mass.

Responses in the monitoring network propagate rapidly after a new hole intersects a conductor, time lags in the network are not a source of ambiguity for interpreting the records. One potential source of error arises from external pressure changes exerted on the pressure measurement tubes. In the GEOSIGMA piezometer and in the Solexperts piezometer in KI0023B, some pressure lines are exposed to external water pressure as they pass through intervals other than those they are monitoring. Pressure changes external to the measurement tube can cause the tube to expand or contract. However, this is a problem only if the tube is monitoring a very low transmissivity interval, of which there are few in the array. The significance of this source of error is consequently regarded to be minimal.

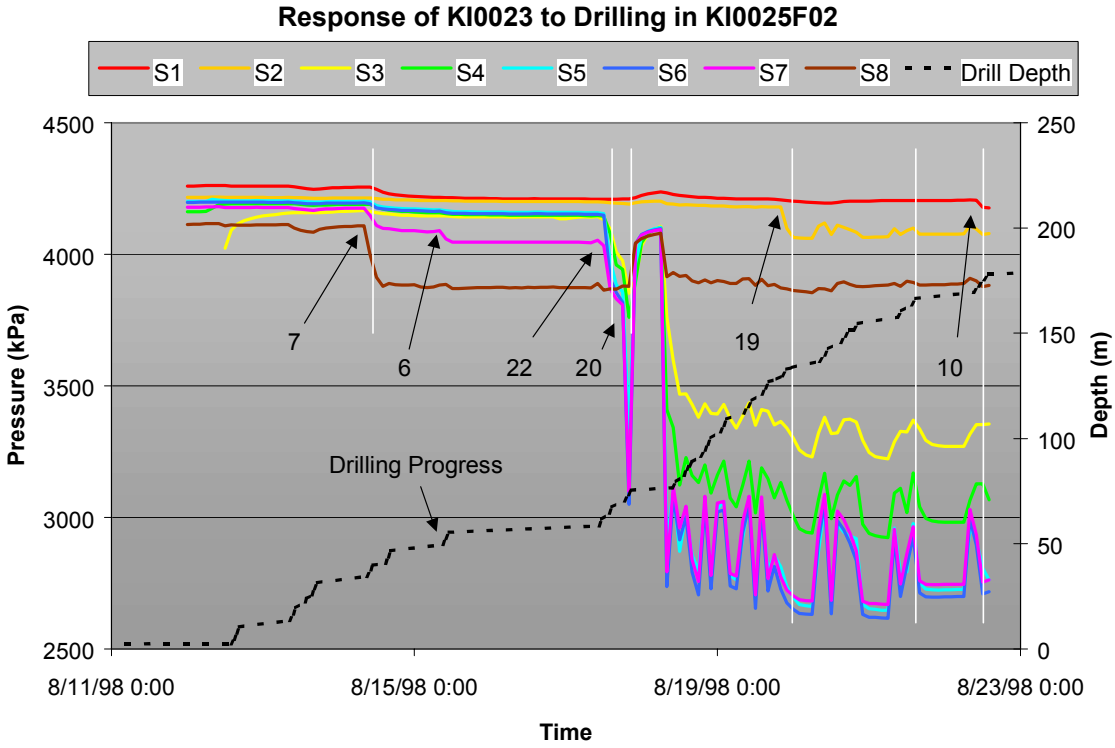

Figure 3-8. *Pressure responses versus time in piezometer intervals of KI0023B during the drilling of KI0025F02. Numbers denote intersection of deterministic structures. White lines show time when inflow increased to KI0025F02.*

3.6 Hydraulic tests

3.6.1 Purpose of hydraulic tests

Hydraulic tests were performed during all stages of the project with different objectives:

- basis for the definition of multi-packer configurations after the drilling of a new borehole,
- estimation of hydraulic parameters (transmissivity and storativity) as an input to the hydro-structural model, cf Chapter 4,
- measure of connectivity between the boreholes as an input for the hydro-structural model, and in combination with tracer dilution tests (see Section 3.7) for the definition of the tracer test configuration,
- to obtain a drawdown data set for numerical modelling,
- to assess the dominant flow regime and the boundary conditions, cf Chapter 6.

The methods used included both single-hole tests and cross-hole tests, the latter also in combination with tracer dilution tests.

3.6.2 Single-hole tests

The single-hole tests were performed with the GEOSIGMA/SKB hydraulic test equipment, (UHT 1), documented in /Gentzschein and Morosini, 2001/. UHT 1 is constructed for underground hydraulic testing in 56 mm and 76 mm diameter boreholes. Maximum borehole length is 300 m and the maximum working depth is 500 metres below sea level. The main parts of the system are (see Figure 3-9):

- **Down-hole System**: including packer system (double or single) for isolating the target test interval, down-hole shut-in valve, central tubing, and control lines for packer inflation and pressure measurement.
- **Hoisting Rig**: for installing and removing the packer system.
- **Surface System**: including data acquisition, flow meters, flow and pressure control and measurement equipment.

The down-hole system includes a flow bypass that connects the guard intervals below the lower packer and above the upper packer (i.e. the entire borehole except the test interval).

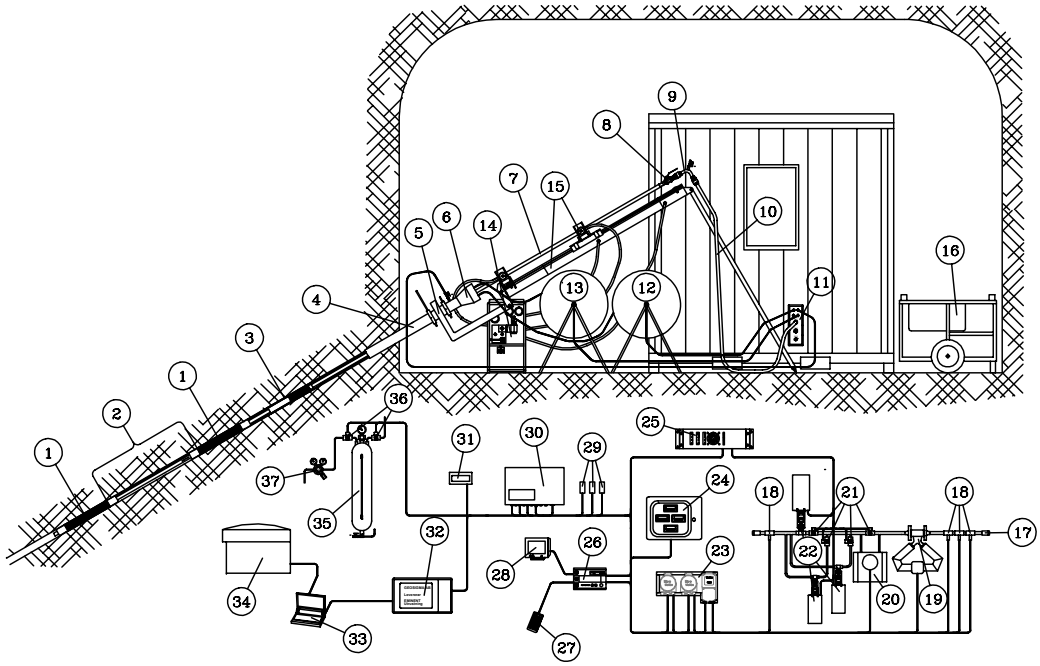

1. Packer
2. Measurement section
3. Test valve
4. Casing
5. Extension beam
6. Sealing device
7. Pipe string
8. Adapter
9. Tube bend with air evacuation valve
10. Measurement hose from borehole
11. Wall leadthrough
12. Hose reel, packer
13. Hose reel, section pressure
14. Control board, hoisting rig
15. Feed beam, hoisting rig
16. Power unit, hoisting rig
17. Inlet to container
18. Sensors, pressure, temperature, electrical conductivity
19. Flow meter “BIG”
20. Flow meter “small”
21. Valves
22. Regulation valves
23. Amplifier to Flow meter unit
24. Display for Flow meter unit
25. Stepping motor
26. Regulation computer
27. Regulation computer, keyboard
28. Regulation computer, monitor
29. Pressure transducers
30. Data scan box
31. External display
32. Measurement computer (SPC Rabbit)
33. Evaluation computer (Compaq)
34. Laser Jet printer
35. Pressure tank, packer inflation
36. Solenoid valves
37. N_2-gas regulator

Figure 3-9. *Overview of the UHT 1-system.*

Single-hole double packer tests were usually performed after the drilling of a new borehole /Gentzschein and Morosini, 2001; Adams, 2001/. The test intervals were chosen based on the results from core analysis, BIPS and flow logging. At some locations the planned duration of the single-hole tests of about 30 minutes was increased and the evaluation included also cross-hole interference responses /Adams et al, 2001; Gentzschein and Ludvigsson, 2001/.

The hydraulic single-hole tests were usually performed by withdrawing water from the test interval at a constant rate between 0.2 and 3 l/min, or by establishing a constant head in the section some 50 to 200 m below the static head of the formation. These tests were followed by a pressure recovery period. Pulse tests were performed in a few test intervals with a very low transmissivity ($<1 \cdot 10^{-10}$ m^2/s).

The analysis of conventional single-hole pumping tests started with an evaluation of diagnostic plots of the pressure or flow rate responses in order to assess the flow regimes and boundary effects. Steady-state conditions were instated rapidly in many tests. This indicates that the tested fractures are connected to dominant structures at a relatively short distance. These tests were analysed with the Dupuit-Thiem formula /Kruseman and de Ridder, 1991/ or Moye's formula /Moye, 1967/.

The diagnostic analysis of tests within dominant structures usually indicated radial flow periods during intermediate times and constant head type boundary effects at late times. The latter can be attributed either high transmissive fractures on a larger scale which bound the experimental site, or to a spherical flow regime. Similar observations were also made in the analysis of the TRUE-1 hydraulic test data /Winberg et al, 2000/.

One step-drawdown test was conducted in an interval of a borehole to evaluate effects of turbulence or fracture aperture variation for typical flow rates between 0.1 and 0.6 l/min, and drawdowns between 50 and 400 m, respectively. This test showed only a relatively small deviation from a linear relationship between drawdown and flow rates at high drawdowns and flow rates, cf Figure 3-10 KI0025F02 /Adams et al, 2001/. In the case of the TRUE-1 characterisation /Winberg et al, 2000/ a compilation of flow rates and drawdowns (from different times) for the main pump section showed a linear relationship for small drawdowns (<300 kPa) and low flow rates (<1 l/min), above which a deviation from the initial trend is visible.

The above result is consistent with the very good agreement, cf Figure 3-11, of specific capacity values (flow rates normalised with drawdown, Q/s) obtained from POSIVA logging with the Q/s values obtained from single-hole double packer tests in KI0025F02. This agreement is not good for Q/s values higher than $2 \cdot 10^{-7}$ m^2/s because the inflows exceed the upper measurement limit of the POSIVA logging of about 3 l/min. It is important to note that the Q/s values are representative for the local transmissivity around the test intervals according to recent research by /Meier et al, 1999/.

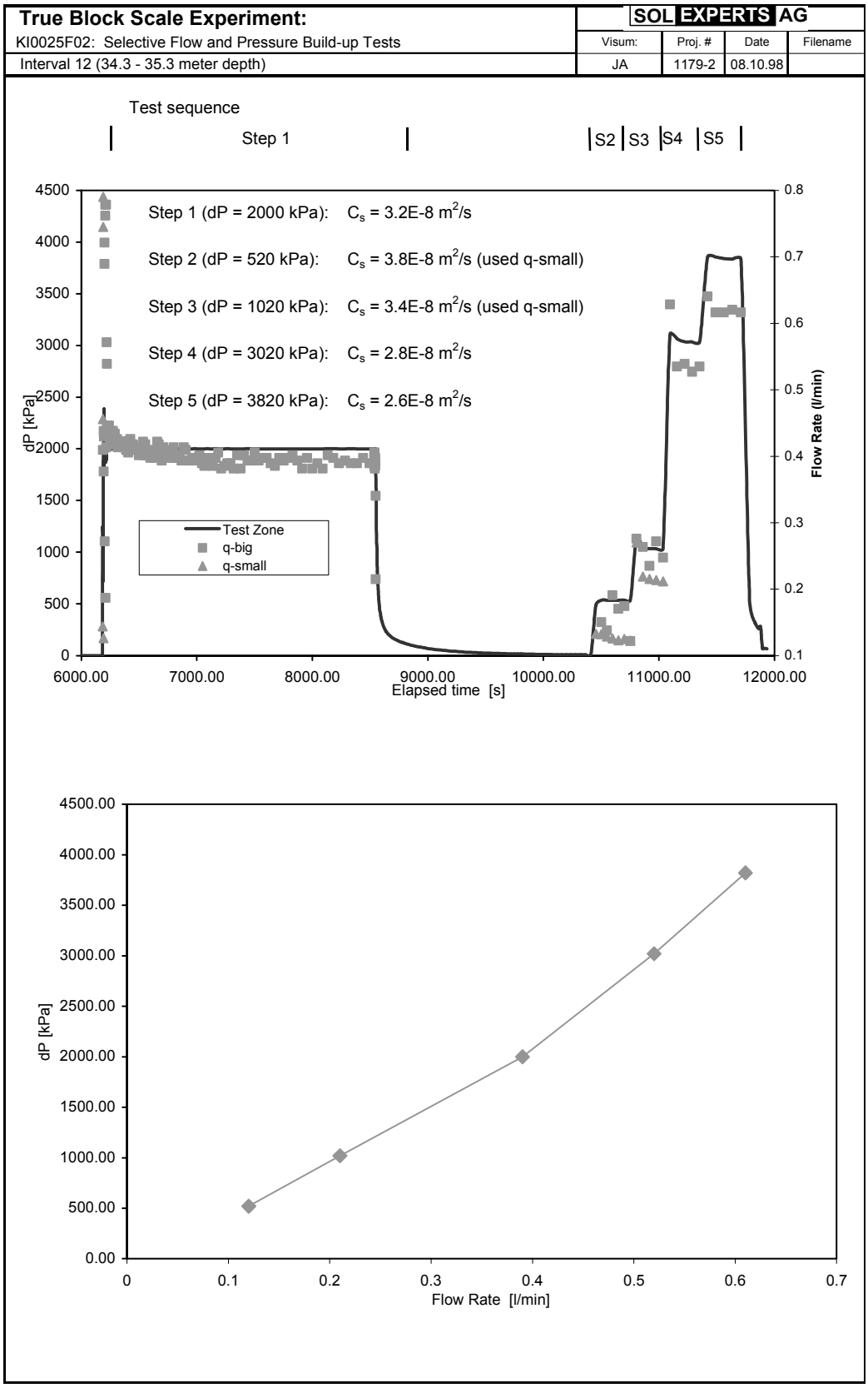

Figure 3-10. *Step-drawdown analysis for the interval L=34.3–35.3 m in borehole KI0025F02 /Adams et al, 2001/. Note that the drawdown-flow rate relation remains linear over a large range.*

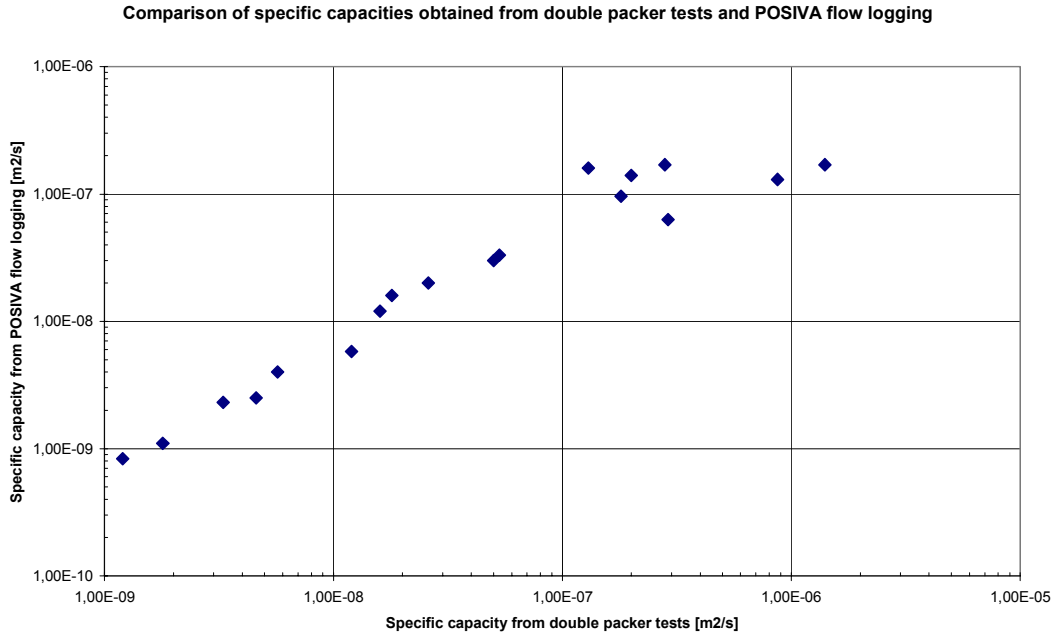

Figure 3-11. *Correlation between specific capacity measurements (Q/S) obtained from POSIVA flow logging and Q/s values obtained from double packer flow and pressure build-up tests. Note that the flow measurement limit of the POSIVA logging was exceeded for values over* $2 \cdot 10^{-7}$ m^2/s.

3.6.3 Cross-hole hydraulic tests

After instrumentation of the borehole with multi-packer piezometer systems, cross-hole hydraulic tests were performed. These tests were sometimes combined with tracer dilution tests, cf Section 3.7. The cross-hole tests were generally performed by establishing sinks through opening of the two flow lines connected to each section. The sinks were in most cases established using maximum possible flow, only restricted by the dimension of the tubing and the transmissivity of the section.

The hydraulic responses have been evaluated in different steps, each at which part of the data has been sorted out for further (quantitative) evaluation. This procedure was necessary in order to restrict the quantitative evaluation to a manageable amount of data.

First, time-drawdown and time-recovery plots were prepared for sections showing a drawdown (or recovery) of more than s_p=1 kPa at the end of the tests. This threshold value was selected with due consideration of the amplitude of the tidal effects. These types of plots were used to estimate the response times (t_R) for each section. The response time is here defined as the time, after start of flowing, when a drawdown (or recovery) of 1 kPa is observed (in the logarithmic plots) for the actual observation section.

To account for the different flow rates used in the tests and to make the response plots comparable between tests, the final drawdown at stop of flowing (s_p) is normalised with

respect to the flow rate (Q). The ratio s_p/Q is plotted on the Y-axis. On the X-axis, the ratio of the response time to the squared distance R in space (t_R/R^2) between the (midpoint of the) source section and (the midpoint of) each observation section is plotted. The latter ratio is inversely related to the hydraulic diffusivity of the rock, a parameter which indicates the speed of propagation of the pressure signal in the rock created by the drawdown in the flowing section.

From the response plots of s_p/Q versus t_R/R^2 for each test, sections with anomalously fast response times (high hydraulic diffusivity) and large (normalised) drawdown can be identified in the upper left corner of the diagram. Such sections, showing primary responses, can be assumed to have a distinct hydraulic connection to the flowing section and may be intersected by fracture zones or other conductive structures in the rock. On the other hand, sections with delayed and weak responses, in the lower left corner, may correspond to sections in the rock mass between such structures. An example is shown in Figure 3-12, where the response to the sink KI0023B:P6 is shown where very good responses are indicated in Structure #20, and in the section KI0023B:P5, which is adjacent to the primary sink section KI0023B:P6.

From the calculated values of s_p/Q (index 1) and t_R/R^2 (index 2) for each observation section, and from each test, a common response matrix, showing the response patterns for all tests, was prepared by classifying the responses by means of the above indexes 1 and 2. This response matrix (see Figure 3-13) was used to get an overview of the response pattern obtained from different tests (sinks).

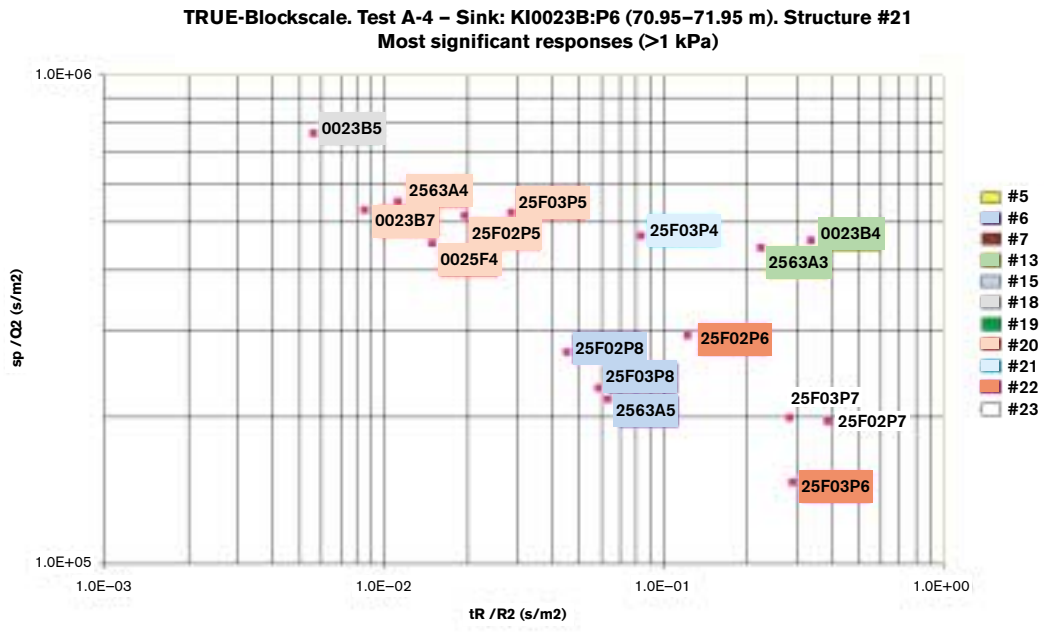

Figure 3-12. *Pressure response plot showing the most significant responses during test A-4. Colour labels refer to structures in the March 2000 hydro-structural model /from Andersson et al, 2000a/.*

Sink in Structure		#20	#21	#20	#21	
Borehole	Interval (m)	A-1	A-2	A-3	A-4	Structure
KA2511A:T1	239-293	B		B	B	#10,11,18
KA2511A:T2	171-238	B		B	B	#19
KA2511A:T3	139-170	B		B	B	# ?
KA2511A:T4	111-138	B		B	B	#20
KA2511A:T5	103-110	B		B	B	#16
KA2511A:T6	96-102	B		B	B	#6
KA2511A:T7	65-95	B		B	B	# ?
KA2511A:T8	6-64	B		B	B	#4,7
KA2563A:S1	242-246	B		B	B	#19
KA2563A:S2	236-241	B		B	B	#19
KA2563A:S3	206-208	M	B	G	M	#13
KA2563A:S4	187-190	E	G	E	G	#20
KA2563A:S5	146-186	G	M	G	G	#6,7
KI0025F:R1	170.5-195.5			B	B	Z
KI0025F:R2	165.5-169.5	B		B	B	#19
KI0025F:R3	90.5-164.5	B		B	B	?
KI0025F:R4	87.5-89.5	G	M	G	E	#20,22
KI0025F:R5	42.5-86.5	B		B	B	#7
KI0025F:R6	5-41.5	B			B	# 5
KI0023B:P1	113.7-200.7				B	#10
KI0023B:P2	111.25-112.7	B		B	B	#19
KI0023B:P3	87.20-110.25	Uncertain				
KI0023B:P4	84.75-86.20	B	B	M	B	#13
KI0023B:P5	72.95-83.75	G	B	G	E	#18
KI0023B:P6	70.95-71.95	G	M	G	S	#21
KI0023B:P7	43.45-69.95	G	G	E	E	#6, 20
KI0023B:P8	41.45-42.45	B		B	B	#7
KI0023B:P9	4.6-40.45	B			B	#5
KI0025F02:P1	135.15-204.18				B	
KI0025F02:P2	100.25-134.15	B			B	#19
KI0025F02:P3	93.35-99.25	B	B	B	M	#13,21
KI0025F02:P4	78.25-92.35	Tight				#?
KI0025F02:P5	73.3-77.25	G	B	S	G	#20
KI0025F02:P6	64.0-72.3	M	B	M	M	#22
KI0025F02:P7	56.1-63.0	B	B	M	B	#23
KI0025F02:P8	51.7-55.1	G	M	G	G	#6
KI0025F02:P9	38.5-50.7	B		B	B	#7
KI0025F02:P10	3.4-37.5	B			B	#5
KI0025F03:P1	101.08-141.72	B		B	B	#19
KI0025F03:P2	93.58-100.08	B		B	B	
KI0025F03:P3	89.08-92.58	B	B	B	B	#13
KI0025F03:P4	85.08-88.08	M	S	M	G	#21
KI0025F03:P5	66.58-74.08	S	B	E	G	#20
KI0025F03:P6	59.58-65.58	B	B	M	M	#22
KI0025F03:P7	55.08-58.58	M	B	M	M	#23
KI0025F03:P8	51.58-54.08	G	M	G	G	#6
KI0025F03:P9	3.58-50.58	B		B	B	#5, 7
KA3510A:P1	122.02-150					
KA3510A:P2	114.02-121.02	B		B	B	#15
KA3510A:P3	4.52-113.02	B			B	#3,4,5,6,8
KA3548A01:P1	15-30				B	
KA3548A01:P2	10-14				B	
KA3573A:P1	18-40				B	#15
KA3573A:P2	4.5-17				B	#5
KA3600F:P1	22-50.1	B		B	B	
KA3600F:P2	4.5-21	B		B	B	#5, 7

INDEX 1=sp/Q
EXCELLENT
HIGH
MEDIUM
LOW
NO RESPONSE

INDEX 2=tr/R2
E=EXCELLENT
G=GOOD
M=MEDIUM
B=BAD

S=SINK

Figure 3-13. *Presssure response matrix for tests A-1 to A-4 /from Andersson et al, 2000a/.*

The results from the qualitative analysis were compared with, and checked for consistency and possible need of revision of the hydro-structural model. The derivative of the drawdown was used as a diagnostic tool in the interpretation of the flow geometry and deduction of hydraulic boundaries, and plotted jointly with the associated drawdown curves.

The main purpose of the quantitative interpretation of the interference tests was to estimate the hydraulic parameters and the hydraulic characteristics of the most significant responses during each test, as identified from the qualitative interpretation. The transmissivity, storativity and hydraulic diffusivity, and in some cases also the leakage coefficient, were estimated from the tests. The estimated hydraulic parameters were assumed to represent the hydraulic properties of some of the fracture zones tested. In addition, the quantitative interpretation also provided (soft) information on the flow geometry during the tests, including effects of outer hydraulic boundaries.

The quantitative interpretation (time-drawdown) was made using the code AquiferTest (Waterloo Hydrologic). As a standard interpretation model, the /Hantush, 1967/ model for constant flow rate tests in a leaky (or non-leaky) aquifer with no aquitard storage was used. This model was used because of its generality and its ability to analyse pure radial flow (Theis' type curve) as well as leaky (pseudo-spherical) flow. The type curve for r/L=0 in the Hantush' model (no leakage) corresponds to the classical Theis' type curve for radial flow. Tests showing periods with (pseudo)-radial flow were analysed using the Cooper-Jacob's /Cooper and Jacob, 1946/ method in semi-logarithmic graphs. For the analysis of the constant head tests, a varying (declining) flow rate was applied at the sink.

A log-log plot of drawdown at different observation intervals during a constant rate cross-hole test in the preferred sink selected for the tracer tests is shown as an example in Figure 3-14. All three methods provided very similar transmissivity and storativity estimates, cf Table 4-12.

In summary, short time single-hole pumping tests provided estimates of transmissivity at a local scale around the borehole intervals in the range between $1 \cdot 10^{-12}$ and $1 \cdot 10^{-5}$ m^2/s, whereas cross-hole tests provided (1) average values for T of about $1 \cdot 10^{-6}$ m^2/s for the interior parts of the TRUE Block Scale rock volume and (2) valuable information on the connectivity between the pumping and the observation wells.

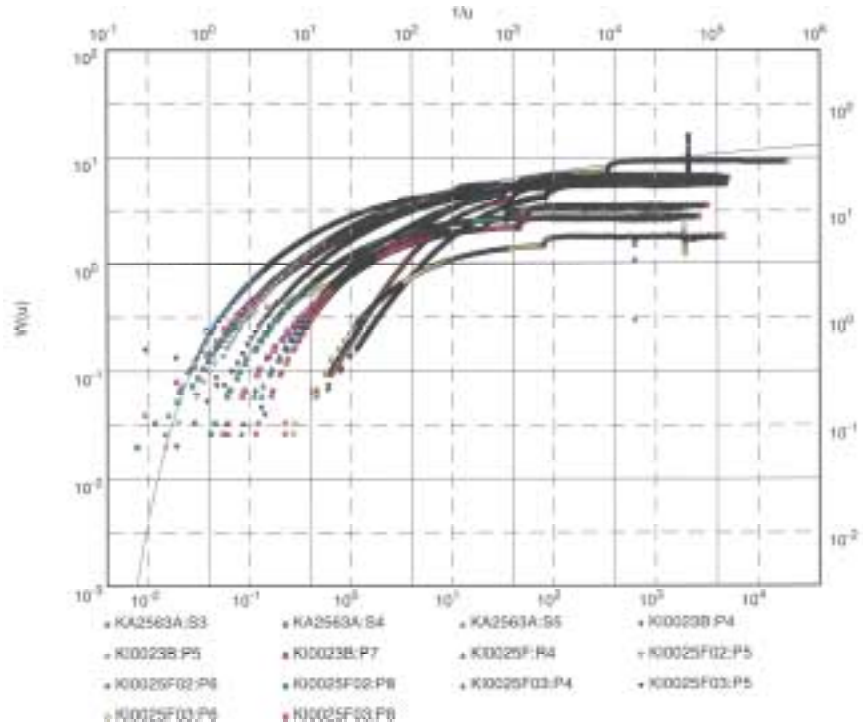

Figure 3-14. *Diagram showing drawdown versus t/R^2 for the combined cross-hole interference and tracer dilution test A-4 with sink in KI0023B:P6 (Structure #21) /Andersson et al, 2000a/. The dashed line represents the Theis' curve for section KI0025F:R4. Evaluated parameters; $T=8.6\cdot10^{-7}$ m^2/s, $S=1.4\cdot10^{-7}$.*

3.7 Tracer dilution tests

Tracer dilution tests have been extensively used throughout all phases of the site characterisation to determine groundwater flow rates /Andersson et al, 2000a, 2001a,b/. The tests have mainly been used to determine background flow and, in combination with pumping, to identify connected flow paths. The tests also aimed at identifying possible points for tracer injection by studying both flow and pressure responses to pumping in selected sinks.

The tests were performed in borehole sections specially prepared for tracer dilution tests by having three connecting lines, two for tracer circulation and one for pressure measurements. These sections were also equipped with volume reducers to minimise the water volumes and thereby also measurement times. The equipment outside the borehole, shown in Figure 3-15, was also used for tracer tests, cf /Andersson et al, 2000a/. The basic idea is to have an internal circulation of the borehole section. The circulation makes it possible to obtain a homogeneous tracer concentration in the borehole section and to sample the tracer concentration outside the borehole in order to monitor the tracer dilution rate.

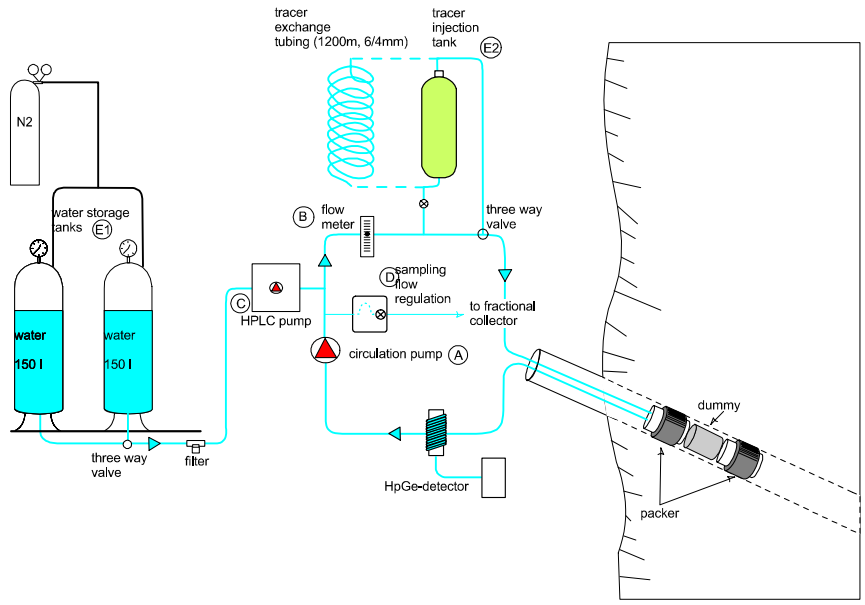

Figure 3-15. *Equipment used for tracer tests and tracer dilution tests in the TRUE Block Scale project. The option for tracer exchange and HpGe-detector were not used for the tracer dilution tests.*

The tests were mostly performed in campaigns with pumping in one to four different sinks and measuring the tracer dilution and pressure responses in up to 18 different sections. This was achieved by using up to six easily movable equipment set-ups. The governing design criterion was to enable measurement of flow rates down to 1 ml/h, which implied measurement times of up to 20 hours for each section.

Figure 3-16 shows an example of a result from a tracer dilution test performed in two steps, with and without sink ("natural" flow). In this case a marked increase of the groundwater flow through the measurement section can be noted by the change in slope of the tracer dilution rate indicating a good connectivity. It should also be noted that the magnitude of change in flow is also dependent on the flow direction. Hence, also a decrease in flow caused by the sink is indicative of the connectivity in that particular flow path.

The groundwater flow rates calculated from tracer dilution tests may also in principle be used to estimate Darcy velocity and hydraulic gradient. However, these parameters should be treated with caution given the influence of the borehole itself. The radius of influence around an ideal borehole is two times the diameter of the borehole but skin effects and short-circuiting of fractures with different hydraulic head may give a radius of influence of between 0.5 to 10 /Bidaux and Tsang, 1991/.

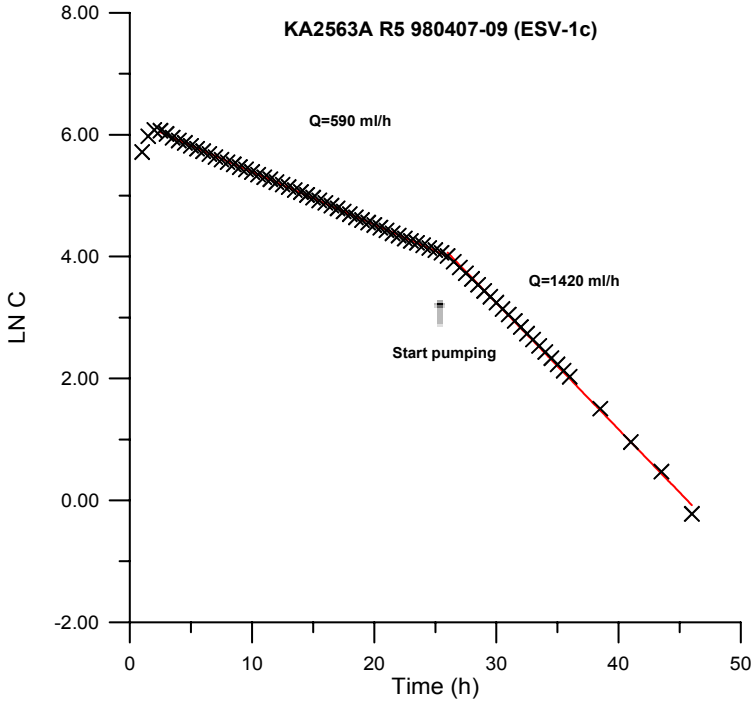

Figure 3-16. *Tracer dilution curve (logarithm of the tracer concentration versus time) in borehole section KA2563A:R5 before and after pump start for interference test ESV-1c (pumping in KI0023B:P6) /Andersson et al, 2001a/.*

3.8 Multiple-hole tracer tests

Tracer tests are one of the main components of the TRUE Block Scale Project. The most important objective of the tests is of course to explore the retention properties of the fractures and fracture network. That part is treated in a separate report /Andersson et al, 2002/ but there are also other purposes with tracer tests, namely to verify the hydro-structural model of the site and to explore the possibility of performing well-controlled (high recovery) tracer tests at the site.

The multiple-hole tracer tests were performed in conjunction with interference tests and tracer dilution test campaigns where results from these tests were used as input for the design of the multiple-hole tests /Andersson et al, 2000a,b, 2001a,b/. The strategy was to pick injection points with good flow response, i.e. borehole sections with high "natural" groundwater flow rate and large increase of the flow rate due to pumping at the selected sink. The idea was to choose injection points where a high mass flux of tracer could be achieved without disturbing the "natural" flow field. This was necessary in order to reduce the dilution of the tracer solution and thereby make it possible to detect the tracer at distances of 15–50 meters in a radially convergent flow field within reasonable time frames.

The tracers used in these verifying tests were the fluorescent dyes Uranine, Amino G Acid, and Rhodamine WT. These tracers are conservative (non-sorbing), well documented and often used as groundwater tracers due to their good dynamic range and low price /Smart and Laidlaw, 1977/. At later stages of the project the repeated use of Uranine resulted in an increase of the background concentration which made it necessary to choose other tracers instead, cf /Andersson et al, 2000b.

The tracers were injected by adding a pulse of concentrated tracer solution into the circulating flow field described in Chapter 3.10 and Figure 3-15. The tracer solution was then diluted by the "natural" groundwater flow through the injection section while circulated through the injection system for sampling and homogenisation. Thus, the procedure is identical to the tracer dilution test producing an input function similar to Figure 3-16. In the later stages of the project tracer injections were also performed by simultaneously injecting water (unequal dipole flow field) and thereby artificially increasing the injection mass flux, cf /Andersson et al, 2000b/.

These verifying tracer tests generally resulted in tracer breakthrough at the sink but not always with full mass recovery. The breakthrough curves were generally single-peak curves with some tailing. The tests were all first interpreted and evaluated with a relatively simple "basic" approach involving inverse modelling with only advection and dispersion and some analytical expressions for "equivalent" or averaged parameters as fracture width and flow porosity. The idea was to have this "basic" evaluation as a means of comparing different flow paths, rather than determining "true" transport parameters. Examples of breakthrough curves and model fits from Phase A /Andersson et al, 2000a/ of the Tracer Test Stage are shown in Figure 3.17. The evaluation and interpretation procedure is more thoroughly described in /Andersson et al, 2002/.

3.9 Porosity

Measurements of connected physical porosity have been carried out at the Swedish National Testing and Research Institute (SP), Sweden and the Research Centre for Energy, Environment and Technology (CIEMAT) in Spain. The samples analysed at SP are fault breccia pieces and wall rock (in two cases sectioned into 5 one centimetre thick slices). The samples are first dried at 110°C until a constant weight is reached (minimum 24 h), and are stored at room temperature under controlled conditions for 24 hours after which a dry weight is measured. The sample is then saturated with water until stable conditions are achieved, and the sample is weighed again. Subsequently, the samples are dried a second time and a new dry weight determined. From this data the bulk density is evaluated. The procedure was made according to the following certified procedures; SS-EN 45001, SS-EN 45002 and ISO/IEC 25.

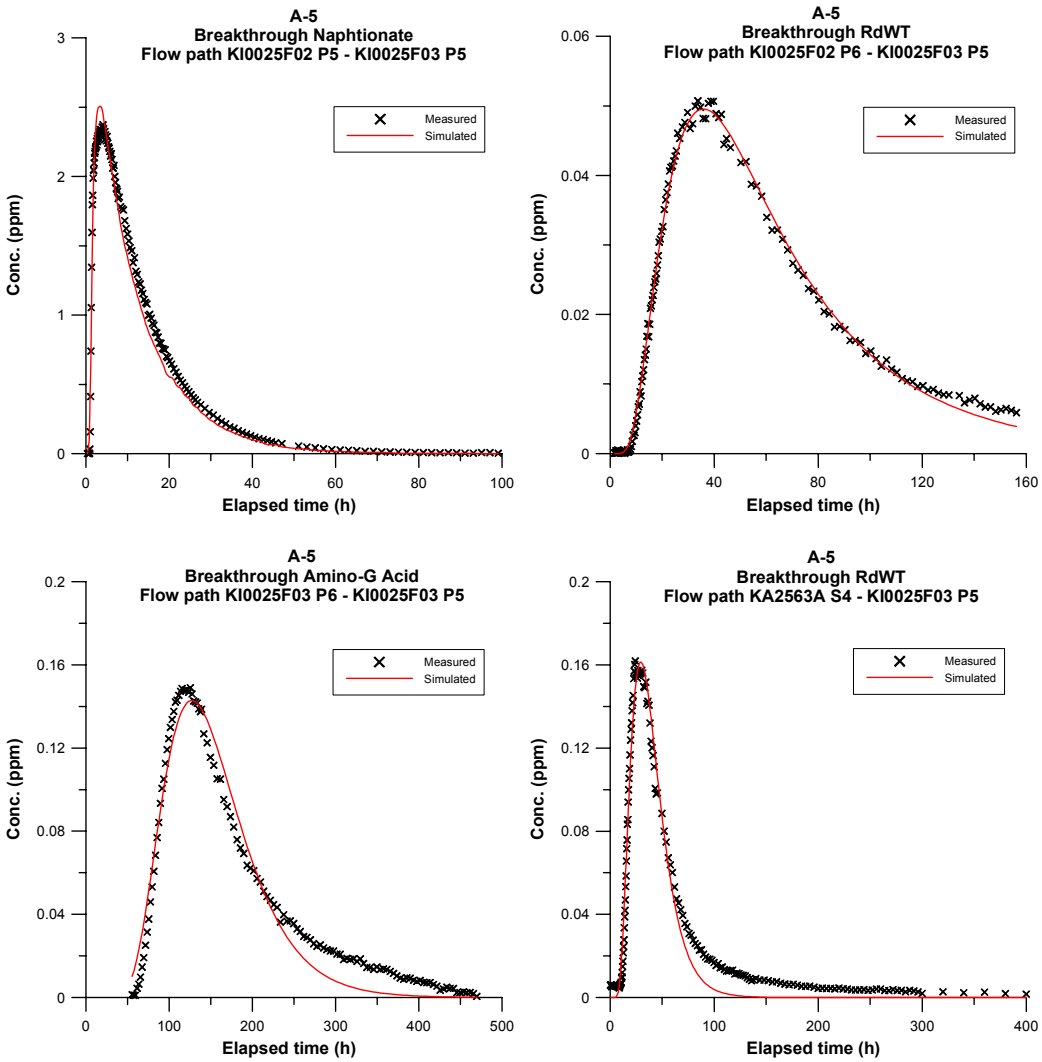

Figure 3-17. *Comparison between measured and simulated tracer breakthrough in KI0025F03:P5 during test A-5 /from Andersson et al, 2000a/.*

Compact density measurements were carried out on fine-ground rock samples. Measurements were carried out using a method denoted “SP method 1338”. The sample volume was measured by use of He-pycnometry. Together with the sample weight this gives the compact density. The procedure for calculation of total porosity is described in Section 7.2.2. The samples measured by CIEMAT were relatively small (<100 g) samples of fault breccia fragments and pieces (>1 mm in size) The water adsorption porosity was measured by the hydrostatic balance method, (ISO 6783-1982 or DIN 52103). The water porosity is defined as the ratio between the weight of the water gained after saturating the sample in water, and the weight of the dried material, expressed as a percentage. The density of the breccia fragments was measured by

the pycnometer method and is defined as the weight per unit volume of a considered substance. In order to determine the volume occupied by a substance, which dried weight is known with precision, the removed water weight by that substance is used.

The ^{14}C-PMMA method involves impregnation of centimetre scale rock cores with ^{14}C labelled methylmethacrylate (^{14}C-MMA) in a vacuum, irradiation polymerisation, autoradiography and optical densitometry with digital image processing techniques /Hellmut et al, 1999; Siitari-Kauppi et al, 1999; Kelokaski et al, 2001/. Impregnation with the labelled low-molecular-weight and low-viscosity monomer 14C-MMA, which wets the silicate surfaces well and can be fixed by polymerisation, provides information on the accessible pore space in crystalline rock that cannot be obtained with other methods. In this work ^{3}H labelled methylmethacrylate was also used to provide porosity information of fault breccia fragments.

Total porosity is calculated using 2D autoradiographs of the sawn rock surfaces. The geometry of porous regions is then visualised. The preconditions for applying this method are: (i) known local bulk density; (ii) presence of only two phases; minerals and PMMA; and (iii) homogeneous distribution of pores and minerals below the limit of lateral resolution of autoradiography.

3.10 Mineralogy

Qualitative mineralogical and textural interpretations were made using transmission light microscopy on thin sections of drillcore samples. Micro-probe analyses with a SEM-EDES equipment and connected Linc-system for evaluation available at the Department of Geology, University of Gothenburg, Sweden and at CIEMAT in Spain were used as complements. Both natural surfaces (gold plated) and thin sections (carbon plated) were analysed.

XRD (X-ray-diffractometry) was used for identification of especially clay minerals. The analyses performed at the Swedish Geological Survey (SGU) in Uppsala were carried out on a Siemens D5000. Diffractograms were obtained before and after treatment with ethyleneglycol, and after heating. The diffractograms obtained were evaluated using the software Diffrac plus. The analyses carried out at CIEMAT in Spain were performed using a Philips diffractometer (model PW 1840). The international ASTM tables were used for identification. All the determinations at CIEMAT were carried out with an Al sample holder, except the coating corresponding to KI0025F03 at 73.1 m, which was done with a Si sample holder due to insufficient amount of sample material. For this reason, this analysis cannot be compared with the results of the other analyses.

3.11 Geochemistry

Major element analyses were determined on fault breccia samples, sieved fraction <0.125 mm, using ICP-AES (Induced Coupled Plasma – Atomic Emission Spectroscopy) at Svensk Grundämmnesanalys AB (SGAB), Sweden. Sample measurements were integrated with measurements of international geological standards. The method has certification number SS-ISO 9002.

Trace elements determined using INAA (Instrumental Neutron Activation Analysis) at Studsvik Nuclear, Sweden have been carried out on the sieved fraction <0.125 mm of the fault breccia material. International geological standards are used for calibration. The certification number of the method is SS-ISO 9001.

Stable isotope analyses of calcites, in fault breccia material and fracture coatings, were carried out at at Institutt for Energiteknikk (IFE), Norway and at Consejo Superior de Investigaciones Cientificas, Spain, using a conventional technique; calcite samples being reacted with ultra-pure phosphoric acid at 25°C, according to the McCrea reaction:

$$2PO_4H_3 + 3CO_3Ca \leftrightarrow (PO_4)2Ca_3 + 3H_2O + 3CO_2 \quad (3\text{-}4)$$

The CO_2 obtained is introduced in a mass spectrometer for its isotope analysis, once it has been separated from the rest of the secondary products and purified by means of a system of cold traps at a vacuum of 4–10 mm Hg. The results are related to the international standard carbonates from the Pee Dee formation.

Uranium series analyses were carried out on the sieved fraction (<0.125 mm) of fault breccia materials. The analyses comprised ^{238}U, ^{234}U, ^{230}Th, ^{232}Th, ^{226}Ra and ^{228}Ra, and were determined by Alpha-Spectrometry at the Radionuclide Analysis Laboratory, AEA Technology, UK using the following method; Accurately weighed aliquots of powdered samples were spiked with U-236 and Th-229 chemical yield monitors and ashed at 450°C. The samples were then dissolved in nitric acid solution followed by treatment with mixtures of hydrofluoric, nitric and perchloric acids. U and Th were co-precipitated with iron(III)hydroxide by the addition of aqueous ammonia to pH 7. The precipitates were then dissolved in hydrochloric acid and U and Th were separated on an anion-exchange resin in chloride form, and further purified by anion-exchange chromatography from nitric acid solution. The U and Th were then electrodepositied onto stainless steel discs and measured by alpha spectrometry. Analyses were also carried out at CIEMAT, Spain using similar procedures; “Procedure for the determination of U isotopes in soils by alpha spectrometry” (PR-X2-09) and “Procedure for the determination of ^{230}Th in soils” (PR-X2-01). ^{226}Ra was determined by gamma spectrometry.

3.12 Hydrogeochemistry

Within the TRUE Block Scale project, groundwater sampling and chemical analyses have been performed following a few standardised Äspö HRL procedures (denoted sampling and analysis classes). The complexity of the sampling (number of bottles, filtering, preservation etc) and the extent of the analysis are defined by the class number (1, 2, 3, 4 or 5). The five chemistry classes differ in the number of analysed components/parameters and thus also in the complexity of the sampling procedure, the higher the number the more complex /SKB, 2001/.

Class 1, Class 2 and Class 3 are simple procedures. Water samples can be collected in any clean bottle of appropriate volume.

Class 4 includes on-line filtering, preservation and special bottles.

Class 5 includes all class 4 analyses and in addition, one or more of the so called special analyses (isotopes, trace elements etc) performed by external laboratories. These latter determinations are all optional and can be combined in a suitable way depending on the purpose of the investigation also to lower classes. In the case of TRUE Block Scale classes 2, 4 and 5 have preferentially be used.

3.12.1 Sampling procedures

The equipment used to collect samples from the boreholes located in the tunnels consists of valves, Tecalan tubing, Swagelok stainless steel fittings, pressure gauges, on-line filters (Nucleopore, complete with holder and tubing) and high capacity filters (Colly Company). The pore size of the filters was 0.45 μm.

The borehole sections are flushed prior to the sampling, such that the quantity of water which is removed from the borehole is equivalent to five times the volume of the test section. This is done in order to collect fresh and representative water from the water bearing fractures and not a mixture containing water which has been staying in the borehole and the tubing system.

Before the sample is collected, the proper sampling flow is measured using a graduated plastic vessel and a stop watch. Details on the sample handling and preservation in relation to different types of analyses are given by /Säfvestad and Nilsson, 1999/.

3.12.2 Analyses

The analyses are performed in the SKB Mobile Field Laboratory stationed at Äspö HRL and by consulted external laboratories. The Mobile Field laboratory and its equipment are described in by /Almén et al, 1986/. The laboratories, methods and measurement uncertainties are listed in Appendix B.

4 Hydro-structural models

The hydro-structural model describes the main geological and hydraulic features in the experimental block in terms of geometrical, geological/mineralogical characteristics and hydraulic material properties. The interpretation is based on the geometrical, geological and hydraulic characteristics of the intersection points of individual fractures or zones along the boreholes, and the hydraulic behaviour (connectivity) between two or more of these intersections points, cf Section 2.3. Radar and seismic investigations have at times provided partial support in the interpretation of the extension of the structures between the observed intersection points and beyond. However, it is important to note that the studied rock volume contains many more fractures, both conductive and non-conductive, that are not explicitly included in the deterministic hydro-structural model. Rather, the model is at all times the simplest explanation (hypothesis) in relation to a series of hydraulic and geological observations. There is most likely more than one fracture involved in many of the interpreted conductive structures. The development of the hydro-structural model has been sequential and iterative over time, adding more geological, geometrical and hydraulic information with each new borehole. In consequence, at the termination of each characterisation stage the hydro-structural model constitutes a hypothesis in it self, to be tested by subsequent investigations.

Independent support for the developed hydro-structural model based on hydrogeo-chemical data is presented in Chapter 6. In this chapter, an account is also given of the hydraulic head and natural flow situation in the investigated rock block.

4.1 Location of the experiment to the –450 m level: The first structural model of the experimental volume

The initial evaluation of the selected experimental site was based on the structural models presented by /Rhén et al, 1997b/ and /Hermanson et al, 1996/. The model by /Rhén et al, 1997b/ was part of the geo-scientific evaluation of the laboratory excavation phase whereas the model by /Hermanson et al, 1996/ constituted a first attempt on a detailed hydro-structural model for the 450 m level of the laboratory, cf Figure 4-1 with the purpose of identifying candidate sites for TRUE Block Scale. Both of the indicated models mainly contain information about large-scale structures cutting through the laboratory and the access tunnel, and essentially consisted of two-dimensional plan view maps of the area. However, the extent and orientation of the largest structures were also estimated in three dimensions.

Prior to the onset of the Scoping Stage of the project, the TRUE Block Scale rock volume was intersected by one pre-existing southeast trending borehole, KA2511A, drilled from the 320 m level towards the southwest, cf Figure 4-1. The hydraulic and structural information from this borehole /Olsson et al, 1994/ indicated at least one highly conductive NNW trending fracture zone (NNW-5) going through the centre part

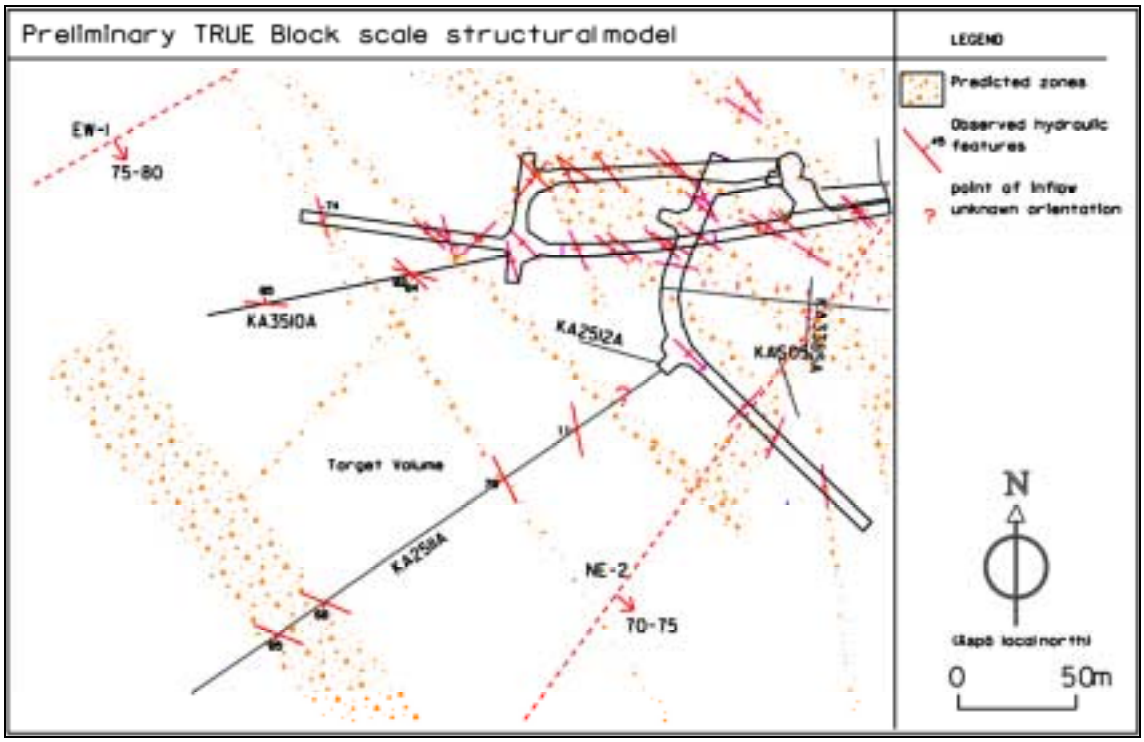

Figure 4-1. *The Preliminary Structural model of the proposed experimental area for the TRUE Block Scale experiment after /Hermanson et al, 1996/.*

of the block and two large bounding structures in the northwestern corner of the block (EW-1) and in the southeastern corner (NE-2) /Rhen et al, 1997b/. Both these latter fracture zones are observed in several boreholes, on the surface or along the main access tunnel.

4.2 Scoping Stage: boreholes KA2563A and KA3510A

The Scoping Stage included drilling of the pilot borehole KA2563A and KA3510A (the latter drilled outside the direct scope of the project). The geological information from these boreholes showed a rock mass of Äspö diorite containing sections of fine-grained granite and greenstone, and transected by sections of tectonised rock. Geological structures which intersect the rock mass show a complex plastic and brittle deformation history and tend to be predominantly northwest trending and steeply dipping. Hydraulic pressure monitoring during drilling and subsequent hydraulic tests between boreholes showed good hydraulic connectivity within the block. Large single inflows complicated the drilling process and required significant grouting in several sections in both boreholes, cf Section 2.1.1. The grouted zones were concentrated to a group of northwest trending steep fractures in the north-eastern part of the investigated block. One of the fractures (at L=103 m in KA2563A) had a notable 700 l/min inflow sustained over time, and was identified to be a single fracture with a 1–2 cm wide aperture at its intersection point in KA2563A as shown in Figure 4-2. This structure corresponds to Structure #5 in the hydro-structural model.

Figure 4-2. *The main contributor to the 700 l/min inflow in KA2563A: a single fracture centimetre wide fracture at L=103 m. The structure was subject to extensive grouting, cf Section 2.1.1. The fracture is interpreted as Structure #5 and is interpreted to be closely linked to several sub-parallel structures.*

In total eighteen deterministic structures were interpreted in the block with variable degree of detail and are shown in the structural model shown in Figure 4-3a. Three of the structures where interpreted to be sub-horizontal with a possible extent through the block. All other interpreted structures were steeply dipping with a predominance of northwesterly trending reactivated plastic deformation features, and single open fractures without any appreciable plastic deformation history.

Borehole KA2511A /Olsson et al, 1994/, cf Figure 4-1, existed prior to the onset of the TRUE Block Scale project. The responses to hydraulic disturbances which were measured in the KA2511A piezometer were atypical of the block as a whole. First, all of the monitored sections in KA2511A appeared to be well connected to one another and to the zone that required grouting in KA2563A (Structure #5). Most of the remaining structures in the TRUE Block Scale rock volume, however, do not appear to have hydraulic connection to KA2511A. The observed connectivity of the monitoring intervals in KA2511A raised concerns that its piezometer might be faulty. However, repeated checks and re-installations of the piezometer did not result in any change in the hydraulic behaviour of the piezometer. The apparent lack of connectivity of KA2511A to the rest of the TRUE Block Scale rock volume implied that the borehole could play little or no role in the subsequent tracer tests.

In summary, the Scoping Stage resulted in a first detailed interpretation and definition of geological structures within the investigated rock volume. As a result, subsequent investigations could be focussed on a smaller rock volume to locate networks of

structures suitable for tracer experiments. This area was laterally delineated by Fracture Structures #6 and #7 in the north, Structures #10, #11 and Fracture NE-2 in the south and east and Structure #8 in the west, cf Figure 4-3a.

4.3 Preliminary Characterisation Stage: boreholes KI0025F and KI0023B

Borehole KI0025F was drilled from the I-niche at the 450 m level with the objective to further confirm the existence of the northeastern fracture set and its geological and hydraulic characteristics, and further to collect information about vertical boundaries and the hydraulic gradient within the studied block. The completion of borehole KI0025F revealed three new structures and resulted in moderate re-interpretations of the geometry of previously interpreted structures /Hermanson, 2001a/, cf Figure 4-3b.

The Fracture Zone Z which was found at the bottom of the KI0025F is the largest structure observed within the block and is interpreted to be a splay of a larger-scale structure, either Fracture zones NE-1 or EW-2, cf Figure 1-3. The geological character of the Fracture Zone Z is dominated by fault crush and intensely deformed host rock, decimetre to metre wide. Mobilised unconsolidated gouge material (cf Section 4.7 for definition of gouge materials) from this structure threatened to fill the bottom of the borehole requiring a packer to isolate the deeper part of the borehole.

Data from KI0025F were used to identify Structures #19 and #20 within the target volume /Hermanson, 2001a/. Both structures are described as reactivated mylonites with widths varying between one to ten centimetres. These structures were likely reactivated to produce gouge material. Structure #19 is considered as an intermediate hydraulic boundary in the southwest of the target area of interest, whereas Structure #20 is centrally located in the foreseen target volume for future in situ experiments.

The observed hydraulic responses in KA2563A (Figure 4-4) to the drilling of KI0025F clearly show connections along the interpreted Structures #7, #20, and #19. The pressure responses to drilling activities were found to be a very useful tool for assessing fracture and structure connections and extents, cf Section 3.5.

The next borehole, KI0023B, was drilled between KI0025F and KA2563A to further define the geometrical, hydraulic and geological character of Structures #19, #20 and #9 and to sample the interior of the proposed target volume. Table 4-1 shows a comparison between predicted and interpreted intercepts of structures in terms of borehole depth.

The double packer flow logging, 3D cross-hole seismic investigation, and a series of interference tests (detailed below) defined a new structure in the target area. This structure was denoted Structure #13, and it is sub-parallel to Structure #20 (Figure 4-3c).

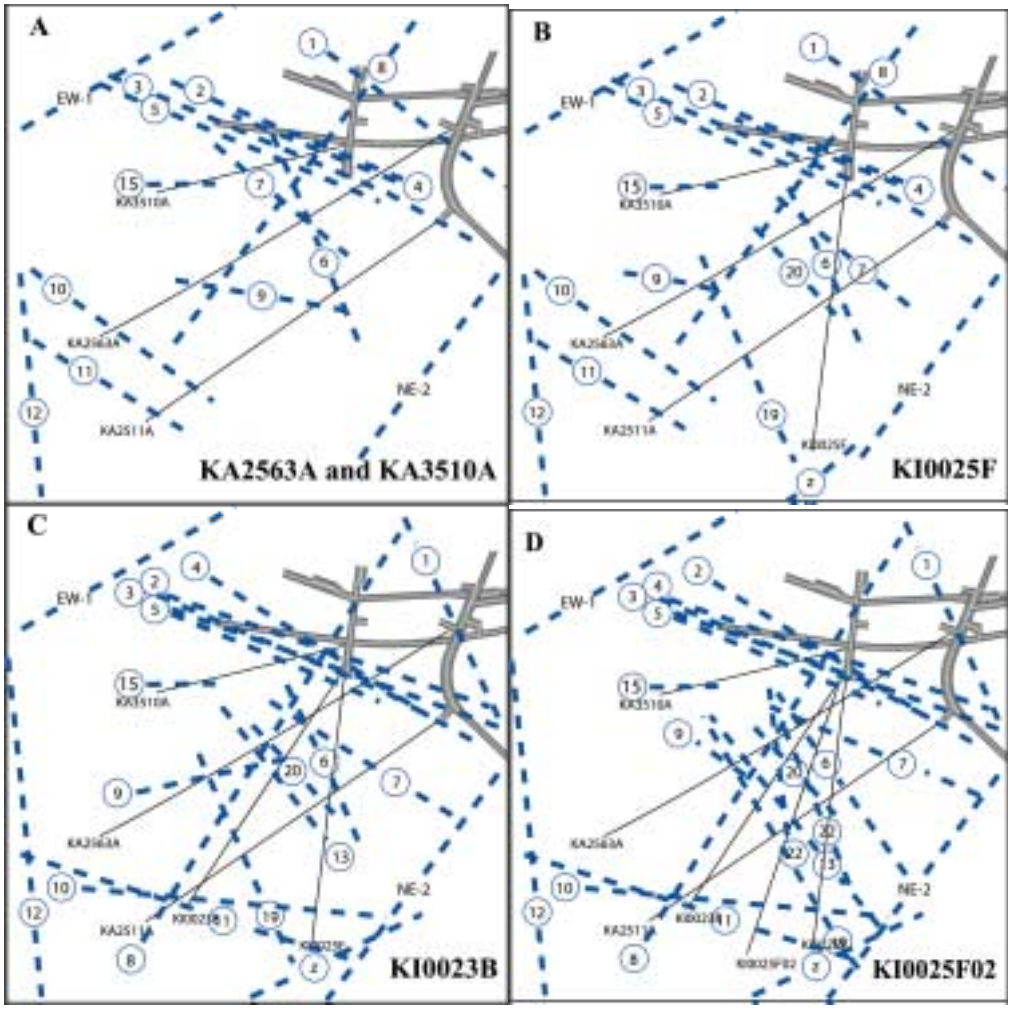

Figure 4-3. *Plan view of the hydro-structural models developed from data collected during the a) Scoping Stage (March '97), Preliminary Characterisation Stage (b) October'97 and c) September'98) and d) Detailed Characterisation Stage (September '99), developed after drilling and characterisation of each respective borehole. Model (a) shows the model after drilling of KA2563A and KA3510A. Models (b), (c) and (d) show the development and refinement of the model after the drillings of KI0025F, KI0023B and KI0025F02, respectively.*

Table 4-1. Comparison between predicted and interpreted (September 1998) structure locations in borehole KI0023B, cf Figure 4-3c.

Structure	Predicted depth (m)	Interpreted depth (m)
5	3–5	7.2
6	36–39	44.2
7	36–39	42.2
9	100–103	71.1
10	178–182	170.7
19	97–100	111.6
20	65–67	69.8

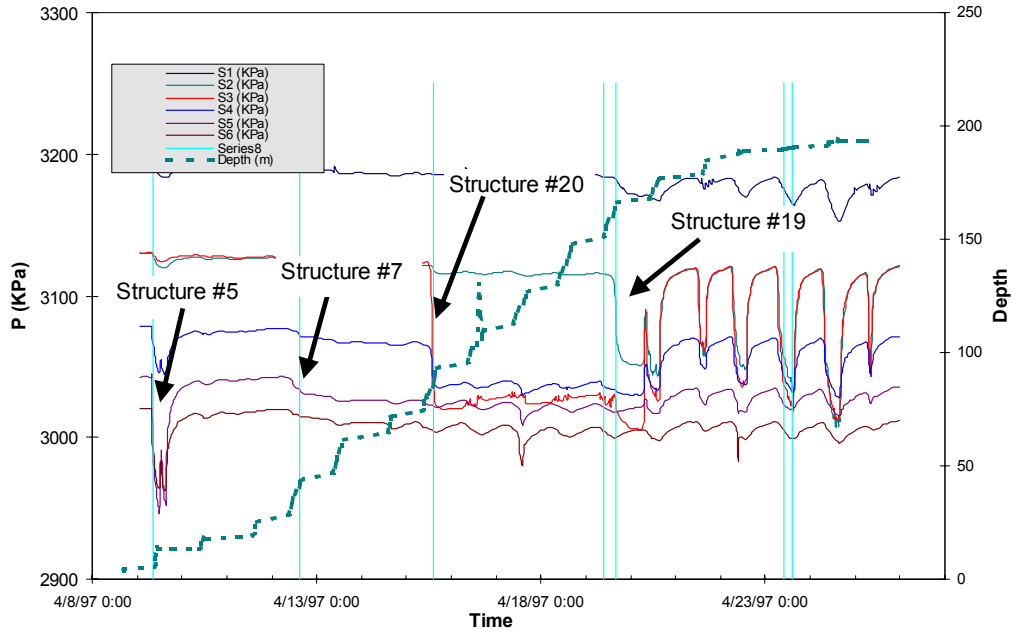

Figure 4-4. *Pressure responses in packed-off sections in KA2563A to drilling of borehole KI0025F. Dashed line shows drilling progress with time.*

Structure #13, as seen in KA2563A and KI0023B, has a similar geological character as #20 with a reactivated mylonites and gouge material in its centre part. The geometry of several of the bounding structures were adjusted given the new information from the borehole /Hermanson, 2001b/.

The pressure responses in KI0025F and KA2563A to the drilling of KI0023B clearly showed the connectivity of Structures #5, #6, and #7, #20, and 19 across the investigated rock volume. The drilling of KI0023B also produced pressure responses in the bottom of borehole KA2511A. These responses are associated with Structure #10, a sub-vertical conductor located south of Structure #19, cf Figure 4.3c Performed interference tests i.a. showed a strong connection between Structure #20 and piezometer intervals including the interpreted Structures #13 and #9, indicating that the three structures are well connected /Andersson et al, 2001a/. This finding making the identified fracture network a strong candidate for future tracer tests. Another inference from the performed interference tests was that sub-horizontal structures, such as Structures #16 and #18, were found to be not hydraulically significant /Andersson et al, 2001a/.

Apart from these important findings, the combined interference and tracer dilution tests confirmed 8 of the 20 interpreted structures (40%) and provided important information about their mutual connectivity. In addition, distance-drawdown plots (s_p/Q vs. t_r/R^2), cf Section 3.6.3, were introduced and used to map out families of responses (structures) with different connectivity and drawdown characteristics. Performed tracer tests indicated the feasibility to run block scale tracer tests.

4.4 Detailed Characterisation Stage: borehole KI0025F02

The Detailed Characterisation Stage aimed at providing sufficient information on the TRUE Block Scale volume to define potential pathways, i.e. sources and sinks for tracer tests. The borehole, KI0025F02, aimed at improving the basic hydro-structural model of the TRUE Block Scale volume and better define the target structures #6, #7, #20, #13 and #9. Detailed characterisation also required a better definition of Structure #19 as a possible boundary in the southeast of the TRUE Block Scale rock volume. Before the onset of drilling, predictions were made of intercepts of the interpreted structures in the new borehole, cf Table 4-2.

The drilling and characterisation of borehole KI0025F02 confirmed the major structures that had been identified in the preliminary characterisation, cf Table 4-2 and Figure 3-8. Performed cross-hole interference tests /Adams et al, 2001/ clearly identified Structures #20, #7 and #19, where Structure #20 is only weakly connected to the latter two structures, to be regarded as bounding structures for future tracer tests. Structures #13 and #9 were found to respond rapidly to hydraulic disturbances in #20. As a verification of Structure #9 in KA2563A, detailed Posiva flow logging was conducted between 189–278 m in KA2563A /Rouhiainen and Heikkinen, 2001b/. Measurements were run both with all other borehole sections shut in, and with section KI0023B:P6 open and flowing. No measurebale flow change was observed rerunning the Posiva log, and it was concluded that the interpreted Structure #9 did not have a hydraulic connevction between its interpreted intecept in KA2563A (at L=265.8 m) and in KI0023B:P6.

With the elimination of Structure #9, the remaining confirmed deterministic structures were largely sub-parallel and oriented northwest, Structures #20 and #13. Hydraulic connection between the two structures was however well established, but the connecting element/-s were not identified. The identification of other potential conductors which may provide hydraulic connections across Structures #13, #20, and #6 became a high priority.

Table 4-2. Comparison between predicted and interpreted (March 1999) structure locations in borehole KI0025F02, cf Figure 4-3d.

Structure	Predicted depth (m)	Interpreted depth (m)
6	69–73	52.3
7	48–52	39.9
10	183–187	Not identified
13	123–127	93.9
19	145–151	133
20	92–97	74.7

A detailed re-evaluation of the drilling responses /Doe, 2001/, cf Figure 3-8, and the borehole television logs from borehole KI0025F02 revealed two new steeply dipping structures, #21 and #22. These structures were interpreted to cross Structures #20 and #13. The new structures were interpreted to be subordinate in width and geological characteristics to both Structures #13 and #20 and could be considered as splay fractures (to Structure #20 and/or #13) connecting the latter two structures.

Subsequently performed pre-tests with the aim of exploring possibilities for block scale tracer tests /Andersson et al, 2001b/ generally confirm the hydro-structural model. For the most part good pressure responses (high and fast) gave corresponding indications of good flow response (increased flow) from tracer dilution tests, indicating a good connectivity. However, exceptions were identified such that the principal conjecture is that a good pressure response is not sufficient to indicate connectivity for transport. Combined interference and tracer dilution tests with sinks in #13, #20 and #21 all show good flow and pressure responses in Structures #6, #13, #20, #21 and #22. Connectivity was also established between Structures #19 and #21. Quantitative analysis revealed predominantly radial flow with indications of leakage at the end of the tests. Analysis of responses in sections containing the bounding Structures #6, #7 and #19 showed effects of constant head boundaries. Tracer tests performed with pumping in Structure #21 in KI0023B and injection of tracer in KA2563A (Structure #19, Structure #20), and KI0025F02 (Structures #13/21 and #22) showed breakthrough from all sections providing final evidence that a workable network of structures (#13, #20, #21 and #22) had been identified for use in the future Tracer Test Stage /Andersson et al, 2001b; Winberg, 2000/.

Based on the Posiva flow log results, an additional structure, Structure #23, was also hypothesised between Structure #22 and Structure #6 /Doe, 2001/, cf Figure 4-3d.

4.5 Tracer Test Stage: borehole KI0025F03

Borehole KI0025F03 was drilled to confirm the geometry and characteristics of the Structures #6, #13, #20, #21 and #22 in the target volume, as well as to provide for alternative/additional injection and pumping points /Winberg, 2000/. The borehole was collared between KI0023B and KI0025F02, but is shorter than the two, because it was targeted to end just beyond Structure #19, cf Table 2-1. The results of the KI0025F03 characterisation largely confirmed the hydro-structural model developed following drilling of KI025F02, cf Table 4.3 and Figure 4-3d. Structure #23 appeared where predicted, cf Table 4-3 and Figure 4-5. The pressure responses to drilling also indicated a Structure #24 located somewhat closer to the collar north of Structures #6 and #7, cf Figures 4-5 and 4-6.

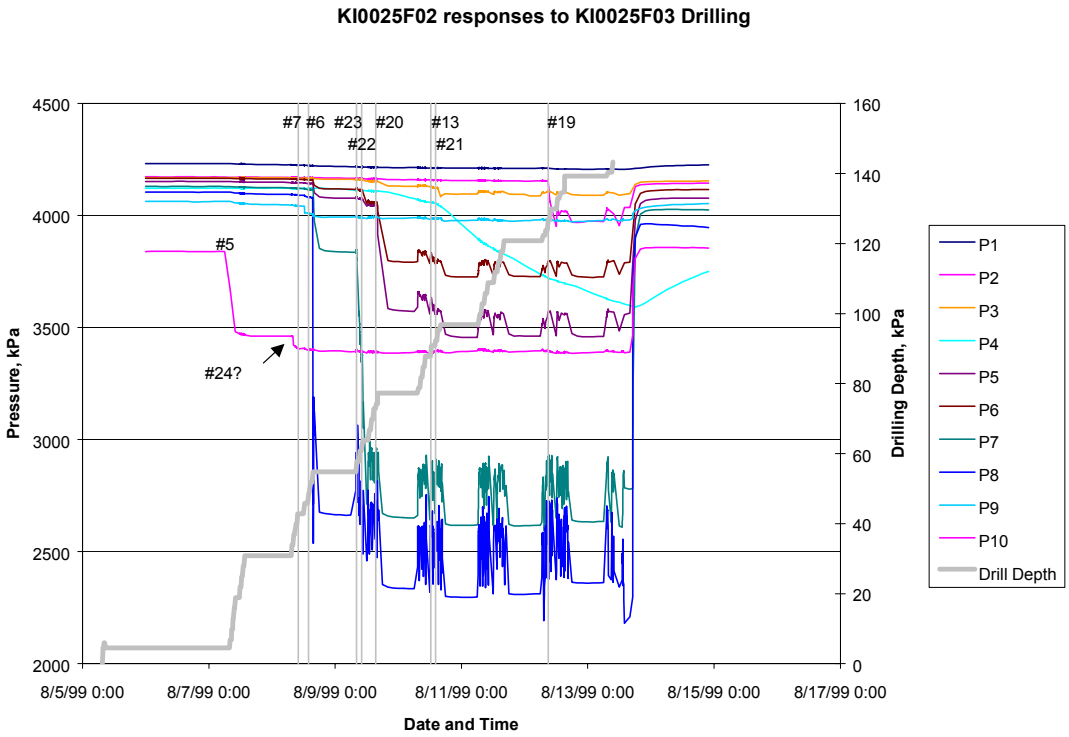

Figure 4-5. *Pressure responses in borehole KI0025F02 to drilling in KI0025F03.*

Table 4-3. Comparison between predicted and interpreted (March 2000) structure locations in borehole KI0025F03.

Structure	Predicted depth (m)	Interpreted depth (m)
#6	52	51.9
#7	?	43
#13	92	87.9
#19	134	124.7
#20	75.5	73.2
#21	83	91.9
#22	62	63.2
#23	59.2	56.8

Performed short-term cross-hole interference tests /Gentzschein and Ludvigson, 2001/ supports the hydro-structural model regarding Structure #20 and also indicates that this structure is well connected with Structure #6, and also with Structure #21. Tests associated with Structure #22 also shows few but significant responses consistent with the hydro-structural model.

The outcome of the drilling and characterisation of KI0025F03 resulted in minor adjustments to the geometry of existing structures, and confirmed the existence of the target structures for tracer tests. Two new structures were included in the model,

Structures #23 and #24, both of which are characterised by single fracture planes in altered dioritic rock. The major geometric conclusions regarding the target structures are /Hermanson and Doe, 2000/:

- Structure #20 is the major structure located in the centre of the tracer test area. It constitutes the core of a network that includes Structures #6, #23, #22, #13, and #21,

- Structure #19 intersects all boreholes except KA2511A. It has possible connections to the Structure #20 network, either through Structure #13 or through background fractures,

- Structure #13 has its strongest geological appearance in boreholes KA2563A and KI0023B. A strong conductor connecting the P3 zones of KI0025F02 and KI0025F03 is a conductor separate from Structure #13 and may be part of Structure 21. Structure #13 does not appear in KI0025F.

- Structure #21 is part of the Structure #20 network with interpreted intersections in boreholes KI0025F02, KI0025F03, KI0023B, and possibly in KA2563A. There are still some ambiguities regarding Structure #21 as it is not sufficiently separated from other structures in the piezometers to show unambiguous pressure responses,

- Structures #22 and #23 are confirmed by the data from KI0025F03,

- The responses due to drilling of KI0025F03 strongly suggest an additional structure, #24, which is located north of Structures #6 and #7. This structure does not, however, connect to Structures #6 and #7. It is steeply dipping and is likely to have little effect on the behaviour of the hydraulics in the planned target area for tracer tests in the TRUE Block Scale rock volume.

Table 4-4. Location of intercepts and geometry of identified structures in the TRUE Block Scale boreholes.

	KA2563A			KA2511A			KA3510A			KI0025F			KI0023B			KI0025F02			KI0025F03		
#	Depth	Strike	Dip	Depth	Strike	Dip	Depth	Strike	Dip	Depth	Strike	Dip	Depth	Strike	Dip	Depth	Strike	Dip	Depth	Strike	Dip
1	12,5	335	82																		
2	68,5	135	87				11,1	309	75												
3	68,5	135	87				37,5	106	81												
4	94,4	296	74	23,1	300	80	12,9	115	89												
5	103,0	114	89				47,7	138	75	4,9	307	57	7,2	112	87						
6	157,2	309	89	100,1	340	71				(61.8)	342	86	44,2	88	83	52,3	317	89	51,9	136	81
7	153,4	111	73	38	143	87				43,5	253	84	42,2	103	87	39,9	126	70	43,0	88	84
8	242,4	26	84				16,1	232	89												
9	230,0	123	88																		
10	351,3	124	80	240,5	127	85							170,7	298	83						
11				258,2	288	88															
12																					
13	207,0	321	86										85,6	318	89	93,9	140	83	87,5	338	87
15							118,0	269	88												
16	56,3	11	40	104,7	233	18															
17	108,9	222	34	132,4	270	16															
18	194,3	12	18	242,5	155	9							75,5	348	41						
19	237,9	343	76	198,2	324	87				166,4	336	84	111,6	342	87	133,0	334	87	124,7	339	86
20	188,7	316	82	122	321	73				87,7	336	77	69,8	157	82	74,7	134	89	73,2	326	64
21										(166.4)	338	74	71,1	123	86	97,9	354	77	91,9	296	59
22										88,8	340	81				66,8	337	88	63,2	154	87
23																59,2	125	80	56,8	301	77
24										37,1	301	82	31,8	308	76	33,9	307	72	33,8	135	75
Z										192,1	243	77									

The final hydro-structural model of the TRUE Block Scale volume is illustrated in plan view in Figure 4-6 at a level of –450 masl. The geometrical information of the location and orientation for each identified structure intercept in the different boreholes are given in Table 4-4. Detailed descriptions of the most important deterministic structures are provided in Section 4.6 and detailed geological interpretations of individual intercepts are provided in Appendix C.

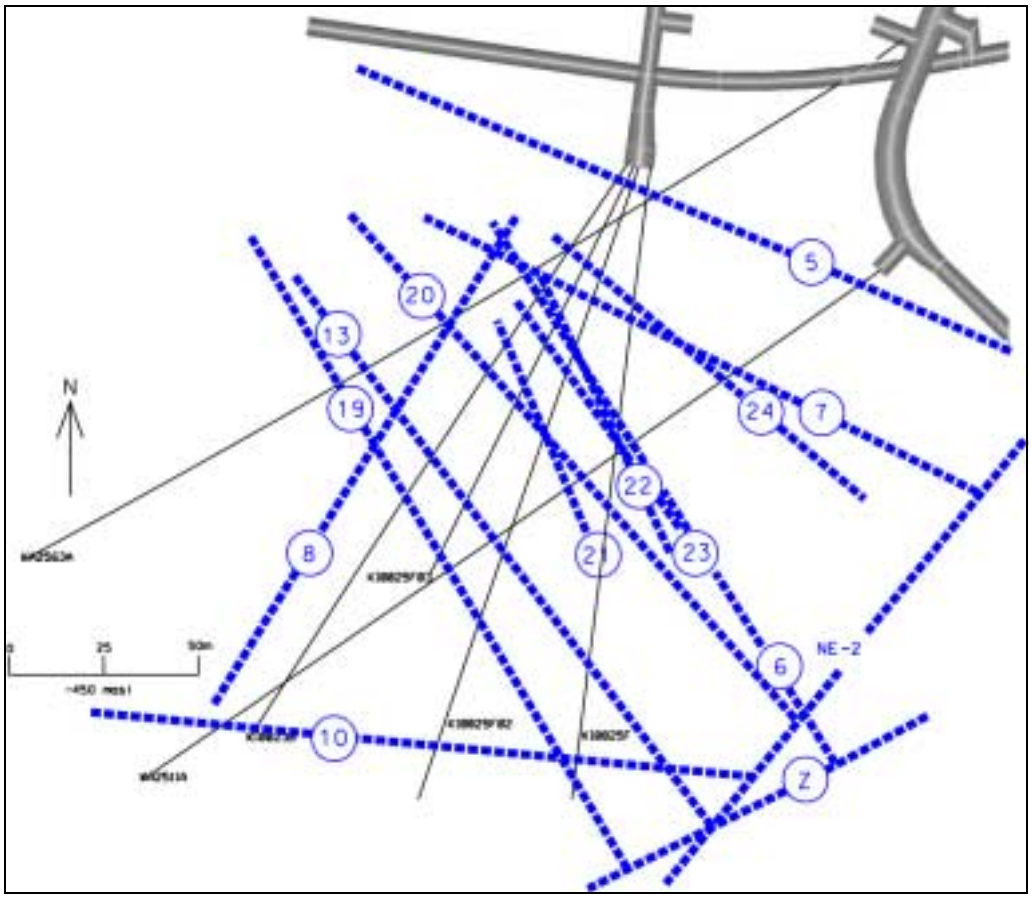

Figure 4-6. *Plan view of the Tracer Test Stage hydro-structural model with focus on the target volume of the block /Hermanson and Doe, 2000/. The model shows the geometry of the interpreted structures based on data from borehole KI0025F03. Structures in the periphery of the experimental target volume are not shown, i.e. Structures #1–#4 (north of Structure #5), #11 and #12 (south of Structure #10) and #15, cf Figure 4-3d.*

4.6 Detailed geological description of the target structures

The geological characteristics of each intersection points of the target structures has been compiled and is presented in Appendix C. Below follows short descriptions of the interpreted geological characteristics along the extension of each major deterministic structure including integrated graphical visualisations of the structures.

4.6.1 Structure #20

Structure #20 is observed in boreholes KI0025F, KI0025F02, KI0025F03, KA2511A, KA2563A and KI0023B, cf Figure 4-7. The geological signature of this structure is complex and variable. The structure is interpreted to either peter out towards boreholes KA2511A and KI0025F as these intercepts show little fracturing in slightly altered diorite. The other intercepts exhibit the same type of fault as found in two of the intercepts with Structure #13, i.e. with a fractured centre with a 10 to 15 cm wide mylonite. The core of the structure most commonly exhibits a double fault plane with mm wide lenses of calcite-rich gouge material. Structure #20 acts as the principal component of the hydraulic network in the tracer test area that includes Structures #6, #23, #22, #13, and #21, the so-called "#20/#13 network".

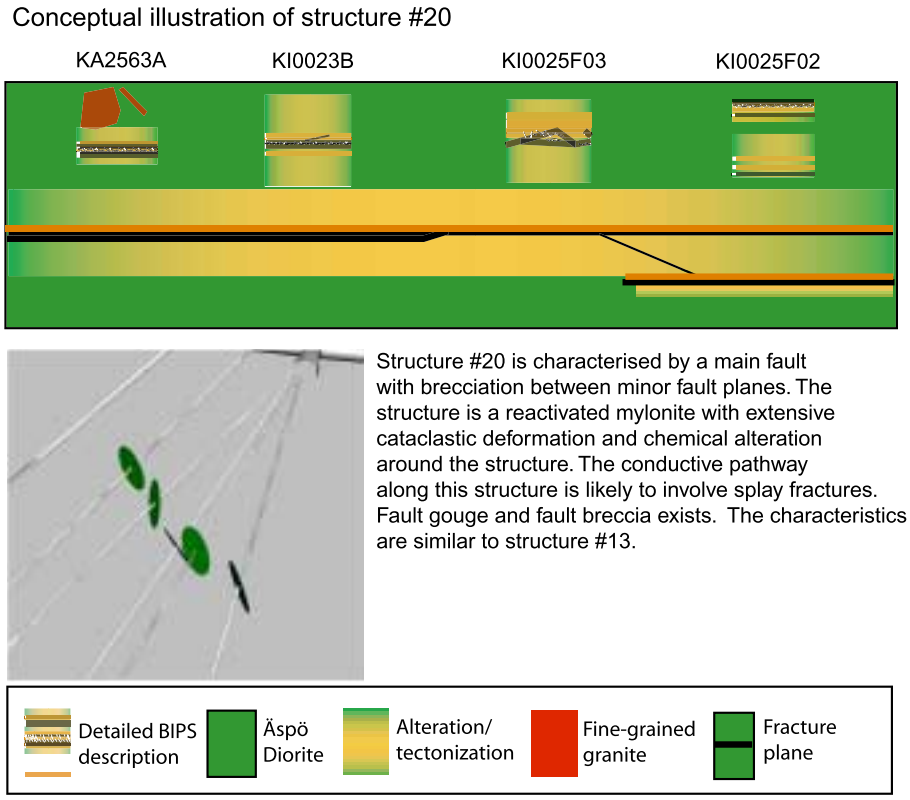

Figure 4-7. *Conceptual structural-geological illustration of Structure #20. A detailed picture of the geological interpretation based on the BIPS image is shown for each intercept at the top of the illustration for reference. The lower half of the green block shows the conceptual model of the character of the structure between the various intercepts.*

4.6.2 Structure #13

Structure #13 is well pronounced and resembles Structure #20 (more distinct fault appearence, fault breccia etc) in the intercepts in boreholes KA2563A and KI0023B. Its appearence in boreholes KI0025F02 and KI0025F03 is less distinct and different from the former, cf Figure 4-8. Structure #13 in KA2563A and KI0023B is a major fault with an estimated maximum width of 25 cm, mainly consisting of altered host rock with mylonite in the central part. The brittle reactivation is located in the centre of the fault. The diorite around the fault is exceptionally black and exhibits a porphyritic character with feldspar crystals in a black matrix. Selected intercepts show that this structure may be correlated to contacts between fine-grained granite, greenstone and Äspö diorite, cf Figure 4-8. A possible reason for the observed difference in appearence in different boreholes may be the difference in bedrock lithology, which in the case of KI0025F02 and KI0025F03 is featured by bodies of fine-grained granite which may act differently mecanically (more brittle deformation) and may be less likely to form clay minerals.

The structure is considered to be a single structure, although several of the other structures are hydraulically connected to this feature. The continuity of Structures #13 and #21, cf Section 4.6.3, are not as clear as some of the other major structures in the TRUE block scale volume. The ambiguity in Structure #13 is the result anomalous

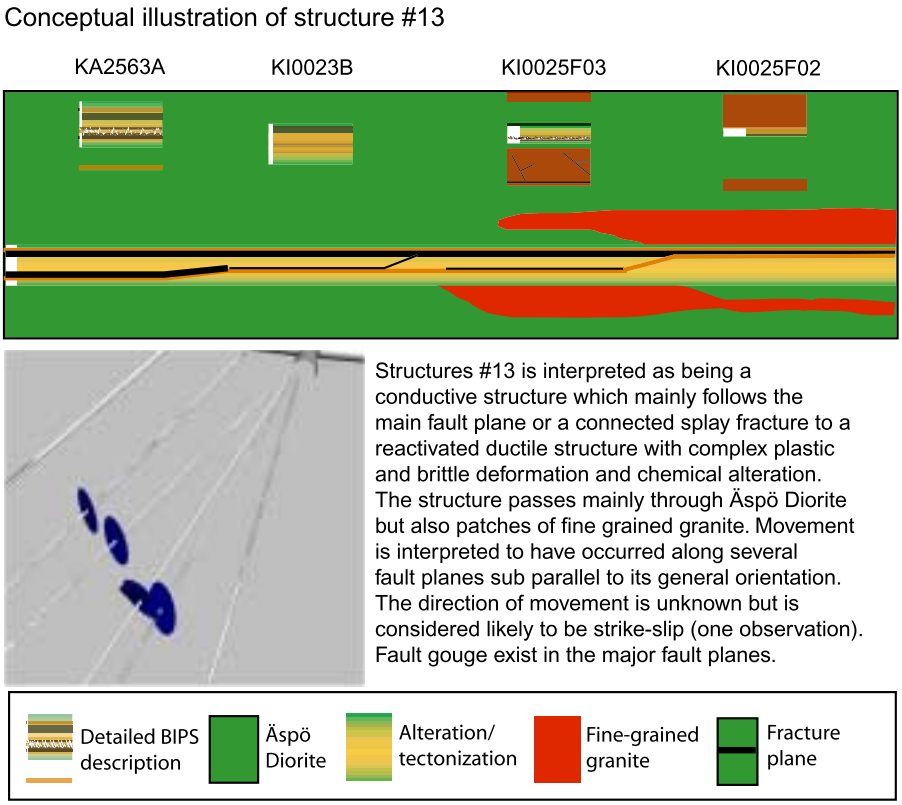

Figure 4-8. *Conceptual structural-geological illustration of Structure #13. A detailed picture of the geological interpretation based on the BIPS image is shown for each intercept at the top of the illustration for reference. The lower half of the green block shows the conceptual model of the character of the structure between the various intercepts.*

drawdowns in response to interference tests. While there are very strong and similar drawdown responses in Structure #13 in KI0023B and KA2563A, the drawdown responses that should be associated with Structure #13 in KI0025F02 and KI0025F03 are unexpectedly small. These small drawdown responses first appeared in tracer pre-test PT-1 /Andersson et al, 2001b/ that used Structure #13 in KI0023B as a sink, and also later during the Phase A interference tests /Andersson et al, 2000a/ which also showed similarly small drawdowns.

4.6.3 Structure #21

Structure #21 is observed in boreholes KI0023B, KI0025F02 and KI0025F03, cf Figure 4-9. The structure consists of several closely spaced fractures that have mineral fillings of calcite and chlorite. The structure cuts through altered diorite or fine-grained granite.

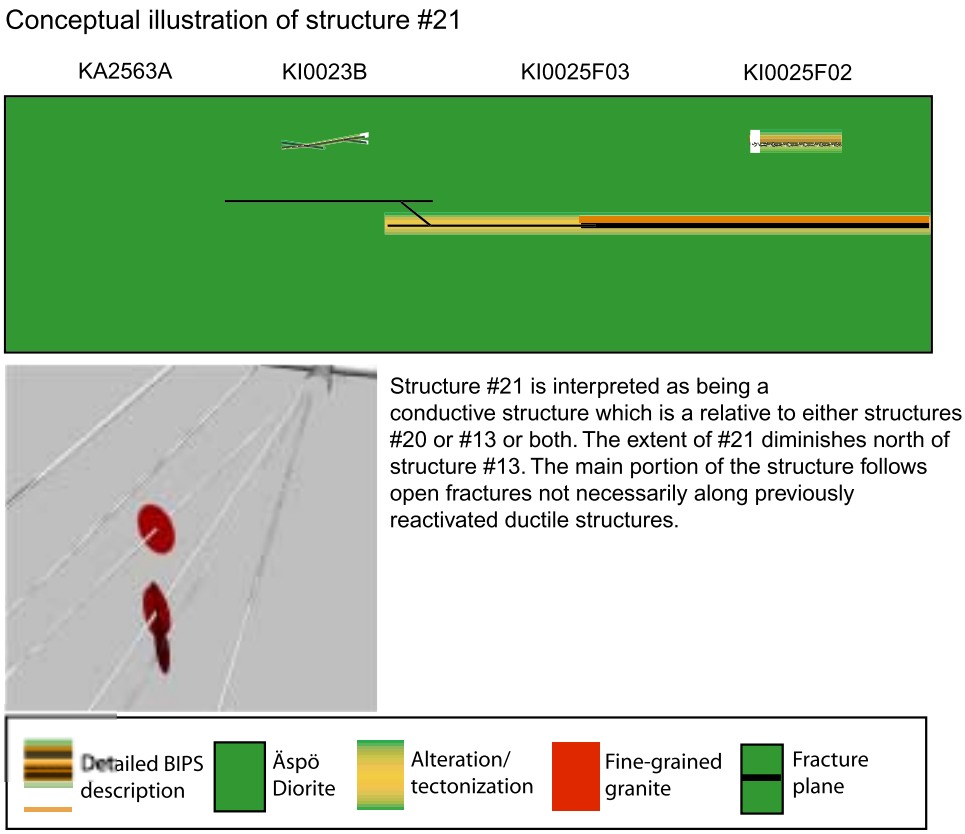

Figure 4-9. *Conceptual structural-geological illustration of Structure #21. A detailed picture of the geological interpretation based on the BIPS image is shown for each intercept at the top of the illustration for reference. The lower half of the green block shows the conceptual model of the character of the structure between the various intercepts.*

However, the character is varied and the variable orientations of the individual intercepts suggest that this is a complex structure made up of two or more splays to a larger geological structure, most likely Structure #20. The intercept in KI0023B is closely related to Structure #20 hydraulically. This means that Structure #21 can be regarded more as a "hydraulic feature" than a well defined geological structure. The continuity of Structures #21 are not as clear as for the remainder of the interpreted major structures in the TRUE block scale volume. The uncertainty in Structure #21 comes from the fact that this structure is isolated from other structures in only one monitoring interval, KI0025F03:P4, cf Section 4.6.4

4.6.4 Hydraulic connectivity within Structures #13 and #21

As indicated in the two preceding sections, the continuity of Structures #13 and #21 are not as clear as for the remainer of the interpreted structures in the TRUE Block Scale rock volume. There are two hypotheses regarding the observed small drawdowns in Structure #13 in KI0025F02 and KI0025F03. These hypotheses are (1) that Structure #13 has a "gap", or it exists as a separate structure in the mentioned boreholes as distinguished from those in KI0023B and KA2563A, or (2) that KI0025F02 and KI0025F03 are located close to a constant pressure boundary, eg provided by a high conductance channel or a fracture intersection zone (FIZ). Because this boundary acts as water source, nearby points show a reduced drawdown compared to more distant sections. Structure #21 is linked to these considerations because it provides a flow path from Structure #13 in the vicinity of KI0025F02 and KI0025F03 and the Structure #20 system in KI0023B. The resolution of these hypotheses lies in several data sources including water chemistry, ambient hydraulic head, pressure responses to drilling KI0025F02 and KI0025F03, and results from tracer dilution performed during interference tests.

The water chemistry data may suggest that portions of Structure #13 are disconnected if the chemistry data are very different. The water chemistry in all of the proposed Structure #13 and #21 intervals is of the high salinity, low $\delta^{18}O$ type, cf Section 6.2. Indeed, Structure #13 contains some of the most saline waters found in the TRUE Block Scale rock volume, and may be acting as a source for these waters. Hence, water chemistry does not indicate separation of the structure.

As points within a common geological structure often have similar ambient hydraulic head values, differences in head may indicate a lack of connectivity. In this case, the ambient heads in KI0025F02:P3 and KI0025F3:P3 are clearly higher than those in Structure #13 in KI0023B and KA2563A. These head data therefore could indicate discontinuity within Structure #13, or a head drop between KI0025F03 and KI0023B.

While the pressure responses to drilling KI0025F02 are ambiguous due to noisy data, the pressure responses to drilling do indicate connectivity between Structure #21 in KI002F03 to the rest of the Structure #21 and #13 intercepts. There is also a widespread response along Structure #13 to the flow anomaly near 92m, or close to Structure #13 in KI0025F03. The pressure response along Structure #13 between KI0025F02 and KI0025F03 is clear but has a relatively small (30 kPa) pressure change.

The clearest indication of hydraulic connection along Structures #13 and #21 comes from the tracer dilution data. KI0025F02:P3 has a strong dilution response to pumping in other zones interpreted to include Structure #21, specifically KI0025F03:P4 and KI0023:P6.

A review of the drilling response, interference test, and tracer dilution data therefore suggests that Structures #13 and #21 are continuous as hypothesized in the hydrostructural model of the TRUE blocks scale volume, cf Figure 4-6. The low pressure responses observed in tracer pre-test PT-1 indicate that a feature such as a flow channel or fracture intersection zone (FIZ) may be acting as a constant pressure boundary. The observed higher hydraulic head in the P3 intervals of KI0025F02 and KI0025F03 may indicate that a conductor near these monitoring points acts as a source for the more saline water in the central portion of the TRUE Block Scale rock volume.

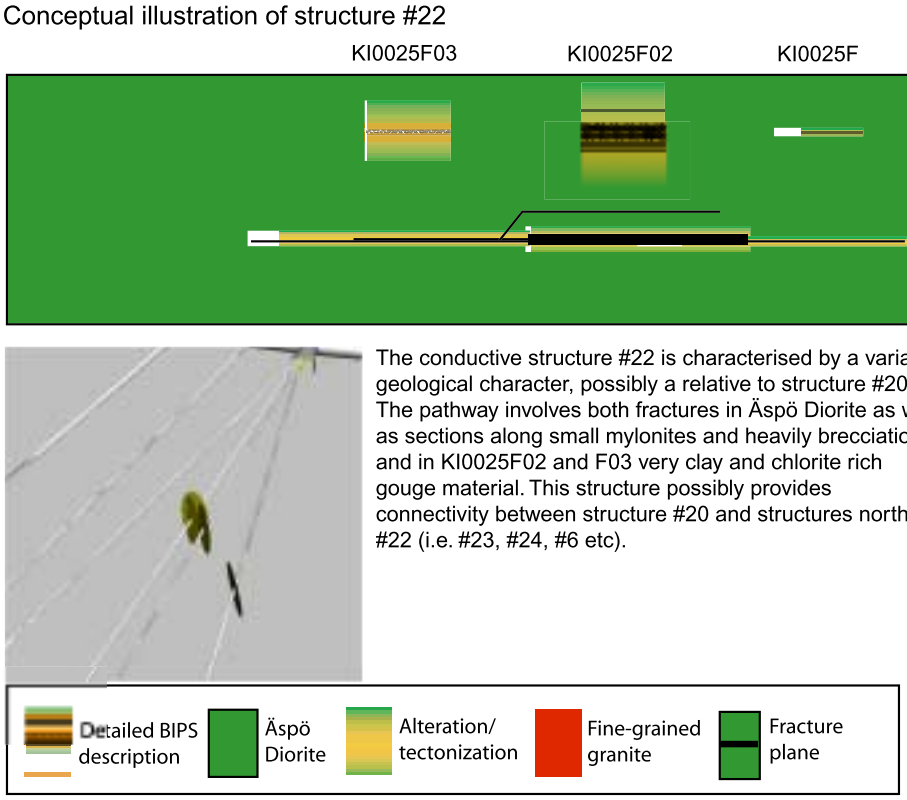

Figure 4-10. *Conceptual structural-geological illustration of Structure #22. A detailed picture of the geological interpretation based on the BIPS image is shown for each intercept at the top of the illustration for reference. The lower half of the green block shows the conceptual model of the character of the structure between the two intercepts.*

4.6.5 Structure #22

Structure #22 is subparallel to Structure #21 and is observed in boreholes KI0025F, KI0025F02 and KI0025F0. The structure constitutes a fault with several subparallel fault planes, cf Figure 4-10. Crushed rock is observed in the core of KI0025F03. However, the interpreted intercept in KI0025F is a small fracture cutting through altered diorite whereas the other intercepts are 15 cm wide faults with a mylonitic core. The host rock is dark diorite with an almost porphyritic character.

4.6.6 Structure #23

Structure #23 is a structure interpreted from the geometry of the fracturing, the Posiva inflow points and results of interference tests run along KI0025F02 and KI0025F03. The geological character of these intercepts is similar to many fractures along the boreholes and is characterised by single fracture planes in altered dioritic host rock. The orientation is consistent in both intercepts.

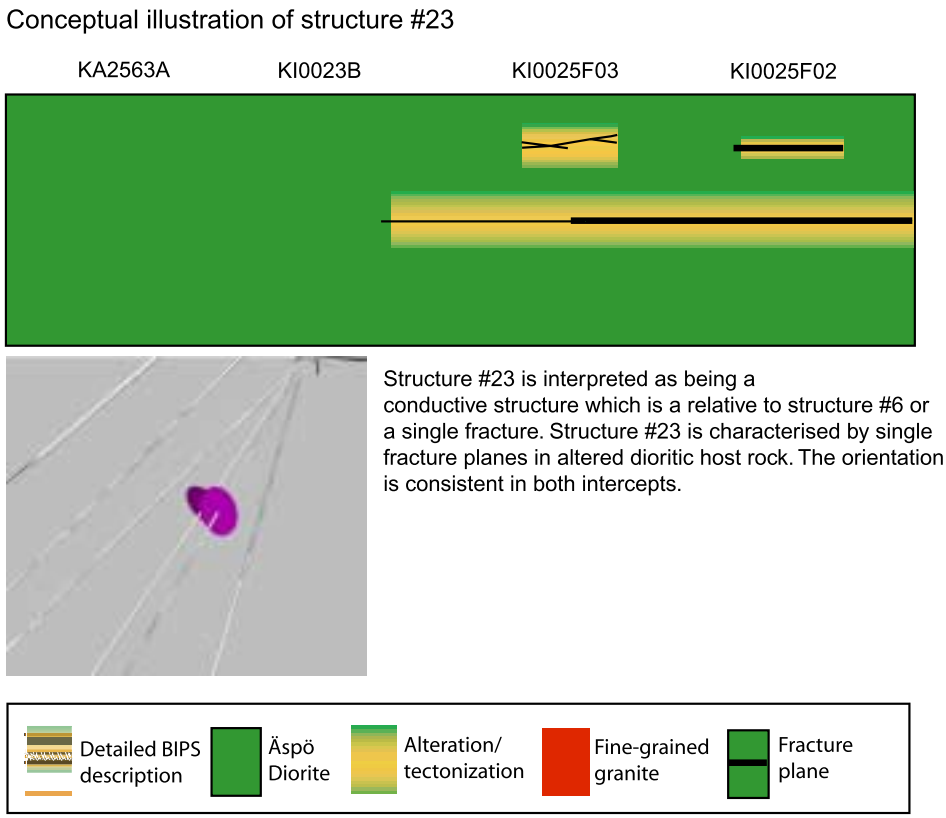

Figure 4-11. *Conceptual structural-geological illustration of Structure #23. A detailed picture of the geological interpretation based on the BIPS image is shown for each intercept at the top of the illustration for reference. The lower half of the green block shows the conceptual model of the character of the structure between the two intercepts.*

4.6.7 Structure #24

An inspection of the pressure responses to drilling of KI0025F03, cf Figure 4-5, suggested the existence of an additional structure located somewhat north of Structures #6 and #7. The main evidence of its existence is a pressure response to drilling at a depth between 33.8 and 36.8 metres in KI0025F03. A review of drilling response records from previous boreholes reveals a consistent response to this structure in all holes except KA2563A.

Posiva flow log anomalies in boreholes KI0025F02 and KI0025F03 also indicate this structure. The interpreted intersection points in KI0023B, KI0025F, KI0025F02 and KI0025F03 align on a near single plane (±10 cm) with an evaluated strike of 130° and a dip of 82°, cf Table 4-4. The structure consists of an open calcite-coated fracture with limited impact of the surrounding host rock. However, the intercept in KI0025F03 shows signs of alteration and plastic deformation around the structure.

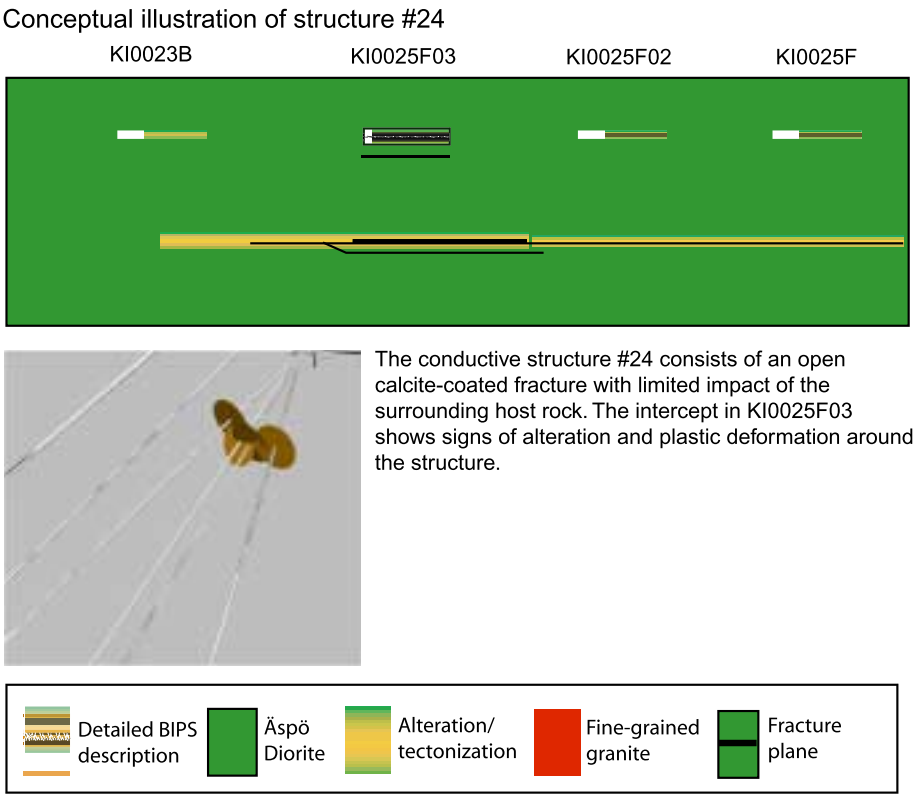

Figure 4-12. *Conceptual structural-geological illustration of Structure #24. A detailed picture of the geological interpretation based on the BIPS image is shown for each intercept at the top of the illustration for reference. The lower half of the green block shows the conceptual model of the character of the structure based on the single intercept available.*

4.7 Mineralogical and geochemical analyses

4.7.1 Lithology and mineralogy

Porphyritic quartz-monzodiorite (denoted Äspö diorite) is the main rock type in the TRUE Block Scale rock volume. In addition, a granodioritic/granitic variety called Ävrö granite has been identified in small portions. Lenses and dikes of fine-grained aplitic granites occur frequently, especially in conjunction with Structures #13 and #21 in boreholes KI0025F02 and KI0025F03. The mineralogical compositions of these rock types are given in Table 4-5.

Table 4-5. Characteristics of the Äspö diorite, Ävrö granite and Fine-grained granite. Based on data from /Wikman and Kornfält, 1995/.

Rock type	Äspö diorite	Ävrö granite	Fine-grained granite
Texture	Medium-grained porphyritic, foliated	Medium to fine grained partly porphyritic, foliated	Fine grained, foliated
Age	approx 1800 Ma	approx 1800 Ma	approx 1800 Ma
Porosity (water saturation)	0.45 ± 0.2 vol%	0.4 ± 0.2 vol%	0.3 ± 0.2 vol%
Mineral composition vol% (average)			
Quartz	14	25	31
K-feldspar	15	29	38
Plagioclase	45	33	23
Biotite	15	7	2.5
Muscovite	0.5	0.5	3
Epidote	6	2.5	1
Amphibole	1	<0.5	–
Titanite	2	1.5	0.5
Apatite	0.5	0.5	<0.5
Opaque	1	1	1

The mineral identification has been carried out on geological material (wall rock and fault breccia) from the borehole intercepts with the major deterministic structures. The methods used in the identification included microscopy, SEM/EDS and XRD analyses. Structural geology and texture have mainly been evaluated from BIPS images and microscopy.

4.7.2 Tectonisation and alteration

Tectonisation of the rock around conductive features are common at Äspö HRL. This tectonisation is manifested in the occurrence of cataclasites and/or mylonites of which cataclasite[1] is characterised by re-crystallisation of quartz, increased frequency of micro fractures, various degrees of chemical alteration (like alteration of biotite to chlorite, saussuritisation of plagioclase, oxidation of magnetite to hematite etc) and in some cases thin shear bands, whereas more localised and intense tectonisation has led to the formation of mylonites, characterised by complete grain size reduction and re-crystallisation/alteration of the wall rock resulting in formation of epidote, quartz, albite and K-feldspar +/–sericite/chlorite.

Almost all of the studied intercepts show alteration and tectonisation of the wall rock and most intercepts follow mylonites (cf Table 4-6). The cataclastic zone around each structure varies in width from centimetres to decimetres around the fractures of the intercepts whereas the mylonites usually vary in width from millimetres up to a few centimetres.

Table 4-6. Type of wall rock and tectonisation. Intercepts contained in injection sections used in the Phase C tracer tests /Andersson et al, 2001c/ areindicated in bold (pumping section is KI0023B, Structure #21). The existence of fault breccia/fault gouge is indicated in Table 4-9.

Borehole	KA2563A	KI0023B	KI0025F	KI0025F02	KI0025F03
#20	ÄG/Cc/My	ÄD/Cc/My		ÄD/Cc/My	ÄD/Cc/My
#21		ÄD/(Cc)		**FKG+ÄD /Cc/My**	**FGG**
#22			ÄG/Cc/My	ÄD/Cc	ÄD/Cc/My
#23				ÄD/Cc/My	**ÄD/Cc**
#13	ÄD/Cc/My	ÄD/Cc/My		FKG/Cc/	ÄD/Cc/My
#6	ÄD/Cc			ÄD/Cc	ÄD/Cc
#19				ÄD/Cc/My	

ÄG= Ävrö granite, ÄD=Äspö diorite, FGG=Fine-granied granite, Cc=Cataclasite, My=Mylonite

[1] Cataclasite is a "rock that has been deformed by the process of shearing and granulation (cataclasis) Cataclasites are the products of dislocation, metamorphism and tectonism" /Allaby and Allaby, 1990/. Cataclasite is the general name given to "fine grained products of cataclasis which possess internal cohesion... " /Ramsay and Huber, 1987/.

Table 4-7. Indication of fault movements along fractures: Slickenlines and lineations on fracture surfaces.

Borehole	KA2563	KI0023B	KI0025F	KI0025F02	KI0025F03
#20	Yes	Yes		Yes	?
#21		Yes		Possibly	No
#22			?	Yes	?
#23				Yes	No
#13	No	Yes		?	?
#6	No			Probably	?
#19				Yes	

A brittle reactivation of old ductile/semi-ductile deformation zones thus seems to have occurred in the case of most of the analysed features/fractures. In addition, slickenlines indicate fault movements along several of the actual fracture planes of the structures, cf Table 4-7.

4.7.3 Characterisation of gouge materials

The movements along fault planes have resulted in formation of fault breccia and fault gouge in variable amounts and proportions. The definitions related to these types of materials employed in TRUE Block Scale are presented in Table 4-8. The locations where the various types of gouge materials have been identified are indicated in Table 4-9. Analysis results of sampled gouge materials are presented in Table 4-10.

The composition of the gouge material is characterised in terms of grain size distribution and mineral composition. However, as unconsolidated material is very easily lost during drilling. The representativity of the fraction of fine-grained fault gouge sampled from drill cores (triple tube drilling) is therefore always questionable. Sampling of fault breccia/fault gouge from the tunnel provides an improved and more complete grain size distribution. /Banwart, 1995/ carried out an analysis of the grain size distribution for a sample from the Redox Zone over the interval 0.002 mm–13 cm, cf Table 4-11 and Figure 4-13.

Of interest to note is that when the data in Table 4-13 is plotted as cumulative mass passing a given mesh size vs. particle size in a log-log diagram, a near linear relation is obtained (slope of ~ 0.7), cf Figure 4-13. According to the fractal theory, this equates to a fractal dimension D_f of 3x0.7=2.1 for a three-dimensional fracture network.

The mineral compositionsof the fault breccia from the sampled intersections are presented in Table 4-12 and the results of the associated geochemical analyses of gouge materials is presented in Appendix D. The fault breccia material consists mainly of altered wall rock fragments (± mylonite fragments). The smaller fractions include single grains of quartz, feldspars, epidote, chlorite, illite ± other clay minerals. Calcite, sulphides and occasionally FeOOHs are observed as mineral phases that have grown on the surfaces of the various fractions of the fault breccia.

Table 4-8. Definitions of Fault Breccia and Fault Gouge employed in the TRUE Block Scale Project.

Material type	Characteristic descriptors
Fault Breccia (FB)	Centimetre (> 2 mm) to decimetre sized pieces of altered wall rock/cataclasite and/or mylonite. The chemical and mineralogical composition is usually similar to that of wall rock. Observable in the BIPS log. The 1–3 cm fraction is also denoted "Fault breccia pieces", cf PMMA analyses results in Section 7.2.3.
Fault Gouge (G)	Fragments and mineral grains (≤ 2mm) of wall rock and secondary minerals (clay minerals and calcite) The smaller fractions (<0.125 mm) are to a variable degree enriched in clay minerals, calcite, pyrite and FeOOH. Not possible to identify from BIPS log. The 1–2 mm fraction is also denoted "Fault breccia fragments", cf PMMA analyses results in Section 7.2.3.

Table 4-9. Fault breccia (FB) (pieces in cm scale) and Fault gouge material (G) (grains and fragments in micrometer to mm scale). Based on observations from BIPS and also from sieving of the geological material.

Borehole	KA2563A	KI0023B	KI0025F	KI0025F02	KI0025F03
#20	FB/G	FB/G		–/–	FB/G
#21		–/–		FB/G?	FB/–
#22			FB/G	FB/G	FB/G
#23				–/–	(FB)/(G)?
#13	FB/G?	FB?/–		FB/–	FB/G?
#6	FB/G			FB/G	FB/G
#19				FB/G	

( ) = minor amounts, ? = indicated from BIPS but lost during drilling.

Fine grained fault gouge (<0.125 mm) sieved from gouge material collected from Structures #6, #19 , #20 and #22 have been analysed for main and trace elements, and for mineralogical composition using XRD. For clay mineral identification the <0.002 mm fraction was analysed separately. Compared to the results from analysis of material from the Redox Zone, /Banwart, 1995/ material from Structures #19, #20 and #22 show larger amounts of clay minerals (shown both by the grain size distribution, the XRD and the chemical composition). Especially Structure #22 exhibits large amounts of extremely fine-grained material consisting of chlorite and mixed-layer clays.

Table 4-10. Mineralogical composition of fault breccia fragments, 0.5–1 mm fraction. Results from microscopy.

Structure **Borehole id.** **Length (m)**	#20 KI0023B 69.9 m	#20 KA2563A 188 m	#22 KI0025F02 66.7 m	#6 KA2563A 154 m	#19 KI0025F02 133 m
Types of fragments %					
Altered wall rock	58	72	54	65	63
Mylonite	21	18		18	33
Cemented grains				14	
Grains dominated by one mineral	14 (Chl) 7 (Ca)	10 (Fl)	24 (Chl) 9 (Ca) 13 (Ad)	6 (Ca) 7 (Qz)	2 (Chl) 2 (Qz)
Fracture coatings pre fragmentation*	Ad, Fl, Ca, Ep, Chl	Fl, Ca, Chl, Ep	Chl, Ca, Ad, Ep	Oz, Ca, Ep	Chl, Ep, Qz
Alteration rims**	Very thin	Very thin	5–20 μm	Very thin	Very thin
New minerals grown on breccia fragments**					
Ca	++	–	+	+	–
Sulphides			+	+	+
FeOOH				+	
Cementation**					
Ca	+				
FeOOH				+	
Clay				+	

Ad=Adularia, Ca=Calcite, Chl=Chlorite, Qz=Quartz, Fl=Fluorite, Ep=Epidote, FeOOH=Fe-oxyhydroxide.

* Fracture coatings that predates the brittle fragmentation; these are mineralisations associated with hydrothermal alteration which has resulted in formation of adularia (low temperature K-feldspar), epidote, quartz, chlorite and calcite.

** Mineralisations in the fracture that post-dates the fragmentation; these are formation of clay minerals and chlorite mostly visible as rims on the fragments and growth of calcite, and sulphides (pyrite) on the fault breccia fragments. Precipitation/cementation of FeOOH is only found in one sample (Structure #6).

Table 4-11. Grain size distribution of fault breccia/fault gouge obtained from a sample collected from the Redox Zone (sample collected from the tunnel wall) /Banwart, 1995/.

Particle size	Weight-%	Cum. mass passing (%)
7–13 cm	45.81	99.98
5–7 cm	21.50	54.17
3–5 cm	21.39	32.67
1–3 cm	6.13	11.28
0.2–1 cm	2.62	5.15
1–2 mm	0.91	2.53
0.5–1.0 mm	0.58	1.62
0.25–0.5 mm	0.37	1.04
0.125–0.25 mm	0.28	0.67
0.090–0.125 mm	0.07	0.39
0.063–0.090 mm	0.07	0.32
0.045–0.063 mm	0.06	0.25
0.032–0.045 mm	0.04	0.19
0.002–0.032 mm	0.10	0.15
<0.002 mm	0.05	0.05

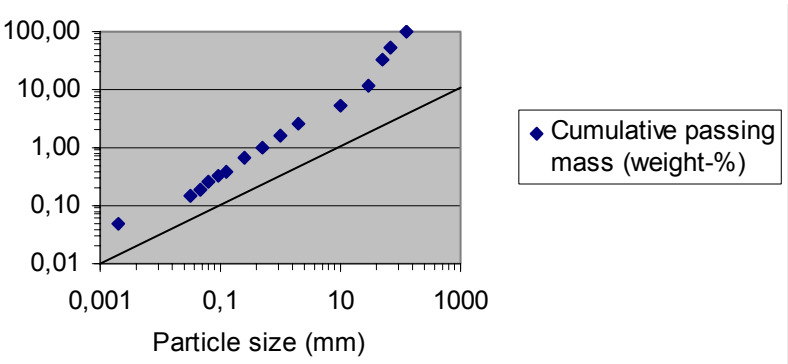

Figure 4-13. *Data in Table 4-11 plotted in a log-log diagram.*

Table 4-12. Mineralogical composition of fine-grained (<0.125 mm) fault gouge based on XRD and chemical analyses of samples extracted from Structures #6, #19, #20 and #22. Values should be regarded as rough estimates. The percentage of the <0.125 mm fraction which is <0.002 mm, and its associated mineral assembly are also indicated.

Mineral	Structure #6 KA2563A L=154 m	Structure #19 KI0025F02 L=133 m	Structure #20 KI0023B L=69.9 m	Structure #22 KI0025F02 L=66.7 m
Chlorite	10	30	20	40
Illite	20	7	20	–
Mica	20	5	–	3
Mixed-layer clay	–	3	2	25
Smectite	–	15	–	–
Calcite	3	–	25	5
Quartz	30	10	10	15
K-feldspar	5	5	10	5
Plagioclase	12	20	10	6
Sulphides	–	–	3	1
Epidote	–	5	–	–
Weight% <0.002 mm (clay fraction)	15	21	28	42
Mineral comp. of <0.002 mm fraction	Illite Chl, Plag (minor; Qz, Kfsp and calcite)	Chl and smectite (minor; illite, mixed-layer clay, Kfsp and Plag)	Chl, (minor; illite and calcite)	Chl and mixed layer clay

The sample with the highest mixed-layer clay content (Structure #22 in the intercept KI0025F02:L=66.7 m) shows a very high Cs value (62 ppm, cf Appendix D), a magnitude which has previously been observed also in the NE-1 zone /Landström and Tullborg, 1993/.

4.7.4 Stable isotopes

$\delta^{13}C$ and $\delta^{18}O$ have been determined on 17 calcite samples from fracture coatings and gouge material. Four samples were analysed at CIEMAT (Spain) whereas the remaining thirteen were analysed at Institutt for Energiteknikk (Norway), cf Section 3.11. Results are shown in Table 4-13. The $\delta^{13}C$ values vary from –14.1 to –4.1‰, with one exception of –23.1‰, the latter interpreted as a result of past in situ biogenic activity causing extremely depleted $\delta^{13}C$ values in bicarbonate. As e.g. sulphate reducing bacteria are not productive at high temperatures, a low temperature origin is suggested for this calcite.

Table 4-13. Stable isotopes in fracture coatings and calcites in fault breccia material.

Borehole	Depth (m)	Structure	$\delta^{13}C$ (‰ PDB)	$\delta^{18}O$ (‰ PDB)
KI0025F03	51.9	#6	–12.7	–12.6
KI0025F03	51.9	#6	–14.1	–11.6
KA2563A	206.85	#13	–9.4	–9.7
KI0023B	86.53	#13	–10.8	–7.4
KI0025F02	74.6	#20	–13.6	–18.2
KI0025F03	73.2	#20	–10.7	–15.2
KI0023B *	69.9	#20	–7.6	–19
KI0023B **	69.9	#20	–4.1	–22.3
KI0023B	69.9	#20	–7.9	–16.3
KI0025F03	73.10	#20	–11.1	–14.1
KI0025F	73. 2	#20	–10.7	–15.2
KI0023B	71.1	#21	–8	–19.2
KI0025F02	97.8	#21	–23.6	–7.5
KI0025F03	91.9	#21	–11.9	–19.9
KI0025F *	88.8	#22	–11.3	–6.6
KI0025F02	59.2	#23	–10.6	–15.6
KI0025F03	56.8	#23	–7.8	–19.8

* Calcite in fult breccia piece
** Idiomorphic crystals

The $\delta^{18}O$ values range from –22.3 to –6.6‰ of which the lowest values are typical for hydrothermal calcites at Äspö. Based on the large variation in both carbon and oxygen isotopes values it can be concluded that calcites from the TRUE Block Scale rock volume represents calcite types of different origins and ages.

In Figure 4-14, $\delta^{18}O$ and $\delta^{13}C$ data of the TRUE Block Scale calcites have been plotted together with previously analysed fracture calcites from Äspö. The very low $\delta^{18}O$ values (around –20‰) accompanied with high $\delta^{13}C$ values (–4 to –8‰) found in samples from Structure #20, the KI0023B intercept of Structure #21 and one sample from Structure #23, indicate precipitation in connection with hydrothermal alteration along these structures. Concerning Structure #20 it is obvious that calcite has been precipitated during different periods although the largest amounts of carbonates have probably been precipitated during hydrothermal conditions, with later redistribution and precipitations of rims etc during later periods. Structure #21 as seen in the intercept in KI0023B (the pumping section for the tracer tests) has been suggested to be a splay fracture to Structure #20, and it is therefore interesting to note the similarity in stable isotope values in calcite from this fracture intercept and the nearby intercept of Structure #20 in KI0023B.

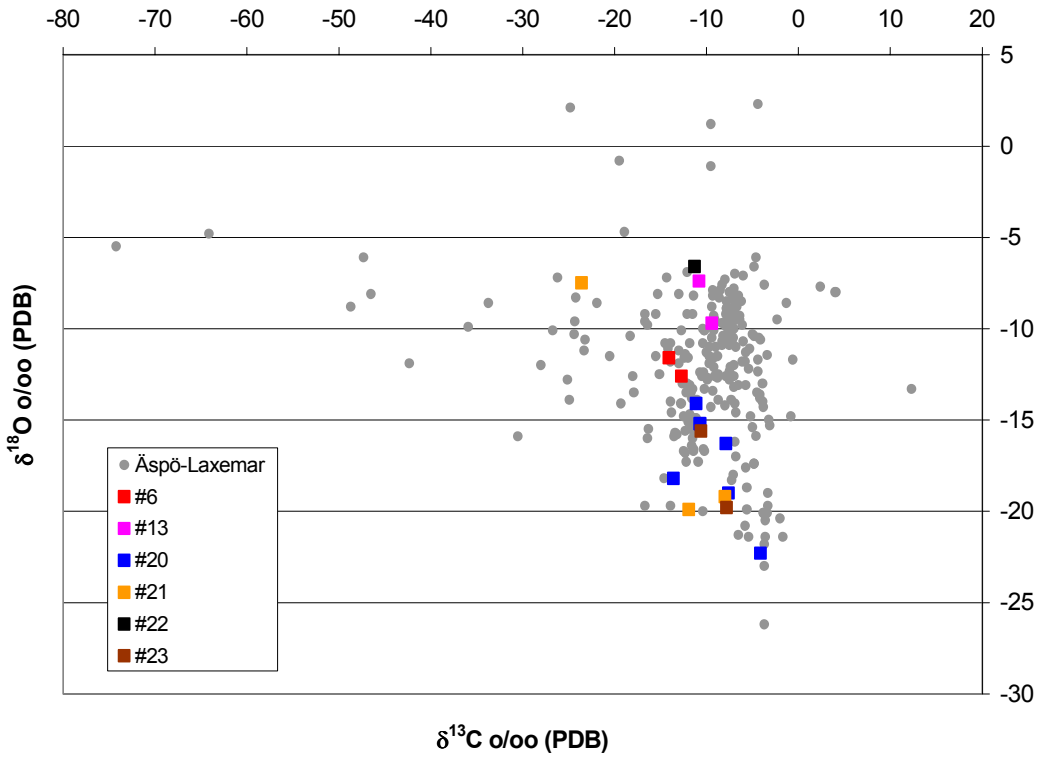

Figure 4-14. *$\delta^{18}O$ versus $\delta^{13}C$ for fracture coating calcites and fault breccia in structures from the TRUE Block Scale (coloured symbols), cf Table 4-13, and all previously analysed fracture coating calcites from Äspö (grey dots).*

The two analyses from Structure 13 (boreholes KA2563A and KI0023B) are very similar underlining the interpretation of this part of the structure as a homogenous part. Unfortunately, no analyses of calcites from the other part of the other leg of Structure #13 (in KI0025F02 and KI0025F03) have been carried out due to limitations in availablility of geological material, cf Section 4.6.4.

As pointed out in Section 4.6.3, Structure #21 is more of a hydraulic feature than a singular geologic structure, which is also indicated by the large variations in $\delta^{18}O$ and $\delta^{13}C$ observed in the calcites from the three intercepts analysed. The intercept in KI0025F02, representing the most pronounced structure with mylonite and fault breccia, showed the most extreme biogenic composition of calcite.

4.7.5 Uranium series analyses

Uranium series analyses have been carried out on a number of gouge material samples from structures within the TRUE Block Scale rock volume, cf Table 4-14. From four of the intercepts clayish fault gouge materials of grain size <0.125 mm, and in one case 0.25 mm, were analysed at Harwell Scientifics, UK. These samples are associated with Structures #6

Table 4-14. Uranium and Thorium series activity concentrations (Bq/kg).

Sample	^{238}U	^{234}U	^{230}Th	^{226}Ra	^{232}Th	^{228}Th
KA2563:154 <0.125 mm #6	47 ± 2	71 ± 3	42 ± 6		44 ± 7	59 ± 9
KI0023B:69.9 <0.125 mm #20	54 ± 3	152 ± 6	21 ± 2		17 ± 2	32 ± 3
KA2563A:188 <0.25 mm #20	85 ± 5	252 ± 10	39 ± 4		22 ± 3	46 ± 4
KI0025F:186 >0.125 mm #Z	78 ± 2	83 ± 2	78 ± 4	82 ± 2	152 ± 6	173 ± 7
KI0025F03:87.9 >1 mm #13	63 ± 3	64 ± 3	58 ± 3	132 ± 47		
KI0025F03:73.1 >1 mm #20	65 ± 3	64 ± 3	48 ± 3	37 ± 30		
KI0025F:88.8 >1 mm #22	37 ± 5	39 ± 5	32 ± 2	125 ± 49		
KI0025F03:63.2 >1 mm #22	28 ± 4	26 ± 4	25 ± 3	180 ± 61		

The fine-grained samples (<0.125 mm and <0.25 mm) were analysed at Harwell Scientifics (UK) and the >1 mm samples were analysed by CIEMAT (Spain), /de la Cruz et al, 2001/.

(KA2563A:L=154 m), Structure #20 (KI0023B:L=69.9 m and KA2563A:L=188 m) and Structure Z (KI0025F:L=186–194 m), cf Figure 4-6. In addition, four samples of fault breccia fragments (>1 mm) were analysed by CIEMAT, /de la Cruz et al, 2001/ associated with Structure #13 (KI0025F03:L=87.9 m), Structure #20 (KI0025F03: L=73.1 m) and Structure #22 (KI0025F:L=88.8 m and KI0025F03:L=63.2 m).

All the samples with fine-grained fault gouge material (<0.125 mm and 0.25 mm) show significant isotopic disequilibria (addition of uranium with $^{234}U/^{238}U$ ratios >1) whereas the >1 mm fault breccia samples show less significant disequilibria, or values close to equilibrium indicating more favourable conditions for sorption of uranium in samples of the fine-grained clayey fault gouge.

The most pronounced disequilibria were detected in the two fine-grained fault gouge samples from Structure #20 showing very high $^{234}U/^{238}U$ ratios (2.79 and 2.95 respectively) in combination with very low $^{234}U/^{230}Th$ ratios (0.14 and 0.15). This indicates recent uranium uptake from a groundwater enriched in ^{234}U.

Six groundwater analyses of uranium series isotopes from the 1999 sampling campaign are available from the TRUE Block Scale volume, and these show $^{234}U/^{238}U$ ratios between 3.3 and 9.4. Interestingly, the groundwater sample from KA2563A:L=187–190 m (Structure #20) shows a very high $^{234}U/^{238}U$ ratio (8.0) and this sample corresponds to the location of the fault gouge sample (<0.25 mm) with a $^{234}U/^{238}U$ ratio of 2.95. The processes behind this uranium accumulation are not fully understood, but at least two events may influence the interpretation:

1. Mobilisation and subsequent deposition of uranium (with enhanced ^{234}U) has occurred during recent geological periods, for example during the latest glaciation/deglaciation cycle, when hydrological and hydrochemical changes were considerable.

2. Changes in flow patterns, caused by the tunnel excavation and additional drilling, may have caused flushing of former stagnant zones/fractures (resulting in groundwater with very high $^{234}U/^{238}U$ ratios) and subsequent sorption of uranium enriched in ^{234}U in the clayish fault gouge material.

A combination of both processes is considered likely.

Sorption of Ra is indicated in the >1 mm fault breccia samples from Structures #22 and #13. Radium isotopes were not analysed in the fine-grained (<0.125 mm and 0.25 mm) samples from Structures #20 and #6, but radium sorption was indicated by $^{228}Th/^{232}Th$ ratios >1 for all four samples analysed, and was found to most pronounced for the two samples from Structure #20.

A more detailed interpretation of the U and Th isotope results taking all the available data form Äspö into account is currently in progress /Tullborg and Smellie, in prep/.

4.8 Generalised detailed conceptual model of target structure

/Winberg et al, 2000/ presented a conceptual model of Feature A studied as part of the First TRUE Stage. This model featured an altered rim zone of Äspö diorite, and also included fault breccia and possible fine grained fault gouge material. Taking the step to TRUE Block Scale, firm evidence of fault breccia pieces and fragments and existence of fine-grained fault gouge has been obtained.

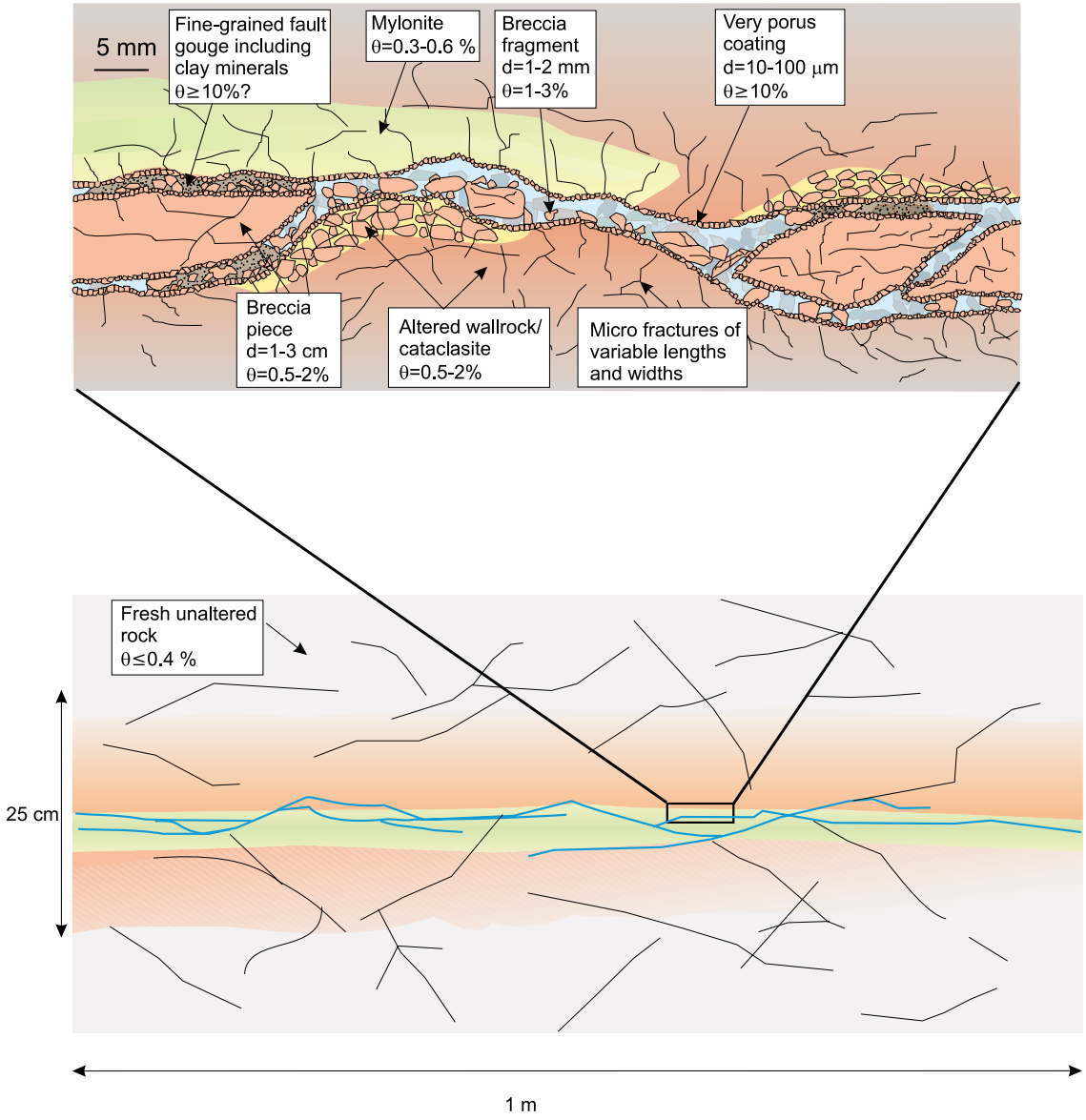

Figure 4-15. *Generalised conceptual model of a typical conductive structure involved in the tracer experiments. Details on porosity estimates are provided in Section 7.2.*

The principal conductor of the target area for tracer tests, Structure #20, is characterised by a fault with a fracture centered on a mylonite. Similar characteristics are also seen to a variable degree for parts of Structure #13 and Structure #22. The generalised conceptual model, cf Figure 4-15, of a typical conductive structure in the TRUE Block Scale rock volume, therefore reflects many of the features of Structure #20, cf Appendix C-3. Emphasised in the conceptual picture is the altered zone centred of the conductive fracture plane. This altered zone is characterised by a highly porous thin layer at the fracture surfaces and a gradually decreasing porosity away from the fracture surface into the intact unaltered wall rock, cf Section 7.2.2 and 7.2.3. The fracture plane is to a variable degree in-filled with fault breccia (cm-sized pieces and mm-sized fragments) and a matrix of fine-grained clayey fault gouge, cf Section 4.7.3. It is envisaged that the

physical distribution of in-filling material is variable such that variably shaped open space (physical flow channels) occur. The actual flow channels for a given situation are dependent on the actual boundary conditions.

4.9 Hydraulic properties of the deterministic structures

Table 4-15 presents the transmissivity values evaluated for the deterministic structures in the TRUE Block Scale rock volume. The sources of data and more detailed explanations appear in /Doe, 2001/ and /Hermanson and Doe, 2000/.

Transmissivity values for the structures in the TRUE Block Scale volume come from several sources including pressure build-up tests, cross-hole interference tests, and different types of flow logs. We separate the performed transmissivity analyses into two types; steady flow and transient flow calculations. Flow logs generally provide only steady flow data. Flow and pump tests may be interpreted using either steady or transient methods provided that transient data are available. Build-up tests are always interpreted using transient methods. There are several steady flow equations for interpreting transmissivity values, but for the most part they all use the specific capacity (flow divided by pressure change expressed as a hydraulic head) multiplied by a constant that reflect assumptions about the flow geometry (cf discussion in Section 3.3 on flow logging for more details). Steady flow methods do not provide information on flow geometry (flow dimension) and they can be strongly influenced by regions in the immediate vicinity of the borehole, particularly regions of lower transmissivity than the tested structure's average transmissivity. Transient interpretations should therefore provide transmissivity values that reflect a larger portion of the structure's area, and the area of influence is a function of the duration of the test.

Table 4-15 also presents well test analyses using the Golder Associates Flowdim code /Enachescu et al, 1997/. For purposes of comparison, the values presented here are for the best matches using an assumed flow dimension of 2. The Flowdim results generally agree well with other transient data interpretations. Where differences appear, they mainly reflect the accounting of skin effects, which appear strongly in some tests.

Table 4-15. Transmissivity data (m^2/s) for the deterministic structures included in the TRUE Block Scale hydro-structural model, cf Figure 4-6.

Structure	KI0025F			KI0025F02			KI0025F03			KI0023B			KA2563A		
	PBU	PTT	PTSS	PBU	PTT	PTSS	PBU	PTT	PTSS	PBU	PTT	PTSS	PBU	PTT	PTSS
7	1.3E-05	3.7E-05	6.2E-08	1.7E-06	1.8E-06	>1.6E-07	x	x	6.3E-08	1.8E-05	1.6E-05	x	x	2.1E-05	x
6	x	x	x	1.5E-08	1.5E-08	1.1E-08	6.8E-08	1.1E-07	2.1E-07	4.0E-07	3.3E-08	1.7E-06	x	x	2.2E-08
24	x	x	x	x	x	x	x	x	3.0E-08	x	x	x	x	x	x
23	x	x	x	5.3E-09	1.1E-08	5.4E-09	1.5E-08	1.3E-08	2.0E-08	x	x	x	x	x	x
22				2.6E-07	3.3E-07	>1.0E-07	8.3E-09	x	3.5E-08	x	x	x	x	x	x
20	5.1E-07	8.5E-07	4.4E-08	6.5E-07	1.1E-06	>1.2E-07	6.1E-07	6.1E-07	7.5E-08	9.6E-07	1.4E-07	8.9E-08	x	8.7E-07	>1.9E-07
21	x	x	x	9.6E-09	5.0E-08	2.8E-08	3.9E-09	9.6E-09	2.1E-08	8.1E-07	6.9E-07	1.5E-07	x	x	6.8E-09
13	x	x	x	1.5E-09	4.6E-09	3.9E-09	3.8E-08	4.4E-08	6.7E-08	5.8E-08	9.8E-08	3.3E-08	x	4.5E-08	2.7E-08
19	2.9E-05	x	8.9E-07	1.7E-06	1.1E-07	>1.1E-07	1.3E-06	x	1.2E-07	3.9E-06	1.2E-06	1.2E-07	x	x	9.4E-08
10	x	x	x	5.3E-08	5.3E-08	3.3E-08	x	x	x	4.5E-06	2.7E-06	2.2E-07	x	x	x

PBU = Pressure Build-Up tests (transient evaluation, Cooper-Jacob)
PTT = Pump Test (Transient evaluation, Cooper-Jacob)
PTSS= Pump Test (packer flow log or Posiva flow log) (Steady State evaluation, Moye)

5 Background fracturing

The purpose of this chapter is to provide a quantitative basis for modelling of background fracturing[1] in the region where TRUE Block Scale boreholes intersect Structures #13, #20, #21, and #22. This area, the "Tracer Test Volume" (TTV), and the structures contained in it, are the focus of the Tracer Test Stage (TTS) of the TRUE Block Scale tracer experiment. It is assumed that "conductive background features" are best identified as the flowing features identified in POSIVA flow logs, other than those which are "deterministic" and numbered features in the TRUE Block Scale Hydro-Structural model.

The following boreholes were analysed:

- KI0025F02
- KI0025F03
- KA2563A
- KA2511A
- KA3510A

The area which has been subject to analyses is given by plus and minus 20 metres from the location where Structures #6 and #19 intersect the above mentioned boreholes, cf Figure 4-6. Borehole KA3510A ends 50 m before it would intersect Structure #6, and is along most of its length intersecting the complex fracture zones around Structure #5, including Structures #1–#4. Borehole KA3510A was analysed as part of the study, but is not included in overall statistics, since it primarily reflects Structure #5 fracture zone and fractures rather than background fractures. Borehole KA2511A intersects Structure #20 approximately 80 m away from the region where the tracer tests of the Tracer Test Stage have been performed. Nevertheless, the fractures intersecting KA2511A were included in the statistics to increase the size of the data set for analysis.

The calculated statistics are based on conductive background fractures identified in the four remaining boreholes.

[1] With background fractures we here denote those conductive fractures/structures which have not been assigned to a deterministic structure. A deterministic structure is defined by at least two hydraulic borehole anomalies correlated in space.

5.1 Fracture intensity

The intensity of conductive background fracturing have been derived directly from the POSIVA flow logs by counting the number of flowing fractures and dividing by borehole length. Anomalies associated with the deterministic structures included in the hydro-structural model have been eliminated from the data to retain only background fractures, cf Table 5-1. Conductive structure transmissivity values in Table 5-1 are based on the simplified approach described in Section 5.3 below.

Table 5-2 presents fracture intensity statistics for conductive background features along the full length of logged boreholes, and in the defined TTV region, here for computational purposes defined as plus and minus 20 metres from the location where Structures #6 and #19 intersect each borehole, cf Section 1.8.2. For the TTV region, the linear intensity P_{10} (m^{-1}) (number of fractures per unit length of borehole) varies from 0.16 to 0.21 m^{-1} amongst the boreholes with an average of 0.19 m^{-1}. This is a relatively small degree of variation, and a value of 0.19 m^{-1} should therefore be an appropriate average value for all modelling of the TTV region.

The fracture volumetric intensity P_{32} (m^2/m^3) (area of fractures per volume of rock mass) is calculated by simulating boreholes with the orientation distribution derived in Section 5.2 and calculating the ratio C_{31} of the volumetric intensity P_{32} to the linear intensity P_{10} from the simulated boreholes,

$$C_{31} = P_{32}\,(\text{sim}) \,/\, P_{10}\,(\text{sim}) \qquad (5\text{-}1)$$

This ratio can then be used to derive and estimate the volumetric intensity.

$$P_{32} = C_{31}\, P_{10} \qquad (5\text{-}2)$$

For the boreholes studied and the fracture orientation distribution in Section 5.2 the value of C_{31} is 1.52, such that the representative value of P_{32} for conductive background fractures is 0.29 m^2/m^3.

Table 5-1. Numbered deterministic structures eliminated from conductive background fracture data base. The derivation of the transmissivity is described in Section 5.3.

	Depth of Feature (m)	Depth (m) BIPS	Trend BIPS	Plunge BIPS	Transmissivity m^2/s
KI0025F02					
#6	53.32	52.5	133	86	1.36E-08
#7	42.57	40.9	313	74	6.78E-10
#13	95.07	94	140	83	4.07E-09
#19	137.14	133.1	141	88	4.07E-08
#20	77.25	74.8	148	85	1.36E-07
#21	95.90	97.9	354	77	3.39E-08
#22	67.07	68.8	165	83	6.78E-08
#10	157.20	164.6	302	87	2.71E-09
KI0025F03					
#6	50.30	51.9	136	81	2.71E-07
#7	42.18	43	88	87	5.42E-08
#13	90.23	87.7	351	72	2.03E-08
#19	131.31	125.5	139	89	4.74E-08
#20	73.88	73.2	291	78	6.78E-08
#21	82.07	85.7	326	87	1.36E-09
#22	60.93	61.3	261	81	2.71E-08
KA2563A					
#6	158.64	157.5	119	86	2.71E-08
#7	153.70	144.9	319	72	1.36E-10
#13	208.01	207	148	79	2.71E-08
#19	239.60	238	343	76	1.36E-07
#20	189.90	188.7	316	82	1.36E-06
#21	182.33	182.6	244	15	6.78E-09
#22	172.64	173.2	275	23	1.36E-09
KA2511A					
#6	87.50	84.8	335	58	6.78E-08
#7	36.54	26.5	297	76	1.36E-07
#10	239.98	240.6	127	85	6.78E-08
#13	148.43	143	98	84	1.36E-07
#19	153.93	150.5	186	19	2.03E-08
#20	120.23	119.5	15	71	1.36E-10
#21	156.10	156.4	232	46	3.39E-09
#22	129.87	124.9	131	65	2.71E-10

Table 5-2. Statistics of background fracture intensity.

	Interval	KI0025F02	KI0025F03	KA2563A	KA2511A	KA3510A	**KI0025F02, KI0025F03, KA2563A, KA2511A**
Posiva Features	Borehole	39	32	69	71	41	211
Length (m)	Borehole	170	129.7	282.9	267.6	112.5	850.2
Intensity P_{10}	**Borehole**	**0.23**	**0.25**	**0.24**	**0.27**	**0.36**	**0.25**
TTV Region Start	TTV Region #19+20 m to #6–20 m	33.32	30.30	138.64	67.50	175.00	
TTV Region End	TTV Region #19+20 m to #6–20 m	157.14	151.31	259.60	173.93	280.00	
Conductive Background Features	TTV Region #19+20 m to #6–20 m	20	24	26	21	0	91
Metres	TTV Region #19+20 m to #6–20 m	123.82	121.01	120.96	106.43	0.00	472.2201
Intensity P_{10}	**TTV Region #19+20 m to #6–20 m**	**0.16**	**0.20**	**0.21**	**0.20**		**0.19**

5.2 Fracture orientation

Orientation distributions were studied for conductive background fractures in the four target boreholes, and also for the subset of fractures in the TTV region interval defined in Table 5-2. Sets were defined by the probabilistic algorithm of /Dershowitz et al, 1996/ using the software FracMan/ISIS. Results of this analysis are provided in Table 5-3 and Figure 5-1.

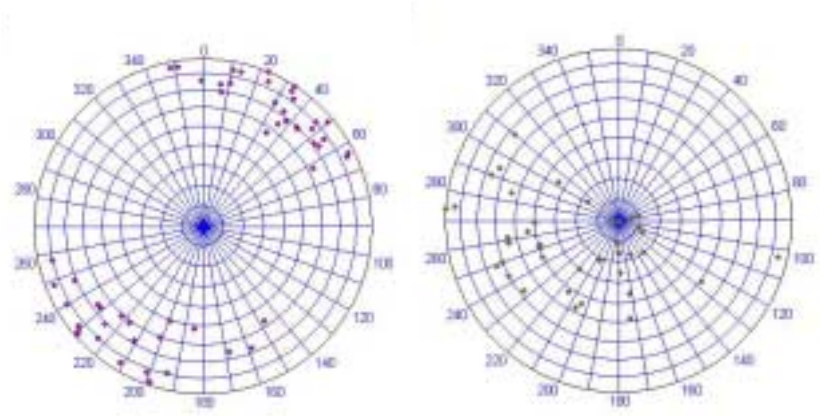

Figure 5-1. *Sets 1 (left) and 2 (right) derived for conductive background fractures.*

Table 5-3. Definitions of conductive background fracturing sets.

Parameter/statistic	Set #1	Set #2
Fractures Assigned	58 (55.2%)	47 (44.8%)
Mean Pole (Trend, Plunge)	(211, 0.6)	(250, 54)
Mean Orientation (Strike(righthand)/Dip)	(121, 89.4)	(160, 36)
Distribution	Fisher	Fisher
Fisher Dispersion κ	9.35	3.8
Kolmogorov-Smirnov Goodness of Fit (% Statistical Significance)	0.085 (79.4%)	0.228 (1.5%)

5.3 Transmissivity of fractures

The simplest approach for derivation of the fracture transmissivity distribution is to apply the radial flow equation to the flow in the POSIVA flow logs.

$$T = (Q/\Delta h) \ln [R/(2 \pi r_w)] \quad (5\text{-}3)$$

where Q is flow, Δh is head drop, R is the "radius of influence", and r_w is the well radius. Assuming R is 0.65 m and r_w is 0.038 m,

$$\ln [R/(2 \pi r_w)] \sim 1 \quad (5\text{-}4)$$

$$T \sim (Q/\Delta h) \quad (5\text{-}5)$$

For these POSIVA flow logs, Δh is approximately 410 m. Based on this transformation, the distributions of POSIVA flow log transmissivity for each of the four wells in the TTV region are shown in Figure 5-2 and summarised in Table 5-4. Although the distributions of fracture transmissivity seem to vary between boreholes, the overall statistics are remarkably stable between boreholes and data sets, even when including data from KA3510A. The background fracture transmissivity mean and standard deviation for model simulations can therefore be taken with some confidence from the TTV Region values in Table 5-4.

Table 5-4. Statistics of transmissivity obtained from POSIVA flow log data.

	KI0025F02	KI0025F03	KA2563A	KA2511A	KA3510A	5 Holes	TTV Region Only
Mean	1.692E-08	1.871E-08	1.210E-08	2.623E-08	6.833E-09	1.762E-08	1.099E-08
St Dev	2.948E-08	7.132E-08	3.860E-08	7.350E-08	1.700E-08	5.374E-08	3.313E-08
Median	3.388E-09	2.033E-09	3.388E-10	1.355E-09	6.098E-10	1.355E-09	6.775E-10
Maximum	1.355E-07	4.065E-07	2.033E-07	4.743E-07	6.775E-08	4.743E-07	2.033E-07
Log10 Mean	–8.53	–8.72	–9.13	–8.76	–9.10	–8.86	**–8.95**
Log10 StDev	0.94	0.95	0.96	1.10	0.90	1.01	**0.93**

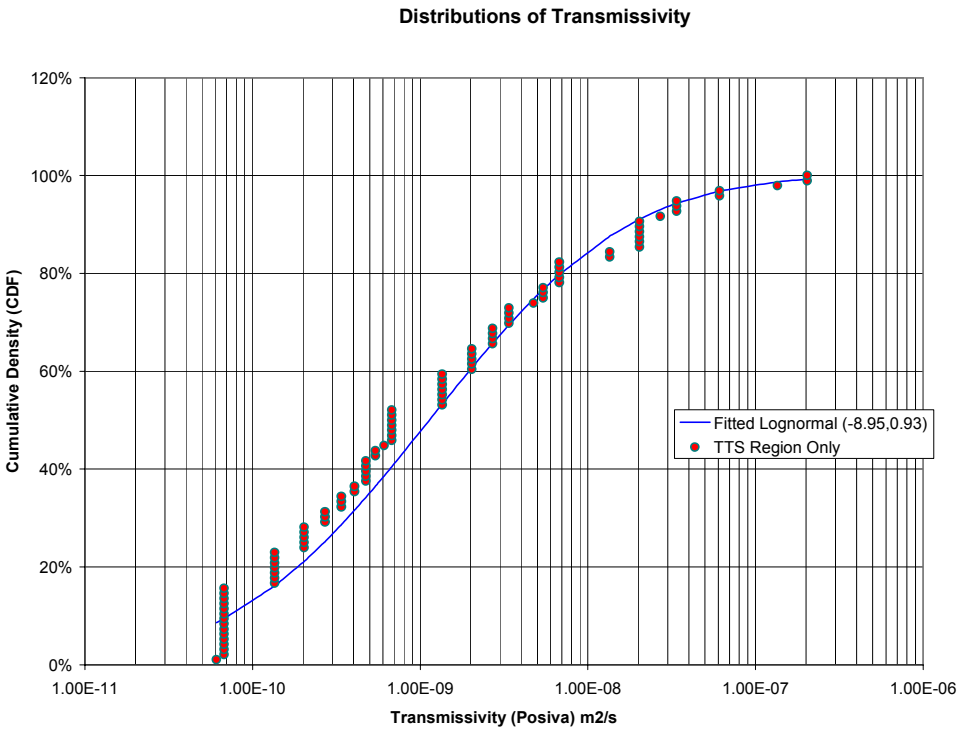

Figure 5-2. *Fit of a lognormal distribution to the TTV region data passing the Kolmogorov-Smirnov test at the 10% level.*

Although the approach given in this section is very rough, a comparison of the values of transmissivity for deterministic structures listed in in Table 5-1 with the more rigorously derived values of Table 4-15 indicates a comforting level of consistency.

5.4 Size distribution

The fracture size distribution is derived from mapping of the tunnels in the vicinity of the experimental site. The fracture size analysis used the simulated exploration size-estimate method /after LaPointe et al, 1993a/ where the observed trace lengths of each fracture around the tunnel perimeter is matched to simulated fracture networks intersecting an identical simulated tunnel. The simulated fracture size distribution was chosen which best mimicked the observed trace length distribution on the tunnel wall. Background fractures were not generated set by set, only the mean size distribution, and as a consequence only a single estimate of fracture size could be derived. The results show a best fit of a fracture radius distribution with a log-normal distribution with mean of 6 m and standard deviation of 2 m.

5.5 Spatial pattern

The spatial pattern of background fracturing affects the pattern of connectivity within rock masses, and has been shown to be an indicator of the geometry of hydraulic compartments /LaPointe et al, 1993b/. A previous analysis was carried out based on fracture data sets from borehole TV (BIPS) logs. The current study repeats this analysis using data on flowing features obtained from the POSIVA flow log interpretations.

5.5.1 Stationarity

Spatial stationarity means that while the occurrence of fractures varies from place to place, certain statistical properties of the fracture population are the same throughout the region. This is evaluated by visual inspection of the fracture patterns and by calculating spatial statistics.

Spatial stationarity has been evaluated based on the pattern of intensity with distance from the borehole collar. The use of relative location rather than absolute location does not effect the analysis results for individual boreholes, and greatly simplifies the analysis. However, since all the boreholes extend into the TRUE Block Scale rock volume, small depths indicate data from near the access tunnel, and larger values indicate locations nearer to the centre of the rock block and deeper.

Visual inspection of the intensity in the TRUE boreholes reveals no spatial trends. Table 5-5 presents the results of simple spatial analysis averaging intensity on 25-m intervals. A systematic spatial trend could be indicated if intensity values more than one standard deviation (σ) from the mean occurred consistently at shallower or deeper portions of the boreholes. Intensity P_{10} values more than one standard deviation from the mean are highlighted in Table 5-5.

Table 5-5. Conductive feature intensity P_{10} vs. distance from borehole collar.

Distance from BH Collar (m)	KI0025F02 (#/m)	KI0025F03 (#/m)	KA2563A (#/m)	KA2511A (#/m)	KA3510A (#/m)
0	0.6 ***	0.12*	0.20*	0.44**	0.24
25	0.12*	0.32	0.36***	0.28*	0.04**
50	0.20	0.08	0.28	0.44***	0.32
75	0.00**	0.40**	0.20	0.00**	0.60
100	0.12	0.16	0.16	0.24	0.16
125	0.32		0.32**	0.04	
150	0.20		0.08**	0.20	
175			0.28	0.24	
200			0.24	0.40	
225			0.32	0.44**	
250			0.16	0.12	
275			0.16		
300					
Summary Statistics					
Mean, μ	0.22	0.22	0.23	0.26	0.27
St Dev, σ	0.19	0.14	0.08	0.16	0.21
$\mu + \sigma$	0.42	0.35	0.31	0.42	0.48
$\mu - \sigma$	0.03	0.08	0.15	0.10	0.06

* Values in the TTV region.
** Intensity values more than one standard deviation from the mean value.
*** Both the above.

No systematic pattern of variation is indicated. This suggests that, at least according to this measure, the rock can be considered statistically homogeneous. Table 5-5 also shows that there is no obvious monotonic decrease or increase in intensity with distance.

5.5.2 Spacing and intensity distributions

The spatial pattern of conductive background fracturing can be indicated by the distribution of intensity P_{10} (fractures/metre), and by the distribution of spacing (S) between successive fractures. A power law (Pareto) distribution of P_{10} implies a fractal process of spatial location, while an exponential distribution of spacing (S) implies a Baecher (Poisson) process of spatial location.

Table 5-6 presents an analysis of spacing distributions for conductive background features observed over the full borehole length, including the TTV Region. For each borehole, the spacing distributions were fitted using 21 different possible distributional forms. Goodness of fit was evaluated using;

- the Chi-squared goodness of fit test, which measures the root mean square (RMS) difference between data and fitted histogram probability density functions (PDF),

- the Kolmogorov-Smirnov goodness of fit test, which measures the magnitude of the worst portion of the match between data and fitted cumulative density functions (CDF), and

- the Anderson-Darling goodness of fit test, which is a modification of the Kolmogorov-Smirnov test to provide higher weight for the tails of the distribution, to better distinguish alternative distributions.

In Table 5-6, the distributions are ranked based on the Anderson-Darling Test. The ranking of distributions varies among the boreholes. The meaning of the goodness of fit is that this is the probability that the tested distribution would be rejected incorrectly. A 95% goodness of fit implies that there is a 5% probability of rejecting a fit even if it were the correct distribution.

Table 5-6. Spacing distribution analysis. Analysis of data from complete borehole lengths and for data from borehole lengths defining the TTV area.

	Full borehole	**Full borehole**	**Full borehole**	**Full borehole**	**Full borehole**	**TTV area only**
	KI0025F	KA2563A	KI0023B	KA3510A	KA2511A	TTV area
Exponential Distribution Parameter λ	5.13	4.181	4.16	3.82	3.41	4.78
Exponential Ranking (of 21)	7	7	6	6	7	5
Goodness of Fit Chi-Squared Test	Rejected	Rejected	>0.09	Rejected	Rejected	Rejected
Goodness of Fit Kolmogorov-Smirnov	Rejected	Rejected	>0.05	>0.01	Rejected	>0.01
Goodness of Fit Anderson-Darling Test	Rejected	Rejected	>0.025	Rejected	Rejected	>0.01
Best Fit Distribution	Lognormal	Inverse Gaussian	Gamma	PearsonVI	PearsonV	Lognormal
Parameter 1	5.12	4.18	1.43	0.95	1.55	5.04
Parameter 2	11.13	1.28	2.92	3.38	1.928	8.75
Parameter 3				9.34		
Goodness of Fit Chi-Squared	Rejected	Rejected	>0.21	Rejected	Rejected	>0.06
Goodness of Fit Kolmogorov-Smirnov	>0.15 *	>0.15 *	>0.15 *	>0.15 *	>0.15 *	>0.15 *
Goodness of Fit Anderson-Darling	>0.15 *	>0.15 *	>0.15 *	>0.15 *	>0.15 *	>0.15 *
Is Baecher Model OK ?	No	No	Yes	No	No	Yes

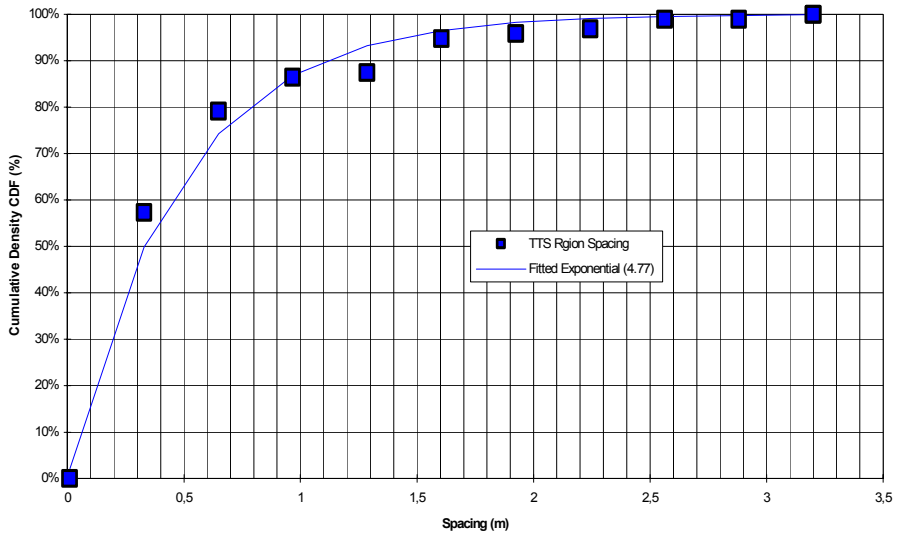

Figure 5-3. *Exponential spacing distribution, TTV area.*

The exponential distribution, however, is never the best fit for data from the complete length of boreholes. However, the exponential distribution does provide a statistically significant fit in the TTV region (Figure 5-3) even though it only fits one borehole for the complete borehole length. This indicates that the Baecher model may be used for background fracturing in the TTV region, although it is not necessarily applicable for the full TRUE Block Scale rock volume.

5.5.3 Intensity distribution

Just as an exponential distribution of spacing is indicative of a Baecher spatial model, a Pareto ("Power Law") distribution of intensity P_{10} implies a fractal process of location /Barton and LaPointe, 1995/. To facilitate this analysis, intensities P_{10} (fractures/metre) were calculated for the data from the four boreholes in the TTV region. This data was then fitted against Pareto and other distributions, omitting data from empty intervals.

The same approach for testing the fits was used as described in Section 5.5.2 above. Results of this analysis are summarised in Table 5-7.

The distribution fitting analysis shown in Table 5-7 does not support the use of Fractal spatial location models. More detailed analyses for alternative spatial models is described in the table.

5.6 Spatial model analysis

The spatial pattern of conductive background fracturing can also be derived by fractal and geostatistical analysis of fracture intersections with boreholes. This section describes a variety of fractal and geostatistical analyses of data from boreholes KI0025F02, KI0025F03, KA2563A, and KA2511A. Due to lack of sufficient data in the TTV region, this analysis was carried out for the full length of each of the four boreholes.

Table 5-7. Distribution fit to 5m interval P_{10} data, TTV area.

	Pareto Distrib (Fractal Process)	Gamma Distrib (Poisson Model)	Best Fit Extreme Value
Number of Intervals with Data	15	15	15
Pareto Distribution Parameter 1	2.52	4.54	0.25
Pareto Distribution Parameter 2	0.20	0.073	0.14
Ranking (of 21)	21	7	1
Goodness of Fit Chi-Squared	Rejected	Rejected	Rejected
Goodness of Fit Kolmogorov-Smirnov	Rejected *	>0.05 *	Rejected
Goodness of Fit Anderson-Darling	Rejected *	>0.15 *	Rejected
Model	Rejected	OK	N/A

5.6.1 Fractal analysis

Three different fractal analyses were carried out. The "box/ruler fractal analysis" evaluates fractal dimension directly from the relationship between the number of boxes necessary to cover all the fractures and the size of the box. The "mass fractal analysis" evaluates fractal dimension from the relationship between the number of fracture centres within a circular region and the circle radius. The "spectral fractal analysis" is based on Fourier spectral analysis of 5m interval fracture intensity patterns. The calculation methodology of the three methods is described by /Barton and LaPointe, 1995/ and /Dershowitz et al, 1999/.

Box/ruler, mass, and spectral fractal analysis results are summarised in Table 5-8. The box dimension analysis produced dimension estimates *D* of 2.5 to 2.59. These values are remarkably consistent. They are also consistent with values for Äspö from trace map analysis,

Table 5-8. Summary of fractal analyses.

Borehole	Spectral Analysis	Ruler (Box) Analysis	Mass (Levy) Analysis
KI0025F02	intercept=–4.80	intercept=27.0	intercept=1.05
	slope β=–2.0	slope β=–0.57	slope β=0.65
	D=3.5	D=2.57	D=2.65
KI0025F03	intercept=–3.40	intercept=31.0	Intercept=0.87
	slope β=–1.41	slope β=–0.59	slope β=0.78
	D=3.8	D=2.59	D=2.78
KA2563A	intercept=–3.9	intercept=41.81	Intercept=0.64
	slope β=–1.22	slope β=–0.59	slope β=0.83
	D=3.9	D=2.59	D=2.83
KA2511A	intercept=–2.87	intercept=27.7	Intercept=0.39
	slope β=–0.68	slope β=–0.50	slope β=0.97
	D=4.16	D=2.50	D=2.97
3D Dimension D	D=4.5+β/2	D=2–β	D=2+β

reported in /LaPointe et al, 1999/. This Box fractal dimension *D* implies that the fractures in the TRUE Block Scale block are fractal in their spatial arrangement, and are not space-filling. In contrast, a Poisson model would have a Box dimension *D* of 3.0.

The dimensions from spectral analyses vary between 3.5 and 4.16. For the spectral analysis, a dimension of 3 implies a completely uncorrelated, i.e., Poissonian field, while a dimension of 4 implies a smoothly varying, well correlated field. Dimensions near 4 are generally indicative of periodic data, or data with a trend. Values between 3 and 4 imply fractal spatial processes. The spectral analysis results for three of the four boreholes thus imply a fractal process of spatial location within the overall TRUE Block Scale rock volume. The spectral analysis was carried out on values obtained from 5 m intervals, and therefore lacks the resolution to detect clustering at scales less than 5 m.

5.6.2 Geostatistical analysis

Geostatistical variograms for conductive fracture intensity P_{10} were fit according to spherical, exponential, Gaussian, de Wijs, and power-law variogram models for 5 metre interval data in boreholes KI0025F02, KI0025F03, KA2563A, and KA2511A. Generally, the best fit was obtained by a pure nugget model, indicating no spatial correlation. A summary of the geostatistical analyses is presented in Table 5-9.

Note that like the spectral fractal this analysis cannot detect spatial correlation at scales less than 5 m due to the binning used for intensity.

Table 5-9. Geostatistical analysis of conductive background fracture intensity P_{10}.

Borehole	Best Fit Model	Parameters	Std. Dev.	Interpretation
KI0025F02	Exponential	Exponent=7.78	0.0075	Weak spatial correlation
KI0025F03	Nugget	Sill=0.095	0.017	No spatial correlation
KA2563A	Nugget	Sill=0.030	0.0039	No spatial correlation
KA2511A	Power law	a=0.0664 c=0.054	0.0082	Weak spatial correlation

5.7 Summary of model of background fractures

Table 5-10 summarises the Background DFN Model based on the analyses above. These parameters were recommended for use in modelling of background fractures in the TTV region of the TRUE Block Scale rock volume.

Table 5-10. Summary of conductive background DFN model.

Parameter	Basis	Set #1	Set #2
Orientation Distribution	Two Fitted Sets (NeurISIS)	Fisher Distribution Mean Pole (Trend, Plunge) = (211, 0.6) Mean orientation (Strike/Dip) = (121, 89.4) Fisher Dispersion κ = 9.4	Fisher Distribution Mean Pole (Trend, Plunge) = (250, 54) Mean orientation (Strike/Dip) = (160, 36) Fisher Dispersion κ = 3.8
Intensity P_{32}	Flowing Posiva Log Features 0.29 m^2/m^3 (total)	0.16 m^2/m^3 (55.2% of fractures)	0.13 m^2/m^3 (44.8% of fractures)
Transmissivity	Flowing Posiva Log Features, OxFilet Analysis of Packer Tests	Lognormal Distribution mean = –8.95 $\log_{10}$ m^2/s st.dev = 0.93 $\log_{10}$ m^2/s	Lognormal Distribution mean = –8.95 $\log_{10}$ m^2/s st.dev = 0.93 $\log_{10}$ m^2/s
Size Equivalent Radius	/Follin and Hermanson, 1997/	Lognormal Distribution mean = 6 m st.dev. = 3 m	Lognormal Distribution mean = 6 m st.dev. = 3 m
Spatial Pattern	Distribution, Fractal, Geostatistical Analyses	Baecher Model in TTV Region Fractal (D≈2.6) for larger scale blocks	Baecher Model in TTV Region Fractal (D≈2.6) for larger scale blocks

6 Groundwater flow system

6.1 Introduction

This chapter describes the site characterisation activities that provided information on the flow system in the investigated TRUE Block Scale rock volume. We will refer to these flow conditions as "ambient" to the extent that they do not involve any of the withdrawal or injection activities associated with tracer tests or hydrologic characterisation.

The flow fields in the investigated rock volume are driven by the flows to the underground openings of the Äspö HRL, and in that sense they do not reflect the virgin flow conditions of the studied block. The flow field may also reflect disturbances due to the presence of existing boreholes. However, the piezometers were designed to isolate separate conductors and hence should return the conductive network to its original state to the extent possible.

Information on the flow fields in the TRUE Block Scale rock volume supports the understanding of tracer transport and retention in several ways, ia;

- Development of pressure or flux boundary conditions for the studied block,
- Providing an understanding of how the fracture networks in the TRUE Block Scale rock volume connect to the larger-scale flow field of the Äspö HRL site, and
- Providing information to test and refine the fracture network conceptual model of the TRUE Block Scale rock volume.

The flow field information comes from several sources including:

- *Groundwater hydraulic head*: The monitoring systems of the TRUE Block Scale experiment have been measuring the groundwater pressure throughout the duration of the program. The ambient data come from time periods with no testing activity. The ambient pressures have not been static, but change with time in response to the long-term inflows and pumping from the entire Äspö laboratory facility as well as due to annual variations.
- *Groundwater chemistry*: The groundwaters sampled at the Äspö HRL come from multiple sources including Baltic seawater, Meteoric water, Glacial waters, and Deep brine, and most samples reflect some mix of waters from these different sources. Some useful indicators of groundwater type are the chloride content, oxygen isotope ratios, and the tritium content. Deeper waters tend to be more saline both due to age and relative density, and they are less likely to contain tritium from meteoric sources. Variations in chemical composition can indicate not only whether or not different parts of the block are well connected, but also whether the fracture

network is preferentially connected to shallow or deeper water sources, respectively. As with the hydraulic head data, chemical compositions of water can vary with time, in response to the flow systems created by the Äspö HRL as a whole.

- *Background groundwater flow:* Tracer dilution experiments have been an important component of the overall block characterisation effort, cf Section 3.7. Changes in flow in response to the pumping of remote monitoring intervals are good indicators of connectivity and for selecting the source-sink pairs for tracer tests. Each of the dilution tests has involved an ambient flow measurement in addition to a measurement under pumping conditions. These ambient measurements indicate the local groundwater flow mainly due to flow to the underground openings. Groundwater flow may be very heterogeneously distributed (governed by the local transmissivity distribution), and the values provided by dilution tests only measure the flow in the immediate vicinity of the borehole. Nonetheless, the distribution of flow values provides a useful, although qualitative, indicator of the overall flow within the block.

Together, the hydraulic head distribution, the groundwater chemistry variation, and the groundwater flow measurements provide information on the flow field within the TRUE Block Scale rock volume. This information, together with larger-scale hydraulic head and chemistry distributions across the Äspö HRL, forms a basis for defining the boundary conditions of the investigated block scale rock volume. This information also supports a better understanding of the network of conductors within the block, and how those conductors connect with the boundaries of the block scale volume.

6.2 Groundwater chemistry

The space and time variations of groundwater chemistry provide information on flow patterns and the connectivity of fracture networks within the studied rock volume to larger structures of the Äspö HRL. Information on these variations comes from two sources; the first is fluid resistivity logging of boreholes that shows variations in salinity of the water in the open borehole, and the second is the chemical analysis of water samples collected from packed-off piezometer sections of a borehole.

6.2.1 General characteristics of Äspö groundwater chemistry

The groundwater in the Äspö HRL has several sources with different chemical signatures. Figure 6-1 shows a principal components analysis (PCA) plot of the groundwaters of the Äspö HRL. The plot indicates four different chemical sources; Meteoric water, Baltic seawater, Deep brine, and old Glacial waters. Groundwater compositions obtained from the TRUE Block Scale water samples plot as mixtures between deep glacial and brine waters and Baltic seawater with a large variability in Baltic component.

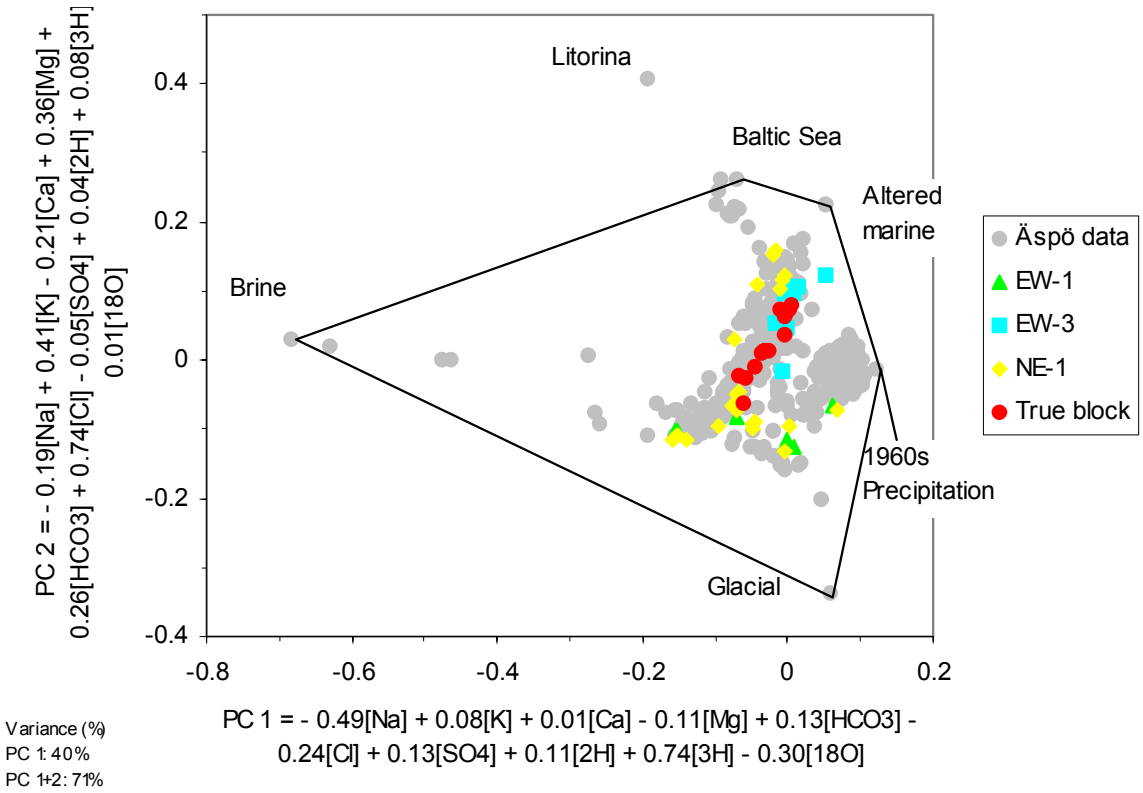

Figure 6-1. *PCA plot of TRUE Block Scale groundwater chemistry data (March 1998) with corresponding data from the Äspö Laboratory.*

The water chemistry at Äspö (after the tunnel excavation) can largely be explained as a mixing of younger Meteoric and Baltic waters with older Deep brine and Glacial water. The glacial component (most easily distinguished by its low $\delta^{18}O$ and ^{3}H values) is the most limited pool of water whereas Baltic seawater and Deep brine are more or less unlimited pools. Meteoric water is limited by recharge.

The groundwater sampling made as part of the TRUE Block Scale program did not measure the full range of elements making up the PCA components at enough locations to enable differentiation of waters within the block to any level of detail. However, samples for a more restricted set of components; Cl^{-}, ^{18}O, and ^{3}H, are more numerous, and are sufficient to broadly identify the groundwater types. Salinity, as measured by Cl^{-}, is not sufficient by itself to differentiate water sources, as there are two different sources of higher salinity water – Deep brine and Baltic seawater. However, these two saline sources differ in their $\delta^{18}O$ values and their exposure to bomb-pulse radioisotopes (^{3}H). Groundwaters with large components of Deep brine should have lower ^{3}H and $\delta^{18}O$ than similarly saline waters from Baltic seawater sources.

For the three main constituents, the groundwater groups are roughly as follows:

- Meteoric: High tritium (10–20 TU), $\delta^{18}O$ about –10‰ SMOW, 20 ppm of Cl^-.
- Baltic seawater: High tritium , $\delta^{18}O$ about –6‰ SMOW, and 3650 ppm of Cl^-.
- Mixtures of Glacial and Deep brine waters: Low tritium (below detection limit), $\delta^{18}O$ greater than –12‰ SMOW, and 2,000 to 12,000 ppm of Cl^- depending on the relative contribution of deep brine.

6.2.2 Variations in groundwater chemistry based on fluid resistivity logs

A clear manifestation of these variations can be seen in measurements of fluid resistivity obtained from borehole logging. Fluid resistivity decreases strongly with salinity. Groundwater fluid resistivity was measured as part of the UCM borehole flow meter logging program. This program measured temperature, flow, and fluid resistivity in KA2563A, KI0023B, KI0025F and KI0025F02. The boreholes that penetrated Structure #10, KI0023B and KI0025F02, show a very distinctive pattern of resistivity along the boreholes, as shown by the example from KI0025F02 in Figure 6-2.

The logs indicate that the deepest waters from Structure #10 have relatively low resistivity. This resistivity decreases at the location of Structure #19, indicating the addition of more saline water from that structure. Structures #13 and #20 increase the fluid resistivity further as they add additional more saline water. The increase in fluid resistivity at the shallow parts of the borehole shows the addition of water from less saline sources carried by Structures #5, #6, and #7. Borehole KI0025F intersects Fracture zone Z rather than Structure #10 at the bottom of the hole. Fracture zone Z is a significant structural feature, but is not a major conductor. The absence of the high resistivity water signature in Fracture zone Z indicates that it does not have the same connection to Baltic seawater that appears in Structure #10.

6.2.3 Results of groundwater geochemical sampling

The TRUE Block Scale program has sampled water regularly for chemical content. Sampling of selected intervals was undertaken roughly at six-month intervals every April and September beginning in September 1998 and the most recent data included in this report are from April 2000. An additional sampling campaign was undertaken in January 1999. This campaign was the most complete in terms of the intervals sampled.

As mentioned above, a discussion of water chemistries the TRUE Block Scale rock volume needs to focus on a few indicator components that have been sampled from a large portion of the monitoring points, preferably at multiple times, hence the focus on Cl^-, $\delta^{18}O$, and ^3H.

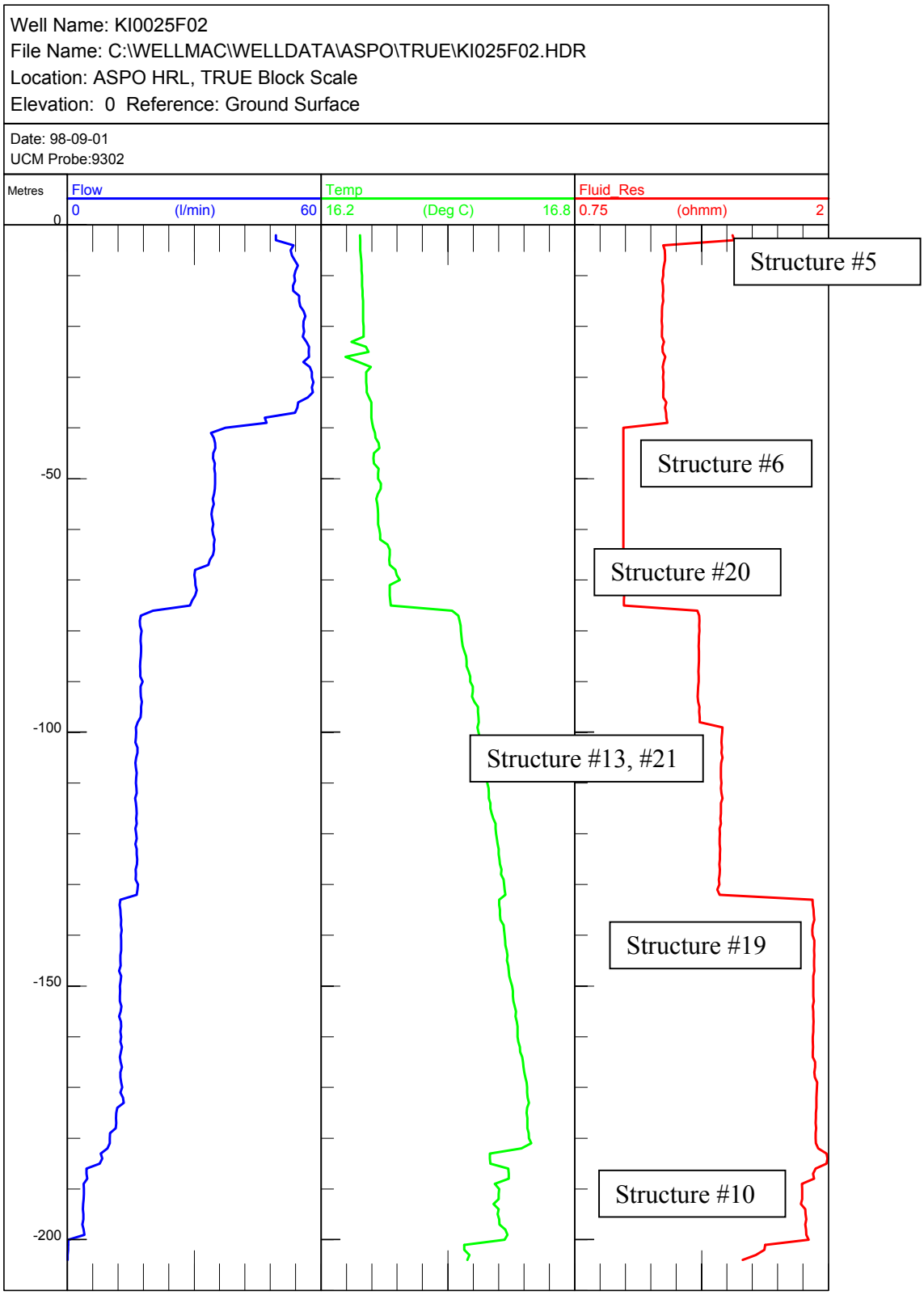

Figure 6-2. *Example of UCM flow, temperature and resistivity logs from KI0025F02.*

Values of $\delta^{18}O$ correlate positively with Cl^-, while ^3H correlates negatively. Figure 6-3 shows the correlation of Cl^- and $\delta^{18}O$. A deviation from this correlation appears in some samples from Structure #13, where the Cl^- values are somewhat smaller for given values of $\delta^{18}O$. These data suggest a slightly higher component of Glacial water in Structure #13, which would decrease the Cl^- without affecting the $\delta^{18}O$.

Sampling episodes did not generally include all piezometer intervals. In recognition of this limitation, two plots are presented, one for the January 1999 sampling campaign, which was the most complete, and one that shows the last values (in time) for any given interval. Most values do not change significantly over time, with the exception of the water of Structure #20 sampled in KA2563A. This one interval progressively changed from relatively saline to relatively fresh water. The KA2511A values are not included in the contouring, but they are shown as labelled values. The KA2511A data (blue text) values appear on the plots for two reasons;

First, the KA2511A sampling points lie a few to several tens of meters above the core of the TRUE Block Scale rock volume. Second, the KA2511A values appear to represent the dominantly more fresh, Baltic seawater-dominated waters, and including them in the kriging would distort the inferred chemistry patterns in the core of the TRUE Block Scale rock volume.

Discussion of January 1999 results

The January 1999 plots (Figure 6-4a–c) show clearly that different water types occupy different parts of the TRUE Block Scale fracture network. Baltic seawater (low Cl^-, high $\delta^{18}O$ and high ^3H) appears in Structure #10 at the bottoms of boreholes KI0023B, KI0025F02, and KA2511A. Similar water is sampled from all points in KA2511A, though the waters become slightly more saline from the bottom of the hole towards the collar. Chloride values that are lower than for Baltic seawater appear in borehole KA2511A suggesting that there may be a component of Meteroric water involved.

Another region with Baltic seawater appears in north of the block in sections of holes KA3548A01, KA3573A, KA3600F, at the Prototype Repository site, and in KA3510A. These holes are all well connected to Structure #5 in the main part of the TRUE Block Scale rock volume, as well as to other numbered structures with a low number.

Water that appears to be a mix of Deep brine and Glacial water is strongly associated with Structures #20 and #13. A second locus for waters with more brine-rich content appears in the deeper parts of boreholes KA3510A and KA3600F. These points appear along a trend that can be extrapolated to the northwest from Structures #13 and #20 in the main part of the TRUE Block Scale rock volume.

Concentrations of Cl^- decrease and $\delta^{18}O$ increase to the northeast and southwest of Structures #13 and #20. Waters in Structure #19 are dominantly Brine-Glacial type, though with greater mixing with Baltic seawater types.

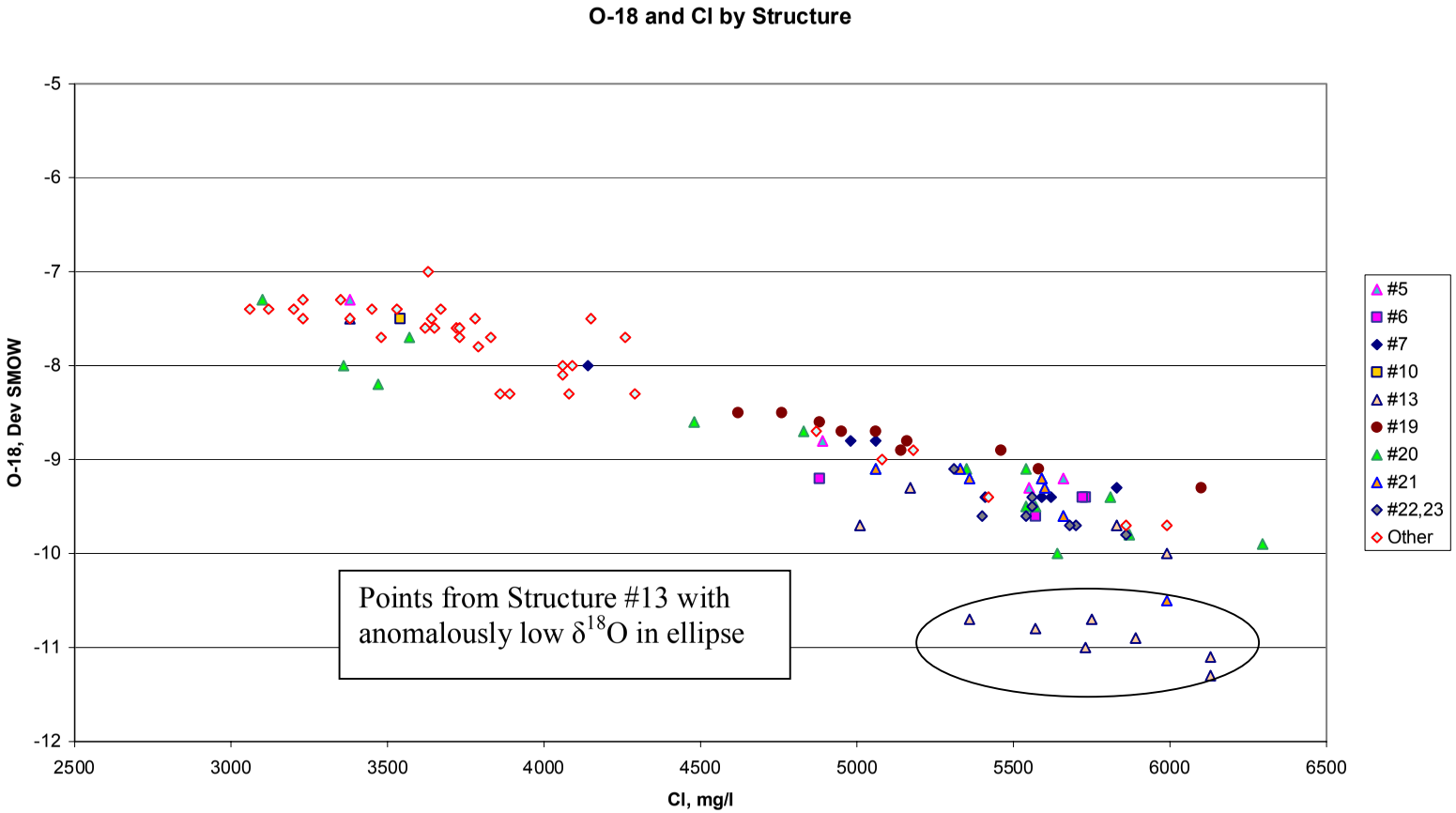

Figure 6-3. *Correlation between Cl^- and $\delta^{18}O$ measurements (identification by interpreted deterministic structure).*

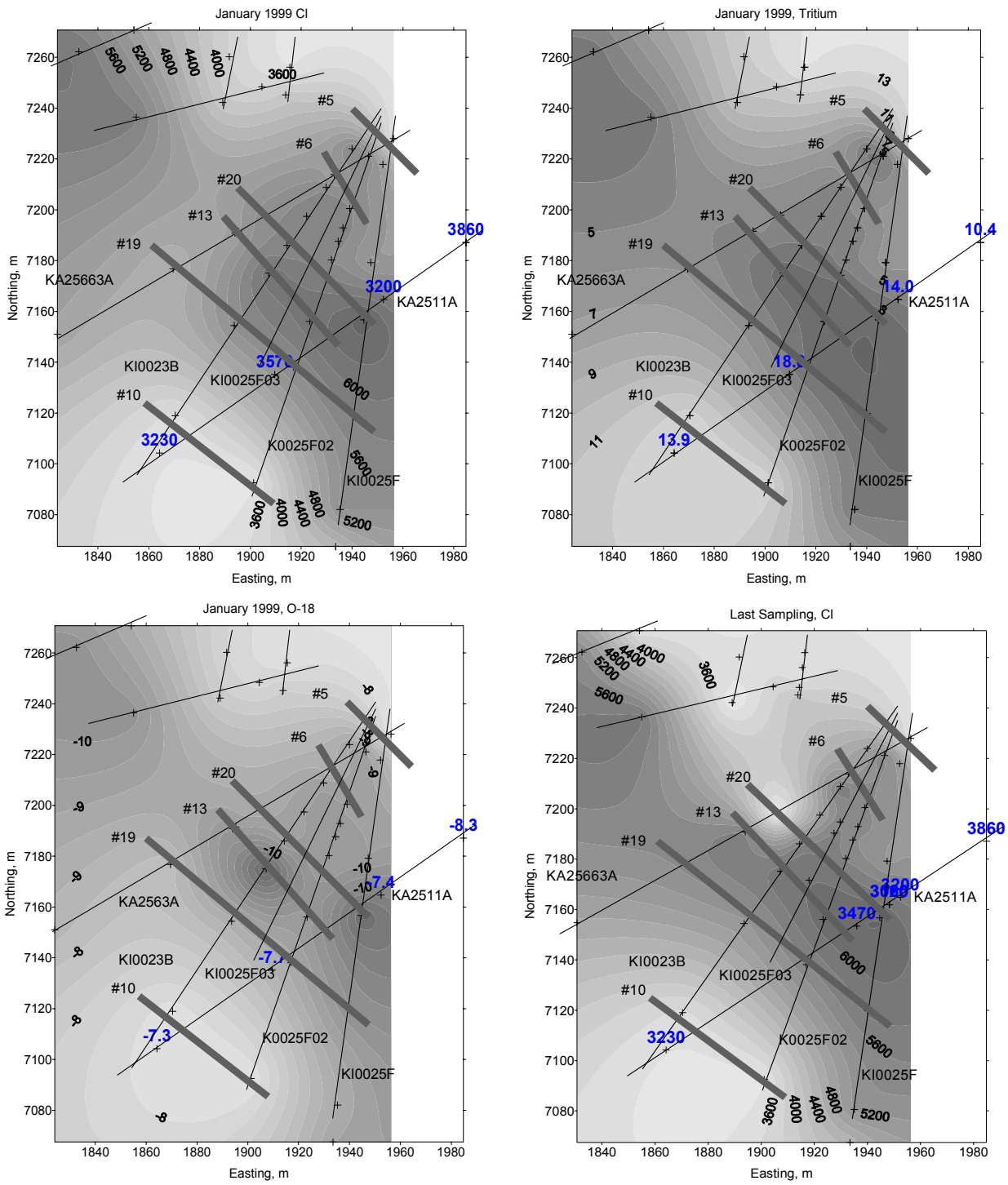

Figure 6-4. *Interpolated chemical variables: a) Cl^- values over the TRUE Block Scale rock volume, January 1999 b) ^3H values over the TRUE Block Scale Volume, January 1999 c) $\delta^{18}O$ over the TRUE Block Scale rock volume, January 1999 d) Cl^- values over the TRUE Block Scale rock volume last sample values showing low chloride waters entering Structure #20 in KA2563A.*

The water chemistry in regions of Structures #6, #7, #22, #23, which are hydraulically downgradient from Structures #20 and #13 are also dominated by Brine-Glacial water types, but, as in the case of Structure #19, these are somewhat diluted, possibly with Baltic water. The pattern of water compositions in the shallower parts of the TRUE Block Scale boreholes (KI0023B, KI0025F02, KI0025F03 and KI0025F) may indicate a plume of more deep-derived saline water moving from Structures #20 and #13 towards the underground openings.

A final feature worth noting in the spatial pattern of compositions is the difference in water composition in KA2563A as compared with the rest of the central part of the TRUE Block Scale rock volume. Specifically, the water collected from each structure is somewhat less brine-rich in KA2563A than the corresponding structure in other boreholes.

Discussion of "latest results"

Figure 6-4d shows the chloride values for the latest sample collected from each sampled piezometer interval. The major change from the January 1999 values, cf Figure 6-4, is the less saline value in Structure #20 in KA2563A. As shown in the data presented in Appendix E there is a progressive freshening of the water in this piezometer interval, hence the change in composition is considered a real phenomenon rather than an anomaly in the sampling. While the tritium data in Figure 6-4b suggests a plume of water with a fresher signature moving from the northeast, this direction is moving up the hydraulic gradient (see section 6.4). A more likely scenario for this change in composition is water movement within the Structure #13–#20 network from above, possibly drawing water from the same source of fresh water that also appears in KA2511A.

6.3 Hydraulic head in the TRUE Block Scale volume

Potential energy provides the drive for groundwater flow, and the common measure of potential energy is hydraulic head. Hydraulic head is best viewed as the elevation of a water column that the pressure at a given point in the flow system will support. As such, head values require a reference datum elevation. The datum for all values discussed in this chapter is the mean sea level.

Hydraulic head information supports the TRUE Block Scale experiments in several ways such as:

- Evaluation of boundary conditions,
- Estimation of background flows, and
- Evaluation of fracture network connectivity.

Hydraulic head data provide insight to *boundary conditions*. The dominant boundary effects are the shallow groundwater system, whose heads are supported by the Baltic Sea and the slightly higher heads due to recharge on Äspö Island, and neighbouring land bodies. The main sinks are the underground openings of the Äspö HRL. Closer openings are the most likely sinks, however, other openings may also contribute depending on the connectivity of the fracture network. Typically, hydraulic gradients are steepest close to the underground openings. This is due in part to the convergent geometry of the flow lines, but it also may reflect low-conductivity parts of the excavation disturbed zones (EDZ) around the openings themselves.

Head information is essential for understanding *background flow* and its distribution. Although underground testing provides good access to fracture networks, the underground openings act as constant head boundaries. Unless there is a complete lack of connection between the target fracture network and the underground openings, background flows, often with considerable hydraulic gradients, will affect underground experiments. Knowing the magnitude of these gradients is important for estimating the background flow and designing tracer tests that minimise the effects of this flow.

In fractured rock, maps of hydraulic head provide useful indicators of *connectivity* among conductors and from networks to boundaries. A common head value among a set of piezometer intervals may indicate a flow compartment, i.e. a part of a rock volume characterised by similar hydraulic head, and possibly similar groundwater chemistry. Networks that preferentially connect to a boundary may have anomalously high or low head values. For example, a strong connection to an underground opening will strongly reduce the head values in the network.

6.3.1 Analysis approach

The focus of this discussion will be maps of hydraulic head in the TRUE Block Scale rock volume. The map data show the head values in an approximate plane that contains the boreholes. As the head data lie within a plane that includes the boreholes and the closest sinks, which are the I-tunnel (collar positions for the KI-boreholes) and the Prototype Repository drift, the two-dimensional views provide an image of the head field that is relevant to understanding flow in the TRUE Block Scale rock volume.

Head maps were prepared by kriging, a geostatistical approach that honours values at known locations and interpolates or extrapolates values to unknown points. The maps were prepared using Surfer©.

The contoured maps do not include values from KA2511A for two reasons.
First, KA2511A lies above the approximate plane that includes the other boreholes.
Second, the head in KA2511A appear to be unrelated to the values in the remainder of investigated rock volume except for the region of Structure #5 near the borehole collars.
For reference, however, the labelled crosses in the figures show the locations and values of hydraulic head in KA2511A. Unlabeled crosses indicate the locations of head values that were used for the contouring.

Hydraulic head data were compiled from four sampling periods: April 1998, November 1998, May 1999, October 1999, and March 2000.

6.3.2 Results

Figures 6-5 and 6-6 present the head data for the TRUE Block Scale rock volume. Figure 6-5 shows a map of the head values from March 2000. Figure 6-6 shows the variation in average head in each structure over time.

The overall hydraulic head field in the TRUE Block Scale rock volume suggests a flow from southwest to northeast, which is towards the nearest underground openings at the collars of the fanned array of boreholes (KI0023B, KI0025F, KI0025F02, and KI0025F03). Head values increase rapidly from the borehole collars, and the highest head values of around –60 masl. Thus, the major part of the head drop occurs within a few metres from the underground openings.

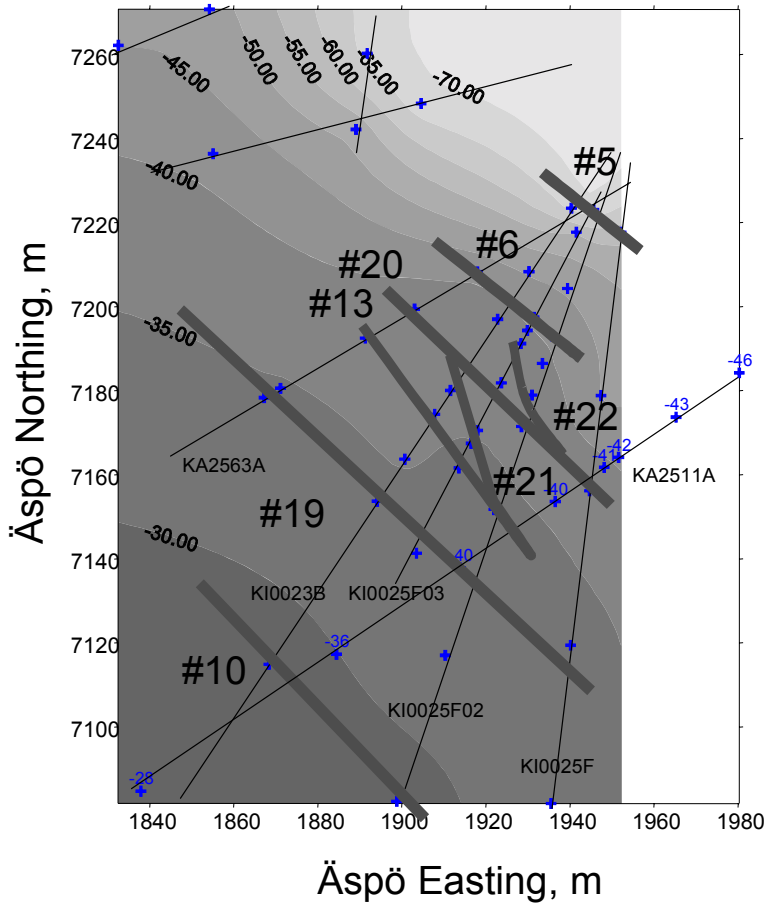

Figure 6-5. *Interpolation of measured hydraulic head (masl). Datum is elevation z=0 (mean sea level).*

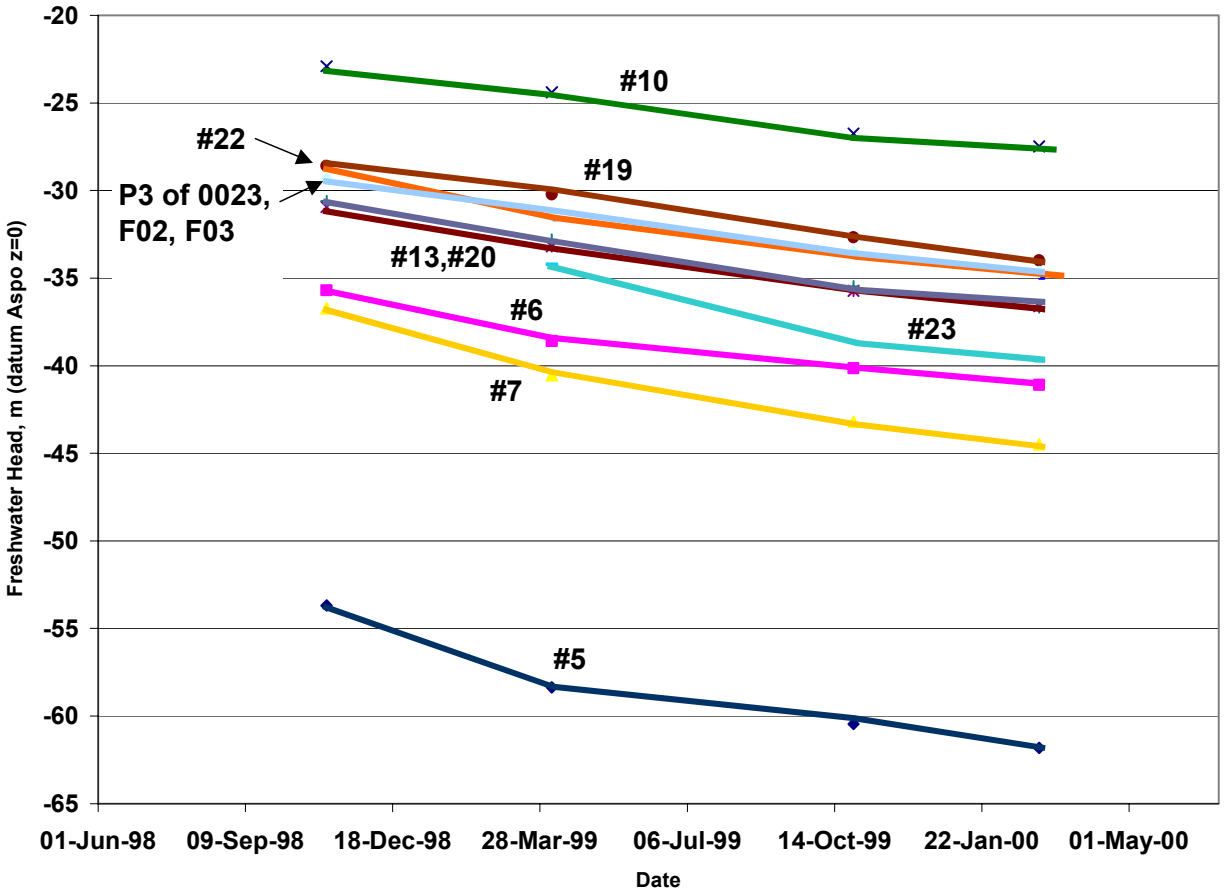

Figure 6-6. *Hydraulic head by structure and time (masl).*

The gradients are generally relatively flat from the innermost structures (Structure #10) to the Structure #19 and the Structure #20–#13 system. These gradients are about 6%. Gradients become more steep towards the borehole collars and the underground openings. The gradient towards the underground openings is inevitable when working underground, however, the relatively low gradients across the core of the TRUE Block Scale rock volume make it a favourable place to conduct tracer experiments.

Each structure has characteristic head values over much of its extent across the investigated block. Within the fanned borehole array, the head values within each structure vary within two metres. The values of hydraulic head in structures progressively decline from southwest to northeast. There is a slight drop of about 0.5 metres that occurs between KI0023B and KA2563A. The sharp bend in the contours between these holes indicates the head change. This indicates that the structures may be draining to the northwest.

The plot of head data versus time shows that the head decrease over the period of the experimentation was between five and ten metres. The largest drops appear closest to the underground openings. For this plot, the P3 intervals of KI0025F02 and KI0025F03 were plotted separately from the rest of Structure #13. These values are clearly higher

than the rest of Structure #13 (KA2563A and KI0023B), and interference test have shown that they are not directly connected with Structure #13. The P3 intervals may rather represent Structure #21.

Another significant feature of the plot of head versus time is the exception from the trend of lower head towards the underground openings that appears for Structures #13 and #20 and Structure #22. Structures #13 and #20 have common head values, which is consistent with the view that they are part of one network. The head in Structure #22, which come from the P6 sections of KI0025F02 and KI0025F03, are slightly higher than those in Structures #13 and #20 despite Structure #22 lying closer to the underground openings. These data suggest that that Structures #13 and #20 are acting as a drain for Structure #22. As the head map in Figure 6-5 shows, there is a slight gradient along Structure #20 to the northwest, towards KA2563A. The head pattern may also reflect drainage due to leakage from Structure #20 to Structure #6 in KI0023B:P7.

6.4 Background flow

Direct measurements of groundwater flow rates complement other information for developing and understanding of flow systems in fracture networks. Although the main motivation for making flow measurements has been tracer test design, the measurement results are also valuable for understanding the flow system in the TRUE Block Scale rock volume. This section discusses how these data support that understanding.

Background flows are an important consideration in designing and interpreting tracer tests. The presence of nearby underground openings assures existence of a background flow. The selection of sinks and sources for tracer tests and proper selection of flow rates at these points need to consider the background flow to assure adequate tracer recoveries.

Aside from measurements of flow at the underground openings, tracer dilution measurements in boreholes, cf Section 3.7, are the primary means of estimating background flow.

Tracer dilution tests are performed under either ambient or disturbed conditions. Ambient conditions mean that no artificial pumping is under way during the measurement, while disturbed conditions mean that there is a pumping sink elsewhere. The primary use of dilution tests in the TRUE Block Scale program has been the verification of connected flow paths by comparing results of dilution tests performed at ambient and disturbed conditions. Typically, a measurement sequence involves a series of ambient tracer dilution measurements. Once a pumping or a tracer test has reached a relatively stable drawdown, a second, disturbed-condition dilution test is performed. A significant change in the flow rate between the ambient and disturbed conditions implies that the dilution measurement point has a hydraulic connection to the pumping point. This confirmation of connectivity requires less time, and is therefore more efficient than a crosshole tracer test to screen potential tracer-injection points.

Over 122 ambient tracer-dilution tests have been performed in 22 different piezometer intervals in the TRUE Block Scale rock volume between March 1998 and March 2000. Table 6-1 and Figure 6-7 summarise these results. For most intervals multiple measurements provide some sense of the variability of flow. Most likely this variability reflects the imprecise nature of flow measurements. Nonetheless, the relative consistency by which intervals yield higher or lower flow rates gives some confidence that the measurement results are significant. Tracer dilution measurements should be used with some caution for quantitative inference of natural flow rates. Dilution tests are essentially point measurements (governed by the local transmissivity), while the flow rate of interest generally is averaged over much larger volumes of rock.

The following paragraphs discuss the major ambient flows that are observed in the TRUE Block Scale rock volume.

The largest ambient flow rate is measured in section KI0023B:P7. This flow exceeds 10 litres per hour. This piezometer section includes the interpreted intercepts of both Structures #6 and #20, hence the large flow rate is the likely result of a short circuit between separate structures at different head values. Difficulties with the piezometer emplacement prevented correction of this problem, which was recognised soon after its installation. The ability to control this short circuit by pumping in KI0023B:P6 was one of the important factors for the selection of that particular interval as the main pumping sink for the subsequent Phase B and Phase C tracer tests.

The second largest flows, about 1 litre per hour, appear in borehole KA2511A. This borehole lies above the main array, and does not appear to have any significant connections to the pathways that have been used for tracer tests. Nonetheless, the borehole is interesting for the information it provides on the larger-scale conductive network. A significant characteristic of KA2511A is the mutual connectivity of the sections along the borehole. Initially this connectivity was thought to reflect problems in the instrumentation. However, repeated attempts to rearrange the packers have not changed the noted connections between the test sections. The fractures that account for this connectivity along KA2511A appear to provide a conduit for Baltic seawater from Structure #10 in the innermost parts of the TRUE Block Scale rock volume towards the underground openings, cf Section 6.2.3. The high flow rates that the dilution tests measure may be a reflection of the connectivity along this hole.

The third highest dilution-test flow rates appear in Structure #20 in KA2563A:S4. The ten dilution measurements performed range from 80 to 590 ml/h with an average of 352 ml/h. This section of KA2563A lies close to the short-circuit in KI0023B:P7, which produces the largest ambient flows in the TRUE Block Scale rock volume. It is tempting to link the high flow in KA2563A:S4 to the short-circuit in KI0023B. However, the hydraulic head in Structure #20 in KA2563A is several metres lower than the head in Structure #20 in KI0023B, thus precluding any movement of water from KA2563A to KI0023B. Another possible explanation for this large flow may be the steeper hydraulic gradient around KA2563A. There appears to be a drop in head along the major northwesterly structures between KI0023B and KA2563A, cf Figure 6-5 and 6-7. This drop appears consistently among all of the mutually intersected structures in

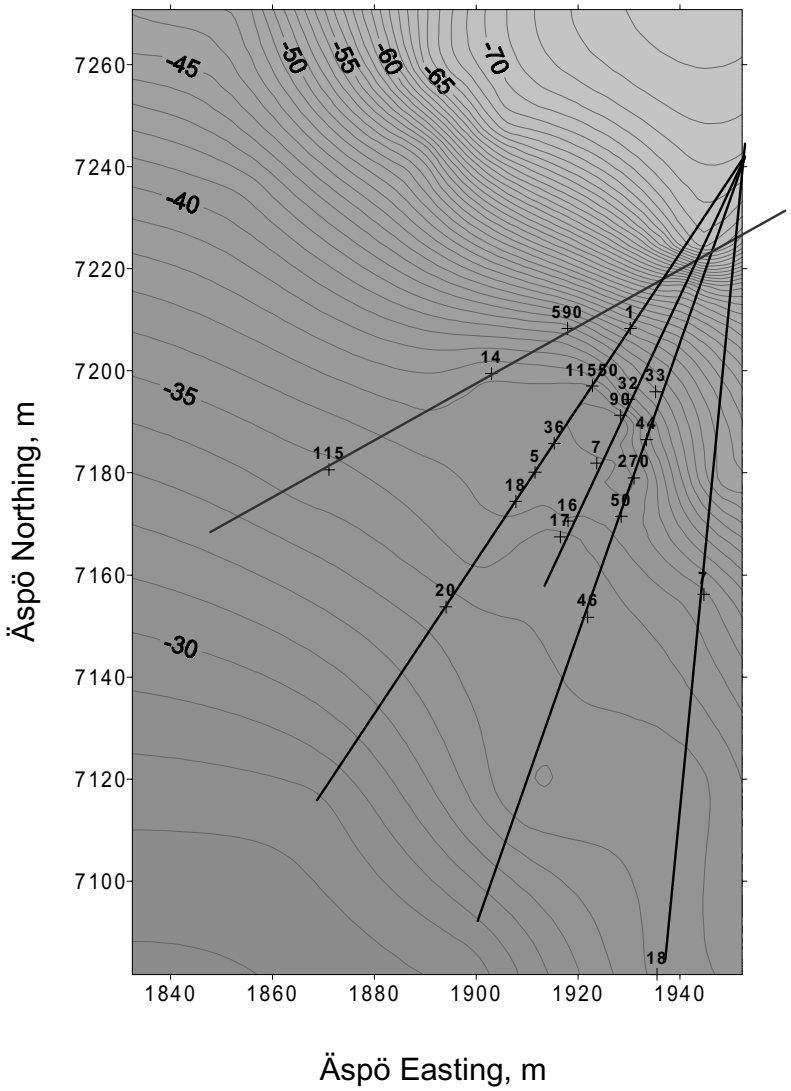

Figure 6-7. *Ambient flows (ml/h) measured in borehole sections using the tracer dilution method. Contours show hydraulic head (masl).*

the tracer test area. However, the relatively high inflow noted in Structure #19 in KA2563A (21–115 ml/h, with the fomer being the most recent measurement) is attributed to a high local transmissivity which in combination with the othgerwise average hydraulic gradient produce the noted flow rate, cf Table 6-3.

The next cluster of high flow rate values appears in Structures #22 and #23 in boreholes KI0025F02 and KI0025F03. The average flows in these sections range from 18–185 ml/h. These structures provide connectivity between the Structure #20–#13 system and downgradient structures such as Structures #5, #6, and #7. Thus, the flow in Structures #22 and #23 may reflect a concentration of the drainage from the centre of the TRUE Block Scale volume towards the underground openings.

Table 6-1. Groundwater flow measurements (ml/h) under ambient conditions in the TRUE Block Scale volume from tracer dilution tests.

Section	Structure	ENW-2 Mar 98	ENW-1 Mar 98	ESV-2 Mar 98	ESV-1a Mar 98	ESV-1b Apr 98	ESV-1c Apr 98	25F02:1 Oct 98	25F02:2 Oct 98	PT-1 Apr 99	PT-2 Apr 99	PT-3 Apr 99	A1 Oct 99	A2 Oct 99	A3 Nov 99	A4 Nov 99	B1 Mar 00	Average
KI0023B:P8	#7	1																1
KI0023B:P7	#6, 20										10120		11070	11030	11550			10943
KA2511A:S4	#6, 16	1100	1100	1150	1200													1138
KI0025F02:P8	#6								30		21	33	6	8				20
KI0025F02:P6	#22										230	100	270	138				185
KI0025F03:P6	#22												64	78	75	90	54	72
KI0025F03:P7	#23												27	22	25	32		27
KI0025F02:P7	#23										7		44	10	9			18
KI0023B:P6	#21		1	3	2	4		5		36		3	21	4				9
KI0025F03:P4	#21												16		6	1		8
KA2563A:S4	#20		540	560		540	590	560		120	130	80	199	201				352
KI0025F02:P5	#20								5	49	50		22	11			21	26
KI0025F03:P5	#20													<1	5	2	7	5
KI0025F:R4	#20	7	5	4	2		2	4		1	3	3	6	2	3			4
KA2563A:S1	#19										115		73	21				70
KI0023B:P2	#19											14	20	16				17
KI0025F:R2	#19	6	16	18														13
KI0025F02:P3	#13, 21								14	38	25		46	25	30			30
KI0025F03:P3	#13												17	9	<1	4		10
KA2563A:S3	#13									1	14		4	5	10			7
KI0023B:P4	#13	1	1	1		1	1				18		2	5	4			4
KI0023B:P5	#?										2		5	5	5			4

6.5 Boundary conditions

The TRUE Block Scale rock volume lies within a larger network of major fracture zones and faults. These conducting zones supply the water that flows through the studied rock volume. As the major conductors of the Äspö HRL site are more transmissive that the structures within the investigated rock volume, these major conductors should act as constant pressure boundaries for the block.

The TRUE Block Scale project has considered boundary conditions in several ways. Qualitatively, one can assess the boundary conditions by looking at the closest major structural features. A more quantitative approach develops the boundary conditions of the investigated rock volume from the site-scale flow models of the laboratory. Both of these approaches are described below.

6.5.1 Major bounding structures

The major structures/fracture zones bounding the TRUE block are shown in Figure 4-1.

- NE-2 lies on the southeast side of the block approximately 200 metres from the centre of the block.
- EW-1 lies to the northwest, on the other side of the access drifts for the TRUE Block Scale rock volume. A less distant bounding feature for that side of the investigated block may be the highly conductive network formed by Structures #1 to #5. This network lies between the centre of the block and nearest underground openings.
- EW-3 lies to the southeast of the block, and may be the ultimate source of the fresher waters that feed Structure #10 in the innermost part of the TRUE Block Scale borehole array.
- No structures, conductive subhorizontal fracture zones and/or lithological bodies, have been identified which could serve as well-defined upper or lower boundaries to the TRUE Block Scale rock volume.

6.5.2 Derivation of boundary conditions from site-scale models for the TRUE Block Scale rock volume

Fracture network modelling supported the main quantitative effort to define the TRUE block boundary conditions /Holton, 2001/. These boundary conditions included both pressure and salinity. A consideration of salinity was necessary because the salinity causes variations in fluid density that may be an additional factor in driving fluid flow.

The modelling work to define boundary conditions began with a 2-km square by 800-m high model of the Äspö HRL site. This model contained the major structural features defined by /Rhén et al, 1997b/. Superposed on this model was a regular network of background fractures as shown in Figure 6-8. The model was run for both undisturbed, pre-laboratory emplacement conditions, and for conditions where water is being

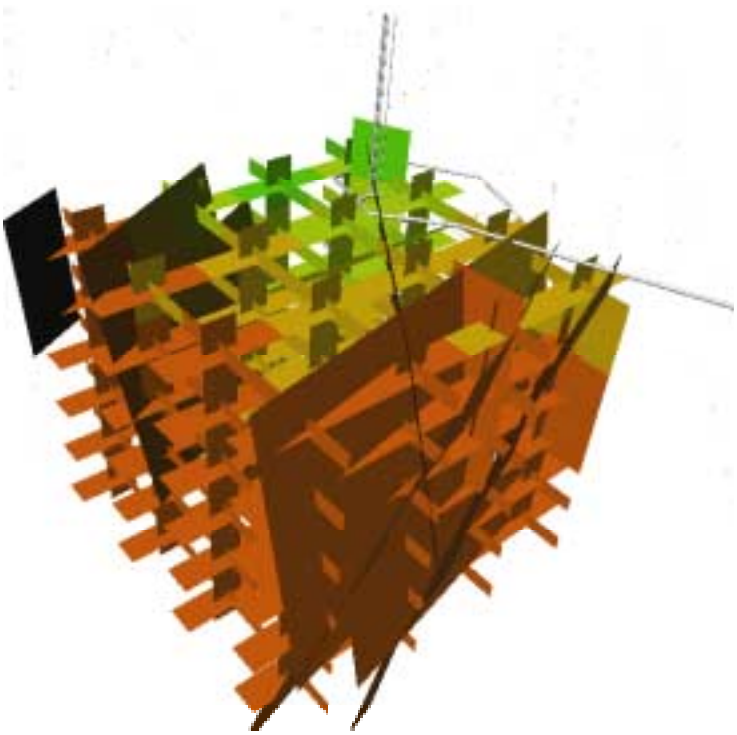

Figure 6-8. *The Site-Scale fracture network model with all of the fractures outside a 500x500x500 m block removed to give an impression of the density variation on the local scale block. The fractures illustrates the distribution of residual pressure in the block. The figure clearly shows the effect of the presence of the tunnel. The colours vary linearly according to drawdown from 60 m in light green to a few metres (1–5 m) shown in red /Holton, 2001/.*

removed from the underground openings of the laboratory. The latter site-scale case used the inflow rates to the tunnels as a boundary condition. The reliability of the fracture network model was checked by comparing drawdowns in selected boreholes and salinity values of water flowing into the tunnels against results from the site-scale continuum model of /Svensson, 1997/.

The boundary conditions for the TRUE Block Scale rock volume were taken from this site-scale fracture network model. The AEA team performed this work using the NAPSAC fracture network model /Holton, 2001/. These pressure and salinity conditions were interpolated to a regular array of 20-m spaced points over a 500-m cube. This cube was centred on TRUE Block Scale rock volume at the following Äspö coordinates: 1900 m, 7170 m, –450 masl (easting, northing, elevation).

7 Retention characteristics

7.1 Overview

This chapter provides an account of the retention characteristics of the investigated rock block with regards to porosity, distribution of porosity, values of diffusivity and distribution coefficients of relevant geological materials. The porosity determinations are of two kinds, derived from water saturation or from impregnation studies. The samples analysed for porosity have been extracted primarily from target structures used in the Phase C tracer experiments employing sorbing tracers. Diffusivity and distribution coefficient are available from laboratory experiments conducted as part of the First TRUE Stage /Byegård et al, 1998; Winberg et al, 2000/. In addition volumetric distribution coefficients have been derived for gouge materials from target structures used in tests with sorbing tracers.

7.2 Porosity and density measurements

7.2.1 Introduction

Definitions

The total or physical porosity in a crystalline rock is the volume not occupied by mineral grains. It therefore incorporates the presence of fractures at different scales (from macro to micro), porous minerals (often secondary minerals) and fluid inclusions. The most frequently cited representation of the total porosity in crystalline rocks is that by /Norton and Knapp, 1977/:

$$\Phi_T = \Phi_F + \Phi_D + \Phi_R \qquad (7\text{-}1)$$

where:

Φ_F = is the effective flow porosity (i.e. where the dominant transport of fluids and aqueous species occurs by advection),
Φ_D = is the diffusion porosity, (i.e. where the dominant transport is by diffusion through the aqueous phase), and
Φ_R = is the residual porosity which is not connected, either to the flow or diffusion porosity.

Although this may seem like an adequate and simple approach to subdivision of porosity, subdivision at more detailed scales of the different types of porosity is highly related to the size and shape of the samples used for measurements, and also to the

prevailing hydraulic pressure situation (gradient). This means that a network of microfractures may correspond mainly to advective transport if the hydraulic pressure gradient is significant, whereas with reduced hydraulic gradients this network should be attributed mainly to diffusion porosity. Another problem is to distinguish the residual porosity from the connected flow and diffusion porosities as the connectivity of the pores of samples in most cases are affected by the drilling and rock stress release. Furthermore, the connected pores available, for example when allowing water to soak into a drill core sample, may deviate significantly from the pores available in, for example, laboratory measurements carried out in cylindrical diffusion cells when only the two end surfaces of the rock cylinder are exposed, and even more under actual in situ conditions. The obvious implication is that the three-fold subdivision of porosity suggested by /Norton and Knapp, 1977/ is basically sound and relevant but difficult to apply *senso stricto* on the types of samples discussed in this chapter. Instead, for the purposes of this study, the connected porosity (Φ_C) is hereby defined as being equal to the pores available for water saturation in the specific sample measured. Compared with the definitions by /Norton and Knapp, 1977/, Φ_C is to large part equal to Φ_D but involves also part of Φ_R (e.g. pores made available by the drilling). The total porosity (Φ_T) has been calculated using bulk and grain density according to /Norton and Knapp, 1977/ to give the minimum values of total porosity as it assumes no mass loss by, for example, evaporation of water in non-connected pores in the bulk sample. Non-connected porosity (Φ_N) can simply be given as; $\Phi_N = \Phi_T - \Phi_C$, since these porosities always relate to the sample measured and the method used, cf Equation (7-1).

Methods used

The determinations of connected porosity were carried out mostly by use of impregnation or saturation techniques. Such measurements on drill core samples or samples from the Äspö HRL have been made within several projects at the Äspö Hard Rock Laboratory /e.g. Mazurek et al, 1997; Sundberg and Gabrielsson, 1999; Johansson et al, 1998/ and during the tunnel construction /e.g. Stanfors et al, 1993a,b/. The method most commonly employed has been water saturation, but He-gas expansion and Hg injection porosimetry have also been tested /Mazurek et al, 1997/.

Despite that a comparison of the three employed methods (water saturation, He-gas expansion and Hg-injection porosimetry) revealed only very small differences /Mazurek et al, 1997/, caution is required since the connected porosity is very small and the error of the methods quite large. It should also be emphasised that the use of the water saturation techniques differs e.g. in time of saturation, procedures for drying of samples, use/non-use of boiling etc. This underlines the necessity to use one common technique/method for all determinations; at least the measurement error will be the same for all samples, thus allowing for direct comparison.

The distribution and orientation of the connected pores can be studied by use of different impregnation techniques. Dye, fluorescent resin or polymethylmethacrylate (PMMA) doped with radioactive tracer (^{14}C or ^{3}H) are different fluids used in such studies /Siitari-Kauppi et al, 1999; Helmuth et al, 1999/. To our knowledge no inter-comparison of different impregnation techniques concerning penetration of different fluids and resolution in pore detection has been carried out so far.

Within the TRUE programme, water saturation measurements have been carried out at the Swedish National Testing and Research Institute (SP). Density and compact density measurements have been carried out at the same institute. The distribution and orientation of pores have been studied using impregnation of samples with ^{14}C-labelled polymethylmethacrylate carried out at the Laboratory of Radiochemistry, University of Helsinki, Finland /Kelokaski et al, 2001/. For description of methods, see Chapter 3.

7.2.2 Connected porosity from water saturation

Porosity measurements using water absorption (water saturation) have been carried out on fresh and altered wall rock samples as well as on centimetre sized fault breccia pieces/fragments from relevant TRUE Block Scale structures, cf Figure 4-13. In addition, fragments (in the size of 2–20 millimetre) from the Redox Zone in the Äspö tunnel have been analysed. This is because available amounts from the TRUE Block Scale drill cores were not sufficient for accurate analyses of porosities of small pieces since at least one hundred grams was required for measurements of such small fractions, whereas from the TRUE Block Scale rock volume single pieces with weights from 9 to 75 grams were used. The results are shown in Appendix E. From the available measurements some general trends are evident, cf Table 7-1 and Figure 4-13; altered wall rock (usually not possible to separate from cataclasite) and fault breccia pieces usually show increased porosity values compared to fresh (unaltered) rock samples, whereas pure mylonites for the most part show lower values. These observations are in good agreement with those presented in previously conducted investigations on Äspö samples /Eliasson, 1993; Mazurek et al, 1997/. An increase in porosity as the result of hydrothermal alteration has been reported also from studies carried out on other sites e.g. /Norton and Knapp, 1977/ and /Siitari-Kauppi et al, 1999/.

Table 7-1. Proposed representative values of connected porosity for geological constituents of a typical structure in the TRUE Block Scale rock volume. Values are based on water saturation porosity data from site-specific material and literature data from /Eliasson, 1993/ and /Mazurek et al, 1997/, cf Figure 4-15.

Geological constituent	Connected porosity (vol%)
Fresh Äspö diorite	0.45 +/–0.2
Altered Äspö diorite/cataclasite	0.45–1.5
Mylonite	0.3–0.6
Fault breccia pieces (cm size)	0.3–2.0
Fault gouge fragments (mm sized)	1.5–3.0

An increased porosity in the altered wall rock has been documented and porosity measurements (water saturation) of cm slices of cores drilled from fracture surfaces into the wall rock have been measured from three fracture intercepts at Äspö HRL (two from the TRUE Block Scale rock volume), cf Figure 7-1. From the two intercepts of Structure #23 (in boreholes KI0025F02 and KI0025F03) porosity profiles obtained on centimetre sized sawed slices show decreasing porosity with higher values (1.0 and 1.5 vol%) <1 centimetre from the natural fracture surface, whereas more distant samples 1–5 centimetres away show lower values.

The alteration responsible for the increase in porosity comprise decomposition of plagioclase to form albite, epidote, sericite +/– calcite. The biotite is more or less chloritised and oxidation of Fe(II) yields small grains of hematite causing red staining frequently observed close to the fracture intercepts (cf Section 4.7). This alteration, which is hydrothermal in origin, is observed along most of the water conducting fractures at Äspö indicating that most of the fractures are formed early in the geological history of the area and then reactivated, probably several times /e.g. Tullborg 1997; Landström et al, 2001/. The higher porosity in the slice adjacent to the fracture surface is also a result of the porous layer of fracture coatings (10–500 μm thick) present on the fracture surface, cf Figure 4-15. It is envisaged that this thin coating can exhibit porosities >10%.

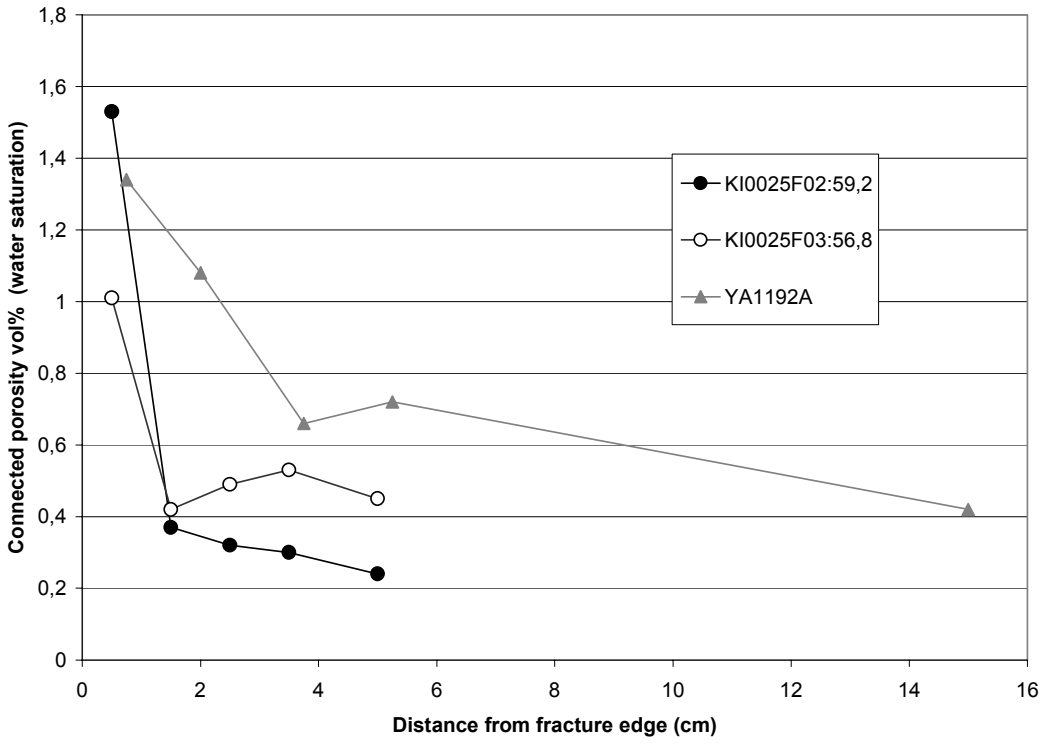

Figure 7-1. *Connected porosity (water saturation) measured on 1cm slices of drill cores. The samples from KI0025F02:L=59.2 m and KI0025F03:L=56.8 m represent profiles from Structure #23 into the altered wall rock. YA1192A represents a profile from a fracture surface exposed in the tunnel /Landström et al, 2001/. The hydrothermal alteration in the wall rock reaches a few cm from the fracture edge and then peters out.*

7.2.3 Density distribution

The three main rock types at Äspö HRL show different densities: Äspö diorite (average 2730–2780 kg/m^3), Ävrö granite (2675 to 2700 kg/m^3) whereas the Fine grained granite shows a slight over-lap with the Ävrö granite with values in the range (2630 to 2680 kg/m^3), cf Figure 7-2. The lower densities measured in the breccia fragments do not imply that they are more granitic in composition, instead these reflect increasing degree of hydrothermal alteration, i.e. increase in amount of clay minerals, carbonates and increase in pore space. There is however one sample of breccia fragments that show relatively high density (2891 kg/m^3) which may indicate a dominating mylonitic composition of the breccia framments.

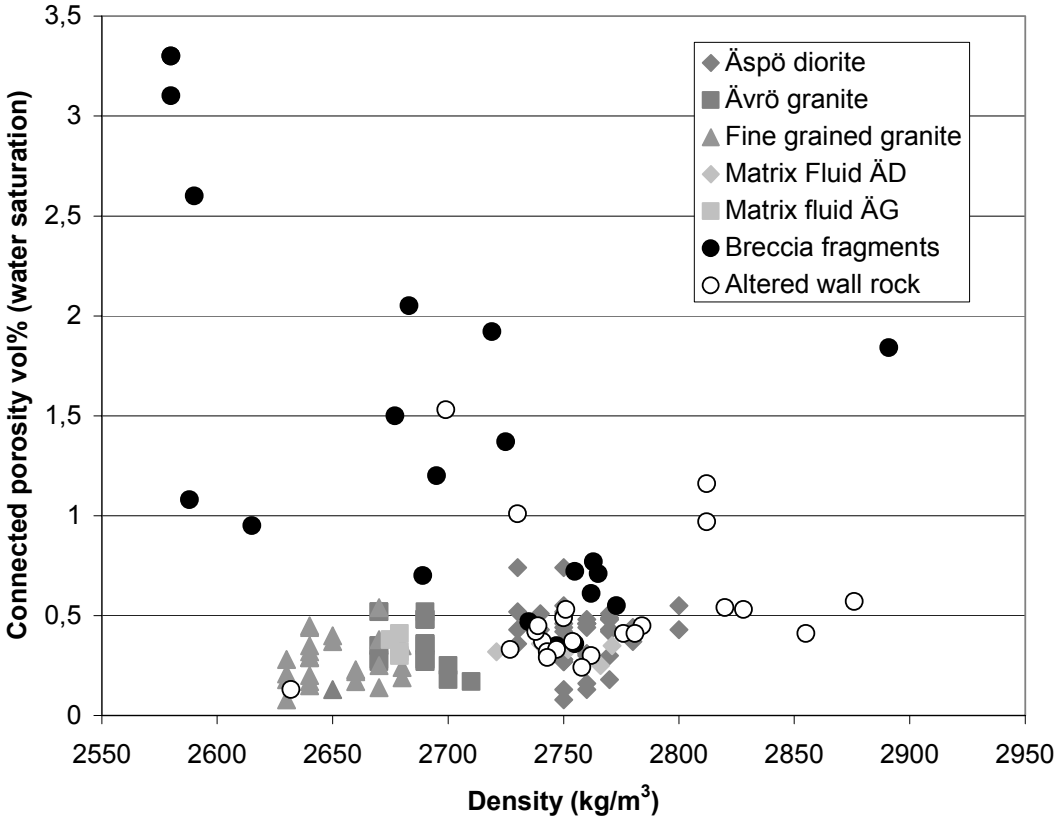

Figure 7-2. *Connected porosity measured in fault breccia pieces (c 2–4 cm in diameter) from the TRUE Block Scale structure intercepts (including fault breccia pieaces and fragments (>1 mm) and small sized (2–20 mm) fault breccia pieces from the Redox Zone (black dots and circles), compared with corresponding values on fresh host rock samples from the Äspö Tunnel /Stanfors et al, 1993a,b; Eliasson, 1993/ and the Matrix Fluid borehole (KF0051A01) at 450 metres depth in the Äspö Hard Rock Laboratory /Smellie, 2000/. All fresh rock samples are shown in grey symbols. All samples are from drill cores except for those from the Redox Zone (these three samples show the highest porosity). ÄG=Ävrö granite, ÄD=Äspö diorite.*

7.2.4 Compact density measurements and total porosity

As mentioned in the introduction (cf section 7.2.1) the total pore space includes micro fractures, porous minerals and fluid inclusions in the rock investigated, whereas the porosity values obtained by the water saturation technique only yield the connected pore volume of the specific sample. In order to get an estimate of the total porosity (also named physical porosity by /Pearson, 1999/) compared with the measured connected porosity (water saturation), compact density measurements (He-pycnometer, cf Section 3.9) were carried out on 9 samples ground to grain size less than 60 μm. Density was measured on the powder (compact density) and compared with previously measured density on whole sample (bulk density). The samples measured were two samples from the Matrix Fluid Chemistry project borehole KF0051A01, (Äspö diorite L=7.71–7.76 m and Ävrö granite L=9.21–9.26 m) and one wall rock sample from the REX fracture (KA2561A), three fault breccia samples from TRUE Block Scale (KA2563A: L=206.85 m, #13, KA2563A:L=54 m, #6 and KI0025F02:L=133 m, #19) and three samples of breccia pieces from the Redox Zone (2–4 mm, 4–8 mm and 8–20 mm, respectively). Figure 7-3 shows a plot of compact density versus bulk density. According to the definition by /Norton and Knapp, 1977/ the bulk and the compact density (=grain density) were used for calculation of the total porosity using the formula:

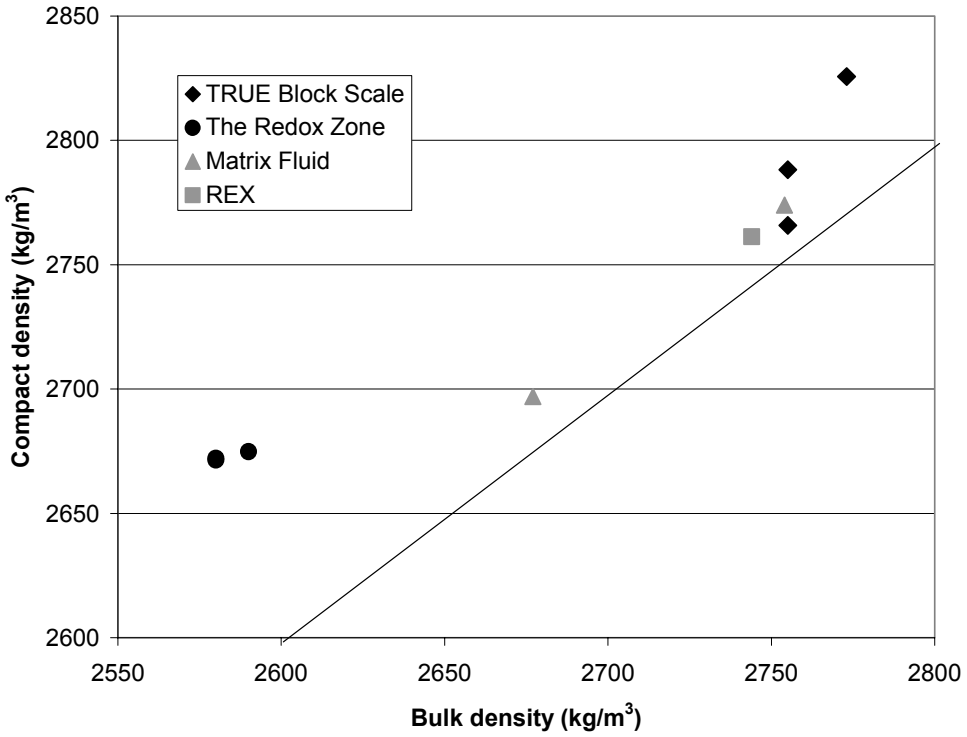

Figure 7-3. *Compact density (grain density) measured on ground samples compared with whole sample densities (bulk density). The line represents a 1:1 ratio.*

$$\Phi_T=[\ 1-(\rho_{\beta/}\ \rho_\gamma] \qquad (7\text{-}2)$$

where ρ_β is the bulk density and ρ_γ is the compact density (grain density).

The values are plotted in Figure 7-4. This calculation is based on the assumption that also the non-connected pores are dry, which is partly not the case since for example fluid inclusions contribute to the total porosity. This means that the total porosity shown in Figure 7-4 should be regarded as minimum values of the total porosity. Based on the few measurements available at this time, it appears that the non-connected porosity constitutes a considerable part of the porosity in most of the samples. However, the mylonitic fault breccia piece from Structure #19 shows a low non-connected porosity. More measurements are required for comparisons between various types of porosity in different rock samples and such measurements will be carried out within the framework of the Matrix Fluid Chemistry project.

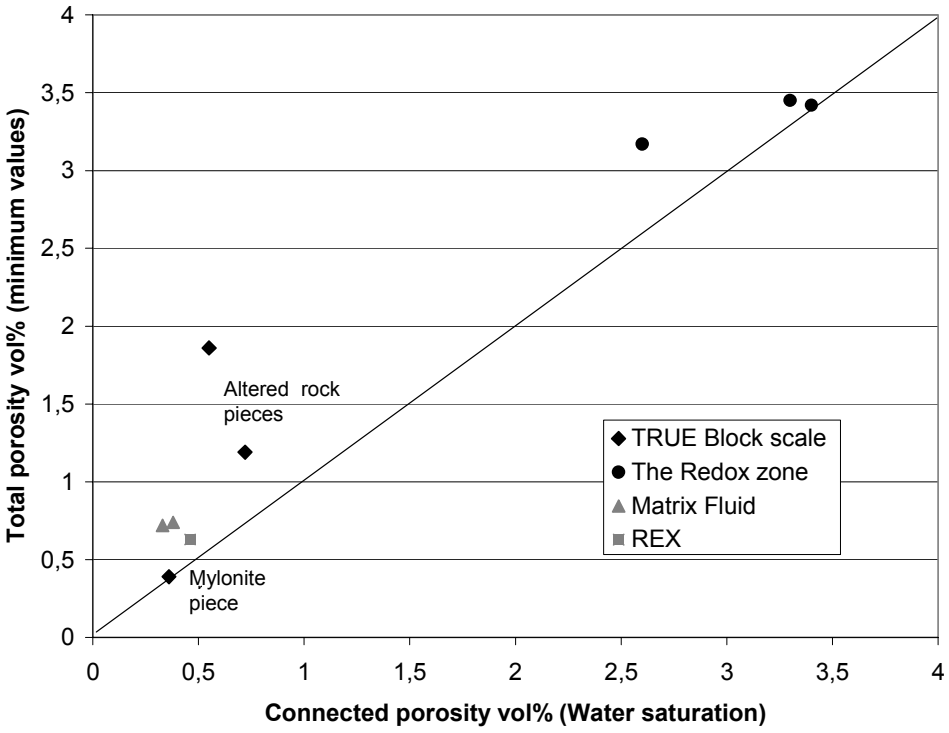

Figure 7-4. *Estimated total porosity based on compact density measurements (see text above for explanation) plotted versus connected porosity (water saturation). Samples from the TRUE Block Scale structures and the Redox Zone represent breccia fragments of altered wall rock (and one mylonitic sample; the lowest values) whereas the Matrix Fluid samples represent fresh Äspö diorite and Ävrö granite and the REX sample represent altered wall rock.*

7.2.5 Porosity distribution – results from impregnations

Distribution of the porosity and the textures of the connected pores can be studied using different impregnation techniques and such studies have been carried out on fresh and altered rock samples from Äspö /e.g. Mazurek et al, 1997; Byegård et al, 1998; Johansson et al, 2000/, which show that the porosity distribution is heterogeneously distributed and that orientation effects may be considerable, especially in foliated and tectonised samples.

The heterogeneous distribution of porosity is demonstrated in Figure 7-5 where an autoradiograph and porosity distribution determined from a ^{14}C-PMMA impregnated sample of fresh Äspö diorite sampled in the Äspö tunnel is shown. It can be noted that 70% of the area has a lower porosity than 0.5 vol% whereas very high porosities (3–5 vol% were encountered in <0.5% of the scanned area /Johansson et al, 2000/.

Higher porosities in the wall rock adjacent to a water conducting fracture have been measured in many samples from Äspö HRL and are e.g. exemplified by the trends in Figure 7-6 where a porosity profile obtained on a centimetre sawed slice show lower porosity values at 1–2 centimetre distance from the fracture edge. A higher porosity close to the fracture wall is also recorded from PMMA studies on samples from TRUE Block Scale /Kelokaski et al, 2001/, where e.g. a higher porosity was recorded in the outer 3–5 mm of a sample from Structure #20 in KI0025F02, L=74.6 m, cf Figure 7-7.

In contrast to the network of micro-fractures found in the altered wall rock of Structure #23 (Figure 7-7), sample KI0023B:69.9 m (Structure #20) shows a preferred orientation of connected pores (micro fractures) parallel to the fracture surfaces (Figure 7-8). Breccia pieces from Structure #20 (Figure 7-9) show evidence of several relatively "large" micro fractures, constituting a connected network in these samples. The results indicate bulk porosities in the wall rock and in centimetre sized fault breccia pieces in the order of 0.4–0.8%-vol, with porosities in the order of 1–3% for the 1–2 mm fault breccia fragments. Due to the heterogeneous nature of the porosity the porosity in places exceeds the bulk porosity significantly /Kelokaski et al, 2001/, e.g. some fragments show porosities >10%, possibly associated with halos of residual fault gouge coatings.

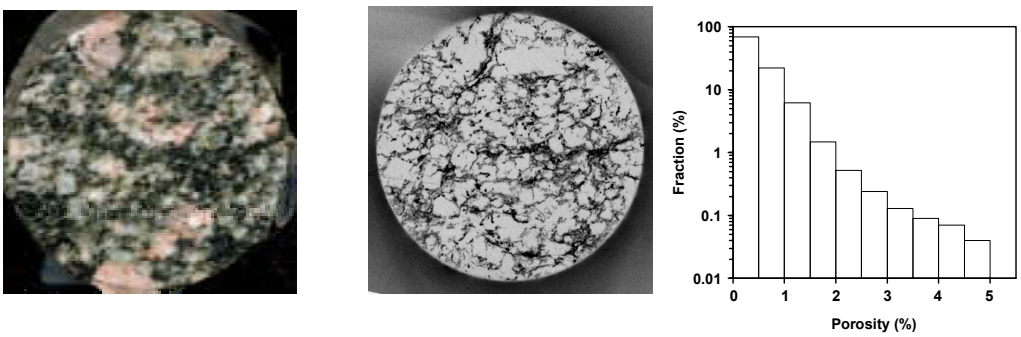

Figure 7-5. *Results of PMMA impregnation of an intact Äspö diorite sample, a) Photograph, b) Autoradiograph, c) Area fraction with different porosity.*

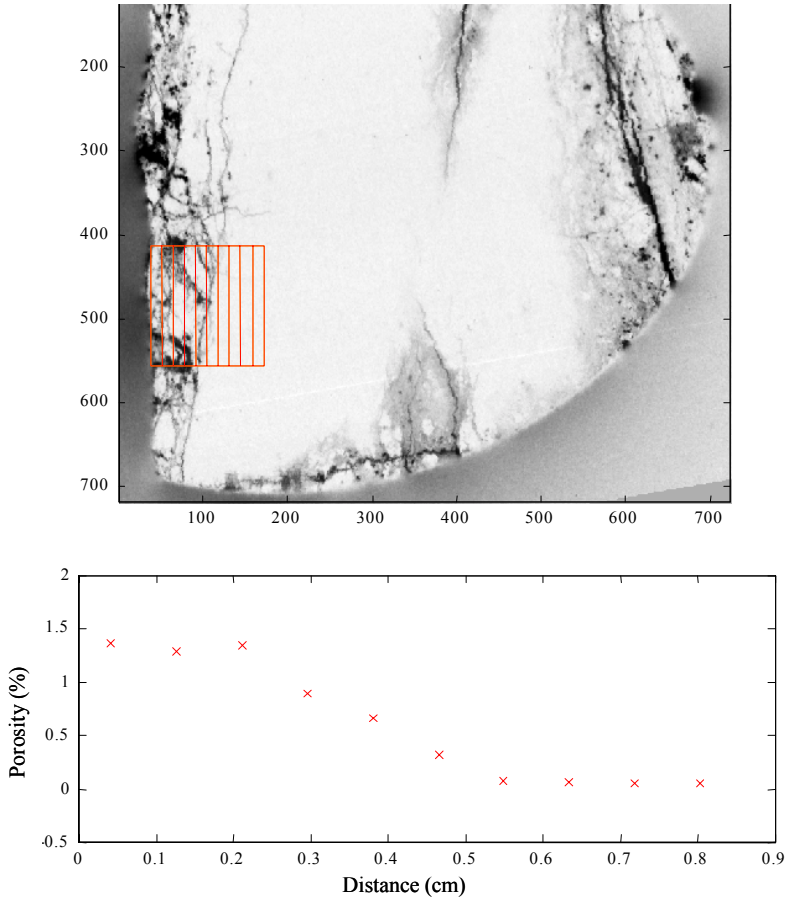

Figure 7-6. *Results of PMMA impregnation of a sample of Feature A from KXTT3 (TRUE-1) /Byegård et al, 2001/, a) Autoradiograph with indicated averaging windows and b) Porosity variation from fracture surface (left) towards interior of fracture wall rock.*

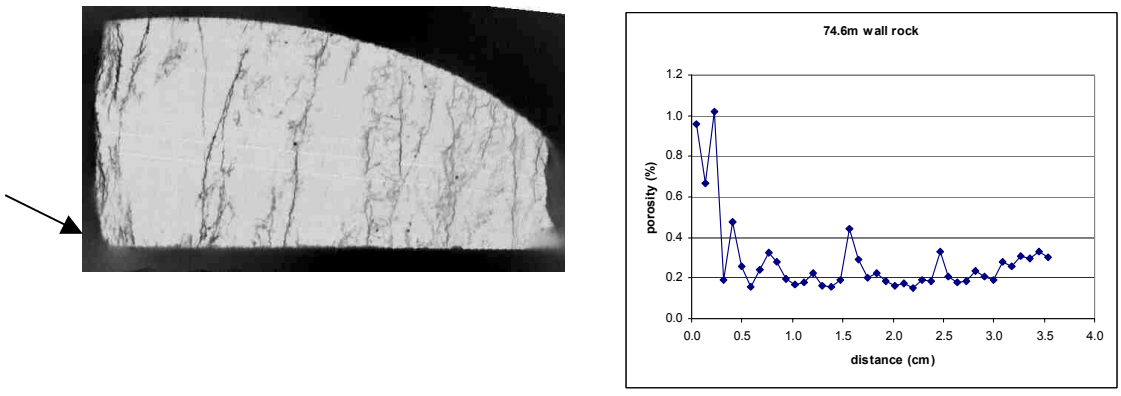

Figure 7-7. *Results of porosity profiling in wall rock of Structure #20 as obtained from a sample from KI0025F02:L=74.6 m. Arrow indicating fracture surface.*

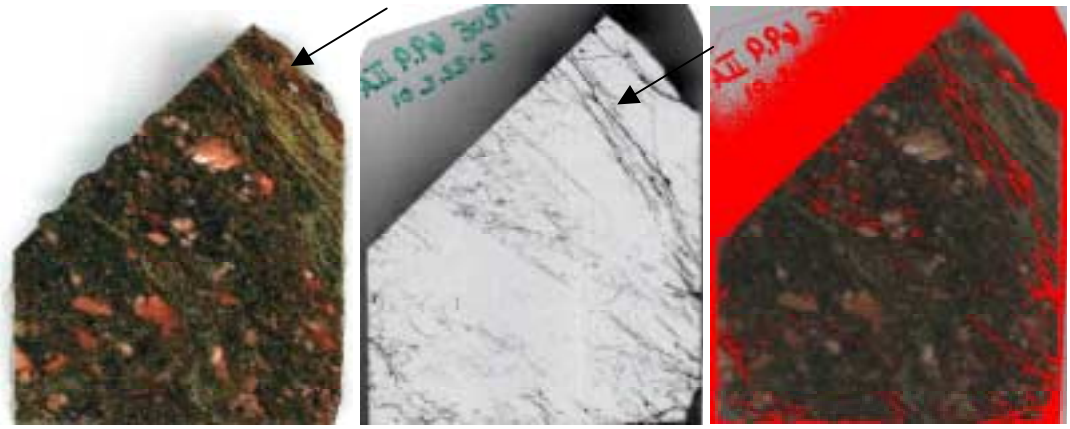

Figure 7-8. *Composite showing photographs of wall rock sample #20 KI0023B:L=69.9 m (left), corresponding autoradiograph (centre) (20 d exposure) and superimposed binary image (right) showing porous areas where MMA was intruded (red). The outer fracture surface and parallel internal fractures are marked with arrows, left and centre.*

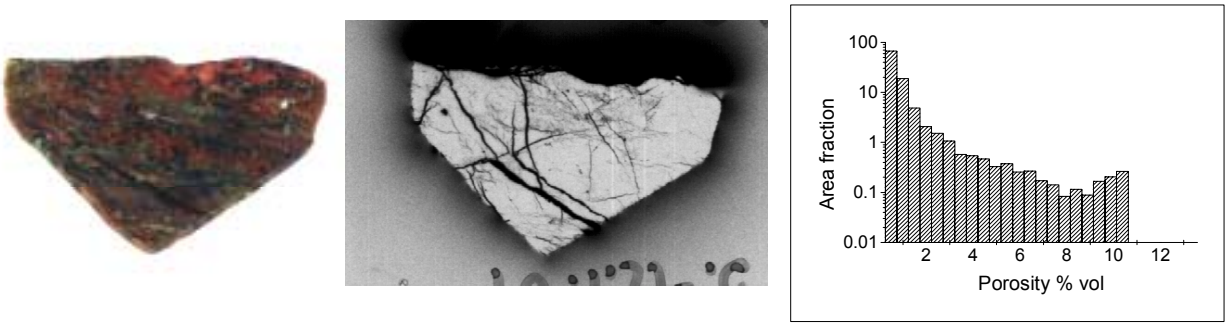

Figure 7-9. *Composite showing a photograph of a cut surface of a cm sized PMMA impregnated fault breccia piece from KI0023B:L=69.9 m (Structure #20) (left), the associated autoradiograph (centre) and the histogram accounting for the area distribution of porosity (right). The total porosity assessed from the exposed surface is 0.8%.*

A general correspondence between porosities derived with the water saturation method and the PMMA impregnation method has been observed in generic rock material /Johansson et al, 1998/, which implies that pores available for water are successfully impregnated with PMMA. It should however, be noted that the samples have been exposed to water (and resin impregnation) from all sides, whereas for example in diffusion experiments (and in situ), this is not the case and a larger variability in the pore connectivity and available porosity have also been noted /Johansson, 2000/. This emphasised the differences in connectivity in different directions and over different distances in the samples, which is discussed below.

7.2.6 Discussion and conclusion

Sample disturbances

It is expected that disturbances imposed on drill core samples are mainly of two types; 1) introduction of new micro cracks caused by the drilling and 2) disturbances of the sample due to rock stress release. Disturbances caused by the drilling have been studied within the Long Term Diffusion Project (LTDE) by /Li, 2001/ using impregnation of core samples with epoxy containing a fluorescent dye follwed by thin-section microscopy. An increase in frequency of newly formed micro-cracks in the outer 2–3 mm of the drill cores was indicated (approximately 2–3 times higher). The micro-cracks formed as a result of drilling were mainly radial and parallel with the core axis and were not preferentially related to grain boundaries.

The disturbance caused by release of rock stresses is much more difficult to evaluate. Estimates by e.g. /Skagius and Neretnieks, 1986/ noted a 2–3 times higher porosity in the drill core samples compared with the situation when the samples were reloaded to in situ stress conditions at repository depth. Decrease in porosity as a result of reloading applied on extracted crystalline rock samples have also been measured in other studies /e.g. Bischoff et al, 1987/. In the latter study a decrease in porosity by a factor of 5–10 was measured when pressure was increased to 30 to 60 MPa. The main explanations for the increase in porosity caused by rock stress release are proposed to be 1) increase in apertures of existing micro-fractures and 2) formation of pores along grain boundaries due to variable response to pressure release by different minerals.

For the TRUE Block Scale samples this implies that the wall rock samples and generic rock material samples probably exhibit an enhanced porosity attributed to sample disturbances. The increase may be a factor 2 to 10 according to the above referred measurements by /Skagius and Neretnieks, 1986/ and /Bischoff et al, 1987/. The breccia pieces/fragments in contrast probably show a lesser degree of mechanical disturbances since they have no, or very small surfaces cut by the drill bit. However, it is noted that these fractions probably have been destressed in situ as a result of the brittle reactivation of the fracture zones. This means that the measured difference in porosity between wall rock samples and breccia fragments can be significantly larger at in situ conditions than shown by the analysed set of data.

Connectivity of pores

The results from the impregnation studies at Äspö /Mazurek et al, 1997; Johansson 2000 and references therein/, show that connected porosity in crystalline rock is mainly made up of micro fractures with some contribution from porous mineral phases (often secondary or altered minerals). For the connectivity of the pores the frequency, size and orientation of the micro fractures are crucial.

A decrease in diffusivity with sample length has been demonstrated in several investigations on crystalline rocks e.g. /Kumpulainen and Uusheimo, 1989; Skagius, 1986; Johansson, 2000/. This decrease is mainly attributed to higher effective porosity (connectivity of the pores) in short samples (1–2 cm). For example /Xu and Wörman, 1998/ measured connected porosity (water saturation) on drillcore slices of different thickness of fresh Äspö diorite, showing mean values of 0.84 vol% (4 mm thick slice) to 0.40 vol% (15 mm slices). The higher porosity in the thinner slabs may be partly due to disturbances caused by sawing, but is probably to a large extent a result of better connectivity of the pores over short distances.

Permeability values evaluated from He-diffusion measurements carried out on Äspö diorite also show a decrease with sample length (1, 2, 4 cm), /Maaranen et al, 2002/.

All the above referred investigations have been carried out on unaltered rock samples. But the effect is also noted (and is even more profound) in the TRUE–1 diffusion experiment carried out on a 1 cm lens of altered Äspö diorite, inter-layered with thin mylonites. In this experiment the effective mean porosity turned out to be approximately 0.1 vol% whereas the water saturation value measured on the same sample was 0.4 vol%. The diffusion pathway was perpendicular to the orientation of the foliation and the thin mylonites and autoradiographs show the preferential orientation of micro fractures parallel to foliation /Byegård et al, 2001/.

The ground water / fracture coating / wall rock contact zone

The gradients in porosity are most obvious close to the coated fracture surfaces. The coatings in the TRUE Block Scale structures, cf Figure 4-13, are mostly thin (<100 μm) and consist of chlorite, calcite, ± illite or mixed-layer clay ± micrograins of pyrite. The soft chlorite/clay surface is interpreted to have a very large active surface with a relief of approximately 10 μm, and then follows a layer of increased porosity about 10–100 μm thick. It has not been possible to evaluate the increased porosity in the thin fracture coatings but porosities between 1–10 vol% appear realistic based on SEM observations and PMMA impregnation studies.

Concluding remarks

The presented porosity values indicate increased porosities (and available active surface areas) in fracture coatings, fault gouge material and partly in fault breccia pieces and fragments. It should in this context be emphasised that no porosity data are available from Äspö on the intact in situ porosity of fault breccia/fault gouge. Likewise, there are no available estimates of the distribution of fault breccia/fault gouge, i.e. the percentage coverage of fault breccia over a given structure plane.

However, /Mazurek et al, 1997/ attributed an in situ porosity of fault gouge to be 10–20% /cf Figure 8-9 in Mazurek et al, 1997/, based on experience from the Grimsel test site, and it was argued that values in the same order of magnitude could be expected for fine-grained fault gouge material from the deterministic TRUE Block Scale structures as well.

As part of the REX experiment at Äspö HRL /Puigdomenech et al, 2001/ a fracture parallel with borehole KA3065A01 was sampled (water conducting fracture zone NW-3 at the Äspö HRL). The fault gouge material (<2 mm particles) collected in this fracture equated to approximately 110 mg fault gouge/cm^2, of which 20 weight-% was in the size fraction <0.25 mm. The physical aperture of the fracture was unfortunately not determined, but a mean value of 1mm was suggested.

Measurements of connected porosity (water saturation) on fault breccia pieces from the TRUE Block Scale deterministic structures show values which are in accordance with altered wall rock, except for some mylonite samples that show values lower than 0.45 vol%. ^{14}PMMA impregnation studies of such breccia fragments, however, show presence of a continuous network of micro fractures transecting the samples possibly yielding higher porosities (1–3%) than those measured by water saturation, cf /Kelokasi et al, 2001/. One should also keep in mind that there are large uncertainties in the water saturation measurements employed on small samples.

Concerning the porosity of the altered wall rock and fresh bedrock compared to the fault breccia pieces, it can be assumed that the sample disturbances (causing increase in porosity) is expected to have influenced the wall rock/bedrock samples more than the breccia pieces. This implies that the difference in porosities between the breccia fragments and the wall rock in situ are probably larger than those accounted for in this study.

A scenario with a pronounced gradient (decrease) in connected porosity going from the partly gouge filled and brecciated centre of water conducting structures through the altered wall rock and further into the unaltered fresh bedrock has been indicated.

7.3 Overview of data used to describe retention processes

Based on the outcome of the modelling of the TRUE-1 experiments with sorbing tracers /Winberg et al, 2000/ and on the observations done at the intercepts of the TRUE Block Scale geological structures, the following retention processes have tentatively been identified:

1. Sorption on the gouge material in the fracture. Due to the heterogeneity observed for this material (see section 4.7), this process has been divided into two types of estimates:
    a. Sorption on the fine-fraction clay-rich fault gouge material. No experimental determination of the sorption parameters of this material is available. An alternative approach has therefore been used where the sorption coefficients have been estimated using the associated mineralogical analysis combined with cation exchange capacities from the literature and selectivity coefficients determined in the TRUE-1 programme /Byegård et al, 1998/ as the basic input.

b. Sorption on the coarse fraction of the fault breccia material (pieces and fragments). Since no experimental determinations are available for this material, the sorption coefficients determined for the 1–2 mm altered Äspö diorite in the TRUE-1 programme /Byegård et al, 1998/ have been chosen as the best available representative estimates for this material.

2. Surface sorption on the fracture walls. Experimental data are available from the TRUE-1 programme /Byegård et al, 1998/.
3. Diffusion into, and sorption within the rock matrix. Experimental data are available from the TRUE-1 programme /Byegård et al, 1998/.

In the following sections, the results, different aspects on the calculations and selection of parameter data for the different processes are described and presented to serve as a base for numerical modelling of the performed tracer experiments.

7.4 Sorption coefficients for gouge material

7.4.1 Size fraction <0.125 mm

Estimation of the cation exchange capacity (CEC) has been performed using the mineralogical composition of the <0.125mm material (Table 4-8) and CEC for "pure" minerals found in the literature, cf Table 7-2, according to the formula;

$$\mathrm{CEC} = \sum_{n} \left(n_{\min} \cdot \mathrm{CEC}_{\min} \right) \qquad (7\text{-}3)$$

Table 7-2. Compilation of Cation Exchange Capacity (CEC) for different minerals found in the literature.

Mineral	$\mathrm{CEC}_{\min}$ (μeq/g)	Reference and comments
Smectite	800	/Allard et al, 1983/
Illite	191	/Comans et al, 1991/
Mixed-layer clay	252	Estimated as 90% illite and 10% smectite
Chlorite	50	/Allard et al, 1983/
Mica	35	Estimated as 50% biotite and 50% muscovite Biotite 17 μeq/g, Muscovite 52 μeq/g, both from /Allard et al, 1983/
Epidote	6	/Allard et al, 1983/
Plagioclase	4	/Allard et al, 1983/
K-feldspar	3.7	/Allard et al, 1983/
Sulphides	1.5	/Allard et al, 1983/
Calcite	0.2	/Allard et al, 1983/
Quartz	0.2	/Allard et al, 1983/

Table 7-3. Cation exchange capacity CEC (μeq/g) estimated from the mineralogy of the gouge material found in the different TRUE Block Scale intercepts. The size fraction <0.125 mm was used.

Sample	#6 KA2563A:154 m		#19 KI0025F02:133 m		#20 KI0023B:69.9 m		#22 KI0025F02:66.7 m	
Mineral	n_{min}·100	n_{min}·CEC_{min}	n_{min}·100	n_{min}·CEC_{min}	n_{min}·100	n_{min}·CEC_{min}	n_{min}·100	n_{min}·CEC_{min}
Smectite	–	–	15	120	–	–	–	–
Illite	20	38	7	13	20	38	–	–
Mixed-layer clay	–	–	3	8	2	5	25	63
Chlorite	10	5	30	15	20	10	40	20
Mica	20	7	5	2	–	–	3	1
Epidote	–	–	5	0.3	–	–	–	–
Plagioclase	12	0.5	20	0.8	10	0.4	6	0.2
K-feldspar	5	0.2	5	0.2	10	0.4	5	0.2
Sulphides	–	–	–	–	3	0.04	1	0.02
Calcite	3	0.006	–	–	25	0.05	5	0.01
Quartz	30	0.06	10	0.02	10	0.02	15	0.03
Sum	100	51	100	159	100	54	100	84

where n_{min} and CEC_{min} are the fraction and the cation exchange capacity, respectively, of a particular mineral. The CEC_{min} used are given in Table 7-2 and the calculated CEC´s are given in Table 7-3.

According to a cation exchange model, the part of the cation exchange capacity occupied by a particular cation (i.e., the fractional occupancy) is determined by the selectivity coefficient for the studied cation relative to a reference cation. In rock-groundwater systems it is most often found that Ca^{2+} occupies a major part of the CEC /e.g., Byegård et al, 1998; Byegård et al, 1995; de la Cruz et al, 2001; Bradbury, 1989/ and Ca^{2+} is therefore used as the reference cation. The selectivity coefficient, K_c, is therefore expressed as:

$$K_c = \frac{\left(\frac{CEC_{M^{\nu+}}}{CEC}\right)^{2/\nu}\left[Ca^{2+}\right]}{\left(\frac{CEC_{Ca^{2+}}}{CEC}\right)\left[M^{\nu+}\right]^{2/\nu}} \qquad (7\text{-}4)$$

where $CEC_{M^{\nu+}}$ and $CEC_{Ca^{2+}}$ are the cation exchange sites occupied by $M^{\nu+}$ and Ca^{2+}, respectively, and $[M^{\nu+}]$ and $[Ca^{2+}]$ are the water concentrations of the $M^{\nu+}$ and Ca^{2+}species, respectively. Rearrangement of Equation (7-4) gives:

$$CEC_{M^{\nu+}} = \left(K_c^{\nu/2}\right)\left(CEC_{Ca^{2+}}^{\nu/2}\right)\left(CEC^{(1-\nu/2)}\right)\left[M^{\nu+}\right]\left[Ca^{2+}\right]^{-\nu/2} \qquad (7\text{-}5)$$

By assuming that the CEC is to major extent occupied by the alkali metals (Na^+–Cs^+) and the alkaline earth metals (Mg^{2+}–Ba^{2+}) (supported by the experimental results of /de la Cruz et al, 2001/) the following expression is obtained:

$$CEC = \sum_{M^{\nu+}} CEC_{M^{\nu+}} = \sum_{M^{\nu+}} \left(K_c^{\nu/2}\right)\left(CEC_{Ca^{2+}}^{\nu/2}\right)\left(CEC^{(1-\nu/2)}\right)\left[M^{\nu+}\right]\left[Ca^{2+}\right]^{-\nu/2} \qquad (7\text{-}6)$$

Knowing the CEC, the water concentrations and the selectivity coefficients of the different cations, the CEC_{Ca2+} can be calculated in order to fulfil Equation (7-6). By inserting the obtained value in Equation (7-5), the $CEC_{M\nu+}$ can be calculated. By applying a cation exchange sorption model, the sorption distribution coefficient (K_d) can be expressed as:

$$K_d = \frac{CEC_{M^{\nu+}}}{\nu \cdot \left[M^{\nu+}\right]} \qquad (7\text{-}7)$$

where ν = number of positive charges for the adsorbing cation.

In the calculation of K_d of the gouge material, the estimated CEC from Table 7-3 has been used for the different intercepts. The water composition data used were obtained from the SICADA database /Säfvestad and Nilsson, 1999/. In cases where a comprehensive water composition data set was not available for an intercept, data was extracted from samples taken at the same feature but in other boreholes. For the trace elements (Rb^+, Cs^+ and Ba^{2+}), very limited amount of data were available and an average of all performed measurements had to be used for some samples.

The selectivity coefficients used in the calculations are from the TRUE-1 investigation of altered Äspö diorite /Byegård et al, 1998/. In that investigation, no measurements of K^+ and Mg^{2+} were performed. The selectivity coefficients obtained for K^+ and Mg^{2+} in the investigation of Finnsjön granodiorite, size fraction 90–250 μm /Byegård et al, 1995/ have therefore been added to the data set used for the calculations. Selectivity coefficients are known to vary between different geologic materials /see e.g. Bruggenwert and Kamphorst, 1982/, so the present approach of using the same selectivity coefficient for all gouge materials is certainly a simplification.

The resulting K_d are given in Table 7-4. For comparison, calculations have also been performed using the average of the CEC experimentally determined by /de la Cruz et al, 2001/ for crushed material of a size fraction <63 μm. It is found that the K_d varies with the CEC. It is likely that the higher K_d in the non-crushed <125 μm gouge material compared to the crushed <63 μm material is explained by the significantly higher contents of clay minerals in the non-crushed material.

Table 7-4. Calculated K_d for the different gouge material, size fraction <125 μm.

		Structure #6 KA2563A:154 m CEC=51 μeq/g (calculated)		**Structure #19 KI0025F02:133 m** CEC=159 μeq/g (calculated)		**Structure #20 KI0023B:69.9 m** CEC=54 μeq/g (calculated)		**Structure #22 KI0025F02:66.7 m** CEC=84 μeq/g (calculated)		**Crushed material[E] <63 μm** CEC=38±6 μeq/g (measured)	
	K_c	Water conc. (M)[A]	K_d (m^3/kg)	Water conc. (M)[B]	K_d (m^3/kg)	Water conc. (M)[C]	K_d (m^3/kg)	Water conc. (M)[D]	K_d (m^3/kg)	Water conc. (M)[F]	K_d[G] (m^3/kg)
Na^+	0.1[H]	8.3e-2	6.6e-5	8.6e-2	2.0e-4	8.8e-2	6.8e-5	8.8e-2	1.1e-4	9.0e-2	4.7e-5
Mg^{2+}	11[I]	1.7e-3	4.7e-3	1.8e-3	1.4e-2	1.7e-3	4.8e-3	1.9e-3	7.4e-3	1.7e-3	3.3e-3
K^+	66[I]	2.2e-4	1.7e-3	2.0e-4	5.2e-3	2.2e-4	1.8e-3	2.4e-4	2.7e-3	2.1e-4	1.2e-3
Ca^{2+}	1	3.4e-2	4.2e-4	3.5e-2	1.3e-3	3.5e-2	4.4e-4	3.4e-2	6.7e-4	3.7e-2	3.0e-4
Rb^+	2.00E+03[H]	3.3e-7	9.3e-3	3.3e-7	2.8e-2	3.4e-7	9.7e-3	3.6e-7	1.5e-2	3.5e-7	6.7e-3
Sr^{2+}	1[H]	2.1e-4	4.2e-4	2.3e-4	1.3e-3	2.5e-4	4.4e-4	2.7e-4	6.7e-4	2.7e-4	3.0e-4
Cs^+	2.00E+05[H]	1.8e-8	9.3e-2	1.8e-8	2.8e-1	1.8e-8	9.7e-2	1.8e-8	1.5e-1	1.8e-8	6.7e-2
Ba^{2+}	20[H]	4.2e-7	8.5e-3	4.2e-7	2.5e-2	4.3e-7	8.7e-3	4.3e-7	1.3e-2	4.3e-7	5.9e-3

[A] Major components from KI0025F, 164–168 m, [Rb], [Ba] and [Cs] = average of all performed trace element measurements.
[B] Major components from KI0023B, 41.45–42.45 m, [Rb], [Ba] and [Cs] = average of all performed trace element measurements.
[C] Water composition from KI0025F02, 73.3–77.25 m.
[D] Water composition from KI0025F02, 64–72.3 m.
[E] Average of the material used in the investigation by /de la Cruz et al, 2001/.
[F] Average of the water composition of the intercepts for the location of the material used in the investigation by /de la Cruz et al, 2001/.
[G] Uncertainties in the range 10–20% due to the variations observed in the CEC and the water composition.
[H] Value from TRUE-1 investigation of altered Äspö diorite, sampled at KXTT2, 15.1 m /Byegård et al, 1998/.
[I] Value from investigation of Finnsjön granodiorite /Byegård et al, 1995/.

It should be acknowledged that all the calculations are based on somewhat rough estimations and that the given K_d values therefore are quite uncertain. A major simplification used is that the selectivity coefficients are assumed independent of the mineral composition of the material. The thorough review of selectivity coefficients done by /Bruggenwert and Kamphorst, 1982/ indicate variations due to the mineralogy. However, large variations are also observed between values given for the same minerals, e.g., the selectivity coefficient for the exchange reaction of K^+ and Ca^{2+} on illite varies in the range of 30.6–1600.

7.4.2 Size fraction 0.125–2 mm

Since the finest fraction of the gouge material is richer in clay minerals and provides a larger surface for sorption, it is assumed that this fraction has the highest sorption capacity, cf Section 7.4.1. However, also the coarser fractions of the fault gouge material may provide higher sorption capacity than the wall rock, and therefore this material deserves its own sets of K_d values.

For the fault gouge material in the size fraction 0.125–2.0 mm, sorption coefficients have therefore been taken from the investigation of the altered Äspö diorite in KXTT2 L=15.1 m performed as part of TRUE-1 /Byegård et al, 1998/. In this work, only the size fraction 1–2 mm was studied. The values obtained are presented in Table 7-5.

Table 7-5. Estimated K_d for the gouge material, size fraction 0.125–2 mm.

Cation	K_d (m3/kg)	Remark
Na^+	3e-6	B
Mg^{2+}	3e-4	C
K^+	1e-4	C
Ca^{2+}	3e-5	B
Rb^+	9e-4	A
Sr^{2+}	4e-5	B
Cs^+	1e-2	A
Ba^{2+}	1e-3	A

A Sorption coefficient, measured in batch experiment from the loss of the tracer in the aqueous phase.

B Desorption coefficient, measured in batch experiment from the desorption of the tracer.

C Calculated using the average ratio of the K_d-values found for Mg/Ca and K/Ca, respectively, cf Table 7-4.

7.5 Surface sorption coefficients

An attempt to estimate surface sorption coefficients, K_a, was made by /Byegård et al, 1998/ on generic Äspö diorite and site-specific material from the TRUE-1 site. As a base for the estimations the geometrical area and the BET-surface area of the largest particle size and the geometrical surface area of the injection side of the diffusion cells were used. However, in a real fracture/structure, the size of the surfaces may vary drastically depending on whether the fracture contains fault breccia, clay minerals etc. K_a values determined from experiments with artificallly crushed material often tend to overestimate the surface areas.

By assuming spherical shape of the particles of the solid phase used in the batch experiments, K_d can be described as

$$K_d = K_{di} + K_a \cdot \frac{6}{\rho \cdot d_p} \qquad (7\text{-}6)$$

where K_{di} is the sorption onto inner surfaces, K_a is the sorption onto the outer surfaces and d_p is the average particle size. K_a evaluated from Equation (7-6) (the slope of a plot of K_d vs $1/d_p$) and from initial sorption onto the injection side of a diffusion cell (Cs sorption) and the TRUE-1 diffusion cell (Cs, Rb) are presented in Table 7-16. K_a has also been calculated from K_d data for the 2–4 mm fraction after the shortest sorption time (1d), when the penetration into the rock matrix is small. However, a slight diffusion into the pores may lead to an overestimation of K_a even after this short contact time. K_a has also been calculated related to the measured BET-surfaces of the 2–4 mm fractions (Kr-gas adsorption).

Table 7-6. Surface sorption coefficients (K_a) for Äspö diorite and Feature A site specific material.

Tracer	Crushed material Geom. surf. 14 d.[1] K_a (m)	Diff.cell Geom.surf. 10 d.[2] K_a (m)	TRUE-1 diff.-cell Geom.surf. 5 d.[2] K_a (m)	Crushed material Geom.surf. 1 d.[3] K_a (m)	Crushed material BET-surf. 14d.[4] K_a (m)
Na^+	$7 \cdot 10^{-7}$			$5 \cdot 10^{-6}$	$2 \cdot 10^{-7}$
Rb^+	$5 \cdot 10^{-4}$		$4 \cdot 10^{-3}$	$1 \cdot 10^{-3}$	$6 \cdot 10^{-5}$
Cs^+	$8 \cdot 10^{-3}$	$9 \cdot 10^{-3}$	$1 \cdot 10^{-2}$	$8 \cdot 10^{-3}$	$5 \cdot 10^{-4}$
Ca^{2+}	$4 \cdot 10^{-6}$			$3 \cdot 10^{-5}$	$3 \cdot 10^{-6}$
Sr^{2+}	$8 \cdot 10^{-6}$			$2 \cdot 10^{-5}$	$4 \cdot 10^{-6}$
Ba^{2+}	$2 \cdot 10^{-4}$			$6 \cdot 10^{-4}$	$4 \cdot 10^{-5}$

1 Plot of K_d vs $1/d_p$ for the four largest particle fractions.
2 Initial sorption onto the surface of the injection side of the diffusion cell.
3 From K_d/A_{geom} 2–4 mm particle size. A_{geom}=0.67 m^2/kg.
4 From K_d/A_{BET} 2–4 mm particle size. A_{BET}=26 m^2/kg.

7.6 Diffusivities and sorption coefficients for the rock matrix

The effective diffusivities for the different tracers are based on mean values from through diffusion measurements on cylindrical core samples of Äspö diorite of 1 and 2 cm lengths /Byegård et al, 1998/. It is observed that D_e decreases with increasing cell lengths used in the experiments. However, since the porosity in the vicinity of a natural fracture is largest near the fracture, the 1 and 2 cm samples may be the most representative (which is a guess, since the Äspö diorite used in the laboratory experiments was fresh and unaltered, which is not the case for the fracture material).

The through diffusion experiment results for the KXTT1 Feature A site specific diffusion cell /Byegård et al, 1998/ showed four times lower diffusivity and porosity than for the Äspö diorite, i.e., ($D_e^{HTO} \approx 4 \cdot 10^{-14}$, $\varepsilon \approx 0.001$) and ($D_e^{HTO} \approx 1.2 \cdot 10^{-13}$, $\varepsilon \approx 0.004$) for the site specific material and the Äspö diorite, respectively. An estimation of effective diffusivities based on this single sample would therefore be to reduce the diffusivities for the tracers obtained for Äspö diorite with a factor of three in order to obtain the effective diffusivities of the Feature A site specific material.

D_e for the sorbing tracers has been calculated from the relation

$$D_e^{sorb} = D_w^{sorb} \cdot F \tag{7-7}$$

where the formation factor for Äspö diorite has been calculated according to:

$$F = \frac{D_e^{HTO}}{D_w^{HTO}} = \frac{1.2 \cdot 10^{-13}}{2.4 \cdot 10^{-9}} = 5 \cdot 10^{-5} \tag{7-8}$$

and the formation factor for the Feature A site specific material has been calculated according to:

$$F = \frac{D_e^{HTO}}{D_w^{HTO}} = \frac{4 \cdot 10^{-14}}{2.4 \cdot 10^{-9}} = 1.7 \cdot 10^{-5} \tag{7-9}$$

where D_w is the diffusivity of the tracer in the water phase /Gray, 1972/. The estimated diffusivities are presented in Table 7-7.

It should be noted that the present calculation of the diffusivity uses the assumption that the porosity of the rock material is homogeneously distributed and fully connected. However, elaborate studies of the porosity of rock fracture material (e.g., Section 7.2 in this report, /Byegård et al, 2001/) show that the porosity is strongly heterogeneously distributed. It is therefore unlikely that the through-diffusion results for experiments using 1–2 cm thick slabs give values representative for the outer mm-layer of the wall-rock that is penetrated during an in situ tracer experiment.

K_d for sorption within the rock matrix (related to matrix diffusion), is based on K_d evaluated from through diffusion experiments on cylindrical core samples of Äspö diorite (Na, Ca and Sr) and on the penetration studies of Äspö diorite (Cs and Ba) /Byegård et al, 1998/. Since no "diffusion K_d" for Rb is available, the K_d for this elements has been estimated based on the K_d measured for the largest particle fraction (2–4 mm) in the batch experiments. These batch K_d values have been divided by a factor of 5, which was the observed relation between the diffusion K_d and batch K_d for Na, Ca and Sr. The estimated K_d values are presented in Table 7-7.

However, it should also be noted that the K_d-values presented are based on the assumption that the porosity is homogeneously distributed and fully connected in the rock matrix. This concept is, as earlier mentioned, somewhat contradicted by experimental observations. In some recently performed studies, attempts have been made to include the observed heterogeneity in porosity distribution in the evaluation of the K_d in some diffusion experiments /Johansson et al, 2000; Byegård et al, 2001/. Through diffusion and penetration profiles evaluated with respect to the experimentally measured distribution of porosity indicated a better consistency between the K_d determined in batch experiments and the K_d values determined from diffusion experiments.

Table 7-7. Matrix sorption and diffusion parameters obtained from diffusion experiments in rock cylinders of Äspö diorite and Feature A site specific material. The K_d´s presented are based on the assumption of homogeneously distributed porosity in the rock.

Tracer	K_d (m^3/kg)	D_w (m^2/s)**	ÄD D_e (m^2/s)***	Feature A D_e (m^2/s)***
HTO	–	$2.4\cdot10^{-9}$	$1.2\cdot10^{-13}$	$4\cdot10^{-14}$
Na^+	$1.4\cdot10^{-6}$	$1.33\cdot10^{-9}$	$6.7\cdot10^{-14}$	$2.2\cdot10^{-14}$
Rb^+	$4\cdot10^{-4}$*	$2.03\cdot10^{-9}$	$1.0\cdot10^{-13}$	$3\cdot10^{-14}$
Cs^+	[1] $8\cdot10^{-4}$****	$2.02\cdot10^{-9}$	$1.0\cdot10^{-13}$	$3\cdot10^{-14}$
Ca^{2+}	$5.2\cdot10^{-6}$	$0.79\cdot10^{-9}$	$4.0\cdot10^{-14}$	$1.3\cdot10^{-14}$
Sr^{2+}	$4.7\cdot10^{-6}$	$0.79\cdot10^{-9}$	$4.0\cdot10^{-14}$	$1.3\cdot10^{-14}$
Ba^{2+}	$2\cdot10^{-4}$****	$0.83\cdot10^{-9}$	$4.2\cdot10^{-14}$	$1.4\cdot10^{-14}$

* From $K_{d(2–4\ mm)}$/5, other K_d are mean values from diffusion experiments.
** Calculated water diffusivities at infinite dilution /Gray, 1972/.
*** $D_e=F\cdot D_w$, $F=5\cdot10^{-5}$ for the Äspö diorite and $F=1.7\cdot10^{-5}$ for the Feature A site specific material.
**** From penetration depth studies in Äspö diorite /Johansson et al, 1998/, the slower of the two processes observed are used.

[1] Typewriting errors of this data entry occurring in the report SKB TR 98-18 have been corrected in this report.

However, explicit recommendations on implementation of heterogeneity concepts and associated data in the evaluation of the TRUE Block Scale experiment is beyond the scope of this report section and reference is instead made directly to the different publications cited in this section.

8 Recommended approach to block scale site characterisation

8.1 Overall premises and strategy

The TRUE Block Scale project capitalises on experiences drawn from investigations performed elsewhere in underground research facilities, mainly Stripa (Sweden), Grimsel (Switzerland) and Kamaishi (Japan). Evaluation of results from TRUE Block Scale i.a. enables definition of an outline of a methodology for site characterisation of fractured rock in the block scale.

The recommended tool kit, as defined in the subsequent sections, is applicable both for assessment of block scale rock volumes using surface boreholes and investigations underground in a rock characterisation facility (RCF). In addition, during the development of an underground repository such a methodology can be applied to define location of storage tunnels and canister positions.

Although the experience from TRUE Block Scale is drawn from characterisation performed over limited length scales (<200 m), the methodology is largely applicable also to investigations on larger scales, e.g. site scale (hundreds of metres to kilometres). However, restrictions in applicability may be imposed by a) the length scale itself (i.e. foreseen distances between boreholes) and b) the surface access (smaller hydraulic disturbances possible compared to what can be achieved in an underground situation).

8.2 Identification of conductive structures

Assessment of conductive structures in a first characterisation borehole at a given site will rely strongly on information from the drilling log combined with borehole radar and BIPS logs. During the drilling of additional boreholes, the location of conductive structures, and even their identity, can be observed/assessed by pressure responses created in existing piezometer test sections in the borehole array. For the most part this is true for the larger, more transmissive structures which can be identified in a deterministic sense. Verification of location of conductors identified from pressure responses, and their relative hydraulic properties, can subsequently be achieved through detailed flow logging. The identification of smaller hydraulic structures is dependent on the refinement of the flow logging technique employed. The POSIVA flow log technique applied to an underground situation enables identification of discrete conductive fractures with a resolution of 0.1 m. The lower measurement limit is about 0.002 l/min (using Equation 5-5 and an average pressure drop of Δh=390 m a measurement limit in transmissivity T of $8.5 \cdot 10^{-11}$ m^2/s is obtained).

The next step is to correlate the hydraulic flow anomaly with a geological structure identified in a borehole television log (e.g. BIPS) and the corresponding corelog. The experience is that the correlation between the major flow log anomalies and the core/BIPS data is relatively straight forward, and should for the most part correlate with identified deterministic structures observed in multiple boreholes. Small inflows are expected to be difficult to correlate to specific geological features extending over longer distances. The latter inflows are instead referred to a background fracture poulation.

The geometry of an identified geological structure/conductor can be obtained by combining the mathematical representation of the mapped trace in the BIPS image with the absolute geometry of the borehole.

8.3 Assessment of fracture network connectivity

The hydraulic connectivity of identified structures can be obtained through different types of measurements performed at various times during the characterisation process. Of particular importance are collected pressure responses to drilling of a new borehole, which can be used to obtain a first hand understanding of connectivity in the studied block. Combined with other characterisation data from the borehole, a first assessment of structure geometry over relevant distances can be made. These inferences are also possible to compare with predicted intercepts made for given structures in the borehole. The use of the pressure responses is primarily qualitative and provides data on the existence and location of structure, but more importantly provides an input on connectivity of structures over larger distances.

Once fixed piezometer installations have been made in the boreholes, cf Section 8.6, cross-hole interference tests, cf Section 8.5, can be used to corroborate the results obtained from analyses of drilling responses. The transient behaviour of the observed pressure responses can be used to identify typical families of responses which can strengthen the interpretation of families of fracture networks with different properties.

Additional support for connectivity may be obtained from hydrogeochemical data, cf Section 8.8.

8.4 Use of borehole geophysics

The directional antenna borehole radar enables assessment of the absolute geometry of a structure beyond the limits of the borehole. The method is however for the most part applicable to larger structures. In a situation with high salinty, as experineced at Äspö HRL, the results may lead to an ambiguity in the interpretation of geometry of a given structure. The primary reason for this restriction is that the salinity (electrical conductivity) of the groundwater provides attenuation of the radar signal. Depending on

the ambient site-specific conditions, the use of the method is primarily recommended for characterisation of a first borehole at a given site to help planning subsequent steps in the drilling programme.

High hopes were attached in TRUE Block Scale to the use of 3D and cross-hole seismics for identification of conductive structures. It is noted that seismics in this particular application in no way could replace the hard geologic and hydraulic data coming from borehole characterisation. This can to some extent be related to the geometry of boreholes and tunnels employed in the survey not being geometrically ideal in relation to the geometry of the structures being characterised.

To the extent that more advanced technologies become available the major contribution would be to enable mapping the continuity and heterogeneity of identified conductive structures between borehole intercepts where hard information is unavailable, e.g. through the use of seismic tomography.

Even with more developed processing techniques it is expected that the contrast in seismic properties of fractured rock at great depth is not sufficient to make crosshole seismics a critical component in the characterisation of conductive structures in the block scale.

8.5 Assessment of hydraulic material properties

The definition of a hydraulic testing programme to a large extent is governed by available resources, primarily the time allotted for hydraulic testing. In addition, the modelling concepts planned to be employed may to a variable degree put constraints/demands on the testing programme.

The block scale is considered to be the smallest scale at which continuum models are applicable for simulation of flow and transport. In addition, if the strategy is one of characterising discrete conductive features, there is a need to make priorities. Continuous logs of equal lenght test sections for statistical inference standing back for a strategy employing focused characterisation of principal conbductors.

In the TRUE Block Scale project the components of hydraulic testing methodology for an individual borehole, which are intimately coupled to flow logging and tracer dilution tests, evolved over time. At the end of the Detailed Characterisation Stage, the methodology comprised the following steps;

1. Identifying location of main conductive structures in the borehole using responses to drilling and flow anomalies in the borehole being drilled.

2. Verification of location and partial quantification (flow) using POSIVA flow logging technique.

3. The combined information from steps 1 and 2 combined with the BIPS TV log were used to select locations for focused flow and pressure build-up tests in defined double packer test sections (mainly 2 m sections). These tests, 10–15 in number per borehole were conducted at constant rate followed by a recovery period. During the tests the pressure responses were monitored in the entire borehole array.

4. The combined and integrated results from steps 1 through 3 where subsequently used to define an optimised array of packers in the new borehole. Due consideration and priority were at this time put on the number of structures present in relation to number of packers possible and, if need be, allocation of circulating sections (usage for e.g. tracer injection).

5. Once the borehole was completed as a multi-packer piezometer it could be utilised in cross-hole interference tests, tracer dilution and tracer tests.

The principal advantage with the employed approach is the speed in that the characterisation is focused to the important conductors of the borehole. The result is that the borehole can be fully equipped with an operational multi-packer system and pressure registration system within two months from completed drilling. The necessary hydraulic data on the principal conductors and the background fractures are available to satisfy the needs of the various modelling concepts employed.

The drawback is that the adopted approach does not furnish a complete log of hydraulic conductivity/transmissivity data along the investigated borehole. From a pure statistical standpoint the collected dataset is incomplete and high-quality data on low-transmissive parts of the investigated borehole are lacking. This may affect the statistical inference necessary for stochastic continuum models. However, it is argued that resources are better spent on that part of the studied rock block which in reality is contributing to the bulk of flow and transport, rather than spending time on the, relatively speaking, less conductive parts of the studied rock volume.

8.6 Borehole piezometer design

Borehole piezometer design differs substantially between surface boreholes and boreholes drilled underground. Underground boreholes completed at repository depth, cf TRUE Block Scale, are typically of relatively limited extent <300 m. Boreholes from the surface can be >1000 m. The advantage is that the underground boreholes, unlike the surface boreholes (dependent on instrumentation concept), can be drilled using one diameter and without telescoping the hole. The limited length of the underground boreholes implies that that the major conductors in most cases can be packed off without difficulties.

Another major advantage is that no special pumping device is needed to induce maximum possible pumping flow from a given sink section. The only thing required is to open the lines connecting a section to atmospheric pressure. In the event a particular flow rate is required this can be achieved by flow regulation.

The experience from the TRUE Block Scale project is that some 8–10 structures require isolation along a 250 m borehole. These sections include both bounding major structures, where only pressure monitoring is required, and some 4–5 sections where possibilities to inject and withdraw water is facilitated (2 additional lines connecting to the section). The constraints on the number of leadthroughs possible are given by the borehole diameter (76 mm in the case of TRUE Block Scale), the diameter of the pressure line (4/2) and the diameter of the circulation lines (6/4 mm, to allow sufficiently high circulation flow and in order to avoid possible chemical clogging of the lines). The employed SKB/GEOSIGMA system at a maximum managed 21 leadthroughs in a 76 mm hole (one common packer inflation line). The ANDRA/Solexperts system managed 40 leadthroughs (including individual packer inflation).

The volumes of borehole sections which are used for circulation of fluids (injection sections for tracer tests, sampling of groundwater) should be minimised to the extent possible to reduce the volume of the circulation system. This is primarily achieved by making the test sections sufficiently short and focused. Additional volume reduction is achieved by introducing material into the sections. The materials should be chemically inert relative to the tracers used to avoid undesired sorption traps. This can be achieved by introducing a liner of suitable material on the central tubing (ANDRA/Solexperts), or by introducing solid dummy bodies (SKB/GEOSIGMA).

Collection of water samples is facilitated primarily by the circulating sections. If there is a demand for a "global" sampling this can be achieved by employing the line used for pressure monitoring in sections devoid of circulation lines.

8.7 Construction of hydro-structural models

A hydro-structural model constitutes a hypothesis regarding the geometry and properties of the conductive network of structures at a given site. Being a hypothesis implies that the model is tested against any new data that emerge from site characterisation and supporting evaluation modelling. In TRUE Block Scale the natural point of model update occurred after completion of each cored borehole and associated characterisation.

In construction of block scale hydrogeochemical models, it is advantageous to start out from a conceptual (hydro-)structural model on a larger scale. The pattern and textures observed on a larger scale is likely to be reoccurring on a smaller length scale. Likewise, information obtained on a smaller scale (including laboratory scale) can be fed back to the larger scale, thus providing mutual support and improvement to models developed on various scales.

The results from high resolution flow logs, borehole TV logs and various types of crosshole pressure interference data are used to construct a first hydrostructutral lattice of structures. This lattice is subsequently further confirmed and informed using results from focused hydraulic tests and detailed geological and mineralogical data associated

with the interpreted structures. Hydraulic structures which are not possible to associate with the identified deterministic structures are associated with a background fracture population described in statistical terms.

The use of computer-based CAD systems is a natural component in the construction of the hydro-structural models. With the powerful computers and software available the complete site characterisation data base can be accessed interactively. The computer-based geometrical models can then be transferred to the end user specialist's desktop for application in his/her special field.

The hydro-structural model is then used to make conjectures and decisions about the next step in the characterisation programme. Is the geometrical context satisfactory well understood? Is the planned experimental array providing the geometrical and areal coverage required? Is the number of packed-off test sections sufficiently large? Is another borehole required?

Originally it was intended to make early use of numerical modelling in the decision making in conjunction with all TRUE Block Scale model updates. It was found, however, that the effort of constructing elaborate discrete feature network models was not feasible during the early stages, while the hydro-structural models were too immature to justify usage of such complex and resource-intensive modelling approaches.

8.8 Use of supporting hydrogeochemical data

The interpretation of hydrogeochemical signatures of a natural geological system can be a valuable tool and independent support when constructing a hydro-structural model. Hydrochemical data can help distinguish an individual conductor, define how various parts/structures of the studied network of structures are connected, and how the system is connected to outside sources of water. In addition, monitoring over time can help follow the dynamics of mixing of waters in the studied rock volume as a result of the evolving borehole array in combination with other sources of disturbance, e.g. existing underground openings and annual variations. The understanding of the evolution of water chemistry is important to correctly interpret possible changes in retention noted over time, e.g. stronger sorption resulting from reduced salinity of the groundwater. The evolution of hydrogeochemistry at a site is a result of; 1) the palaeo end members of groundwater compositions seen at present, 2) the conductive geometry of structures and their hydraulic properties, 3) the distribution of hydraulic head (hydraulic gradient), and 4) the result of water rock interaction over time.

The puncturing of a natural groundwater system with boreholes entails mixing of waters of potentially variable composition. In order to capture the virgin groundwater chemistry of a given part of the studied system it is recommended to collect (pressurised) water samples during drilling using downhole samplers. Care should be placed to enable identification of contamination of drilling water, which should be tagged with a suitable tracer (the dye tracer uranine used at Äspö HRL).

An as complete as possible element analysis and isotope analysis is desired if the resources are available. The experience from TRUE Block Scale, where the groundwater chemistry is largely known, is that valuable inferences can be made also on low intensive analysis schemes including i.e. HCO_3, Cl, Electrical conductivity, pH, ^{18}O, ^{2}H and ^{3}H. The exact palette of analyses has to be tailored to the type of groundwater chemistry experienced.

8.9 Use of laboratory data

The laboratory data in this context constitute a broad suite of techniques by which a more detailed understanding is obtained about the constitution and physical and chemical properties of conductive structures and the rock matrix of the studied system. The properties/entities analysed include; mineralogy and geochemistry, porosity and distribution of porosity, diffusivity and sorption properties (volumetric and surface distribution coefficients). A general problem faced is that the investigated structures only are accessible at their borehole intercepts, which may or may not be potential injection and sink sections for subsequent tracer tests. However, the actual flow path of a given tracer experiment between the source and the sink essentially is unknown. The flow path can be traced in a numerical model, but basically we only have a "source – sink pair", defined by the respective borehole sections. This also implies that the material properties along the flow path essentially are unknown. A first approximation must be that the available intercepts (and associated drill core materials) provide a representative description of the flow path in question. However, the uncertainties embedded in this assumption should be made clear.

Of the mentioned techniques/methods those associated with mineralogy and geochemistry are pretty straight forward (i.e. microscopy, XRD and chemical analyses). From a transport viewpoint is worth mentioning that there is a need to collect and characterise non-consolidated materials of fault breccia/fault gouge type because this material can have a significant impact on the retention over experimental time scales, and possibly also over performance assessment time scales. Sorption experiments should be conducted on relevant materials (wall rock and un-consolidated materials) and on relevant size fractions and sorption times.

Diffusivity measurements on cores are relatively time consuming and the results are dependent on the length of the (core) samples. In addition it is noted that the results of laboratory diffusion tests (in through-diffusion cells) to a variable degree will be affected by the unloading of the rock stresses resulting from the coring, and by mechanical damage induced by the drilling itself and by sample preparation. The combined effects being widening of existing micro fractures and possible opening of grain boundaries/sealed microfractures (ubiquitous) and creation of new fractures (along the periphery of the core), e.g. /Li, 2001/. Ongoing in situ work at the high-stressed rock at the Canadian URL indicates that core-based determinations of diffusivity may be overestimated by 1-2 orders of magnitude /Vilks et al, 2001/. Correlation between electrical conductivity and diffusivity has been established in the laboratory /Ohlsson, 2000/. Based on these findings in situ determination of diffusivity based on electrical

logging methods in boreholes have been proposed /Ohlsson et al, 2001/. These types of measurements would potentailly also allow the possibility to correlate variability in resistivity (and possibly diffusivity) to geological variability. It is envisaged that core-based determinations of diffusivity, remain the principal means for calibrating diffusivity estimates based on in situ borehole geophysical logging. One should however be aware of the potential errors and uncertainties associated with in situ logging methods. These are embedded in artefacts (effects of conductive minerals) and the need to know the electrical conductivity of the matrix pore fluids. In addition, the calibration made on drillcore samples is to a variable degree affected by mechanical damage and stress redistribution effects on the drill cores. Similarly, stress concentrations at depth on the borehole periphery may entail a local reduced porosity/connectivity/diffusivity from the in situ measurements.

9 Discussion and conclusions

The following sections discuss the essential results and experiences from the characterisation of the TRUE Block Scale rock volume and the construction of hydro-structural models and conceptual flow models. In addition the principal conclusions associated with this work are presented.

9.1 Characterisation tools and methodology

The principal aim of the performed characterisation has been to build a robust hydro-structural model of major deterministic conductive structures which could serve as a basis for planning, design and interpretation of subsequent tracer tests in a block scale network of structures. The steps in the characterisation has involved identification of the location of deterministic structures along the boreholes and their connectivity within the borehole array. Subsequent steps have involved assessment of material and transport properties of the identified different types of structures.

9.1.1 Location and geometry of conductive features

The identification of hydraulic structures in the TRUE Block Scale rock volume has been made and corroborated with a number of different methods;

- The use of pressure responses and associated flow anomalies for assessment of connectivity is primarily qualitative but has provided important early information/ confirmation on the existence and location of a given hydrulic structure and its extent between boreholes. Comparison of structure locations interpreted in a given borehole with predictions made on the basis of the hydro-structural model at a given time has shown improved predictive capability as the hydro-structural model has evolved/matured.

- Verification of conductors identified from pressure responses has been achieved using various flow logging techniques. The usage of the POSIVA difference flow log technique has enabled identification of discrete conductive fractures with a flow rate as low as 0.002 l/min and with a spatial resolution of 0.1 m.

- Correlation of a hydraulic flow anomaly to a geological feature has for the majority of identified conductors been achieved with the BIPS borehole television log, cf Section 3.4, and the BIPS-based BOREMAP corelog. The correlation is straight forward for the major inflow points, which for the most part correlate readily with identifiable geological structures. These structures make up the identified deterministic structures which appear in multiple boreholes.

- The directional antenna RAMAC borehole radar enables assessment of the absolute geometry of larger structures, but generally provide ambiguous geometry, i.e. two alternate geometries. This is primarily attributed to the attenuation of the radar signal imposed by the high salinity of the groundwater experienced at the Äspö HRL. In the case of the radar survey in KI0025F02 the number of reflectors where a preferred geometry could be singled out was in the order of 30%. However, it should be emphasised that the borehole radar during the early phases of site characterisation (few boreholes available) provided valuable support to the construction of the hydro-structural model.

- Before the POSIVA difference flowmeter was introduced as a standard flow logging technique, the high-frequency borehole radar provided support to the identification of conductive structures, thereby filling up the blind zone near the borehole periphery existent in the directional borehole radar maps.

- The integrated interpretation of performed cross-hole, VSP and HSP seismic techniques have confirmed the bounding larger structures, i.e. Structure # 10 and possibly also Structures #19 and #8. In addition the integrated evaluation of the seismic data has indicated the existence of three subhorizontal structures, with lateral extents less than 250 m, located between –525 and –475 masl. It should in this context be emphasised that the hydraulic characterisation attributes no significance to the subhorizontal structures.

9.1.2 Connectivity of identified conductive structures

The connectivity of identified structures has been assessed through a series of different measurements performed at various times of the characterisation sequence.

- During the drilling of a borehole, pressure responses have been used to obtain a first assessment of connectivity between two boreholes. By careful registration of drilling advance vs. time it has been possible to relate pressure responses in packed off sections to a given inflow point/conductor in the borehole being drilled.

- Indexed pressure responses in the form of so-called response matrices were identified as an efficient means to compile and visualise complex connectivity relationships.

- Tracer dilution tests have been made in conjunction with most of the long-term cross-hole interference tests. By combining dilution tests at ambient (non-pumped) conditions with tests at pumped conditions a transport connectivity has been assessed. The results have been used to select suitable source (injection) sections for tracer. For the most part sections showing good hydraulic connectivity (fast and high pressure responses) correlate well with sections showing good transport connectivity. However, exceptions occur, showing the necessity for tracer dilution tests for effectively identifying and screening among possible source sections for tracer tests.

9.1.3 Hydraulic tests

In the hydraulic characterisation of the TRUE Block Scale rock volume a selective approach has been adopted. The selection of locations for more elaborate transient hydraulic tests has been based on preceding flow logging in combination with the BIPS/BOREMAP logs. During the characterisation in the two last boreholes the performed constant head flow and pressure build-up tests were closely linked to a programme of short-term cross-hole interference tests in selected sections which enabled rapid establishment of packer positions in the piezometers in the new boreholes.

Analysis of transient behaviour of the responses collected during cross-hole interference tests in packed off boreholes combined with distance–drawdown analyses have been used to identify families of responses. The latter have been shown to correlate well with the identified principal families of structures/fracture networks. In the case of the responses in the TRUE Block Scale rock volume, two main groupings can be identified; the #13/#20/#21 (#22/#23) and the #5/#6/#7 (#24) systems. Complexity in the fracture system studied combined with practical inability to pack off every single structure has made it difficult to fully differentiate/resolve Structures #21 and #13.

The UHT-1 equipment for performing transient hydraulic tests underground has proved to work well.

9.1.4 Piezometer design

In the TRUE Block Scale Project two different piezometer (multi-packer system) designs have been employed in 76 mm boreholes. The SKB/GEOSIGMA system, used in KA2563A, KA3510A, KI0025F and KI0025F03 is centred on a 20 mm central rod to which packers are positioned at selected intervals, cf Section 2.2.2. Tubings are clamped to the central rod. The packers systems are inflated with water pressurised by nitrogen gas using one common inflation line for all packers. An individual packer has up to 21 leadthroughs allowing up to 7 circulation sections and/or up to 21 sections where pressure can be monitored depending on how the leadthroughs are distributed. Circulation sections are equipped with dummy bodies to reduce the volume of the sections.

The ANDRA/Solexperts system installed in borehole KI0023B and KI0025F02 consists of up to 10 inflatable packers connected to a central tubing. All tubing and leadthroughs (up to 40) are led through the central tubing. All packers have individual inflation lines.

All ten sections are equipped to facilitate circulation of fluids. No dummy materials in the test sections are required while the diameter of the central tubing is large in itself. In the case of the Solexperts system a length of uncoated central tubing collapsed in KI0023B due to the load of the fluid pressure, cf Section 2.2.2. This resulted in partial loss of functionality of the packer system.

Table 9-1 compiles advantages and disadvantages associated with the two types of equipment. It should in this context be noted that only minor problems with faulty inflation have been experienced. In addition no serious constraints were imposed by the limited number of leadthroughs in the SKB/GEOSIGMA system.

Table 9-1. Comparison between advantages and disadvantages of utilised multi-packers systems with regards to re-instrumentation, system maintenance, collection of water samples and performance of hydraulic tests.

SKB/GEOSIGMA packer system	ANDRA/Solexperts system
Advantages	**Advantages**
Flexible configuration	Large number of leadthroughs
Easy re-instrumentation	Separate inflation lines
Disadvantages	**Disadvantages**
Limited number of leadthroughs	Cumbersome re-instrumentation
One common inflation line	Clogging of sinter filters in injection sections

In the case of the early piezometers installed in KA2563A, KI0025F and KI0023B, need for re-instrumentation was identified, and was also done repeatedly. In the case of KI0023B, re-instrumentation was impossible, as was also complementary flow logging because of the collapsed tubing. The imposed restrictions were not found to seriously restrict the planned in situ test programme.

9.2 Building of hydro-structural models

9.2.1 Structural and geometrical aspects

- The conductive geometry of the investigated rock block is made up of deterministic NW structures (easy to predict/characterise) and NNW structures (connections more difficult to assess), both characterised by a steep dips.

- The noted high inflows in a borehole are for the most part associated with geologically or geometrically identified conductors.

- No evidence of subhorizontal conductive structures is available. This finding is also supported by observations from the nearby access and ventilation shafts. Although the integrated 3D seismic evaluation indicates existence of subhorizontal reflectors, these have been interpreted to be of no, or negligible significance. However, scrutiny of the hydrogeochemical data provides an indication of possible subhorizontal structure/lithological body loacted above TRUE Block Scale rock volume, cf Section 9.3.

- It is identified that the first three boreholes (KA2563A, KI0025F and KI0023B) were required to develop the basic model of the network of major structures. The last two boreholes (KI0025F02 and KI0025F03) basically confirmed and refined the initial basic model. The latter included interpretation of four new structures (#21, #21, #23 and #24) and an additional insight into the heterogeneous natures and interrelation of Structures #13 and #21. The implications of the above finding is that scopings and assessment using complex numerical models may not be very useful and cost effective until a mature basic hydro-structural model has been formulated.

- The remainder of the conductive fractures/structures, once the components of the deterministic structural model have been identified, are assigned to the background fracture population. The two sets of background fractures is one NW with steep dips (mean strike/dip 121/89.4) and a less inclined NNW set (mean strike/dip 160/36), cf Chapter 5.

9.2.2 Hydraulic aspects

The transmissivity of the identified deterministic structures which are part of the TRUE Block Scale volume ranges between $1.5 \cdot 10^{-9}$ and $3.7 \cdot 10^{-5}$ m^2/s. The transmissivity of those structures which are involved in the performed tracer tests range between $1.5 \cdot 10^{-9}$ and $1 \cdot 10^{-7}$ m^2/s.

The transmissivity distribution of the background fracture population derived from POSIVA flow logs from the area where tracer tests have been performed is featured by a log-normal distribution ($^{10}\log T = -8.95$ and $\sigma_{10\log T}=0.93$).

Low pressure responses in boreholes KI0025F02 and KI0025F03 have suggested that Structure #13 is discontinuous, or possibly that some intercepts interpreted associated with Structure #13 are associated with a different structure /Hermanson and Doe, 2000/ as discussed in Section 4.6.2 and 4.6.3. However, the interpreted discontinuity in Structure #13 is disputed by tracer dilution responses in the test section in question /Andersson et al, 2000a/. An alternative cause for the noted lack of response may be that some other water source acts as a reservoir and constant head boundary that reduces pressure responses to pumping in more distant pumping sections. A possible candidate for such a reservoir is the fracture intersection zone (FIZ) between Structure #13 and #21 that extends close to intersections of Structure #13 in boreholes KI0025F02 and KI0025F03. It is also noted that the groundwater chemistry does not indicate a discontinuity in Structure #13. The available data thus supports the interpretation of a continuouis Structure #13 as included in the hydrostructural model. The difference in drawdown response is attributed to a flow channel or fracture intersection effect.

9.2.3 Major conclusions

- The principal experience from the characterisation and subsequent construction of a hydro-structural model is that it is not possible to discouple structural-geological and hydraulic data/elements in building the hydro-structural model.

For the most part the hydraulic information and geological structural information are integrated simultaneously in the interpretation. However, at times a hydraulic anomaly does not have a straightforward geological/geometrical interpretation, and a more thorough examination of the geological data is required. An example is the identification of Structures #21 and #22 in TRUE Block Scale.

- The main set of tools for determining the conductive geometry is combined borehole television (BIPS) and flow logging (POSIVA difference flow log) and pressure responses (drilling/cross-hole tests),

- The major conducting structures and their terminations between holes have been determined. The basic hydro-structural model was established using information from the three first boreholes. No major changes to the model was required on the basis of the additional information acquired from the last two boreholes. However, additional detail (new structures and insight into heterogeneity) was added to the model. Difficulties remain with regards to the actual extent of interpreted deterministic structures outside the borehole array,

- In terms of hydraulic connectivity and hydraulic response characteristics the interpreted structures form two main groupings; "#20/#13-system" (incl #21, #22 and the "#6/#7/#5-system" (incl #24), which are featured by distinct differences in response times and response characteristics,

- The developed hydro-structural model combined with the understanding of the hydraulic behaviour obtained from performed cross-hole and tracer dilution tests made it possible to identify a target area for well-controlled tracer experiments.

9.3 Conceptual flow model

Site characterisation of the TRUE Block Scale volume has produced data on groundwater head, chemistry, and groundwater flow that increase the understanding of the connection of the studied block to the larger Äspö HRL flow system. The data also provide further understanding of the structures within the block.

Chemical data show that Baltic seawater has penetrated downwards along structures such as EW-3, EW-1, and NE-2. These structures bounding the TRUE Block Scale volume in turn feed water to structures within the block, specifically Structure #10 and Structures #1 to #5. Baltic seawater from Structure #10 or a similar source has moved along an unidentified feature that parallels KA2511A somewhere between that hole and

centre of the block. The vertical flow paths feeding water to KA2511A may also contain a component of Meteoric water, as some chloride values in the central part of that hole have lower salinity than Baltic seawater. The source of these fresher waters cannot be deeper Glacial water as the tritium values are also enhanced.

The core of the TRUE Block Scale rock volume contains waters that constitute mixtures of Deep brine water and Glacial waters. These waters may be coming from depth towards the underground openings along Structures #13 and #20. One inconsistency in this interpretation is the observation from the UCM logs (Figure 6-1) that the inflows of more saline water around Structure #13 and Structure #20 also are cooler than the fresher water that flows in from Structure #10.

The hydraulic head information shows the expected movement of water across the studied block towards the underground openings of the Äspö HRL. The gradient over the central part of the TRUE Block Scale rock volume is about 0.05 m/m. The gradient becomes steeper toward the underground openings. Over the period of the experiment, heads in the block have dropped about 5 metres from gradual de-pressurisation of the rock mass.

The head data are generally consistent within each structure. One exception to this observation is Structure #13 where there is an apparent barrier to flow and an accompanying head drop between KI0025F03 and KI0023B. This head difference is attributed to the KI0025F03 intercept being located to a close proximity constant head boundary, cf Section 9.2.2.

The differences in hydraulic head as well as the chemical information indicate a hydraulic discontinuity between the core of the TRUE Block Scale rock volume and the overlying borehole, KA2511A. Given the high degree of connectivity between piezometer sections in KA2511A, this discontinuity may be a subhorizontal conductor/lithological body that has not yet been penetrated by a borehole in the area.

Ambient flow measurements from tracer dilution tests provide a useful complement to other information on the flow field. The major anomaly of the measurements is the flow within KI0023B between Structure #20 and Structure #6, which are both contained in piezometer interval KI0023B:P7. The tracer test design had to consider this ambient flow carefully to avoid loosing tracer. As to other measurements, the higher values appear associated with feeding the KI0023B:P7 short circuit, except for the flow in Structure #19 in KA2563A, which is well-connected to the Structure #13–#20 system based also on tests during pumping.

9.4 Transport parameters

Transport parameters (D_e and K_d) presented for the wall rock of structures involved in the TRUE Block Scale tracer tests are not based on laboratory diffusion and batch sorption measurements on site-specific materials from TRUE Block Scale. Instead, data have been imported from the previously presented results from studies performed in conjunction with the TRUE-1 experiments /Byegård et al, 1998/. The basis for this import is the structural and geological/mineralogical kinship between the TRUE Block Scale structures and the feature investigated as part of the TRUE-1 investigations.

However, an elaborate mineralogical and geochemical study has been performed on material collected from TRUE Block Scale structure intercepts of interest including fault breccia material. Assessments of the cation exchange capacity have, together with mineralogical distribution and site-specific hydrogeochemical data, been used to estimate volumetric distributions coefficients, K_d, for the size fractions <0.125 mm and 0.125–2 mm. As an example the calculated K_d values of Cs for the <0.125 mm fraction is significantly higher (K_d=0.093–0.28 m^3/kg) than that calculated for the 0.125–2 mm fraction (K_d=0.01 m^3/kg) which in turn is significantly higher than the value assigned to intact Äspö diorite (K_d=0.0008 m^3/kg).

Further, a comprehensive petrophysical programme has been performed with the aim to assess the porosity and porosity distribution/texture related to relevant structure intercepts. Measurements have been performed using both conventional water saturation/water absorption techniques and impregnation techniques using ^{14}C labelled PMMA /Hellmuth et al, 1999/. In this context measurements have been taken beyond measurements on wall rock samples alone, in that porosity determinations have been performed on 1–2 cm fault breccia pieces and even on 1–2 mm fault breccia fragments from the investigated target structures. The results show average bulk porosities for the fault breccia pieces (about 0.4–0.8%) which are comparable to that of wall rock samples. The fault breccia fragments, however, show distinctly higher porosities varying between 1–3%, with (with highs >10%).

9.5 What have we learned?

The characterisation of the TRUE Block Scale rock volume has demonstrated that it is important to monitor all possible hydraulic and chemical entities and parameters during the development of the block scale experimental volume. The recording of pressure responses to drilling, combined with a record of the advancement of the drill bit and associated flow anomalies proved to be an effective qualitative instrument in the construction/reconciliation of the hydro-structural model. In this context it is important in an underground research facility like Äspö HRL to keep a good record of any peripheral events which may affect the interpretation of the hydraulic and or/chemical situation in the investigated rock volume.

In order to obtain a useful basic model of the network of major structures, three boreholes were required (KA2563A, KI0025F, KI0023B). The remaining two boreholes (KI0025F02 and KI0025F03) basically confirmed and refined the developed hydro-structural model (including addition of four additional structures and a more detailed understanding of the hetereogeneity of the studied network of structures).

Relatively simple and resource non-intensive characterisation tools have been found to provide the basis for building a hydro-structural model satisfying the requirements for design, performance and evaluation of block scale tracer tests. An initial model update has been made using pressure responses to drilling and flow logging. Careful correlation of flow logging results with borehole TV data allows identification of the geological and structural characteristics of the conductive features. Quantification and further substantiation of the initial model is provided by transient single hole tests, crosshole interference tests and tracer dilution tests. Support for the developed hydro-structural model and the identified experimental volume in relation to other parts of the Äspö HRL is provided by hydrogeochemical and isotope data.

Numerical modelling was originally regarded as a tool to help decision making in conjunction with all TRUE Block Scale hydro-structural model updates. It was found, however, that the effort of constructing elaborate discrete feature network models was not feasible during the early stages, because the hydro-structural models were not mature enough to justify usage complex and resource-intensive modelling approaches.

The TRUE Block Scale characterisation has demonstrated the ability to build a robust hydro-structural model of a network of structures on a length scale of hundreds of metres. The model has subsequently been possible to verify (and modify) using additional boreholes and associated characterisation. The validity of the hydro-structural model, which should be regarded as a hypothesis in itself, will be subject to further testing as part of the evaluation of performed tracer tests. Of particular interest here is the possible role of background fractures for transport in the block scale rock volume.

10 Acknowledgement

The careful reviews of early versions of this report by Carmen Bajos (Enresa), Les Knight (Nirex), Juhani Vira (Posiva), Marin Mazurek (University of Bern), Olle Olsson (SKB), Jan-Olof Selroos (SKB) are gratefully acknowledged.

11 References

Adams J, 2001. Preliminary results of selective pressure build-up tests in borehole KI0023B. Swedish Nuclear Fuel and Waste Management Company, Äspö Hard Rock Laboratory, International Progress Report IPR-01-43.

Adams J, Andersson P and Meier P M, 2001. Äspö Hard Rock Laboratory, TRUE Block Scale project, Preliminary results of selective pressure build-up tests in borehole KI0025F02. International Progress Report IPR-01-56.

Ahlbom K and Smellie J A T, 1991. Overview of the Fracture Zone Project at Finnsjön, Sweden. J. of Hydrology, 126, pp. 1–15.

Allaby A and Allaby M (eds), 1990. The concise Oxford dictionary of earth sciences. Oxford University Press, Oxford. ISBN 0-19-286125-5

Allard B, Karlsson M, Tullborg E-L and Larsson S-Å, 1983. Ion exchange capacity and surface areas of some major component sand common fracture filling materials of igneous rock. Swedish Nuclear Fuel and Waste Management Company. SKB Technical Report TR 83-64.

Almén K-E et al, 1986. Site investigation – Equipment for geological, geophysical, hydrogeological and hydrogeochemical characterization. Swedish Nuclear Fuel and Waste Management Company (SKB), Technical Report TR-86-16.

Andersson P, Ludvigsson J-E, Wass E and Homqvist M, 2000a. Interference tests, dilution tests and tracer tests, Phase A, Swedish Nuclear Fuel and Waste Management Company, International Progress Report IPR-00-28.

Andersson P, Wass E, Holmqvist M and Fierz T, 2000b. Tracer tests, Phase B. Swedish Nuclear Fuel and Waste Management Company, Äspö Hard Rock Laboratory, International Progress Report IPR-00-29.

Andersson P, Ludvigsson J-E and Wass E, 2001a. Preliminary Characterisation Stage – Combined interference tests and tracer tests – Performance and preliminary evaluation. Swedish Nuclear Fuel and Waste Management Company, Äspö Hard Rock Laboratory, International Progress Report IPR-01-44.

Andersson P, Ludvigsson J-E, Wass E and Holmqvist M, 2001b. Detailed Characterisation Stage – Interference tests and tracer tests PT-1 – PT-4. Swedish Nuclear Fuel and Waste Management Company, Äspö Hard Rock Laboratory, International Progress Report IPR-01-52.

Andersson P, Byegård J, Holmqvist M, Skålberg M, Wass E and Widestrand H, 2001c. Tracer Test Stage – Tracer test, Phase C. Swedish Nuclear Fuel and Waste Management Company, Äspö Hard Rock Laboratory, International Progress Report IPR-01-33.

Andersson P, Byegård J and Winberg A, 2002. TRUE Block Scale Project Final Report no. 2(4) – Tracer tests in the block scale. Swedish Nuclear Fuel and Waste Management Company (SKB), Technical Report TR-02-14, in prep.

Banwart S (ed), 1995. The Redox experiment in block scale – Final reporting of results from the three year project. Swedish Nuclear Fuel and Waste Management Company, Äspö Hard Rock Laboratory, Progress Report PR 25-95-06.

Barton N and LaPointe P, 1995. Fractals in the Earth Sciences. Plenum Press, New York.

Bidaux P and Tsang C-F, 1991. Fluid flow patterns around a well bore or an underground drift with complex skin effects. Water Resour. Res., vol. 27, no. 11, pp. 2993–3008.

Billaux D and Rachez X, 2002. Investigation of the correlation between early-time hydraulic response and tracer breakthrough times in fractured media, Phase II. Swedish Nuclear Fuel and Waste Management Company, Äspö Hard Rock Laboratory, International Progress Report IPR-02-16.

Bischoff K, Wolf K and Heimgartner B, 1987. Hydaulische leitfähigkeit, porosität und uranruckhaltung von kristallin und mergel: Bohrkern-infiltrationsversuche. Nagra Technical Report series NTB 85-42, Nagra, Baden, Switzerland.

Black J H, 2001. Flow accounting – a new hybrid of hydrogeological and tracer test techniques to improve site characterization in fractured crystalline rocks. In: Proc. of the XXXI Int. Ass. of Hydrogeologists Congress. Munich, Germany, 10–14 September 2001. New Approaches Characterizing Groundwater Flow Volume 2, ISBN 90 2651 850 1.

Bossart P, Hermanson J and Mazurek M, 2001. Analysis of fracture networks based on the integration of structural and hydrogeological observations at different scales. Swedish Nuclear Fuel and Waste Management Company (SKB), Technical Report TR-01-21.

Bradbury M H, 1989. Laboratory investigation in supports of the migration experiments. Nagra Technical Report 88-23.

Bruggenwert H G M and Kamphorst A, 1982. Chapter 5 In: Soil Chemistry B. Physico-chemical models, G.H. Bold (ed). Elsevier, Amsterdam.

Byegård J, Skarnemark G and Skålberg M, 1995. The use of some ion-exchange sorbing tracer in in situ experiments in high saline groundwaters, Mat. Res. Soc. Symp. Proc. 353, 1077–1084.

Byegård J, Johansson H, Skålberg M and Tullborg E-L, 1998. The interaction of sorbing and non-sorbing tracers with different Äspö rock types. SKB Technical report, TR 98-18. ISSN 0284-3757.

Byegård J, Widestrand H, Skålberg M, Tullborg E-L and Siitari-Kauppi M, 2001. Complementary investigation of diffusivity, porosity and sorptivity of Feature A-site specific geological material. Äspö Hard Rock Laboratory International Cooperation Report ICR-01-04.

Comans R N J, Haller M and Preter P D, 1991. Sorption of cesium on illite: Non-equilibrium behaviour and reversibility, Geochim. Cosmochim. Acta 55, 433–440.

Cooper H H Jr and Jacob C E, 1946. A generalized graphical method for evaluating formation constants and summarizing well-field history, Eos Trans. AGU,27(4), 526–534.

Cvetkovic V, Cheng H and Selroos J-O, 2000. Evaluation of Tracer Retention Understanding Experiments (first stage) at Äspö. Swedish Nuclear Fuel and Waste Management Company, International Cooperation Report ICR-00-01.

de la Cruz B, Fernández A M, Rivas P, Cózar J and Labajo M A, 2001. TRUE Block Scale Experiment – Mineralogical and geochemical analyses of fracture filling materials (gouge and cuttings) from drillcore samples. Swedish Nuclear Fuel and Waste Management Company. Äspö hard Rock Laboratory, International Progress Report IPR-01-59.

Dershowitz W, Busse R, Geier J and Uchida M, 1996. A Stochastic Approach for Set Definition. In Aubertin, M. et al, Rock Mechanics: Tools and Techniques. Balkema, Rotterdam. pp. 1809–1813.

Dershowitz W, Burago A, Lee K and LaPointe P, 1999. User Documentation: Fractal 1.0, Spatial Data Analysis. Golder Associates Inc.

Doe T, 2001. TRUE Block Scale Project – Reconciliation of the March'99 structural model and hydraulic data. Swedish Nuclear Fuel and Waste Management Company, International Progress Report IPR-01-53.

Elert M, 1999. Evaluation of modelling of the TRUE-1 radially converging tests with conservative tracers, The Äspö Task Force on Modelling of Groundwater Flow and Transport of Solutes., Tasks 4C and 4D. Swedish Nuclear Fuel and Waste Management Company (SKB), Technical Report TR-00-07.

Elert M and Svensson H, 2001. Evaluation of modelling of the TRUE-1 radially converging tests with conservative tracers, The Äspö Task Force on Modelling of Groundwater Flow and Transport of Solutes., Tasks 4E and 4F. Swedish Nuclear Fuel and Waste Management Company (SKB), Technical Report TR-01-12.

Eliasson T, 1993. Mineralogy, geochemistry and petrophysics of red coloured granite adjacent to fractures. SKB Technical Report, TR 93-06, ISSN 0284-3757.

Enachescu C, Lavanchy J-M, Ostrowski L, Senger R and Wozniewicz J, 1997. Hydraulic investigations at Wellenberg: Hydraulic Packer Testing in Boreholes SB4a/v and SB4a/s. NAGRA Technical Report NTB 95-01, Nagra, Wettingen.

Follin S and Hermanson J, 1997. A discrete fracture network model of the Äspö TBM tunnel rock mass. Swedish Nuclear Fuel and Waste Management Company. Progress Report AR-97-001.

Frost LH, Kozak E T, Everitt R A, Serzu M H, Lodha G S, Gascoyne M and Davison C C, 1998. Transport properties in moderately fractured rock experiment, Stage 1 Groundwater flow domain characterization report. Ontario Hydro, Nuclear Waste Management Report No: 06819-REP-01200-0021 R00.

Gentzschein B, 2001. Detailed flow logging of core boreholes KA2511A, KI0025F and KA3510A using a double packer system. Swedish Nuclear Fuel and Waste Management Company. Äspö Hard Rock Laboratory. International Progress Report IPR-01-69 (in prep).

Gentzschein B and Morosini M, 2001. Selective pressure build-up tests in borehole KI0025F. Swedish Nuclear Fuel and Waste Management Company, Äspö Hard Rock Laboratory, International Progress Report IPR-01-01-45.

Gentzschein B and Ludvigsson J-E, 2001. Single-hole hydraulic tests and short-term interference tests in KI0025F03. Swedish Nuclear Fuel and Waste Management Company, Äspö Hard Rock Laboratory, International Progress Report IPR-01-58.

Gnirk P, 1993. OECD/NEA International Stripa Project 1980–1992 – Overview Volume II – Natural Barriers, January 1993. ISBN 91-971906-3-2.

Gray D E, 1972. American Institute of Physics Handbook, McGraw-Hill, New York.

Guimerà J, Vives L, Carrera J, Martinez L, Gómez P, Turrero M J, Alonso J and Hernán P, 1996. Hydrogeochemical implications in the flow analysis of El Berrocal site. In: Use of hydrogeochemical information in testing groundwater flow models. Proceedings of an International OECD/NEA Workshop, Borgholm Sweden, 1–3 September 1997, pp. 175–194. OECD/NEA ISBN 92-64-16153-8.

Guimerà J, García-Gutiérrez M, Yllera A, Carrera J, Hernández-Benítez A and Saaltink M, 1997. "Design, performance and interpretation of tracer tests at El Berrocal site (Spain). In: Field tracer experiments. Role in the prediction of radionuclide migration. Synthesis and Proceedings of an international NEA/EC GEOTRAP workshop, pp. 171–187. NEA/OECD. ISBN 92-64-16013-2.

Gustafson G, Stanfors R and Wikberg P, 1988. Swedish Hard Rock Laboratory. First evaluation of preinvestigations 1986–1987 and target area characterization. SKB Technical Report TR 88-16, Stockholm.

Hantush M S, 1967. Flow to wells in aquifers separated by a semipervious layer. J. Geophys. Res., vol. 72, no. 6, pp. 1709–1720.

Hautojärvi A and Taivassalo V, 1994. The INTRAVAL Project – Analysis of the Tracer Experiments at Finnsjön by the VTT/TVO Project Team, Report YJT-94-24, Nuclear Waste Commission of Finnish Power Companies, December 1994, Helsinki.

Hellmuth K-H, Siitari-Kauppi M, Klobes P, Meyer K and Goebbels J, 1999. Imaging and Analyzing Rock porosity by Autoradiography and Hg-Porosimetry/X-ray Computertomography-Applications, Phys. Chem. Earth (A), Vol. 24, No. 7, pp. 569–573.

Hermanson J, Nilsson P, Stenberg L, Follin S, Nyberg G and Winberg A, 1996. TRUE Block Scale – Updating of the structural-hydraulic model and compilation of scoping data set. Swedish Nuclear Fuel and Waste Management Company, Äspö Hard Rock Laboratory, Unpublished Progress Report.

Hermanson J and Doe T, 2000. March'00 structural and hydraulic model based on borehole data from KI0025F03. Swedish Nuclear Fuel and Waste Management Company (SKB), Äspö Hard Rock Laboratory, International Progress Report IPR-00-34.

Hermanson J, 2001a. October 1997 structural model – Update using characterisation data from KA2511A and KI0025F. Swedish Nuclear Fuel and Waste Management Company (SKB), Äspö Hard Rock Laboratory, International Progress Report IPR-01-41.

Hermanson J, 2001b. September 1998 structural model – Update using characterisation data from KI0023B. Swedish Nuclear Fuel and Waste Management Company (SKB), Äspö Hard Rock Laboratory, International Progress Report IPR-01-42.

Holton D, 2001. TRUE Block Scale Project – Boundary conditions for submodels at the äspö TRUE Block Scale site. Swedish Nuclear Fuel and Waste Management Company (SKB), Äspö Hard Rock Laboratory, International Progress Report IPR-01-50.

Jensen M R, 2001. The moderately fractured rock experiment. Background and overview. In: First TRUE Stage – Transport of solutes in an interpreted single fracture – Proc. from the 4th International Äspö Seminar, September 9–11, 2000.

Johansson H, Siitari-Kauppi M, Skålberg M and Tullborg E-L, 1998. Diffusion pathways in crystalline rock-examples from Äspö-diorite and fine-grained granite. Journal of Contaminant Hydrology, 35, 41–53.

Johansson H, 2000. Retardation of tracers in crystalline rocks. PhD Thesis, Chalmers University of Technology, Series 1582, ISSN0346-718x.

Johansson H, Byegård J and Skålberg M, 2000. Impact of porosity heterogeneity on the diffusíon of some alkali and alkaline earth metals in crystalline rock. In: Scientific Basis for Nuclear Waste Management XXIII, Editors: R.W. Smith, D.W. Shoesmith, Materials Research Society Symposium Proceedings, 2000, vol. 608, pp. 191–198.

Kelokaski M, Oila E and Siitari-Kauppi M, 2001. Investigation of porosity and microfracturing in granitic rock using the 14C-PMMA technique on samples from the TRUE Block Scale site at the Äspö Hard Rock Laboratory. Swedish Nuclear Fuel and Waste Management Company (SKB), Äspö Hard Rock Laboratory, International Progress Report IPR-01-27.

Kornfält K-A and Wikman H, 1988. The rocks of the Äspö island. Description of the detailed maps of solid rocks including maps of 3 uncovered trenches. Swedish Nuclear Fuel and Waste Management Company (SKB), Äspö Hard Rock Laboratory, Progress Report PR 25-88-12.

Kruseman G P and de Ridder N A, 1991. Analysis and evaluation of pumping test data. Publication no. 47, International Institute for Land Recalamation and Improvement, Wageningen, The Netherlands. ISBN 90 70754 207.

Kumpulainen H and Uusheimo K, 1989. Diffusivity and electrical resistivity measurements in rock matrix around fractures Report YJT-89-19, Nuclear waste Commision of Finnish Power Companies, Helsinki.

Landström Y and Tullborg E-L, 1993. Results from a geochemical study of Zone NE-1, based on samples from the Äspö tunnel and drill core KA16 (395–451 m). Swedish Nuclear Fuel and Waste Management Company, Äspö Hard Rock Laboratory, Progress Report PR 25-93-01.

Landström O, Tullborg E-L, Eriksson G and Sandell Y, 2001. Effects of glacial/post-glacial weathering compared with hydrothermal alteration – implications for matrix diffusion. Results from drillcore studies in porphyritic quartz monzodiorite from Äspö, SE Sweden. SKB Report R-01-37.

LaPointe P, Wallmann P and Dershowitz W, 1993a. Stochastic Estimation of Fracture Size Through Simulated Sampling. International Journal of Rock Mechanics and Mining Science, Vol. 30, No. 7, pp 1611–1617.

LaPointe P, Dershowitz W and Wallmann P, 1993b. Flow and Conductivity Properties of Fracture Networks as a Function of the Fractal Dimension in Proc. Geol. Soc. Amer. Annual Meeting, October 25–28, 1993. Boston, MA.

LaPointe P, Cladouhos T and Follin S, 1999. Calculation of Displacement of Fractures Intersecting Canisters Induced by Earthquakes. Aberg, Beberg, Ceberg, examples. Swedish Nuclear Fuel and Waste Management Co. Technical Report TR 99-03. SKB, Stockholm.

Li C-L, 2001. Long-Term Diffusion Experiment – Microscopic observation of disturbance in drill core samples from KA3065A02 and KA3065A03. Swedish Nuclear Fuel and Waste Management Co, Äspö Hard Rock Laboratory. International Progress Report IPR-01-03.

Liedke L and Zuidema P, 1988. The fracture system flow test. In: Grimsel Test Site from 1983 to 1990. Nagra Bullentin, Special Edition 1988, pp. 41–45.

Liedke L, Götchenberg A, Jobman M and Siemering W, 1994. Grimsel Test Site – Fracture system flow test – Experimental and numerical investigations of mass transport in fractured rock. NAGRA Technical Report 94-02E.

Maaranen J, Lehtioksa J and Timonen J, 2002. Determination of porosity, permeability and diffusivity of rock samples from Äspö HRL using the helium gas method. Swedish Nuclear Fuel and Waste Management Company. Äspö Hard Rock Laboratory. International Progress Report IPR-02-17 (in prep).

Marschall P and Vomvoris S (eds), 1995. Grimsel test Site – Devleopments in hydrotesting, fluid logging and combined salt/heat tracer experiments in the BK site (Phase III). NAGRA Technical Report 94-02E.

Mazurek M, Bossart P and Eliasson T, 1995. Classification and characterization of water-conducted features at Äspö: Results of phase I investigations. SKB Progress Report PR 25-95-03, Stockholm.

Mazurek M, Bossart P and Eliasson T, 1997. Classification and characterization of water-conducting features at Äspö: Results of investigations on the outcrop scale. SKB ICR 97-01, ISSN 1104-3210.

Meier P M, Carrera J and Sánchez-Vila X, 1999. A numerical study on the relationship between transmissivity and specific capacity in heterogeneous aquifers, Ground Water, Vol. 37, No. 4, July–August 1999.

Moye D G, 1967. Diamond drilling for foundation exploration. Civil Engineering Transactions, April 1967, pp. 95–100.

Munier R, 1995. Studies of geological structures at Äspö. Comprehensive summary of results. SKB Progress Report PR 25-95-21, Stockholm.

Norton D and Knapp R, 1977. Transport phenomena in hydrothermal systems; the nature of porosity. American J. Science, 277 (8), 913–936.

NRC, 1996. Rock Fractures and fluid flow – Contemporary understanding and applications. National Research Council. National Academy Press, Washington D.C. ISBN 0-309-04996-2.

Ohlsson Y, 2000. Studies of Ionic Diffusion in Crystalline Rock. Doctoral thesis at the Royal Institute of Technology, Stockholm, Sweden. ISBN 91-7283-025-5.

Ohlsson Y, Löfgren M and Neretnieks I, 2001. Rock matrix diffusivity determinations by in situ electrical conductivit measurements. Journal of Contaminant Hydrology, Vol 47, pp. 117–125.

Olsson O (ed), 1992. Site characterization and validation – final report. OECD/NEA International Project. Swedish Nuclear Fuel and Waste Management Company. Stripa Project Technical Report 92-22.

Olsson O, Stanfors R, Ramqvist G and Rhén I, 1994. Localization of experimental sites and layout of turn 2 – Results of investigations. Swedish Nuclear Fuel and Waste Management Co, Äspö Hard Rock Laboratory. Progress Report PR 25-94-14.

Pearson F J, 1999. What is the porosity of a mudrock? In Aplin, A. C., Fleet, A.J. and J.H.S Macquaker (eds) Muds and Mudstones: Physical and Fluid flow properties, Geological Society London. Special Publications. 158. 9–21.

Poteri A, Billaux D, Cvetkovic V, Dershowitz B, Gómez-Hernández J-J, Hautojärvi A, Holton D, Medina A and Winberg A, 2002. TRUE Block Scale Project. Final Report – 3. Modelling of flow and transport. Swedish Nuclear Fuel and Waste Management Company. Technical Report TR 02-15 (in prep).

Puigdomenech I, Ambrosi J-P, Banwart S A, Bateman K, Eisenlohr L, Griffoult L, Gustafsson E, Hama K, Kotelnikova S, Lartige J-E, Michaud V, Milodowski A E, Pedersen K, Rivas Perez J, Trotignon L, Tullborg E-L, West J M and Yoshida H, 2001. O_2 depletion in granitic media: The REX project. SKB Technical Report TR 01-05.

Ramsay J G and Huber M I, 1987. The techniques of modern structural geology; Volume 2; Folds and fractures. 1987, Acadademic Press, London, UK.

Rhén I, Bäckblom G, Gustafsson G, Stanfors R and Wikberg P, 1997a. Äspö HRL-Geoscientific evaluation 1997/2. Results from pre-investigations and detailed characterization. Summary report. SKB Technical Report TR 97-03, Stockholm.

Rhén I, Gustafsson G, Stanfors R and Wikberg P, 1997b. Äspö HRL-Geoscientific evaluation 1997/5. Models based on site characterization 1986–1995. SKB Technical Report TR 97-06, Stockholm.

Rivas P et al, 1998. El Berrocal project – Summary Report. European Commission. EUR 17830 EN. ISBN 92-828-2147-1.

Rouhiainen P, 2001. Posiva groundwater flow measuring techniques. In: Proc. of the XXXI Int. Ass. of Hydrogeologists Congress. Munich, Germany, 10–14 September 2001. New Approaches Characterizing Groundwater Flow Volume 2, ISBN 90 2651 850 1.

Rouhiainen P and Heikkinen P, 2001a. Difference flow measurements in borehole KI0025F02 at the Äspö Hard Rock Laboratory, Äspö Hard Rock Laboratory International Progress Report IPR-01-46.

Rouhiainen P and Heikkinen P, 2001b. Difference flow measurements in boreholes K2563A and KA2511A at the Äspö HRL, Äspö Hard Rock Laboratory International Progress Report IPR-01-48.

Rouhiainen P and Heikkinen P, 2001c. Difference flow measurement in borehole KI0025F03 at the Äspö HRL. Äspö Hard Rock Laboratory International Progress Report IPR-01-55.

Sandberg E, Olsson O and Falk L, 1990. Site characterization and validation – borehole radar investigations, Stage 3. Stripa Project TR 90-01.

Sawada A, Uchida M, Shimo M, Yamamoto H, Takahara H and Doe T W, 2000. Non-sorbing tracer migration experiments in fractured rock at the Kamaishi mine, northeast Japan. Eng. Geology 56, pp. 75–96.

Shimo M, Yamamoto H, Uchida M, Sawada A, Doe T W and Takahara Y, 1999. In situ test on flow and mass transport properties of fractured rocks. In: Proc. of 9th International Congress on Rock Mechanics, Paris, 1999 (Vouille, G and Beretst, P. eds), pp. 1401–1404. Balkema Publishers.

Siitari-Kauppi M, Marcos N, Klobes P, Goebbels J, Timonen J and Hellmuth K-H, 1999. Physical rock matrix characterization. The Palmottu Natural Analogue Project.

Skagius K, 1986. Diffusion of dissolved species in the matrix of some Swedish crystalline rocks. Ph. D Thesis, Royal Institute of Technology, Stockholm.

Skagius K and Neretnieks I , 1986. Porosities and diffusivities of some non-sorbing species in crystalline rocks. Water Resour. Res. 22, 389–397.

SKB, 2001. Site investigations – Investigation methods and general execution programme. Swedish Nuclear Fuel and Waste Management Company. SKB Technical Report TR-01-29.

Smart P L and Laidlaw I M S, 1977. An evaluation of some dyes for water tracing. Water Resources Research Vol. 13, No 1, p. 15–33.

Smellie J (ed), 2000. Status report of the Matrix Fluid Experiment. IPR-00-35.

Stanfors R, Liedholm M, Munier R, Olsson P and Stille H, 1993a. Geological-structural evaluation of data from tunnel section 700–1475 m. SKB Progress Report 25-93-05.

Stanfors R, Liedholm M, Munier R, Olsson P and Stille H, 1993b. Geological-structural and rock mechanical evaluation of data from tunnel section 1475–2265 m. SKB Progress Report 25-93-10.

Sundberg J and Gabrielsson A, 1999. Laboratory and field measurements of thermal properties of the rocks in the prototype repository at Äspö HRL. IPR 99-17.

Svensson U, 1997. A site scale analysis of groundwater flow and salinity distribution in the äspö area. Swedish Nuclear Fuel and Waste Management Company. SKB Technical Report TR 97-17, Stockholm.

Säfvestad A and Nilsson A-C, 1999. Äspö hard Rock Laboratory – Compilation of groundwater chemistry data. January 1995 to April 1998. Swedish Nuclear Fuel and Waste Management Company. Äspö Hard Rock Laboratory. International Progress Report IPR-99-13.

Tullborg E-L, Larson S Å and Stiberg J-P, 1996. Subsidence and uplift of the present land surface in the southeastern part of the Fennoscandian Shield. Geologiska Föreningens I Stockholm Förhandlingar 118, 126–128.

Tullborg E-L, 1997. Recognition of low-temperature processes in the Fennoscandian shield. PhD thesis, Earth Science center, Göteborg University. A 17, 1997 ISSN 1400-3813.

Tullborg E L and Smellie J A T (in prep). Uranium series disequilibrium studies of fracture filling material from major fracture zones at Äspö (in manuscript).

Vilks P, Cramer J J, Jensen M, Miller N H, Miller H G and Stanchell F W, 2001. In situ diffusion experiment in granite: Phase I. Submitted for publication in the Proceedings of the 8th International Conference on Chemistry and Migration Behaviour of Actinides and Fission Products in the Geosphere (Migration '01), Bregenz, Austria, Sept. 16–21, 2001.

Vomvoris S and Frieg B (eds), 1992. Grimsel Test Site – Interpretation of crosshole hydraulic tests and a pilot fluid logging test for selected boreholes within the BK-site. NAGRA technical Report 91-09.

Wikberg P, Gustafson G, Rhén I and Stanfors R, 1991. Äspö Hard Rock Laboratory. Evaluation and conceptual modelling based on the pre-investigations 1986–1990. SKB Technical Report TR 91-22, Stockholm.

Wikman H and Kornfält K-A, 1995. Updating of the geological model at Äspö. SKB Progress Report 25-95-04, Stockholm.

Wikström A, 1989. General geologic-tectonic study of the Simpevarp area with special attention to the Äspö island. SKB Progress Report 25-89-06, Stockholm.

Winberg A (ed), 1996. First TRUE Stage – Tracer Retention Understanding Experiments: Descriptive structural-hydraulic models on block and detailed scales on the TRUE-1 site. Swedish Nuclear Fuel and Waste Management Company. Äspö Hard Rock Laboratory. International Cooperation Report ICR 96-04.

Winberg A, Andersson P, Hermanson J and Stenberg L, 1996. Results of the SELECT Project – Investigation Programme for Selection of Experimental Sites for the Operational Phase. Swedish Nuclear Fuel and Waste Management Company. Äspö Hard Rock Laboratory Progress Report PR HRL-96-01.

Winberg A, 1997. Test plan for the TRUE Block Scale Experiment. Swedish Nuclear Fuel and Waste Management Company. Äspö Hard Rock Laboratory. International Cooperation Report ICR 97-02.

Winberg A (ed), 1999. Scientific and technical status. Position report prepared for the 2nd TRUE Block Scale review meeting, Stockholm, Nov 17 1998. Swedish Nuclear Fuel and Waste Management Company. Äspö Hard Rock Laboratory. International Progress Report IPR-99-07.

Winberg A (ed), 2000. Final report of the detailed characterisation stage – Compilation of premises and outline of programme for tracer tests in the block scale. ICR-00-02 – Report on Detailed characterisation stage. Swedish Nuclear Fuel and Waste Management Co, Äspö Hard Rock Laboratory. International Cooperation report ICR 00-02.

Winberg A, Andersson P, Hermanson J, Byegård J, Cvetkovic V and Birgersson L, 2000. Äspö Hard Rock Laboratory, Final report of the first stage of the tracer retention understanding experiments, Swedish Nuclear Fuel and Waste Management Company, SKB Technical report TR-00-07.

Winberg A, Andersson P, Byegård J, Poteri A, Cvetkovic V, Dershowitz B, Doe T, Hermanson J, Gómez-Hernández J-J, Hautojärvi A, Billaux D, Tullborg E-L, Meier P, Medina A, 2002. TRUE Block Scale Project. Final Report – 4. Synthesis of flow, transport and retention in the block scale. Swedish Nuclear Fuel and Waste Management Company. Technical Report TR-02-16 (in prep).

Xu S and Wörman A, 1998. Statistical patterns of geochemistry in crystalline rock and effect of sorption kinetics on radionuclide migration. Swedish Nuclear Power Inspectorate. SKI Report 98:41. ISSN 1104-1374.

Åberg G, Löfvendahl R and Levi B, 1984. The Götemar granite – isotopic and geochemical evidence for a complex history of an anorogenic granite. Geologiska Föreningens I Stockholm Förhandlingar 106, 297–400.

Appendix A

Evolution of packer configurations in boreholes. Test section delimiters (SECUP and SECLOW) are given in metres.

Ceneration code:	P	R	S	T
Idcode	**to 970429**	**to 980209**	**to 990201**	**present**
KA2511A : 8				6 - 64
KA2511A : 7				65 - 95
KA2511A : 6		6 - 63		96-102
KA2511A : 5		64 - 91	52 - 54	103 - 110
KA2511A : 4	6- 30	92 - 138	92 - 109	111 - 138
KA2511A : 3	31 - 80	139 - 170	110 - 216	139 - 170
KA2511A : 2	81 - 170	171 - 230	217 - 241	171 - 238
KA2511A : 1	171 - 293	231 - 293	242 - 244	239 - 293
Idcode	**to 980218**	**to 990120**	**present**	
KA2563A : 7	6 - 75	76 - 145		
KA2563A : 6	76 - 112	146 - 186		
KA2563A : 5	113 - 145	187 - 190	146 - 186	
KA2563A : 4	146 - 186	191 - 219	187 - 190	
KA2563A : 3	187 - 196	220 - 224	206 - 208	
KA2563A : 2	197 - 265	225 - 228	236 - 241	
KA2563A : 1	266 - 362	262 - 362	242 - 246	
Idcode	**present**			
KI0023B : 9	4,6 - 40,45			
KI0023B : 8	41,45 - 42,45			
KI0023B : 7	43,45 - 69,95			
KI0023B : 6	70,95 - 71,95			
KI0023B : 5	72,95 - 83,75			
KI0023B : 4	84,75 - 86,20			
KI0023B : 3	87,2 - 110,25			
KI0023B : 2	111,25 - 112,70			
KI0023B : 1	113,7 - 200,71			
Idcode	**to 980225**	**to 990728**	**present**	
KI0025F : 8	0 - 2,5			
KI0025F : 7	3,5 - 40			
KI0025F : 6	41 - 85	3,5 - 40	5 - 41,5	
KI0025F : 5	86 - 88	41 - 85	42,5 - 86,5	
KI0025F : 4	89 - 151	86 - 88	87,5 - 89,5	
KI0025F : 3	152 - 157	89 - 163	90,5 - 164,5	
KI0025F : 2	158 - 168	164 - 168	165,5 - 169,5	
KI0025F :1	169 - 193.7	169 - 193.7	170,5 - 193,7	
Idcode	**present**			
KI0025F02 : 10	3,4 - 37,50			
KI0025F02 . 9	38,5 - 50,70			
KI0025F02 : 8	51,7 - 55,10			
KI0025F02 : 7	56,1 - 63,00			
KI0025F02 : 6	64 - 72,30			
KI0025F02 : 5	73,3 - 77,25			
KI0025F02 : 4	78,25 - 92,35			
KI0025F02 : 3	93,35 - 99,25			
KI0025F02 : 2	100,25 - 134,15			
KI0025F02 : 1	135,15 - 204,18			
Idcode	**present**			
KI0025F03 : 9	3,58 - 50,58			
KI0025F03 : 8	51,58 - 54,08			
KI0025F03 : 7	55,08 - 58,58			
KI0025F03 : 6	59,58 - 65,58			
KI0025F03 : 5	66,58 - 74,08			
KI0025F03 : 4	85,08 - 88,08			
KI0025F03 : 3	89,08 - 92,58			
KI0025F03 : 2	93,58 - 100,08			
KI0025F03 : 1	101,08 - 141,72			

Appendix B

Analyses of groundwater sampled in the TRUE Block Scale rock volume. List of laboratories, analysis methods, detection limits and measurement uncertainties.

Components/ parameters	Laboratory	Method/SIS-Standard number	Detection limit or range	Measurement uncertainty
pH Conductivity Cl Cl HCO_3	SKB Chemlab	Potentiometric Mohr titr. (SIS 028120) IC Alkalinity titr. (SIS 028135)	0–14 0–10000 mS/m 10 mg/l 0.5 mg/l 0.6 mg/l	± 0.1 pH unit ± 5% ± 5% ± 10% ± 5%
Na, K Ca, Mg, S, Mn, Fe, Si, Li, Sr	SGAB	ICP-AES	0.1 mg/l <0.1 mg/l <0.03 mg/l <0.005 mg/l	± 5% ± 5% ± 5% ± 5%
SO_4 Br	SKB Chemlab	IC	0.05 mg/l 0.1 mg/l	± 10% ± 10%
Fe (tot) Fe (+II) HS^- NH_4_N	SKB Chemlab	Spect. (Ferrozine) Spect. (Ferrozine) Spect. (SIS 028115) Spect. (SIS 028134)	0.002 mg/l 0.002 mg/l 0.01 mg/l 0.005 mg/l	± 10% ± 10% ± 10% ± 20%
DOC	Fortum	UV oxidation, IR	0.2 mg/l	± 0.1 mg/l
^3H ^2H ^{18}O	U. Waterloo IFE	Natural decay counting MS MS	8.4 TU	± 4.2 TU ± 1.0 * ± 0.2 *
^{14}C age	Ångström lab.	Accelerator measurement	– – –	– – –
U and Th isotopes	Studsvik	Chem. Sep. and Alfa-spectrometry	–	± 30%
Ra and Rn isotopes	Studsvik	Chem. Sep. and Alfa-spectrometry, Gamma spectrometry	– –	– –
Trace metals	SGAB	ICP-MS ** INAA	Depending on element	± 15–20%

* In unit ‰ deviation from SMOW (Standard Mean Oceanic Water).
** In June 1997 HR ICP-MS was introduced for trace metals at SGAB.

For explanations of abbreviations and laboratory acronyms, see overleaf.

Abbreviations and explanations

titr.	Titrimetric method
IC	Ion Chromatography
Spectr.	Spectrophotometric method
ICP-AES	Inductively Coupled Plasma Atomic Emission Spectroscopy
ICP-MS	Inductively Coupled Plasma Mass Spectroscopy
DOC	Dissolved Organic Carbon (filtered sample)
UV-oxidation, IR	UV-oxidation and IR-measurement
MS	Mass Spectroscopy
INAA	Instrumental Neutron Activation Analysis

Laboratories

SKB Chemlab	SKB Chemistry Laboratory, Äspö HRL, Sweden
SGAB	SGAB Analytica AB, Luleå, Sweden
IFE	Institutt For Energiteknikk, Kjeller, Norge
Fortum	Fortum Power and Heat OY, Vantaa, Finland
Studsvik	Studsvik Nuclear AB, Nyköping, Sweden
Ångström lab	Ångströmlaboratoriet, Uppsala, Sweden
U. Waterloo	University of Waterloo, Ontario, Canada

Detailed interpretation of Structure #13 intercepts – 1.

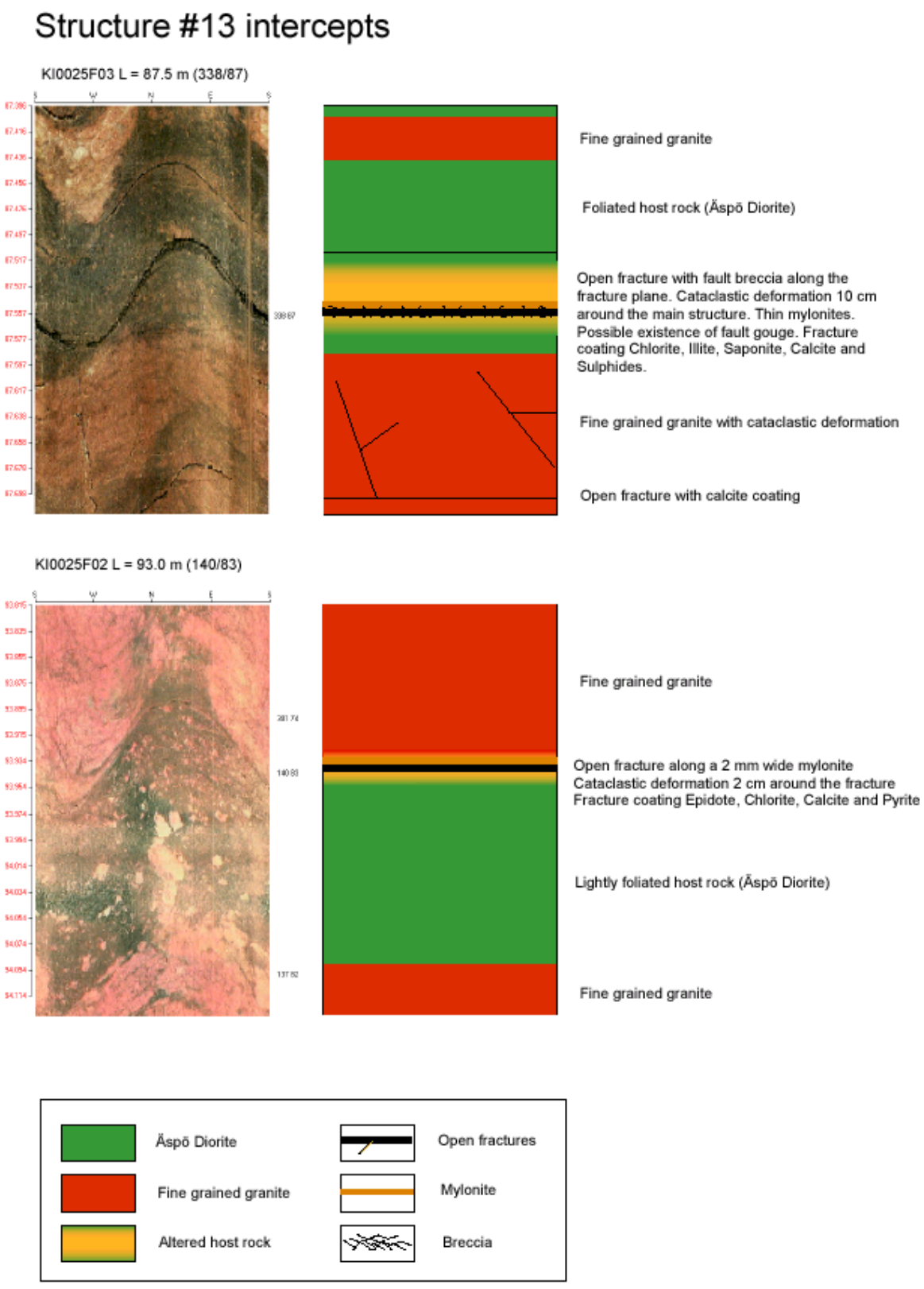

Appendix C-2

Detailed interpretation of Structure #13 intercepts – 2.

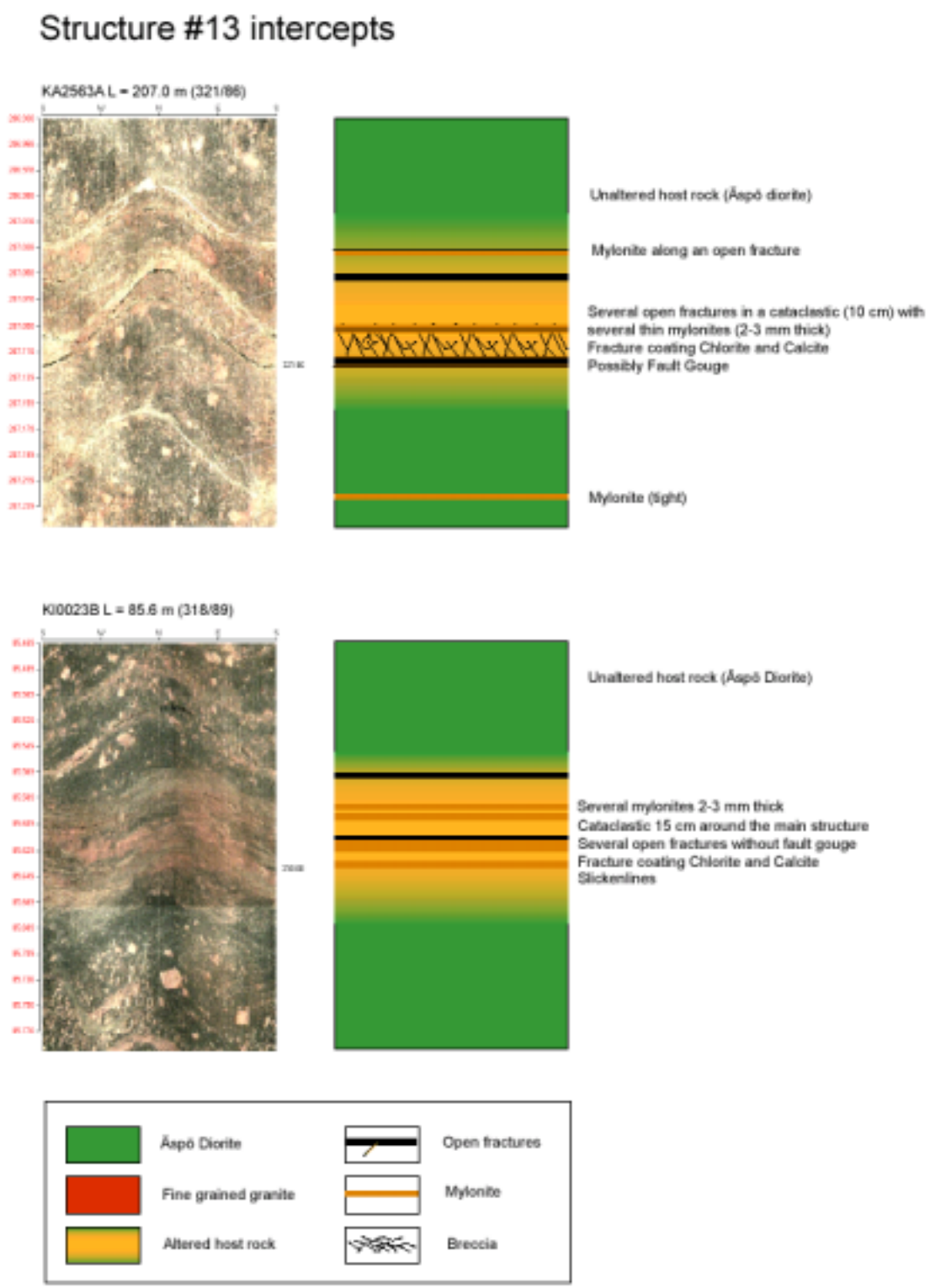

Detailed interpretation of Structure #20 intercepts – 1.

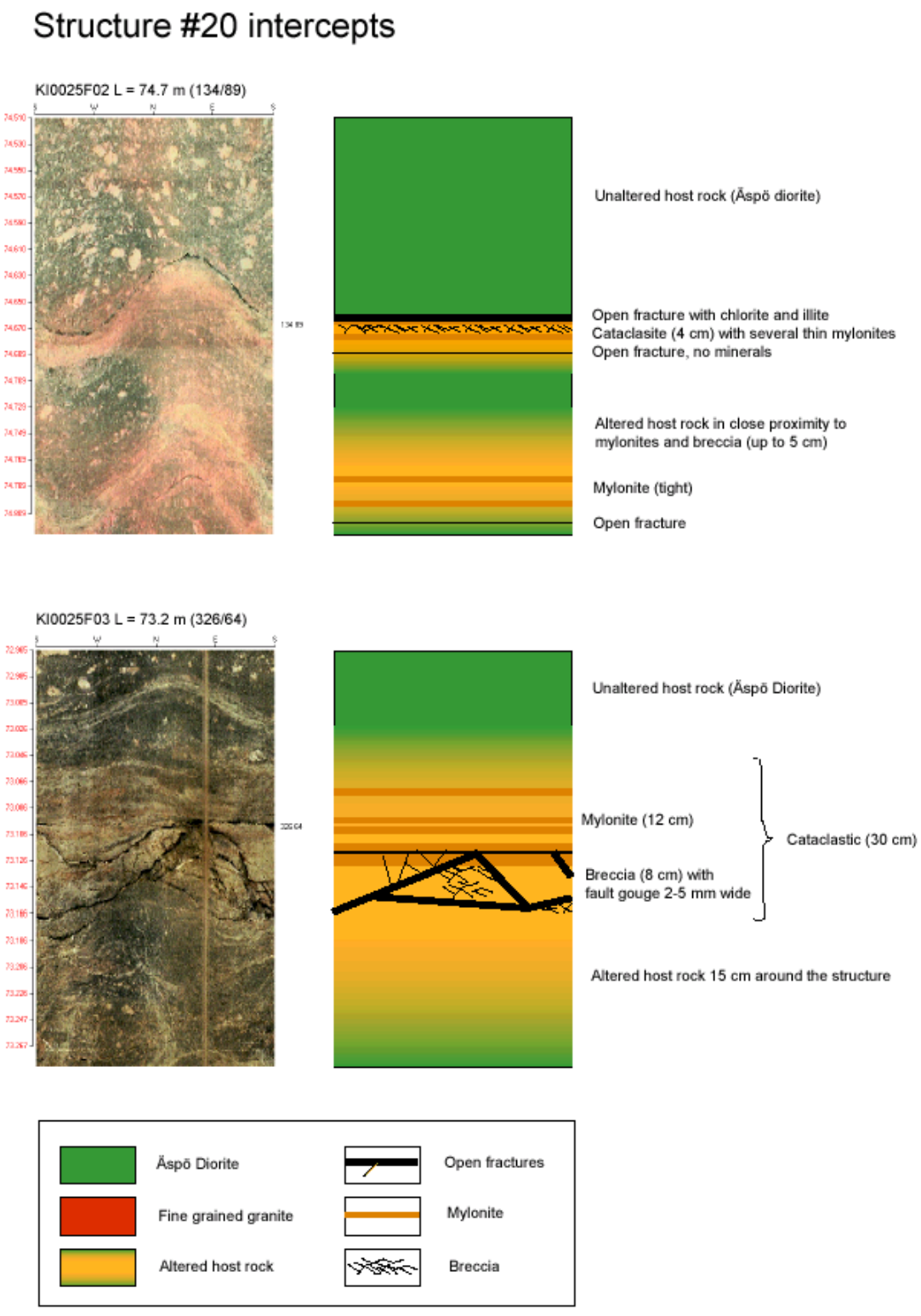

Appendix C-4

Detailed interpretation of Structure #20 intercepts – 2.

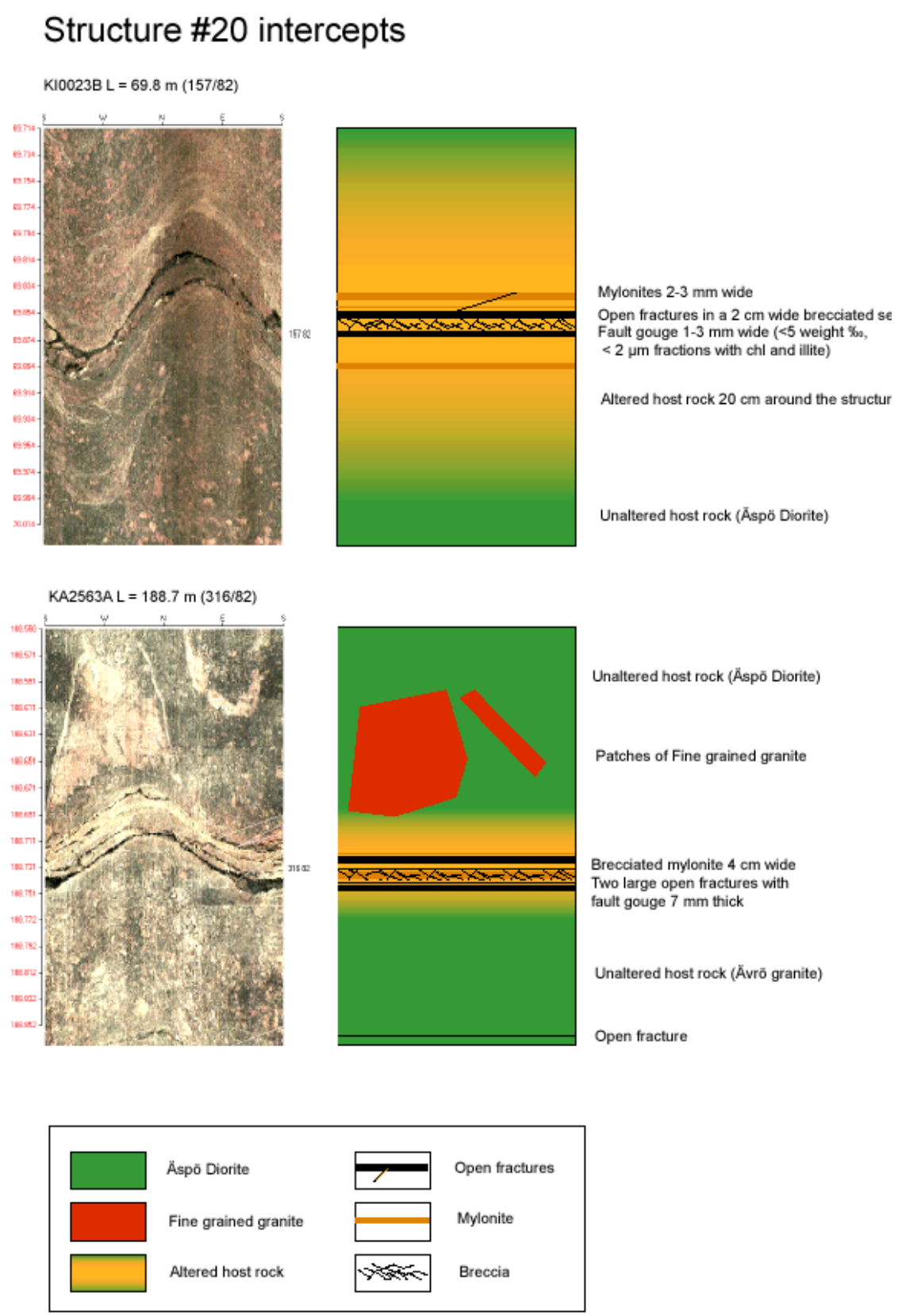

Appendix C-5

Detailed interpretation of Structure #21 intercepts.

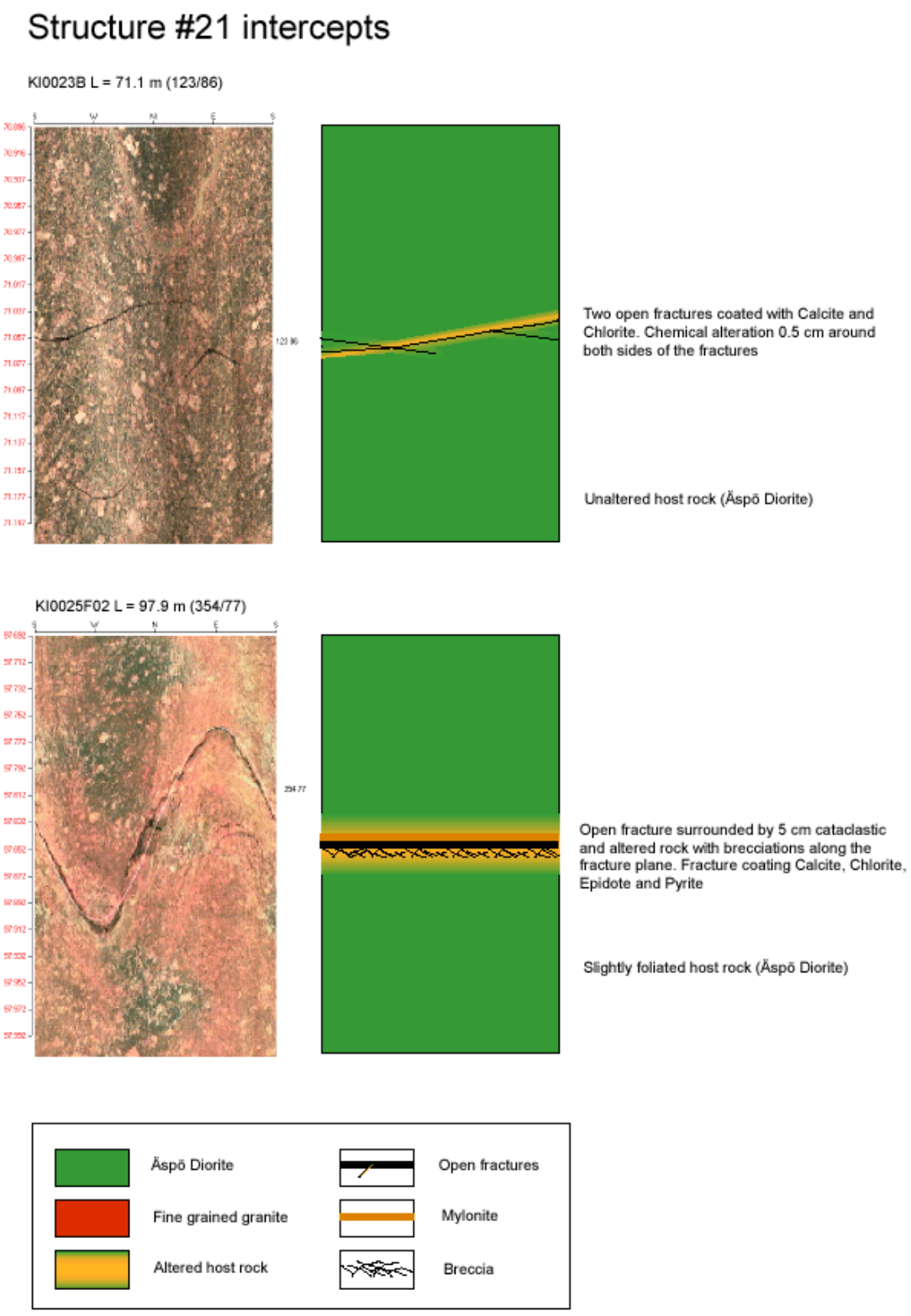

Appendix C-6

Detailed interpretation of Structure #22 intercepts – 1.

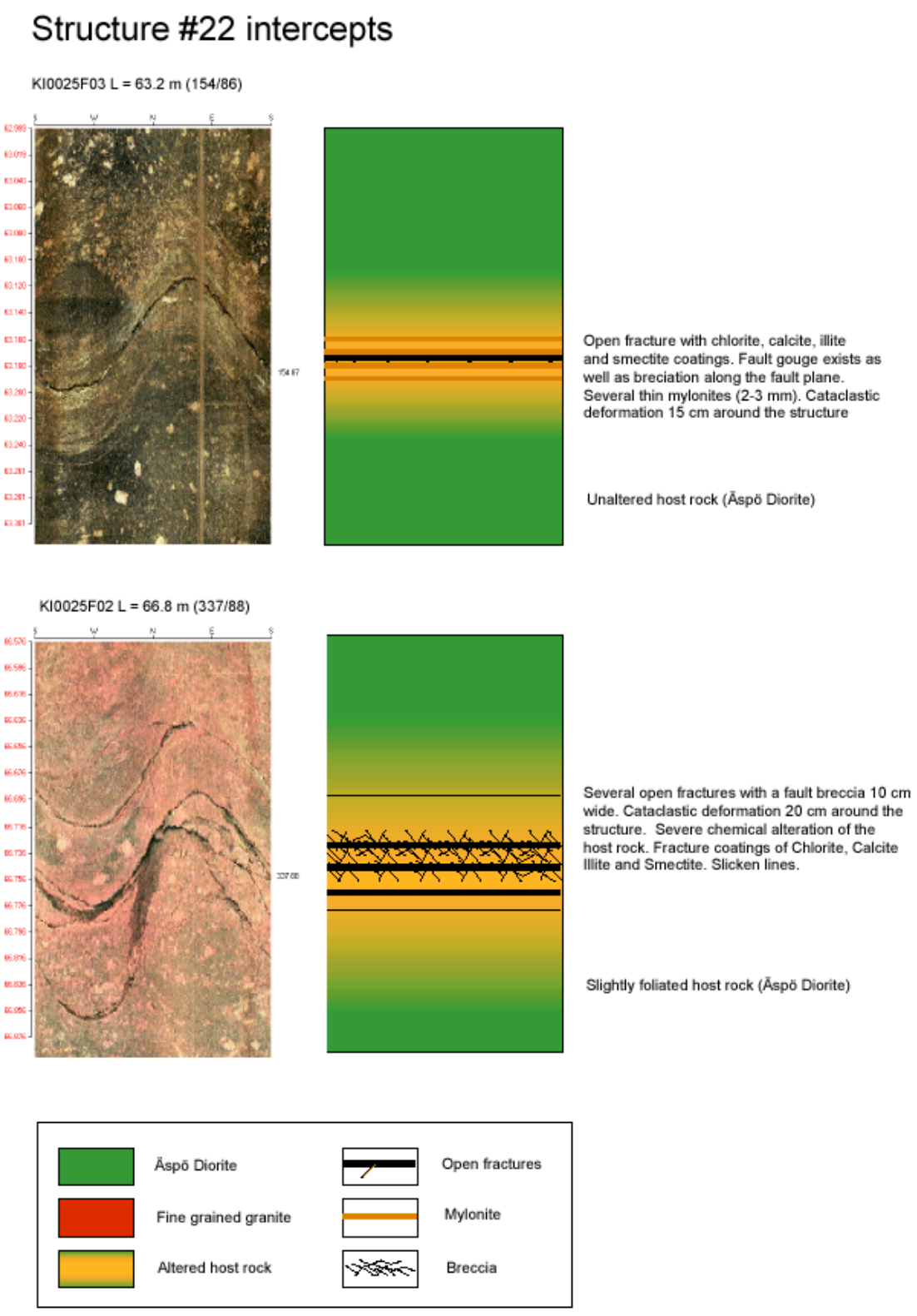

Appendix C-7

Detailed interpretation of Structure #22 intercepts – 2.

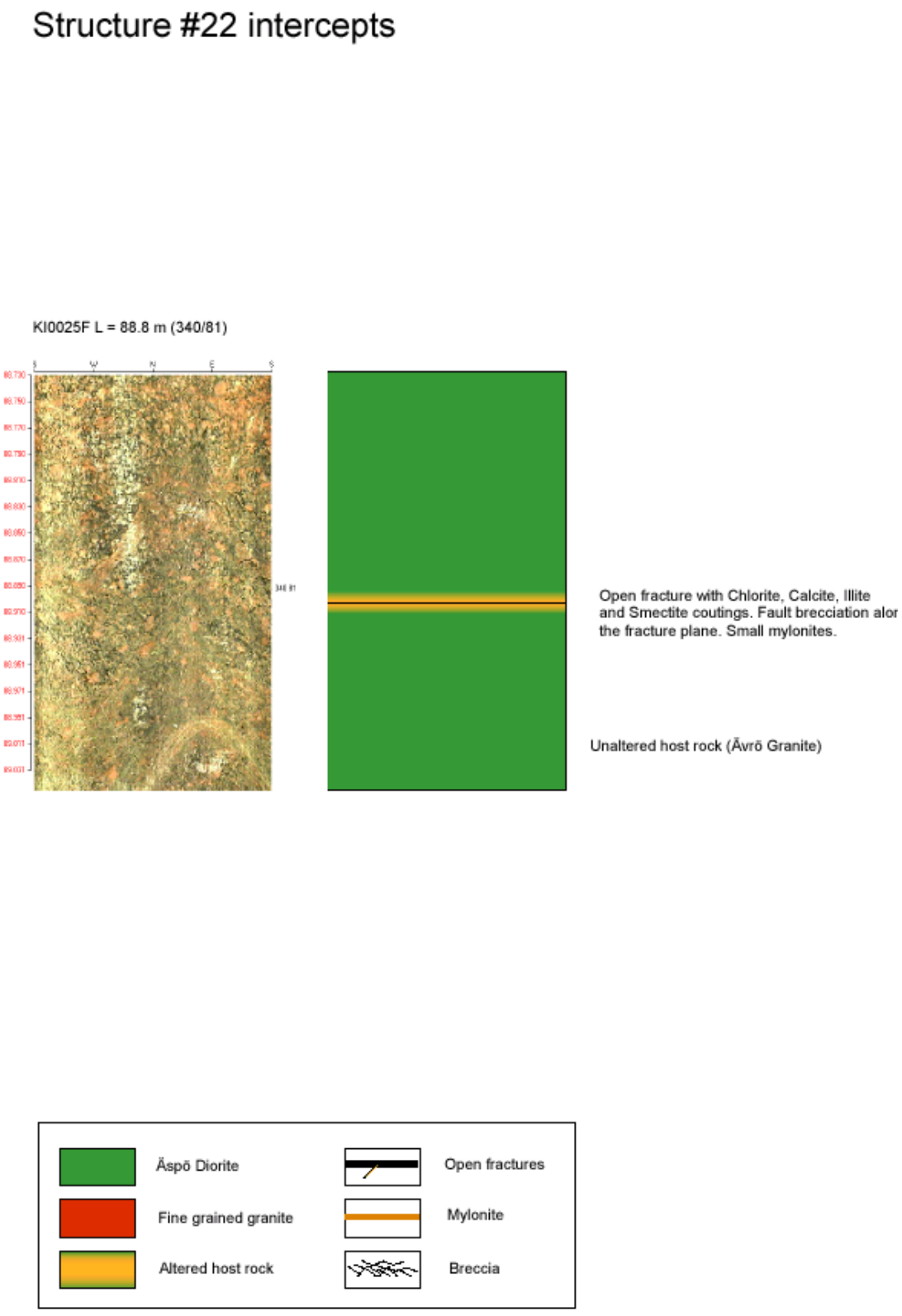

Detailed interpretation of Structure #23 intercepts.

Structure #23 intercepts

KI0025F03 L= 56.8 m (300/64 alt 301/77)

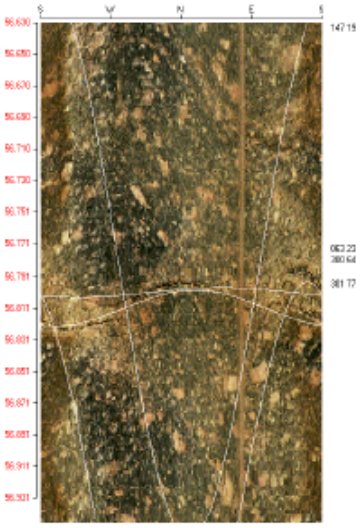

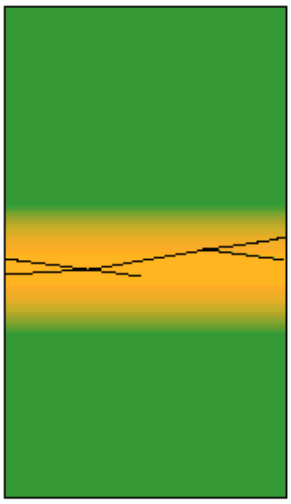

Open fractures with Chlorite, Calcite, Pyrite and Illite
Cataclastic and altered host rock 5 cm wide
Extensive formation of Albite, Sericite, Epidote and Calcite from plagioclase and Chlorite from Biotite

Unaltered foliated host rock (Äspö Diorite)

KI0025F02 L = 59.2 m (125/80)

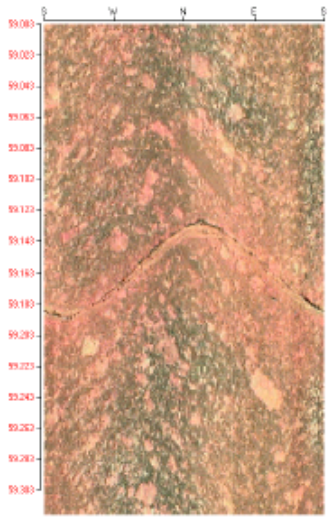

Unaltered foliated host rock (Äspö Diorite)

Open fracture with chlorite and calcite coatings
Mylonite 3 mm wide
Cataclasite 2 cm around the open fracture

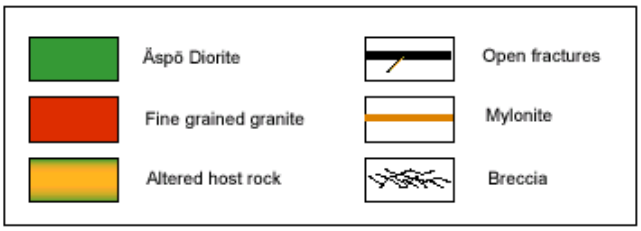

Appendix D

Analyses of gouge material (<0.125 mm fraction) from four TRUE Block Scale structure intercepts. Analyses of generic fresh Äspö diorite is presented for comparison. Shade = elements analysed using INAA, the remainder is analysed using ICP-MS.

Sample	**KA2563A:154 m** #6	**KI0025F02:133 m** #19	**KI0023B:69.9 m** #20	**KI0025F02:66.7 m** #22	**Äspö diorite** Generic
Mineralogy	Qz, Kfsp, Bi, Illite, Pl, Ca	Chl, Pl, Qz, Ep? Smectite, Illite	Ca, Chl, Illite, Kfsp, Qz, M-lc?	Chl, Qz, M-lc Kfsp,Pl,	Pl, Kfsp, Qz, Bi
% <0.002 mm (clay fraction)	15 illite, Chl, Pl,	21 Chl, smectite	28 Chl, illite, M-lc?	42 Chl, M-lc	N.A.
Oxides					
SiO_2 (weight-%)	60.5	48.7	25.7	45.1	61
Al2O3	15	15.7	10.1	17.4	17.8
CaO	4.4	4.3	14.5	2.9	4.1
Fe_2O_3	7.1	14	7.4	12.5	4.6
K_2O	3.3	1.7	2.2	5.3	3.2
MgO	2.1	4.1	3.9	6.3	2.2
MnO_2	0.12	0.18	0.27	0.33	0.09
Na_2O	3	3.8	1.3	0.7	4.4
P_2O_5	0.4	0.5	(13.9)*	0.2	0.3
TiO_2	0.87	1	0.36	0.3	0.8
Total	96.8	94.1	79.6	91.1	98.5
Element					
Ba (ppm)	1920	1100	807	916	1600
Sr	877	1080	632	356	1100
Rb	95.4	45.7	58.2	238	120
Cs	3.1	3.7	5	62.4	3
Hf	13	7.6	2.9	3.3	7.3
Zr	573	330	162	144	250
Ta	1.4	3	8.3	0.7	
U	3.4	5.2	4.7	1.8	4.5
Th	10	11.1	3.9	2.4	11
Co	18.7	43.4	25	62.6	
Cu	145	328	2960	165	20
Zn	142	386	2100	683	70
V	88	105	99	198	
La	59.9	59.1	35.9	25.3	57
Ce	144	136	71.2	49.5	120
Nd	54.1	52.4	20.3	14.6	58
Sm	8.4	9.7	5	3.2	10
Eu	1.9	1.9	1	0.8	2.1
Tb	1	1	1.2	0.5	1.3
Yb	1.4	3.1	2.3	2	2.3
Lu	0.4	0.5	0.3	0.3	0.4

Chl = chlorite, Qz = Quartz, Kfsp = K-feldspar, Pl = plagioclase (including albite)

Ca = calcite, M-lc = mixed-layer clay

* The P_2O_5 content in sample KI0023B:66.9 m is due to contamination

Appendix E-1

Groundwater chemistry data for the TRUE Block Scale volume.

Borehole	Structure	Secup	Seclow	Sampling	^{3}H	$\delta^{18}O$	Cl^-
		m	m	yy/mm/dd	Tritium Units	‰ SMOW	ppm
KA2511A	Unclear	52.0	54.0	980928	9.1	–8.3	3890
KA2511A	Unclear	52.0	54.0	990112	10.4	–8.3	3860
KA2511A	Unclear	92.0	109.0	980305	14.6	–7.3	3350
KA2511A	Unclear	92.0	109.0	980928	14.4	–7.3	3230
KA2511A	Unclear	92.0	109.0	990112	14.0	–7.4	3200
KA2511A	Unclear	103.0	110.0	990408	14.3	–7.4	3120
KA2511A	Unclear	103.0	110.0	990930	14.2	–7.4	3060
KA2511A	Unclear	110.0	216.0	990112	18.0	–7.7	3570
KA2511A	Unclear	111.0	138.0	990408	10.7	–8.0	3360
KA2511A	Unclear	111.0	138.0	990930	11.7	–8.2	3470
KA2511A	Unclear	217.0	241.0	990112	13.9	–7.3	3230
KA2563A	#5	76.0	145.0	990112	13.3	–7.3	3380
KA2563A	#6, #7	146.0	148.0	990112	6.9	–8.8	4980
KA2563A	#20	187.0	190.0	980928	7.6	–8.7	4830
KA2563A	#20	187.0	190.0	990112	4.9	–9.1	5540
KA2563A	#20	187.0	190.0	990408	4.2	–9.1	5350
KA2563A	#20	187.0	190.0	990928	6.4	–8.6	4480
KA2563A	#20	187.0	190.0	000411	14.1	–7.3	3100
KA2563A	#20	191.0	219.0	990112	5.4	–9.3	5170
KA2563A	#13	206.0	208.0	990408	4.3	–9.7	5010
KA2563A	#13	206.0	208.0	990928	5.4	–11.0	5730
KA2563A	#19	242.0	246.0	990928	5.9	–8.5	4620
KA2563A	#19	242.0	362.4	000411	4.9	–8.5	4760
KA2563A	#19	262.0	362.0	990112	7.3	–8.7	4950
KA3510A	#5 System	4.5	113.0	990115	11.6	–7.7	3730
KA3510A	#5 System	114.0	121.0	990115	3.5	–9.7	5860
KA3548A01	#5 System	5.0	6.0	980805	10.2	–7.0	3630
KA3548A01	#5 System	9.0	14.0	990113	14.1	–7.5	3380
KA3548A01	#5 System	15.0	30.0	990113	11.8	–8.0	4090
KA3548A01	#5 System	18.0	21.0	980807	12.4	–7.6	3650
KA3573A	#5 System	4.5	17.0	980928	11.4	–7.4	3670
KA3573A	#5 System	4.5	17.0	990115	11.7	–7.8	3790
KA3573A	#5 System	4.5	17.0	990407	8.9	–8.0	4060
KA3573A	#5 System	4.5	17.0	990929	14.3	–7.4	3450
KA3573A	#5 System	18.0	40.0	980928	10.7	–7.5	3640
KA3573A	#5 System	18.0	40.0	990115	10.7	–8.1	4060
KA3573A	#5 System	18.0	40.1	990407	10.9	–8.3	4290
KA3573A	#5 System	18.0	40.1	990929	14.3	–7.5	3230

Appendix E-2

Groundwater chemistry data for the TRUE Block Scale volume.

Borehole	Structure	Secup	Seclow	Sampling	^{3}H	$\delta^{18}O$	Cl^-
		m	m	yy/mm/dd	Tritium Units	‰ SMOW	ppm
KA3600F	#5 System	4.5	21.0	980309	10.0	–7.6	3730
KA3600F	#5 System	4.5	21.0	980928	9.8	–7.7	3830
KA3600F	#5 System	4.5	21.0	990113	7.2	–9.0	5080
KA3600F	#5 System	4.5	21.0	990409	6.8	–8.7	4870
KA3600F	#5 System	4.5	21.0	990929	11.9	–7.7	3480
KA3600F	#5 System	22.0	50.1	980928	8.1	–7.5	4150
KA3600F	#5 System	22.0	50.1	990113	3.5	–9.7	5990
KA3600F	#5 System	22.0	50.1	990409	5.5	–8.9	5180
KA3600F	#5 System	22.0	50.1	990929	5.3	–9.4	5420
KI0023B	#5	4.6	40.5	990111	3.7	–9.2	5660
KI0023B	#5	4.6	40.5	990407	4.1	–8.8	4890
KI0023B	#7	41.5	42.5	980928	13.9	–8.0	4140
KI0023B	#7	41.5	42.5	990111	3.9	–9.4	5590
KI0023B	#7	41.5	42.5	990407	4.6	–9.3	5830
KI0023B	#6, #20	43.5	70.0	990111	4.6	–9.4	5730
KI0023B	#6, #20	43.5	70.0	990927	5.7	–9.2	4880
KI0023B	#21 (#20)	71.0	72.0	980928	4.2	–9.1	5330
KI0023B	#21 (#20)	71.0	72.0	990111	4.0	–9.3	5600
KI0023B	#21 (#20)	71.0	72.0	990407	5.3	–9.2	5360
KI0023B	#21 (#20)	71.0	72.0	990927	4.2	–9.1	5060
KI0023B	#21 (#20)	71.0	72.0	000410	4.5	–9.6	5660
KI0023B	#13	84.8	86.2	980928	2.7	–10.7	5750
KI0023B	#13	84.8	86.2	990111	2.4	–11.1	6130
KI0023B	#13	84.8	86.2	990407	4.6	–10.8	5570
KI0023B	#13	84.8	86.2	990927	1.2	–10.7	5360
KI0023B	#13	84.8	86.2	000410	3.0	–10.9	5890
KI0023B	#19	111.3	112.7	980928	7.6	–8.6	4880
KI0023B	#19	111.3	112.7	990111	5.5	–8.9	5460
KI0023B	#19	111.3	112.7	000410	4.4	–8.9	5140
KI0023B	#10	113.7	200.7	990111	12.4	–7.5	3540

Appendix E-3

Groundwater chemistry data for the TRUE Block Scale volume.

Borehole	Structure	Secup	Seclow	Sampling	^{3}H	$\delta^{18}O$	Cl^-
		m	m	yy/mm/dd	Tritium Units	‰ SMOW	ppm
KI0025F	#5	3.5	40.0	990113	5.4	–9.0	5070
KI0025F	#6	41.0	85.0	990113	6.5	–9.4	5160
KI0025F	#20	86.0	88.0	980305	3.6	–9.8	6050
KI0025F	#20	86.0	88.0	980928	5.1	–10.6	6200
KI0025F	#20	86.0	88.0	990113	2.2	–10.8	6510
KI0025F	#20	86.0	88.0	990407	3.0	–10.6	6560
KI0025F	#20	86.0	88.0	000412	2.8	–10.5	6220
KI0025F	#20	87.5	89.5	990929	2.8	–10.4	6210
KI0025F	#13?	89.0	163.0	990113	2.2	–9.8	5860
KI0025F	#19	164.0	168.0	980928	5.5	–8.8	5410
KI0025F	#19	164.0	168.0	990113	3.7	–9.0	5450
KI0025F	#19	164.0	168.0	990407	4.8	–8.5	5380
KI0025F	#19	165.5	169.6	990929	5.1	–8.8	5270
KI0025F	#Z	169.0	193.7	990113	6.6	–9.2	4460
KI0025F02	#5	3.4	37.5	990114	3.6	–9.3	5550
KI0025F02	#7	38.5	50.7	990114	6.1	–9.4	5620
KI0025F02	#7	38.5	50.7	000411	5.5	–9.4	5410
KI0025F02	#6	51.7	55.1	990114	4.4	–9.4	5720
KI0025F02	#6	51.7	55.1	000411	4.4	–9.6	5570
KI0025F02	#23	56.1	63.0	990114	4.4	–9.7	5700
KI0025F02	#23	56.1	63.0	990407	2.4	–9.7	5680
KI0025F02	#23	56.1	63.0	990928	7.1	–9.6	5400
KI0025F02	#22	64.0	72.3	990114	4.8	–9.4	5560
KI0025F02	#22	64.0	72.3	990408	5.1	–9.1	5310
KI0025F02	#22	64.0	72.3	990928	4.4	–9.5	5560
KI0025F02	#20	73.0	75.4	980818	1.9	–10.0	5640
KI0025F02	#20	73.3	77.3	990114	3.2	–9.4	5810
KI0025F02	#20	73.3	77.3	990408	3.4	–9.5	5540
KI0025F02	#20	73.3	77.3	990928	5.8	–9.5	5570
KI0025F02	#20	73.3	77.3	000411	2.6	–9.8	5870
KI0025F02	#21	93.4	99.3	990114	2.5	–9.5	6090
KI0025F02	#21	93.4	99.3	990408	2.3	–10.2	5990
KI0025F02	#21	93.4	99.3	990928	3.0	–10.3	6110
KI0025F02	#19	100.3	134.2	990114	2.8	–9.1	5580
KI0025F02	#10	135.2	204.2	990114	12.7	–7.4	3350
KI0025F03	#23	55.1	58.6	000412	4.3	–9.6	5540
KI0025F03	#22	59.6	65.6	000412	4.9	–9.6	5690
KI0025F03	#13	85.1	88.1	000412	3.3	–10.5	5990
KI0025F03	#21	89.1	92.6	000412	4.7	–10.0	5990

Compilation of porosity data (water saturation technique).

Sample	Intercept (m)	Density (kg/m3)	Porosity (weight%)	Porosity (volume%)	Weight (g)	Feature id.	Rock type/type of sample
1A	KA2563A: 206.85 m	2755	0.26	0.72	19.22	Structure #13	Altered ÄD partly mylonitic, Piece of fault breccia
1B	KA2563A: 206.85 m	2763	0.28	0.77	39.62	Structure #13	Altered ÄD partly mylonitic, Piece of fault breccia
2	KA2563A: 154.3 m	2773	0.2	0.55	40.49	Structure #6	Slightly altered ÄD, Piece of fault breccia
3	KI0025F02: 66.7 m	2677	0.56	1.5	17.91	Structure #22	Extensive chemical alteration in ÄD, Piece of fault breccia
4	KI0025F02: 133 m	2755	0.13	0.36	75.84	Structure #19	Mylonite and altered ÄD, Piece of fault breccia
5A	KI0025F02: 133 m	2735	0.17	0.47	11.67	Structure #19	Mylonite and altered ÄD, Piece of fault breccia
5B	KI0025F02: 133 m	2747	0.13	0.35	7.84	Structure #19	Mylonite and altered ÄD, Piece of fault breccia
6	KI0023F: 69.9 m	2689	0.26	0.7	23.19	Structure #20	Altered and partly mylonitic ÄD, Piece of fault breccia
7A	KA2563: 188 m	2695	0.45	1.2	15.68	Structure #20	Altered ÄD, Piece of fault breccia
7B	KA2563: 188 m	2762	0.22	0.61	13.69	Structure #20	Altered ÄD, Piece of fault breccia
	KI0025F02:59.2 A	2699	0.57	1.53	53.26	Structure #23	Part of section through fracture coating+wall rock, d=0–1 cm
	KI0025F02:59.2 B	2741	0.14	0.37	51.41	Structure #23	Part of section through fracture coating+wall rock, d=1–2 cm
	KI0025F02:59.2 C	2743	0.12	0.32	68.29	Structure #23	Part of section through fracture coating+wall rock, d=2–3 cm
	KI0025F02:59.2 D	2762	0.11	0.3	56.129	Structure #23	Part of section through fracture coating+wall rock, d=3–4 cm
	KI0025F02:59.2 E	2758	0.09	0.24	115.07	Structure #23	Part of section through fracture coating+wall rock, d=4–6 cm
	KI0025F03:56.8 A	2730	0.37	1.01	43.59	Structure #23	Part of section through fracture coating+wall rock, d=0–1 cm
	KI0025F03:56.8 B	2738	0.15	0.42	52.56	Structure #23	Part of section through fracture coating+wall rock, d=1–2 cm
	KI0025F03:56.8 C	2750	0.18	0.49	39.58	Structure #23	Part of section through fracture coating+wall rock, d=2–3 cm
	KI0025F03:56.8 D	2751	0.19	0.53	36.37	Structure #23	Part of section through fracture coating+wall rock, d=3–4 cm
	KI0025F03:56.8 E	2739	0.16	0.45	55.33	Structure #23	Part of section through fracture coating+wall rock, d=4–6 cm
	KI0025F03:51.9	2588	0.42	1.08	<100	Structure #6	Gouge and breccia pieces >1 mm
	Ki0025F03:63.2	2891	0.65	1.84	<100	Structure #22	Gouge and breccia pieces >1 mm
	KI0025F03:73.1	2765	0.26	0.71	<100	Structure #20	Gouge and breccia pieces >1 mm
	KI0025F03:87.9	2683	0.78	2.05	<100	Structure #13	Gouge and breccia pieces >1 mm
	KI0025F:88.8	2719	0.72	1.92	<100	Structure #22	Gouge and breccia pieces >1 mm
	KA2563A:154	2725	0.51	1.37	<100	Structure#6	Gouge and breccia pieces >1 mm
T2:15,10	KXTT2: 15.10	2776	0.16	0.41	189,41	Feature A	Mylonite and altered ÄD (W)
T2:15,10	KXTT2: 15.10	2812	0.41	1.16	14,56	Feature A	Altered Äspö diorite (W)
T2A	KXTT2: 15.10	2820	0.19	0.54	10,45	Feature A	Mylonite plus chlorite coating (W)
T2B	KXTT2: 15.10	2855	0.15	0.41	6,89	Feature	Dominated by mylonite
T2C	KXTT2: 15.10	2747	0.12	0.33	16,59	Feature A	Mylonite and Äspö, variable proportions
T2D	KXTT2: 15.10	2754	0.13	0.37	52,01	Feature A	Mylonite and Äspö, variable proportions
T2E	KXTT2: 15.10	2784	0.16	0.45	12,38	Feature A	Mylonite and Äspö, variable proportions
T2F	KXTT2: 15.10	2828	0.19	0.53	5,38	Feature A	Mylonite and Äspö, variable proportions

Appendix F2

Compilation of porosity data (water saturation technique).

Sample	Intercept (m)	Density (kg/m3)	Porosity (weight%)	Porosity (volume%)	Weight (g)	Feature id.	Rock type/type of sample
T2G	KXTT2: 15.10	2743	0.11	0.29	9.34	Feature A	Mylonite and Äspö, variable proportions
T2H	KXTT2: 15.10	2812	0.34	0.97	14.56	Feature A	Mylonite and Äspö, variable proportions
T2I	KXTT2: 15.10	2727	0.12	0.33	16.77	Feature A	Mylonite and Äspö, variable proportions
T2J	KXTT2: 15.10	2781	0.15	0.41	13.59	Feature A	Mylonite and Äspö, variable proportions
T3:14,10	KXTT3:14.10	2876	0.2	0.57	236	Feature A	Slightly altered Äspö diorite (W)
T4:12.10	KXTT4:12.10	2632	0.05	0.13	140	Feature A	Fine-grained granite (W)
8	The Redox Zone	2615	0.36	0.95	11	Redox Zone	Fault breccia material from altered Ävrö granite, 40 mm piece
	The Redox Zone	2580	1.2	3.1	> 100	Redox Zone	2–8 mm fault breccia, average grain porosity of sieved fraction
	The Redox Zone	2580	1.3	3.3	> 100	Redox Zone	2–4 mm fault breccia, average grain porosity of sieved fraction
	The Redox Zone	2590	1	2.6	> 100	Redox Zone	4–8 mm fault breccia, average grain porosity of sieved fraction
	The Redox Zone	2580	1.3	3.3	> 100	Redox Zone	8–20 mm fault breccia, average grain porosity of sieved fraction

(W) = Wall rock sample
d = depth from fracture surface

ISSN 1404-0344

CM Digitaltryck AB, Bromma, 2002